Viscoplastic-Damage Model Parameter Identification via Bayesian Methods

Ehsan Adeli

Viscoplastic-Damage Model Parameter Identification via Bayesian Methods

Von der
Fakultät Architektur, Bauingenieurwesen und Umweltwissenschaften
der Technischen Universität Carolo-Wilhelmina
zu Braunschweig

zur Erlangung des Grades eines
Doktor-Ingenieurs (Dr.-Ing.)
genehmigte

Dissertation

von
Ehsan Adeli
geboren am 30.07.1988
aus Isfahan

Eingereicht am: 7. Dezember 2018
Disputation am: 12. Februar 2019

Berichterstatter: Prof. Dr. Hermann G. Matthies
Prof. Dr.-Ing. Dieter Dinkler

2019

Abstract

The state of materials and accordingly the properties of structures are changing over the period of use, which may influence the reliability and quality of the structure during its life-time. Therefore identification of the model parameters of the system is a topic which has attracted attention in the content of structural health monitoring.

The parameters of a constitutive model are usually identified by minimization of the difference between model response and experimental data. However, the measurement errors and differences in the specimens lead to deviations in the determined parameters. In this thesis, the focus is on the identification of material parameters of a viscoplastic damaging material using a stochastic simulation technique to generate artificial data which exhibit the same stochastic behavior as experimental data. It is proposed to use Bayesian inverse methods for parameter identification. To do so, two steps are considered, solving the forward and the inverse problem. Therefore, first the propagation of the a priori parametric uncertainty through the model including hardening behavior and damage describing the behavior of a steel structure is studied. A non-intrusive stochastic finite element method based on polynomial chaos is applied.

From the forward model, material parameters can be identified using measurement data such as displacement via Bayesian approaches. In this thesis, two methods are applied. The first one is a Transitional Markov chain Monte Carlo method that generates the samples of the posterior probability distribution functions. The second one is a linear approximation of the conditional expectation, the so-called Gauss-Markov-Kalman filter, which is a modification of the Kalman filter, by using the polynomial chaos expansion as the spectral approximation. The applicability of these methods on the desired model is evaluated and the results of both these methods are studied. Further, the efficiency of these identification methods is discussed. Moreover, the evaluated efficient approach is applied to a well-known CT-Test to identify its model parameters by using the data from a pure surface measurement of strain. As the damage parameters can also be determined by considering a minor damage, i.e. not a collapsing damage, the selected Bayesian approach can be proposed for the purpose of structure health monitoring for mechanical material models considering real tests.

Kurzfassung

Der Zustand von Materialien und dementsprechend die Eigenschaften von Konstruktionen ändern sich über die Nutzungsdauer, was die Zuverlässigkeit und Qualität der Konstruktion während ihrer Lebensdauer beeinflussen kann. Daher ist die Identifizierung der Modellparameter des Systems ein Thema, das inhaltlich beim strukturellen Zustandsmonitoring Interesse gefunden hat.

Die Parameter eines konstitutiven Modells werden normalerweise durch Minimierung der Differenz zwischen der Modellantwort und den experimentellen Daten identifiziert. Die Messfehler und Unterschiede in den Proben führen jedoch zu Abweichungen in den ermittelten Parametern. In dieser Arbeit liegt der Fokus auf der Identifizierung von Materialparametern eines viskoplastischen Materials mit Möglichkeit der Schädigung unter Verwendung einer stochastischen Simulationstechnik, um künstliche Daten zu erzeugen, die dasselbe stochastische Verhalten wie experimentelle Daten zeigen. Es wird vorgeschlagen, Bayes'sche inverse Methoden zur Parameteridentifikation zu verwenden. Um dies zu tun, werden zwei Schritte betrachtet: das vorwärts- und das inverse Problem. Daher wird zunächst die Ausbreitung der a priori parametrischen Unsicherheit durch das Modell untersucht, einschließlich des Verfertigungsverhaltens und der das Verhalten einer Stahlstruktur beschreibenden Schädigung. Es wird eine nicht-intrusive stochastische Finite-Elemente-Methode angewendet, die auf polynomialem Chaos basiert.

Aus dem Vorwärtsmodell können Materialparameter anhand von Messdaten wie Verschiebungen über Bayes'sche Ansätze identifiziert werden. In dieser Arbeit werden zwei Methoden angewendet. Die erste ist eine Transitional-Markov-Chain-Monte-Carlo-Methode, die die Stichproben der a posteriori Wahrscheinlichkeitsverteilungsfunktionen generiert. Die zweite ist eine lineare Approximation an die bedingte Erwartung, das sogenannte Gauss-Markov-Kalman-Filter, das eine Modifikation des Kalman-Filters ist, indem die Polynom-Chaos-Expansion als spektrale Näherung verwendet wird. Die Anwendbarkeit dieser Methoden auf das gewünschte Modell wird bewertet und die Ergebnisse dieser beiden Methoden werden untersucht. Ferner wird die Effizienz dieser Identifikationsmethoden diskutiert. Darüber hinaus wird der effizientbewertete Ansatz auf einen bekannten CT-Test angewendet, um seine Modellparameter anhand der Daten einer reinen Oberflächenmessung der Dehnung zu ermitteln. Da die Schadensparameter auch bestimmt werden können, indem ein geringer Schaden betrachtet wird, d. h. kein schwerer schaden, kann der ausgewählte Bayes'sche Ansatz zum Zweck der Zustandsüberwachung für mechanische Materialmodelle unter Berücksichtigung realer Tests vorgeschlagen werden.

Acknowledgments

This work would have not been accomplished without the help and support of several people.

Above all, I would like to express special appreciation to Prof. Hermann G. Matthies, who gave me the opportunity of working on my thesis topic in the Institute of Scientific Computing where I have gained a lot of experiences. I also thank him for being supportive, helpful, and kind, and also for the constructive discussions during this thesis.

I would like to thank Prof. Dieter Dinkler for letting me work as a scientific researcher in our graduate school "GRK 2075", and also for his continuous support, kindness, and encouragement during the last three years.

I would like to thank Dr. Bojana Rosić and Dr. Sven Reinstädler for always being available for questions and discussions, despite their busy schedules, so that I could proceed with my work smoothly. I also thank Dr. Noémi Friedman, Dr. Thilo Moshagen, Mr. Muhammad Sadiq Sarfaraz, Dr. Jaroslav Vondřejc, and Dr. Elmar Zander in alphabetical order for being available for discussions.

I also want to thank all members of GRK 2075, Institute of Scientific Computing and Institute of Structural Analysis at TU Braunschweig for the time we spent together and for making good memories. My special thanks go to Ms. Cosima Meyer who with her support and help is not forgettable for me.

I am very pleased to have some great friends. I thank Florian, Jörn, Nane, Paul, Leona, Ahmed, Sid, Mark, and Hendrik for always being there for me. My immense gratitude goes to Sahel, whose support and company truly boosted me to keep going ahead especially during the days when my father was suffering badly from his disease.

My deepest acknowledgment goes to my beloved family who suffered through this work with me with their unconditional support and understanding which was such a great energy to keep me going over this milestone. I would like to thank my mother who taught me to become a self-motivated and a patient person and my father for teaching me to stay strong and to never give up.

Contents

List of Tables

List of Figures

List of Algorithms

List of Symbols

Abbreviations

CE	Conditional expectation
CT	Compact-Tension test
GMKF	Gauss-Markov-Kalman filter
KLE	Karhunen-Loève expansion
MCMC	Markov Chain Monte Carlo method
MH	Metropolis-Hastings algorithm
ODE	Ordinary differential equation
PCE	Polynomial chaos expansion
PDE	Partial differential equation
PDF	Probability distribution function
RV	Random variable

General Notations

a	Scalar
$\boldsymbol{a}$	Vector
$\boldsymbol{A}$	Tensor

Mathematical Notations

$\cdot$	Scalar product
$:$	Double scalar product
$\times$	Cartesian product
$\otimes$	Tensor product
tr	Trace of a tensor
∇	Nabla operator
∂	Partial derivative
δ	Dirac delta function
$\left\langle \right\rangle$	McAuley brackets

Probability Notations and Symbols

$(\Omega, \mathfrak{B}(\mathcal{M}), \mathbb{P})$	Probability space
$\mathbb{E}$	Expectation
$\mathbb{P}$	Probability measure
$\mathbb{R}$	Set of real numbers
$\mathcal{U}(-r,\, r)$	Uniform distribution on the interval $[-r,\, r]$
$\mathcal{U},\, \mathcal{V}$	Some general vector spaces
$\mathfrak{B}(\mathcal{M})$	Sub-σ-algebra of Borel sets of join domain $\mathcal{M}$
μ	Mean value of Gaussian distribution
Ω	Space of all events ω
σ	Standard deviation of Gaussian distribution
$\boldsymbol{r}(\omega)$	Random variable
$H_\alpha(\boldsymbol{\theta}(\omega))$	Hermite polynomials
$L_1(\Omega, \mathfrak{B}(\mathcal{M}), \mathbb{P})$	Space of integrable RVs
w	Event
cov	Covariance
var	Variance

Mechanical Material Notations

All mechanical material notations are defined in Section 3.

1. Introduction

In recent decades, many practical efforts in civil and mechanical engineering have been dedicated to introduce models which estimate the behavior of systems under time-varying loads by a set of equations. The repetition of such dynamic loads results in the deterioration of the material and consequently every load cycle leads to different displacement levels and it can be addressed to material aging. In such cases, hysteresis, which has been introduced in lots of literatures, appears as a natural mechanism of materials to supply restoring loads against movements and dissipate energy. Hence the studied model should take into account the displacements of the structure and history of the structure. Thus a nonlinear constitutive equations model is required to fulfill the necessities.

After simulating the behavior of the model using the determined parameters existed in a set of inelastic constitutive model equations, it is great of interest to identify the model parameters as the reverse solution given the output measurement of the system. To achieve this purpose, some methods have been developed which lead to estimate the true values of parameters within the hysteresis model by using the probability descriptions. In recent years stochastic simulation methods and Bayesian model updating techniques are paid more attention. The development of these stochastic methods has led to a renaissance in Bayesian and probabilistic methods across all disciplines in science and engineering.

The Bayesian updating approaches treat the probability of all uncertain model parameters within a set of candidate model parameters for a system and consequently have the advantage of being able to quantify all of the uncertainties associated with the modeling of a system and to handle ill-conditioned identification problems. Although Bayesian methods are widely used in many fields, their application to identification of mechanical material models seems to be very limited.

1.1. Problem Statement

To predict the behavior of loaded metallic materials, constitutive models are applied, which present a mathematical frame for the description of elastic and inelastic deformation. The Miller, Krempl, Korhonen, Aubertin, Chan and Bodner models can be addressed as such well-known constitutive models for isotropic materials [1, 2, 3, 4, 5]. In 1983, Chaboche [93, 94] put forward what has become known as the unified Chaboche viscoplasticity constitutive model, which has been widely accepted. In this thesis, the desired model to identify its model parameters is based on the Choboche model and

some enrichments of this model by considering kinematic and isotropic hardening and the damage model introduced by [95] are also evaluated.

In order to estimate the desired model parameters when the uncertainty [111] is considered, which is basically what can not be avoided in the engineering, the probabilistic regularization is applied to solve the ill-posed problem [84, 85]. Hence the uncertain parameters are not represented any more by single values, but by distributions of the random variables. Therefore the process of probabilistic regularization can be divided in two steps. One step is to solve the so-called forward problem, where the uncertainty is propagated to the system and the response of the system should be quantified. The second step is to solve the inverse problem, where the response of the model is compared to the response of the system, which is basically an ill-posed problem.

In order to solve the inverse problem two main approaches can be highlighted that are used in this thesis. The first one is based on generating the samples of the final probability distribution by considering the prior distribution and the additional information, i.e. the observation. It is called Transitional Markov Chain Monte Carlo method [168, 170, 171] which is basically a Markov Chain Monte Carlo method [151, 152, 153, 157, 158] inspired by an adaptive Metropolis-Hastings algorithm [159, 166, 155, 167, 169]. The second approach is an estimation of conditional expectation which leads to a filter called Gauss-Markov-Kalman filter [115, 186, 195, 196, 207, 208]. As it is an approximation some information which possibly from the measurement could be obtained is lost but on the other hand, it is a much faster approach than the first method. Moreover, the functional approximation is applied to the filter which makes the computation much faster.

The problem statement of this thesis is to investigate the possibility of application of the mentioned probabilistic approaches or some other modifications of them in the Bayesian setting and their performance efficiency on the mechanical material models to identify their model parameters, and to track the uncertainty of the desired parameters. Applicability of these probabilistic approaches to estimate the model parameters and whether these approaches can be applied on the real test specimens and engineering tests, and possibly on the health monitoring purpose are the issues which are studied. The review of literature work is discussed in the forthcoming subsection.

1.2. State of the Art

There are tons of references available to address the deterministic approach to identify the model parameters [6, 7, 8, 9, 10, 11, 12, 13, 14, 15, 16, 17, 18, 25] and references therein but only a few investigations are found to address the stochastic approaches to estimate the mechanical material model parameters.

A non-linear approximation by the least-squares method in the Marquardt-Levenberg variant to estimate the parameters of an inelastic model without considering any kind of error is applied by Klosowski and Mleczek [19]. A similar method to solve the inverse problem for parameter identification of a one-dimensional viscoelastic model that incorporates Kelvin-Voigt damping is applied by Banks et al. [20]. Gong et al. [21] have also used some modification of the least-squares optimization method to identify the parameters for a modified Chaboche unified viscoplasticity model where the uncertainty is not considered and the obtained results do not show a good match between the estimated parameters and truth values. Harth and Lehn [22] identified the model parameters of a model by employing the generated artificial data instead of experimental data using stochastic technique. They applied an optimization algorithm which contains stochastic elements to estimate the model parameters where the method has high computational time. A similar study by Harth and Lehn has been carried out for other constitutive models like Lindholm and Chan [23]. The possibility of parameter updating in a Bayesian setting for few linear mechanical material examples is also observed by Arendt et al. [24] and by Cividini et al. [25].

There are few investigations on the simplest material model, elasticity model, to identify only very few parameters of the model where the sampling approach like Metropolis algorithm and its modifications are employed. Pacheco et al. [26] investigated a three-point bending test with an elasticity behavior and calibration is done by solving the inverse problem through a Bayesian perspective by using the Metropolis-Hastings algorithm. Only elasticity moduli are identified without considering the error. Slonski et al. [32] are also applied a sequential particle filter on an elastic model and the Young's modulus is estimated where the Bayesian setting is compared to the deterministic approach and the Bayesian setting is proffered. The elastic modulus of a polymeric material is updated by Zhang et al. [38] where a Markov Chain Monte Carlo method is used by considering very high computation time needed. Further, the Young's modulus is estimated for a considered material by Gallina et al. [27] by applying a multi dimensional Markov Chain Monte Carlo method. A similar Bayesian approach for composite materials to estimate the Young's modulus is carried out by Pieczonka et al. [28]. Arnst et al. [29] have applied a Markov Chain Monte Carlo method by using polynomial chaos expansion to identify Young's modulus of an elasticity model.

Only a few investigations were carried out on the enriched material models such as viscoelastic model to identify the few parameters by employing the Metropolis-Hastings technique and the classical Markov Chain Monte Carlo method. Rappel et al. [30, 31] studied an elastic and a viscoelastic model where the measurement error is considered. Bayesian inference is applied to estimate only the elasticity modulus parameter by applying an adaptive Metropolis-Hastings technique. An et al. [33] investigated a crack model by a classical Markov Chain Monte Carlo method in order to estimate the parameters of a model which represent the size and position of the crack in the Bayesian setting. Also Hernandez et al. [34] applied a Markov Chain Monte Carlo method on a viscoelastic model in order to update its model parameters in the Bayesian setting but the posterior

distribution of the parameters are not updated properly. In fact, the parameters are not identified properly. Mahnken [35] has also applied a Markov Chain Monte Carlo method to estimate few parameters of a plasticity model. The damage parameters of a truss structure under model uncertainties is studied by Zheng et al. [36] where the multi level Markov Chain Monte Carlo method is applied and the true values are not well estimated. Further, this approach suffers from high computation time. Another damage detection approach is applied by Nichols et al. [37] by applying a modified version of Markov Chain Monte Carlo method.

There are other investigations in the Bayesian setting using Markov Chain Monte Carlo method and Madireddy et al [39], Wang and Zabaras [40], and Oh et al [41] have carried out an investigation on the identification of material model by using its modified method. In studies carried out by Alvin [42], Marwala and Sibusiso [43], Daghia et al. [44], Abhinav and Manohar [45], Gogu et al. [46, 47] and Koutsourelakis [48, 49], the elastic parameters of the model are estimated stochastically. Fitzenz et al. [50], Most [51] and Sarkar et al. [52] investigated the elastoplastic materials and thermodynamical material models to identify their model parameters. Other studies on viscoelastic models are carried out by Zhang et al. [53], Mehrez et al. [54] and Miles et al. [55]. Further investigations on the viscoelastic models to estimate more number of model parameters are studied by Zhao and Pelegri [56] and by Kenz et al. [57]. The estimation of fatigue parameters using Markov Chain Monte Carlo method is also studied by [58].

Few investigations in which the Kalman filter and its modifications are employed to identify the material model parameters can be found in literature. Hoshi et al. [59] have estimated the Young's Modulus and Poisson's ratio parameters of an organ model by an extended version of Kalman filter. The same study on an elastic model is carried out to identify the elastic constants of anisotropic materials using Kalman filter by Furukawa et al. [60]. Conte et al. [61] applied some modifications of Kalman filter on a nonlinear structural model to identify its parameters. Hendriks [62] investigated the possibility of identification of few parameters on a viscoelastic model representing the behavior of solid materials by using Kalman filter. Few parameters to identify on the crack path is carried out by Bolzon et al. [63] by employing Kalman filter. Nguyen et al. [64, 65, 66, 67, 68] applied an extended Kalman filter on an elastoplastic model to identify the model parameters. Wall [69] and Nakamura et al. [70] also applied a modification of Kalman filter on a viscoplastic model to determine its model parameters probabilistically. Further, Rosić et al. [88] have applied an accelerated version of Markov Chain Monte Carlo method and also the ensemble Kalman filter by using the polynomial chaos expansion on an elastoplastic model to identify its bulk and shear modulus. It is turned out that the applied methods performed successfully on the studied model. Further, Agmell et al. [71] have determined the Johnson–Cook constitutive model constants for an orthogonal cutting process by using the Kalman filter.

Elastic–plastic graded materials are observed by Bocciarelli et al. [72] and Gu et al. [73] in order to identify their model parameters by employing Kalman filter. The parameters

of an elastic-damage interface model are also identified by Corigliano et al. [74, 75] where the extended Kalman filter method is applied. Further, Ebrahimian et al. [76, 77, 78, 79] investigated the damage parameter identification in the framework of structural health monitoring by using an extended version of Kalman filter. Damage detection for the purpose of health monitoring is also done by Yan et al. [80] by using the Kalman filter.

Although these discussed research into the identification of mechanical material models has been carried out, most of these previous research did not identify many parameters e.g. hardening and damage parameters of the complex mechanical material models, did not quantify mostly the modeling uncertainties, did not properly deal with the ill-conditioning inherent based on the available data, and the methods employed have a high computation time even for the simplest material model considering a very few uncertain parameters. However, the uncertainty associated with the material model predictions can have a significant impact on the decision-making process in design, control, and health monitoring process.

1.3. Objectives

In this thesis as a first step it is aimed to investigate the possibility of identification of the parameters of a viscoplastic-damage model enriched with hardening behavior using a modification of Transitional Markov Chain Monte Carlo (TMCMC) method [168, 170, 171] and a linear approximation of conditional expectation leads to Gauss-Markov-Kalman filter by employing the polynomial chaos expansion (PCE) [115, 186, 195, 196, 207, 208].

The performance of the mentioned methods is evaluated by applying them on the simplest mechanical material model (Elasticity) which is basically a linear system to the most complex considered model, i.e. viscoplastic-damage model with isotropic and kinematic hardening which is a nonlinear system on a three dimensional element. A step by step verification procedure is carried out since a lot of factors can have a partial influence on the identification of the model parameters in the Bayesian setting. It should be noted that the virtual simulation of the model is assumed to represent the data model.

The Transitional Markov Chain Monte Carlo method is applied on the mentioned mechanical material models by considering the uniform distribution of the prior distribution functions of the parameters and it is determined whether the material model parameters including the hardening parameters which do not have much influence on the output displacement are identifiable without any pre-knowledge information of the model parameters. If the estimated parameters are correct, then this method can be applied for further application to identify the model parameters, even if the less knowledge of parameters are available.

The Gauss-Markov-Kalman filter approach is applied in two ways, i.e. the history matching update approach and the sequential updating approach to update the model parameters like model, hardening and damage parameters. The other objective of this thesis is to observe the efficiency of the mentioned update method even for the damage parameters which have very little effect on the measured displacement. The other issue which is discussed in this thesis is to improve the efficiency of the estimated parameters. It is also observed whether the history matching updating where the parameters are updated only one time provides acceptable results for all the model and damage parameters. The applicability of the sequential Gauss-Markov-Kalman filter approach to estimate the model, hardening and damage parameters is also observed. The number of update in terms of time steps and a balance between number of update and quality of the results is also studied. The lesser number of update to save the computation time on particular time intervals is also discussed. As updating on some other time intervals does not provide new information which leads to no update and hence choosing the exact time steps play a very important role.

It is important to consider the computation time for updating the model parameters. Using functional approximation instead of sampling leads to a much cheaper calculation as the functional approximation plays a crucial role when the real tests with high computation times are considered. Comparison of hardening and damage parameter identification for two different main approaches, i.e. Transitional Markov Chain Monte Carlo method and Gauss-Markov-Kalamn filter by considering the fact that these parameters do not have a strong influence on the final measured displacement is also studied and if this fact really should be considered for each of these methods. In this thesis, it can also be seen that the study is carried out by applying the load path in such a way that all set of equations such as hardening and damage evaluation equations are activated so that their parameters can be properly updated when the employed approach is Gauss-Markov-Kalamn filter.

The preliminary study carried out by these approaches will be validated and the evaluated efficient approach is applied to a well-known engineering test called as CT-Test to identify its model parameters. The goal is to investigate the possibility of Bayesian identification of a model parameters for a specimen using data from pure surface measurement of strain. Further, investigating the existed uncertainty for the virtual engineering tests in the form of virtual digital image correlation can be carried out. When the Gauss-Markov-Kalman filter is employed, the effect of different number of measurements considered on the final estimated parameters is studied. Moreover, it is clearly investigated by updating the parameters by considering the model error which literally means considering different identification and model data.

It is also aimed to detect the damage and its parameters in the Bayesian setting. If the damage and damage parameters before a real collapse or at least an immense damage can be identified, then the Bayesian approaches discussed in this thesis to identify the model and damage parameters can be recommended to be employed for the purpose of

health monitoring for mechanical material models considering the real tests. Besides the achieved goals and objectives set above, the other achieved results and observations are encapsulated and discussed in the following.

The Transitional Markov Chain Monte Carlo method to identify the model parameters of the viscoplastic model is well suited, though this method is computationally expensive. On the other hand, the Gauss-Markov-Kalman filter approach using history matching update is fast enough but the estimated parameters are not true at all time for all the model parameters and their uncertainties are not reduced greatly especially for the hardening and damage parameters which do not have a great influence on the measured displacement. Therefore, for the case such as a viscoplastic-damage model with isotropic and kinematic hardening when a well-known test like CT-Test with high computation time is studied, neither the Transitional Markov Chain Monte Carlo method nor the Gauss-Markov-Kalman filter approach using history matching update is recommended.

The sequential Gauss-Markov-Kalman filter approach is highly recommended to apply on a viscoplastic-damage model, especially when the parameters of a test like CT-Test is to be identified. The estimated parameters are accurate and the uncertainties of the parameters are reduced significantly even when the model error is also considered by observing a lot of measurement data which provides us with much information. However, the updating should be carefully designed in such a way that only at special time steps the parameters should be updated.

1.4. Outline of the Thesis

The structure of this thesis is briefly explained in this subsection.

Chapter two: Abstract Problem Setting

In this chapter, the idea of the probabilistic identification is explained. The reasons that stochastic approaches in the presence of uncertainty are considered to estimate the model parameters given the measurements is clearly described. Identification and data model are defined and forward and inverse problem are also introduced. The Bayes' theorem which is the main theorem of this thesis is presented in this chapter.

Chapter three: Mechanical Material Models

In this chapter, the constitutive equations of continuum mechanics and the models representing the behavior of steel material are discussed. From the simplest model (Elasticity) to the most complex model such as a viscoplastic-damage model with isotropic and kinematic hardening behavior are throughly discussed. The desired models are considered to identify their model parameters in the Bayesian setting.

Chapter four: Uncertainty and Forward Model

Uncertainty, its different types and the ways it can be stochastically modeled are discussed in this chapter. The formation of the forward model by propagating the uncertainty using random variables into the deterministic model is also discussed. The quantification of the uncertainty in the response of the system using direct integration and stochastic collocation method is also explained. Moreover, Karhunen-Loève expansion and polynomial chaos expansion representing the functional approximation are discussed.

Chapter five: Bayesian Updating via Markov Chain Monte Carlo

In this chapter, one of the main Markov Chain Monte Carlo approaches which solve the very high conditional ill-posed problem in the Bayesian setting is discussed. Transitional Markov Chain Monte Carlo method is clearly described. Its modifications, improvements, advantages, and disadvantages of this method are explained in detail.

Chapter six: Bayesian Updating via Conditional Expectation

This chapter explains a method based on the linear approximation of the conditional expectation. This approximation is applied to develop a filter so-called Gauss-Markov-Kalman filter by considering the polynomial chaos expansion. This filter is used to solve the inverse problem probabilistically and to identify the parameters of the desired model by updating the uncertainty of the parameters.

Chapter seven: Bayesian Parameter Identification for Mechanical Material Models

This chapter is dedicated to evaluate the discussed Bayesian approaches in Chapter 5 and 6 on the mechanical material models described in Chapter 3 to estimate their model parameters. The methods are applied on the variety of the material models and their efficiency and validation are investigated in this chapter.

Chapter eight: Parameter Identification of a CT-Test using SGMKF

In this chapter the selected method, so-called the sequential Gauss-Markov-Kalman filter, from the Chapter 7 is applied on the well-known CT-Test in order to update its model parameters by considering a viscoplastic-damage model with hardening behavior. The applicability of these methods under different conditions in different scenarios is studied.

Chapter nine: Conclusions and Outlook

In this chapter summary of the discussed methods and their applicability on the desired viscoplastic-damage model to identify its model parameters for different tests are stated. Further, a brief outlook of the future work that can be proposed is discussed.

2. Abstract Problem Setting

In the presented thesis with two type of problems are confronted, i.e. the forward problem and the inverse problem. Predicting the output or in other words, the response of the system from the given input is called forward problem [112, 115, 130, 24, 81, 82]. In contrast, adopting the parameters in a mathematical computational model is denoted as the inverse problem where the response of the model is compared to the response of the system. The response of the system which can be a real-world system or a complex computational model is obtained by solving the forward problem. Hence matching the model response with the system response is called inverse problem [186, 195, 24, 81, 82] and this problem can be solved in different ways.

As the observations do not contain enough information to uniquely determine the parameters, the inverse problem to solve is mostly ill-posed and this can be solved by adding an additional information to find a unique solution. Classically the deterministic approaches are applied where the mean square error (MMSE) is minimized which is a type of optimization problem to find the optimal parameters [83]. These sort of approaches are called deterministic regularization which are not of concern in this thesis.

Probabilistic regularization facilitate us to convert the ill-posed problem to a well-posed problem in a probabilistic setting however it is achieved at a cost [84, 85, 186, 195]. Indeed the unknown parameters are considered as uncertain and modeled as random variables and the information which is added is the prior probability distributions. In other words, the parameters are not considered as single values but distributions of random variables. Hence the result of identification is also distributions and as the distributions are considered, the computational cost increases significantly. The procedure to model the uncertainty into the model using random variables and to compute the response of the system by solving the forward model is presented in Chapter 4.

Although the probability distributions of parameters are considered as the additional information in the probabilistic setting, the evaluation of the residual uncertainty following the identification procedure via the distributions is an advantage of probabilistic setting in comparison to deterministic setting. Hence the probabilistic setting is assumed to model our knowledge about the parameters value in the probability theory language and our knowledge of parameter values are updated by conditioning on the observation. The main probabilistic background for any kind of probabilistic regularization in the probabilistic setting is Bayes's theorem [84, 85, 81, 82] which will be introduced later.

In some cases the probabilistic methods in the probabilistic setting generate the sam-

ples of the updated parameter distributions. These frequently used methods refer to Bayes's theorem in terms of distributions and liklihood functions and typically employ Markov chain Monte Carlo (MCMC) methods [152, 155, 87, 88] to generate the samples of posteriors. A modification of Markov chain Monte Carlo is discussed in Chapter 5 and employed on the desired models in Chapter 7.

In some other cases the Bayesian update is theoretically based on the notion and definition of conditional expectation (CE) [191, 84, 186, 195] as a computational tool. A linear approximation of conditional expectation approach [86] related to the Bayes linear is also discussed in Chapter 6 where the functional representation of the uncertain parameters is considered by employing the polynomial chaos expansion (PCE) [115, 186, 195, 196, 88]. This method is applied on the desired models as described in Chapter 3 and its evaluations are discussed in Chapter 7 and 8.

2.1. Mathematical Set-up

The Bayesian identification is explained by considering an example. The governing equation of linear elastodynamics material [99] as shown in Equation 2.1a and the boundary condition as shown in Equation 2.1b and 2.1c are considered.

$$\text{governing equation} \qquad \rho \frac{\mathrm{d}^2 \boldsymbol{u}(X,t)}{\mathrm{d}t^2} - \rho \boldsymbol{b} = \nabla \cdot (\boldsymbol{C} : \nabla^{\mathrm{sym}} \boldsymbol{u}(X,t)) \tag{2.1a}$$

$$\text{Neumann boundary condition} \qquad \boldsymbol{\sigma} \cdot \boldsymbol{n} = \bar{\boldsymbol{t}} \tag{2.1b}$$

$$\text{Dirichlet boundary condition} \qquad \boldsymbol{u} = \bar{\boldsymbol{u}} \tag{2.1c}$$

In Equation 2.1 where $\ddot{\boldsymbol{u}}(X, t_0) = \ddot{\boldsymbol{u}}_0(X)$, $X \in \mathcal{G}$ is a spatial coordinate in the domain $\mathcal{G} \subset \mathbb{R}^n$, $t \in [0, T]$ is the time, $\boldsymbol{u}$ a vector displacement, ρ the density, $\boldsymbol{\sigma}$ the Cauchy stress tensor, $\boldsymbol{n}$ the normal vector, $\bar{\boldsymbol{t}}$ the traction and ∇ the Nabla operator. Assuming that some parameters e.g. tangential modulus of elasticity $\boldsymbol{C}$, which consists of the bulk and shear modulus, etc., are unknown and thus uncertain, i.e. some uncertainty should be considered and added to their precise values. According to [186, 195], the data and identification model can be introduced and differentiated as described in Subsection 2.1.1.

2.1.1. Data Model

Considering the Equation 2.1 where the $\boldsymbol{u}(t) := \boldsymbol{u}(\cdot, t)$ is considered as an element of a Hilbert space $\mathcal{U}$ which is a closed subspace of the Sobolev space $H^1(\mathcal{G})$ [186, 195]. Then the Equation 2.2 represents $A_{\mathcal{U}} : \mathcal{Q} \times \mathcal{U} \to \mathcal{U}$ which is possibly a non-linear operator in $\boldsymbol{u} \in \mathcal{U}$ and the unknown parameters are with $\boldsymbol{q} \in \mathcal{Q}$ where $\mathcal{Q}$ is some Hilbert space.

$$\frac{\mathrm{d}^2\boldsymbol{u}}{\mathrm{d}t^2}(t) = \ddot{\boldsymbol{u}}(t) = A_{\mathcal{U}}(\boldsymbol{q};\, \boldsymbol{u}(t)) + \boldsymbol{b}(\boldsymbol{q},\, t), \quad \boldsymbol{u}(0) = \boldsymbol{u}_0(\boldsymbol{q}) \in \mathcal{U}, \quad t \in [0,\, T] \tag{2.2}$$

Equation 2.2 is assumed as an instance of stochastic evolution as both $A_{\mathcal{U}}$, $\boldsymbol{u}_0$ and $\boldsymbol{b}$ could involve some noise. It should also to be noted that the observed data is generated from this Equation 2.2.

It is assumed that observation function $\hat{Y}(\boldsymbol{q};\, \boldsymbol{u}(t))$ of the state $\boldsymbol{u}(t)$ i.e. $\hat{Y} : \mathcal{Q} \times \mathcal{U} \to \mathcal{Y}$ is evaluated at regular time intervals $t_n = n \cdot \mathbf{1}t$ where $y_n = \hat{Y}(\boldsymbol{q};\, \boldsymbol{u}_n)$ and $\boldsymbol{u}_n := \boldsymbol{u}(t_n)$. The solution operator Υ of Equation 2.2 results in Equation 2.3 providing the solution from t_n to t_{n+1}.

$$\boldsymbol{u}_{n+1} = \Upsilon(t_{n+1}, \boldsymbol{q}, \boldsymbol{u}_n, t_n, \boldsymbol{b}) \tag{2.3}$$

Hence the observation function results in the Equation 2.4 where some noise u_n is considered because of the inaccuracy of the observation.

$$\hat{y}_{n+1} = \hat{h}(\hat{Y}(\boldsymbol{q};\, \Upsilon(t_{n+1}, \boldsymbol{q}, \boldsymbol{u}_n, t_n, \boldsymbol{b})), \mathsf{u}_n) \tag{2.4}$$

2.1.2. Identification Model

The generation of the data from the data model is described in Subsection 2.1.1 and the identification model is presented in the following. Similar to Equation 2.2, the identification model can be defined as shown in Equation 2.5 where the unknown parameters $\boldsymbol{q}$ are to be identified [186, 195].

$$\frac{\mathrm{d}^2\boldsymbol{v}}{\mathrm{d}t^2}(t) = \ddot{\boldsymbol{v}}(t) = A(\boldsymbol{q};\, \boldsymbol{v}(t)) + \boldsymbol{b}(\boldsymbol{q},\, t), \quad \boldsymbol{v}(0) = \boldsymbol{v}_0(\boldsymbol{q}) \in \mathcal{V}, \quad t \in [0,\, T] \tag{2.5}$$

A solution operator V is defined for the Equation 2.5 from t_n to t_{n+1} and it results in the Equation 2.6.

$$\boldsymbol{v}_{n+1} = \mathsf{V}(t_{n+1}, \boldsymbol{q}, \boldsymbol{v}_n, t_n, \boldsymbol{b}) \tag{2.6}$$

It should be noted that two spaces $\mathcal{U}$ in Equation 2.2 and $\mathcal{V}$ in Equation 2.5 are not the same as it is not assured that $\boldsymbol{u} \in \mathcal{U}$, while the observations $y \in \mathcal{Y}$ is assured.

As the parameters $\boldsymbol{q}$ and the state $\boldsymbol{v} \in \mathcal{V}$ in Equation 2.5 are identified sequentially, i.e. the estimated parameters change from step n to step $n+1$, an extended state vector $x = (\boldsymbol{v},\, \boldsymbol{q}) \in \mathcal{X} := \mathcal{V} \times \mathcal{Q}$ are introduced which describes the change from n to $n+1$ via

the Equation 2.7.

$$x_{n+1} = (\boldsymbol{v}_{n+1}, \boldsymbol{q}_{n+1}) = \hat{f}(x_n) := (\mathsf{V}(t_{n+1}, \boldsymbol{q}_n, \boldsymbol{v}_n, t_n, \boldsymbol{b}),\ \boldsymbol{q}_n) \tag{2.7}$$

A noise $\mathsf{w} \in \mathcal{W}$ representing the stochastic contribution or modeling errors between the models introduced in Equations 2.2 and 2.5 is considered and it results in the Equation 2.8.

$$x_{n+1} = f(x_n, \mathsf{w}_n) \tag{2.8}$$

The identification observation operator for the extended state is introduced resulting in the Equation 2.9 where some noise u_n, as given in Equation 2.4, representing the inaccuracy of the observation is also taken into account.

$$y_{n+1} = h(x_n, \mathsf{u}_n) = H(x_{n+1}, \mathsf{u}_n) = H(f(x_n, \mathsf{w}_n), \mathsf{u}_n) \tag{2.9}$$

The Equation 2.10 can be considered as a simple example with additive noise where $\mathsf{u} \in \mathcal{U}$ refers to the random vector and a bounded linear map $\mathsf{S}_{\mathcal{U}}(x) \in \mathscr{L}(\mathcal{U}, \mathcal{X})$ from $\mathcal{U}$ to $\mathcal{X}$ for each $x \in \mathcal{X}$ exists.

$$h(x_n, \mathsf{u}_n) := Y(\boldsymbol{q}; \mathsf{V}(t_{n+1}, \boldsymbol{q}_n, \boldsymbol{v}_n, t_n, \boldsymbol{b})) + \mathsf{S}_{\mathcal{U}}(x_n)\mathsf{u}_n \tag{2.10}$$

The true observation without noise u_n are predicted by mapping $Y : \mathcal{Q} \times \mathcal{V} \to \mathcal{Y}$. The Equation 2.8 representing the time evolution of the extended state and Equation 2.9 representing the observation are the main equations of this section that aids in identification.

2.2. Synopsis of Bayesian Estimation

Ideally the observation $\hat{y}$ determined from Equation 2.4 depending on the unknown parameters $\boldsymbol{q}$ should be equal to y determined from the Equation 2.9. As the parameter $\boldsymbol{q}$ can not be uniquely determined or there are many $\boldsymbol{q}$ conforming to $\hat{y}$, the mapping $\boldsymbol{q} \mapsto y = Y(\boldsymbol{q}; u(\boldsymbol{q}))$ is not invertible even when no distracting errors such as w and v are considered. Hence the problem is confronted as an inverse problem in which the $\boldsymbol{q}$ is determined from the observation $\hat{y}$ [81, 186, 195, 82]. It is basically an ill-posed problem as shown in Equation 2.11 where ϵ is a random variable. This random variable ϵ is represented as the errors of the measurement device in case of data model and as the model error in case of identification model i.e. the difference between the model and reality. The Equation 2.11 is obtained by simplifying the Equation 2.4 and 2.9.

$$\hat{y} = y + \epsilon = Y(\boldsymbol{q}) + \epsilon \tag{2.11}$$

The ϵ represents the error in the Equation 2.4 and 2.10. The Equation 2.11 aids in estimating the $\boldsymbol{q}$ from the given measurement $\hat{y}$.

In order to overcome the ill-posed problem and estimate the parameters q_n, the difference between the observed $\hat{y}_n$ and the predicted system output y_n is minimized. However the evaluated parameters from the minimizing approaches are unique. In order to determine the unique parameters a regularization should be performed [81, 83, 85] which is a kind of optimization procedure.

In this thesis, the stochastic regularization in a Bayesian setting is assumed. Hence each unknown parameter is assumed to have uncertain value due to lack of knowledge and is modeled by initial random variable distribution called as prior probabilistic model [84, 85, 82, 81]. Hence the problem becomes well-posed but now a probability distribution conforming to the data is to be determined instead of single value. The considered additional information are the measurement or observation which changes the probabilistic description to the so-called posterior model. This approaches are described in Chapter 5. The other approach used in this thesis is the updating of the probabilistic description based on the additional information, i.e. by considering the measurements, the unknown parameters and the remained uncertainty are estimated while the probabilistic description is updated. This approach based on conditional expectation is discussed in Chapter 6.

As the parameters are assumed to be uncertain and accordingly are represented by the random variables, the computational cost in the probabilistic approach is higher than the deterministic approach. Therefore to accelerate the computation the spectral representation such as the functional approximation of stochastic problems are employed. The polynomial chaos expansion, a type of functional approximation, is used numerically and it is described in Chapter 4.

The theorem of Bayes and Laplace is introduced in the following subsection. A sampling method based on the Bayes's theorem where the posterior distribution is computed from the prior and the additional information i.e. measurements is described in this thesis. However the other approach described in this thesis is not based on the Bayes's theorem but based on conditional expectation and its computation. In this approach, the prior represented by the random variables is manipulated to obtain the new random variables with the correct posterior distribution. Meanwhile all the relevant information from the conditioning can also be computed. The relation between the condition expectation approach and Bayes's theorem is also discussed later.

2.2.1. The Theorem of Bayes and Laplace

The Bayes's theorem [84, 81, 85, 186, 82, 195] incorporates the new information into a probabilistic description. The Bayes's theorem can be defined by the conditional probability such as $\mathcal{I}_q \subset \mathcal{Q}$, i.e. it is subset of possible q's from which new information is gained and $\mathcal{M}_y \subset \mathcal{Y}$ is the information obtained from the measurement. $\mathbb{P}(\mathcal{I}_q)$ is called as prior and it is known before the observation $\mathcal{M}_y$. The quantity $\mathbb{P}(\mathcal{M}_y|\mathcal{I}_q)$ refers to the likelihood i.e. it refers to the conditional probability of $\mathcal{M}_y$ by assuming $\mathcal{I}_q$ is given. The term $\mathbb{P}(\mathcal{M}_y)$ referring to the probability of observing $\mathcal{M}_y$ is called as evidence and this can be expanded by using law of total probability. This term allows to choose between different models. Hence the posterior term $\mathbb{P}(\mathcal{I}_q|\mathcal{M}_y)$ reflecting the knowledge on $\mathcal{I}_q$ after observing $\mathcal{M}_y$ results in the Equation 2.12 where the quotient $\frac{\mathbb{P}(\mathcal{M}_y|\mathcal{I}_q)}{\mathbb{P}(\mathcal{M}_y)}$ is called as Bayes factor and it reflects the relative change in probability after observing $\mathcal{M}_y$.

$$\mathbb{P}(\mathcal{I}_q|\mathcal{M}_y) = \frac{\mathbb{P}(\mathcal{M}_y|\mathcal{I}_q)}{\mathbb{P}(\mathcal{M}_y)}\mathbb{P}(\mathcal{I}_q), \quad \text{if } \mathbb{P}(\mathcal{M}_y) > 0 \tag{2.12}$$

As it is known from the formulation of Bayes's theorem obtained from the Equation 2.12 that if $\mathbb{P}(\mathcal{M}_y) = 0$ then the set observations $\mathcal{M}_y$ has vanishing measure. This problem can be resolved by reformulating the Bayes's theorem obtained from the Equation 2.12 and this carried out by considering the continuous random variables for the probability density functions (PDFs) or distributions representing it.

The Equation 2.12 is reformulated by using the probability density functions. The Equation 2.13 is obtained when y and q have a joint PDF $\pi_{y,q}(y,q)$ as y is essentially a function of q.

$$\pi_{q|y}(q|y) = \frac{\pi_{y,q}(y,q)}{Z_s(y)} \tag{2.13}$$

The condition PDF term in the Equation 2.13 is $\pi_{q|y}(q|y)$ and Z_s is the evidence. The term Z_s as shown in the Equation 2.14 is a normalizing factor and it integrates the conditional PDF $\pi_{q|y}(\cdot|y)$ to unity.

$$Z_s(y) = \int_{\Omega} \pi_{y|q}(y|q(\omega))\,\mathbb{P}(\mathrm{d}\omega) \tag{2.14}$$

The joint PDF can be split into the likelihood density $\pi_{y|q}(y|q)$ and the prior PDF $\pi_q(q)$ as shown in the Equation 2.15.

$$\pi_{y,q}(y,q) = \pi_{y|q}(y|q)\pi_q(q) \tag{2.15}$$

Eventually the Equation 2.16 is obtained by reformulation of the Equation 2.12 using

the probability density functions.

$$\pi_{q|y}(q|y) = \frac{\pi_{y|q}(y|q)}{Z_s(y)}\pi_q(q) \tag{2.16}$$

Some stochastic approaches determine the probability density function by generating the samples as one of them is described in Chapter 5. However some other approaches involving the random variables instead of probability density function and conditional probability. One of this kind of approaches is discussed in Chapter 6. Hence the concept of conditional expectation (CE) [191, 84, 186, 195, 85] and its relation to Bayes's theorem is considered. Classically for any measurable function Ψ of q, the conditional measure or probability density function implies the conditional expectation as defined by the Equation 2.17.

$$\mathbb{E}(\Psi|\mathcal{M}_y) := \int_{\mathcal{Q}} \Psi(q)\mathbb{P}(\mathrm{d}q|\mathcal{M}_y) \tag{2.17}$$

The conditional expectation $\mathbb{E}(\cdot|\mathcal{M}_y)$ can be defined as an integral over the conditional measure $\mathbb{P}(\cdot|\mathcal{M}_y)$ respectively the conditional PDF $\pi_{q|y}(\cdot|y)$. The conditional expectation and related discussions are clearly explained in the Chapter 4.

2.3. Summary

In this chapter, the problem is defined and the disadvantages of the deterministic regularization was discussed. The forward and inverse problem in the Bayesian setting were also defined in this chapter. Moreover the probabilistic space, uncertain parameters and the methodology to solve the forward model were addressed. The forward and inverse problem for a case study was mathematically defined and expressed in terms of the two considered model, i.e. data model and identification model. In addition, the approaches to solve the inverse problem were specified. Accordingly the random walk approaches e.g. MCMC methods and a method based on conditional expectation using polynomial chaos expansion are addressed. In the following, the material mechanical models will be described in Chapter 3 and then in Chapter 4 forward problem and the method to solve it is described. Two main inverse approaches are studied in Chapter 5 and 6. The validation of the discussed methods on the desired models will be evaluated in the Chapter 7. Finally the application of the validated methods on a well-known test will be investigated in the Chapter 8.

3. Mechanical Material Models

The constitutive equations of continuum mechanics and the models representing the behavior of steel material are discussed in this chapter. Models can be distinguished into microscopic model and macroscopic model. Microscopic models describe for instance the density of dislocations while macroscopic models describe as an example the evaluation of material by defining the isotropic and kinematic hardening behavior by means of external variables (stress, strain) and a set of internal variables. Before studying the models, the basic equation of continuum mechanics which are material independent are briefly discussed in the following.

Under restriction of small strain, the fundamental balance equations of continuum mechanics such as conservation of mass (Balance of mass), conservation of momentum (Balance of momentum and angular momentum) and conservation of energy (first and second law of thermodynamics) are shown below [90, 91].

$$m = \int_{\Omega} \rho \, \mathrm{d}\Omega \quad \text{(mass)} \tag{3.1a}$$

$$\int_{\partial\Omega} \bar{\boldsymbol{t}} \, \mathrm{d}\partial\Omega = \int_{\Omega} \nabla \cdot \boldsymbol{\sigma} \, \mathrm{d}\Omega \quad \text{(momentum)} \tag{3.1b}$$

$$\sigma_{ij} = \sigma_{ji} \quad \text{(moment of momentum)} \tag{3.1c}$$

$$\rho \dot{e} = \boldsymbol{\sigma} : \dot{\boldsymbol{\epsilon}} + \rho r - \nabla \cdot \boldsymbol{q} \quad \text{(energy)} \tag{3.1d}$$

$$\boldsymbol{\sigma} : \dot{\boldsymbol{\epsilon}} + \rho T \dot{s} - \rho \dot{e} - \boldsymbol{q} \cdot \frac{\nabla T}{T} \geqslant 0 \quad \text{(entropy)} \tag{3.1e}$$

$$\Psi = e - \frac{\partial e}{\partial s} s = e - Ts \quad \text{(definition of Helmholtz free energy)} \tag{3.1f}$$

In the Equation 3.1a, m is the mass of a body and ρ is the density where Ω specifies the considered volume. In the Equation 3.1b, $\bar{\boldsymbol{t}}$ and $\boldsymbol{\sigma}$ represents the vector of surface traction and the Cauchy stress tensor respectively. The Nabla operator is indicated by ∇. The terms e, r, and $\boldsymbol{q}$ in Equation 3.1d represent the internal energy density per mass unit, a heat source inside a volume and a heat flux through the surface respectively. In Equation 3.1e, s indicates the entropy density per unit mass and T is the absolute temperature.

Two more useful equations are derived from the balance laws such as in the Clausius-Duhem inequality 3.1e as the Helmholtz free energy is substituted into it where the

partial derivatives of Helmholtz free energy with respect to $\boldsymbol{\epsilon}$ results in Equation 3.2.

$$\boldsymbol{\sigma} = \rho \frac{\partial \Psi}{\partial \boldsymbol{\epsilon}} \tag{3.2}$$

Also the dissipation potential (ϕ) is introduced such that the partial derivatives of it with respect to $\boldsymbol{\sigma}$ results in Equation 3.3 where the inelastic part of strain is represented by $\dot{\boldsymbol{\epsilon}}^{in}$.

$$\dot{\boldsymbol{\epsilon}}^{in} = \frac{\partial \phi}{\partial \boldsymbol{\sigma}} \tag{3.3}$$

The other equations of state variables are determined from the partial derivative of Helmholtz free energy (Ψ) and dissipation potential (ϕ). From the Equations 3.2 and 3.3, it can be inferred that constitutive and evolution equation for elastic, inelastic and damaged material can be described through thermodynamics of irreversible process.

3.1. Material Equations

In this section, the simplest material model (Elasticity) and enriched models (Inelasticity) are discussed. Inelastic deformations are accompanied by the phenomenon of hardening such as isotropic and kinematic hardening. The behavior of steel material by considering the cyclic loading are clearly described by defining the hardening phenomenon. The mechanical material damage described by continuum damage mechanics is also considered in the model to express the material behavior of steel under cyclic loading in the reality.

In the following subsection, the equations of state and evolution equations for viscoplastic material model with isotropic and kinematic hardening and anisotropic ductile and creep damage according to [101, 106, 100, 92, 105, 93, 94, 96] are discussed and the models introduced will be used as case studies in the next chapters.

3.1.1. Viscoplastic-Damage Model Considered

The mechanics of the investigated structures with the elasto-viscoplastic material behavior by neglecting inertia and infinitesimal strain theory are described in Equations 3.4a and 3.4b [92, 99].

$$\text{equilibrium} \qquad -\nabla \cdot \boldsymbol{\sigma} = \rho \boldsymbol{g} \tag{3.4a}$$

$$\text{strain decomposition} \qquad \boldsymbol{\epsilon}_{el} + \boldsymbol{\epsilon}_{vp} = \boldsymbol{\epsilon} \tag{3.4b}$$

The Cauchy stress ($\boldsymbol{\sigma}$) is caused by the body force ($\rho\boldsymbol{g}$) as specified by density (ρ) and gravity ($\boldsymbol{g}$). The boundary conditions are given in Equations 3.5a and 3.5b.

$$\boldsymbol{u} = \bar{\boldsymbol{u}} \tag{3.5a}$$
$$\boldsymbol{\sigma} \cdot \boldsymbol{n} = \bar{\boldsymbol{t}} \tag{3.5b}$$

The boundary condition such as the displacement is represented by $\bar{\boldsymbol{u}}$ and the acting surface tension is represented by $\bar{\boldsymbol{t}}$ on the Dirichlet and Neumann part, respectively. The Cauchy stress is mapped to the outward normal vector ($\boldsymbol{n}$) in the boundary of the structural body as shown in Equation 3.5b. As the kinematics of the structure is considered the equilibrium 3.4a and the strain balance 3.4b are taken into account in the differential equation form. The kinematics is described by the Cauchy strain tensor which describes it as the gradient of the displacement field as shown in Equation 3.6.

$$\boldsymbol{\epsilon} = \frac{1}{2}\left(\nabla \boldsymbol{u} + (\nabla \boldsymbol{u})^T\right) \tag{3.6}$$

The constitutive equations of the elastic strain ($\boldsymbol{\epsilon}_{el}$) and viscoplastic strain ($\boldsymbol{\epsilon}_{vp}$) along with the governing equations such as Equation 3.4a and Equation 3.4b are discussed in detail.

For mild steel under cyclic loading the isotropic and kinematic hardening are taken into account. For viscoplastic material the material behavior is characterized by the modified Chaboche model [93, 94, 96] as introduced by Kowalsky et al. [95] where the damage is described by continuum damage mechanics. The spatially distributed differential equation with internal length (l_c) as model parameter defines the isotropic ductile damage (D). Equation 3.7 is used to introduce a non-local damage variable ($\bar{D}$) to evaluate effective strains and stresses [96, 97, 98].

$$D = \bar{D} - l_c^2 \nabla^2 \bar{D} \tag{3.7}$$

The Equation 3.7 is considered as it is assumed that the damage occurs locally but acts non-locally. Here the stresses are only affected by damage while the strains remain unaffected as it shown in Equation 3.8.

$$\tilde{\boldsymbol{\sigma}} = \frac{1}{1-\bar{D}}\,\boldsymbol{\sigma}\,, \qquad \tilde{\boldsymbol{\epsilon}} = \boldsymbol{\epsilon} \tag{3.8}$$

The cross section of a material which is damaged is shown in Figure 3.1 where the damage parameter (D) is derived from the damaged area of the cross section of model denoted in Figure 3.1 by blue color by its total area [96, 97, 98].

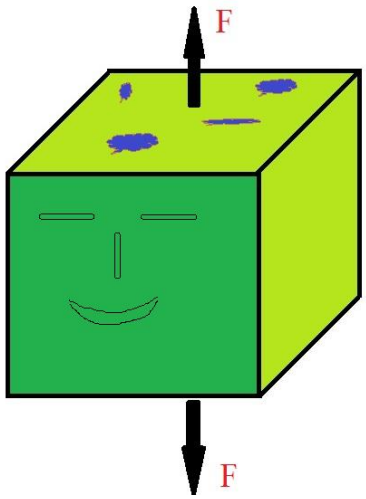

Figure 3.1.: Cross section of a damaged material

The elastic behavior of the material is described by the potential of a St. Venant-Kirchhoff material [106, 91, 90] as in Equation 3.9.

$$\phi_{el}(\boldsymbol{\epsilon}_{el}) = \frac{\lambda}{2}\left(\mathrm{tr}(\boldsymbol{\epsilon}_{el})\right)^2 + \mu\,\boldsymbol{\epsilon}_{el} : \boldsymbol{\epsilon}_{el} \tag{3.9}$$

The second Lamé-coefficients (μ) is also called as shear modulus (G). Along with the first Lamé-coefficient the elastic behavior of the material is from so on in this thesis described by the bulk modulus ($\kappa = \lambda + \frac{2}{3}\,\mu$) [100, 101, 106]. By using the tensor of elasticity as it is shown in Equation 3.10, the rate of effective strain from the constitutive equation of the elastic part can be written as in Equation 3.11.

$$\boldsymbol{C} = \frac{\partial^2 \phi_{el}}{\partial \boldsymbol{\epsilon}_{el}^2} \tag{3.10}$$

$$\dot{\tilde{\boldsymbol{\epsilon}}}_{el} = \boldsymbol{C}^{-1} : \dot{\tilde{\boldsymbol{\sigma}}} = \frac{1}{1-\bar{D}}\,\boldsymbol{C}^{-1} : \dot{\boldsymbol{\sigma}} + \frac{\dot{\bar{D}}}{(1-\bar{D})^2}\,\boldsymbol{C}^{-1} : \boldsymbol{\sigma} \tag{3.11}$$

If elasticity model [101, 106, 100] is the case, i.e. viscoplastic part of the effective strain is zero, the strain follows the stress immediately and it becomes zero once the stress is removed as shown in Figure 3.2. A reversible direct relation between stress, strain and elastic deformation characterizes the material behavior.

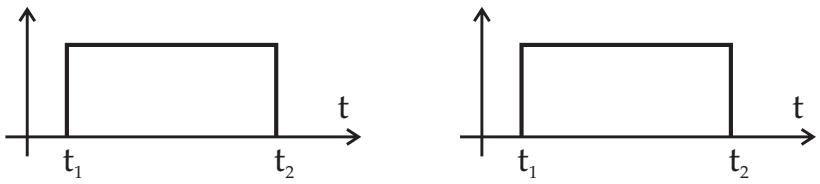

Figure 3.2.: Elastic material response

A linear elastic behavior is represented by a one-dimensional device called as spring as shown in Figure 3.3.

Figure 3.3.: Rheological model of Elasticity

For viscoplasticity [96, 101] the dissipation potential in terms of the effective equivalent stress ($\tilde{\sigma}_{eq}$) and the isotropic hardening (R) as time-varying variables is shown in Equation 3.12.

$$\phi_{vp}(\tilde{\boldsymbol{\sigma}}) = \frac{k}{n+1}\left\langle\frac{\tilde{\sigma}_{ex}}{k}\right\rangle^{n+1} \quad \text{with} \quad \tilde{\sigma}_{ex} = \tilde{\sigma}_{eq} - \sigma_y - R \quad \text{and} \quad \langle\cdot\rangle = \max(0,\cdot) \tag{3.12}$$

On contrary the model parameters such as yield stress (σ_y), k and n are constant in time. From the von-Mises yield-criterion [91, 100], the equivalent effective stress as in Equation 3.13 described by the second invariant (I_2) as given by Equation 3.14 which is applied to the deviatoric part of the effective stress tensor ($\tilde{\boldsymbol{\sigma}}^{\text{ef}} = \tilde{\boldsymbol{\sigma}} - \boldsymbol{\chi}$) taking into account the kinematic hardening back stress tensor ($\boldsymbol{\chi}$) [96, 101, 98, 106, 100].

$$\tilde{\sigma}_{eq} = \sqrt{3\,I_2\left(\tilde{\boldsymbol{\sigma}} - \boldsymbol{\chi}\right)^d + \bar{D}\left(I_1\left(\tilde{\boldsymbol{\sigma}} - \boldsymbol{\chi}\right)\right)^2} \tag{3.13}$$

$$I_2\left(\tilde{\boldsymbol{\sigma}} - \boldsymbol{\chi}\right)^d = \frac{1}{2}\,\mathrm{tr}\Big(\left(\tilde{\boldsymbol{\sigma}} - \boldsymbol{\chi}\right)^d \cdot \left(\tilde{\boldsymbol{\sigma}} - \boldsymbol{\chi}\right)^d\Big) \tag{3.14}$$

The second term in Equation 3.13 is considered as the damage of material results in the reduction of elastic capacity of the material. It is noted that the first invariant (I_1) is equivalent to hydrostatic stress as given in Equation 3.15.

$$I_1\left(\tilde{\boldsymbol{\sigma}} - \boldsymbol{\chi}\right) = \frac{1}{3}\mathrm{tr}\left(\tilde{\boldsymbol{\sigma}} - \boldsymbol{\chi}\right) \tag{3.15}$$

The partial derivative of the dissipation potential (ϕ_{vp}) with respect to $\tilde{\boldsymbol{\sigma}}$ results in the Equation 3.16 referring to the rate of effective viscoplastic strain [96, 101, 106, 100].

$$\dot{\tilde{\boldsymbol{\epsilon}}}_{vp} = \frac{\partial \phi_{vp}}{\partial \tilde{\boldsymbol{\sigma}}} = \left\langle \frac{\tilde{\sigma}_{ex}}{k} \right\rangle^n \frac{\partial \tilde{\sigma}_{ex}}{\partial \tilde{\boldsymbol{\sigma}}} \tag{3.16}$$

Considering a perfect viscoplasticity model, i.e. a viscoplastic model without kinematic and isotropic hardening, then time dependent behavior is accompanied by permanent deformation as shown in Figure 3.4.

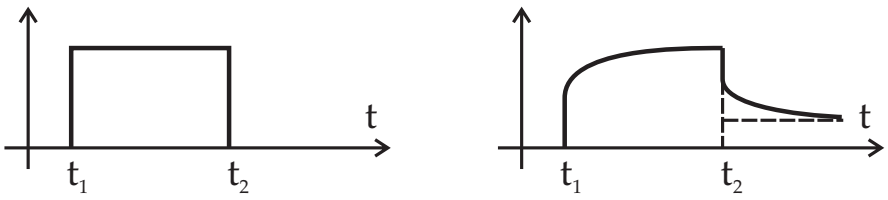

Figure 3.4.: Viscoplastic material behavior

A combination of springs, dash pot and a friction slider are used to model a perfect viscoplastic behavior. A simple system with viscosity (η) and yield stress (σ_y) is shown in Figure 3.5.

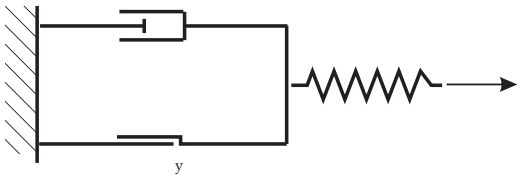

Figure 3.5.: Rheological model of viscoplasticity

The enriched Chaboche model [93, 94, 96] with isotropic and kinematic hardening is considered to describe the Bauschinger effect in steel under high cyclic loading [96, 101, 96, 98] where the evolution of the isotropic and kinematic hardening is described by the ordinary differential equations as shown in Equation 3.17 and Equation 3.18 respectively.

$$\dot{R} = b_R \left(H_R - R \right) \dot{p} \tag{3.17}$$

$$\dot{\boldsymbol{\chi}} = b_{\boldsymbol{\chi}} \left(\frac{2}{3} H_{\boldsymbol{\chi}} \frac{\partial \tilde{\sigma}_{eq}}{\partial \tilde{\boldsymbol{\sigma}}} - \boldsymbol{\chi} \right) \dot{p} \tag{3.18}$$

Isotropic and kinematic hardening Equations 3.17 and 3.18 depend on the accumulated equivalent viscoplastic strain which is written by using McAuley bracket as shown in Equation 3.19.

$$\dot{p} = \left\langle \frac{\tilde{\sigma}_{ex}}{k} \right\rangle^n \tag{3.19}$$

The parameter b_R represents the speed of evolution and the parameter H_R represents the threshold of the isotropic hardening. Similarly the parameters $b_{\boldsymbol{\chi}}$ and $H_{\boldsymbol{\chi}}$ control the kinematic hardening behavior.

To comprehend the effect of hardening equations on the behavior of material, a perfect plastic model with a plastic model with isotropic and kinematic hardening is compared. A perfect plastic material is loaded such that the strain/time function as shown in Figure 3.6 is obtained and the stress response as shown in Figure 3.7 is calculated.

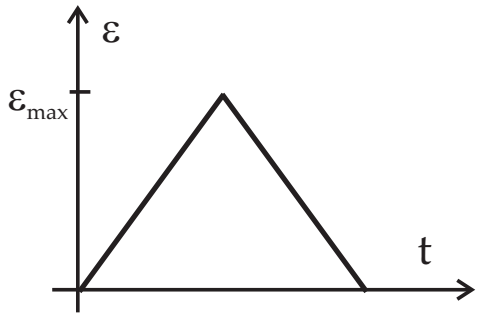

Figure 3.6.: Strain–time function applied in subsequent tension tests

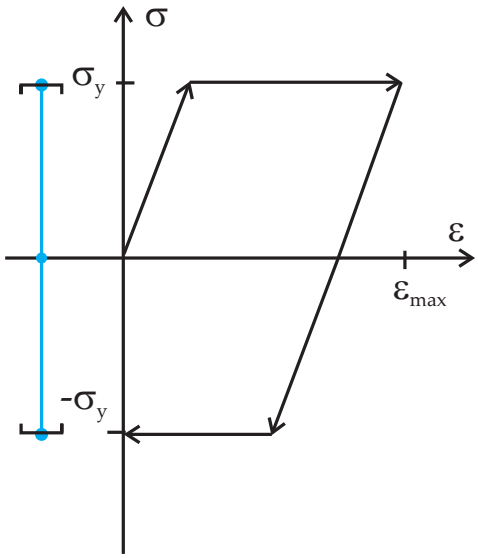

Figure 3.7.: Stress–strain response of the perfect plasticity model

Considering a plastic model with isotropic hardening subjected to the strain–time function as shown in Figure 3.6 results in the stress response of the material as shown in Figure 3.8 which represents the influence of isotropic hardening in the two dimensional stress-strain space. As seen in Figure 3.8, the yield surface is expanded by the isotropic hardening variable (b_R) and the stress increases until the saturation value (H_R) is reached. The shape of the hysteresis loop for the various number of cycles remains same on reaching the saturation.

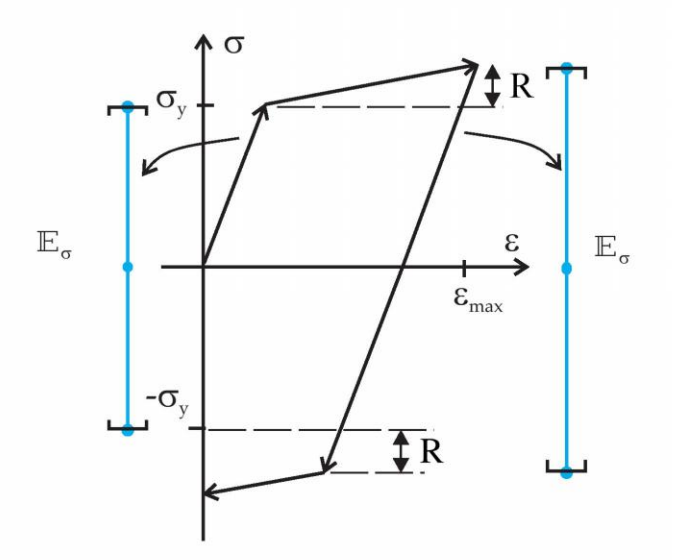

Figure 3.8.: Stress–strain response of the isotropic hardening model

Considering a plastic model with isotropic and kinematic hardening which is subjected to the strain–time function as shown in Figure 3.6 results in the stress response of the material as shown in Figure 3.9.

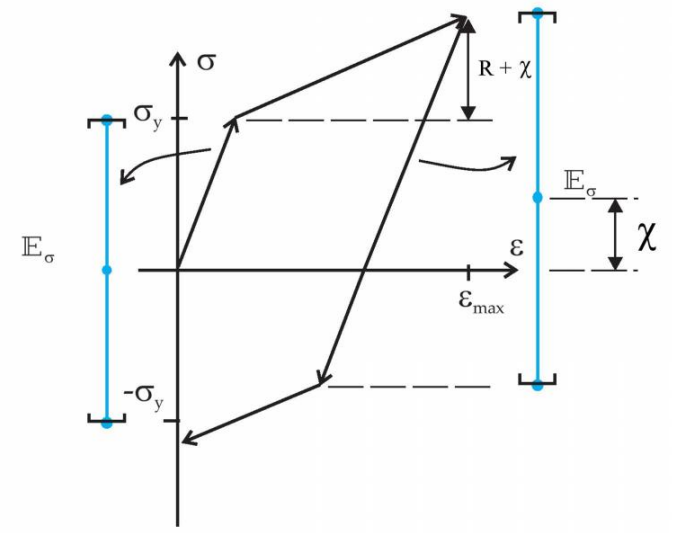

Figure 3.9.: Stress–strain response of the isotropic and kinematic hardening model

As seen in Figure 3.9, the yield surface is translated by the value of kinematic hardening back stress tensor ($\boldsymbol{\chi}$).

The evolution equation for the local damage proposed by Kowalsky et al. [95] as shown in Equation 3.20 is regularized by the model parameter c_1 up to c_5 and it is activated only when the threshold ϵ_{vp}^{eq} for the viscoplastic strain is reached. Hence it results in $\sqrt{2/3\,\boldsymbol{\epsilon}_{vp} : \boldsymbol{\epsilon}_{vp}} > \epsilon_{vp}^{eq}$ [97, 98, 102, 103].

$$\dot{D} = \left(c_1 + c_2 e^{-c_3 p^+}\right) \dot{p}^+ + c_4 \left(c_5 - \bar{D}\right) \left\langle \mathrm{tr}\left(\frac{\partial \tilde{\sigma}_{eq}}{\partial \tilde{\boldsymbol{\sigma}}} \dot{p}^+\right)\right\rangle \tag{3.20}$$

The damage accumulates only with the positive hydrostatic stress which literally means that the damage occurs in the ductile material when it is under tension [104]. An active accumulated plastic strain (p^+) which is an internal variable increasing with as given in Equation 3.21 results in the formulation of Equation 3.20.

$$\dot{p}^+ = \dot{p} \left\langle \frac{I_1}{|I_1|} \right\rangle \tag{3.21}$$

Initial conditions such as $R(0) = 0$, $\boldsymbol{\chi}(0) = \mathbf{0}$ and $D(0) = 0$ are assumed and the complete material model is summarized in Table 3.1.

Table 3.1.: Chaboche-type material with hardening and damage

Elastic strains

$$\dot{\tilde{\boldsymbol{\epsilon}}}_{el}(t) = \boldsymbol{C}^{-1} : \dot{\tilde{\boldsymbol{\sigma}}}(t) \quad \text{with} \quad \boldsymbol{C}\,(G, \kappa)$$

Viscoplastic strains

$$\dot{\tilde{\boldsymbol{\epsilon}}}_{vp}(t) = \left\langle \frac{\tilde{\sigma}_{eq}(t) - \sigma_y - R(t)}{k} \right\rangle^n \frac{\partial \tilde{\sigma}_{ex}}{\partial \tilde{\boldsymbol{\sigma}}}$$

Isotropic and kinematic hardening

$$\dot{R} = b_R \left(H_R - R\right) \dot{p}$$

$$\dot{\boldsymbol{\chi}} = b_{\boldsymbol{\chi}} \left(\frac{2}{3} H_{\boldsymbol{\chi}} \frac{\partial \tilde{\sigma}_{eq}}{\partial \tilde{\boldsymbol{\sigma}}} - \boldsymbol{\chi} \right) \dot{p}$$

Local damage

$$D = \bar{D} - l_c^2 \, \nabla^2 \bar{D}$$

$$\dot{D} = \left(c_1 + c_2 e^{-c_3 p^+} \right) \dot{p}^+ + c_4 \left(c_5 - \bar{D} \right) \left\langle \mathrm{tr} \left(\frac{\partial \tilde{\sigma}_{eq}}{\partial \tilde{\boldsymbol{\sigma}}} \, \dot{p}^+ \right) \right\rangle$$

Initial conditions

$$\tilde{\boldsymbol{\epsilon}}_{el}(0) = \mathbf{0}, \;\; \tilde{\boldsymbol{\epsilon}}_{vp}(0) = \mathbf{0}, \;\; R(0) = 0, \;\; \boldsymbol{\chi}(0) = \mathbf{0} \text{ and } D(0) = 0$$

Parameters

G, κ,	(elastic strains)
σ_y, k, n,	(viscoplastic strains)
b_R, H_R, $b_{\boldsymbol{\chi}}$, $H_{\boldsymbol{\chi}}$,	(hardening)
c_1, c_2, c_3, c_4, c_5	(local damage)

The governing equations described in this chapter are numerically solved in the deterministic way using the Space-Time Finite Element method (ST-FEM) [105]. The ST-FEM is the consistent extension of the finite element method [106] with a time integration scheme which is performed according to the Galerkin method [105, 107].

3.2. Summary

The simplest mechanical material model, viscoplasticity model and viscoplastic model with isotropic and kinematic hardening are discussed in this chapter. Similarly a complicated viscoplastic-damage model with isotropic and kinematic hardening is studied in this chapter along with its constitutive equations as shown in Table 3.1. The in-

troduced uncertain parameters are identified by using Bayesian method. The desired uncertain material parameters are in vector notation as $\boldsymbol{q} = \left[\kappa\ G\ b_R\ b_{\boldsymbol{\chi}}\ \sigma_y\ c_1\ c_2\ c_3\right]$ and this vector $\boldsymbol{q}$ has to be determined as shown in Equation 3.22 where $Y(\boldsymbol{q})$ represents the operator which maps unknown parameters $\boldsymbol{q}$ to the measurement $\hat{y}$ which is the observed displacement u in this case and ε represents the measurement and model error.

$$u = Y(\boldsymbol{q}) + \varepsilon \tag{3.22}$$

As Equation 3.22 is an ill-posed problem, it is difficult to estimate the material parameters in $\boldsymbol{q}$ from u and it requires regularization which can be achieved either in a deterministic or in a probabilistic way as discussed in Chapter 2. Further the stochastic methods to solve the forward model is described in Chapter 4. Chapter 5 and 6 are dedicated to the methods used to solve the inverse problem in the Bayesian setting. The validation of the methods to identify the material model parameters is evaluated in Chapter 7. Finally the model parameters of the viscoplastic-damage model are identified by the application of suitable probabilistic method.

4. Uncertainty and Forward Model

The concept of uncertainty, its different types, method of modeling uncertainty and the formation of the forward model are discussed in this chapter. The quantification of the uncertainty in the response of the system is also explained in this chapter. The uncertainty is expressed through probabilistic models using random variables to quantify the uncertainty in the response of the model. It should be noted that the partial differential equation (PDE) with spatial differential operators is used as a mathematical model to define the mechanical system introduced in Chapter 3 and it is discretized by finite elements which can be addressed to the stochastic finite element methods (SFEM) [108, 112, 109, 115] as the probabilistic setting is considered.

4.1. Uncertainty

Uncertainty in engineering problems can not be neglected in design and calculations. Therefore the uncertainty has to be studied significantly because of its influence on the reliability of the structure. The parameters which affect the uncertainties are loading conditions, excitation force, material properties, accuracy of modeling the problems, etc., as it is shown in Figure 4.1.

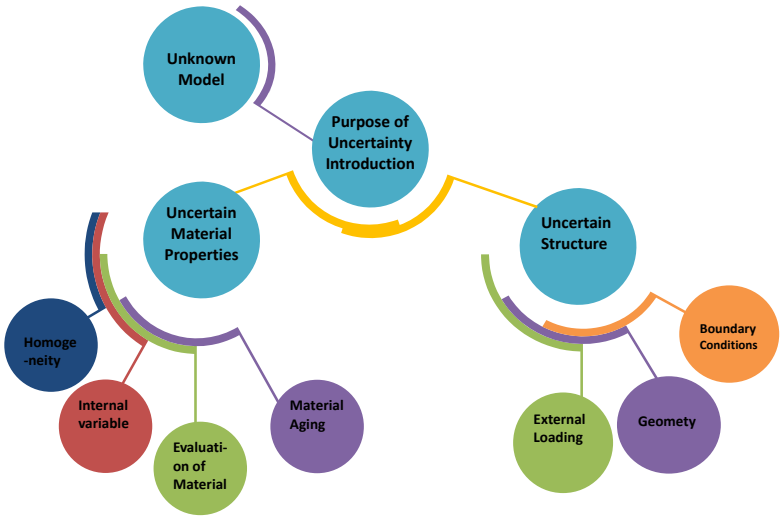

Figure 4.1.: Uncertainty in engineering

The uncertainty is defined in different types in the engineering world and they are to be distinguished clearly. The different types of uncertainty according to [111] are:

- **Model uncertainty**:
  In most of cases it is difficult to model the problem. Hence a simplified mathematical relationship instead of complex ones are employed to represent the problem.

- **Prediction uncertainty**
  In some cases it is necessary to predict the future state of the variables in the problem and this method of estimating the future positions are called as prediction uncertainty.

- **Decision uncertainty**
  In some cases the observer decides the occurrence of the phenomenon and this decision which determines the uncertainty of the problem is called decision uncertainty.

- **Human ratio uncertainty**
  Involvement of humans to design, model and fabricate results in uncertainty called as human error. This uncertainty is called as human ratio uncertainty.

- **Statistical uncertainty**
  Some uncertainty is observed from the statistical estimation of the available data and this uncertainty is due to lack of information.

- **Physical uncertainty**
  The models created from the insufficient values of material properties results in uncertainty and this uncertainty can be reduced by the large availability of data but it cannot be completely eliminated. Hence this uncertainty is chosen subjectively.

As the other classification, the uncertainty is classified generally into two main categories such as aleatoric uncertainty and epistemic uncertainty [112, 113]. Aleatoric uncertainty deals with the unknowns that varies each time on doing the same experiment and this uncertainty cannot be avoided or reduced. Epistemic uncertainty arises from our incomplete knowledge and principally it can be reduced but practically it is not possible.

From the different methods available, uncertainty is described as probabilistic or stochastic models. Indeed, the epistimic uncertainty arising from lack of knowledge can be defined better by the probability theory. Practically, the probabilistic approach is used

more than any other methods with that uncertainty may be described [84, 114]. By employing probabilistic approach uncertainty and certain quantities in the model are represented by random variables which will be defined in the following [115, 117].

The probability space of $(\Omega, \mathfrak{B}, \mathbb{P})$ is introduced for the realization of the uncertain elements as a proper mathematical setting where the probabilistic approach can be used on its setting. The $\mathfrak{B}(\mathcal{M})$ refers to the σ-algebra of Borel sets of $\mathcal{M}$ from Ω which is a set of random elementary events so that to each $B \in \mathfrak{B}$ a real number $\mathbb{P}(B) \in [0, 1]$ may be assigned and mathematically the probability of occurrence is a measure $\mathbb{P}$ [185, 118, 120]. Reminding Hilbert space $\mathbb{S}$, it is now simplified to $\mathbb{S} = L_2(\Omega)$ which is the random variables of finite variance [119]. Abstractly here the space S represent random variables which are measurable functions from Ω to $\mathbb{R}$.

4.2. Stochastic Modeling of Uncertainty

As the probabilistic aspects are considered as a part of the model and as a computational device, the uncertainty defined in the model should be traceable and quantified in the response of the model [130, 115].

In a vector space $\mathcal{V}$ consisting mostly of real numbers $\mathbb{R}$, random variable $\boldsymbol{r}$ is a $\mathcal{V}$-valued and it is also a measuring function relating to each $\omega \in \Omega$ an element $\boldsymbol{r}(\omega) \in \mathcal{V}$. Also, the random variables as functions of Ω representing the uncertainty helps in employing the approximation process more conveniently [115]. Therefore, random variables (RVs)

$$\boldsymbol{r}(\omega) \in L_2(\Omega, \mathfrak{B}(\mathcal{M}), \mathbb{P}) \tag{4.1}$$

provide the measurable maps. In the definition above, $\mathfrak{B}(\mathcal{M})$ is the sub-σ-algebra of Borel sets of join domain $\mathcal{M}$ from Ω where the sub-σ-algebra $\mathfrak{B}$ is a subset of the underlying σ-algebra $\mathfrak{A}$, i.e. $\mathfrak{B} \subset \mathfrak{A}$ [185, 118, 120]. It should be noted that the σ-algebra is basically representing the collection of subsets of Ω on which statements about their probability can be made. Also, L_2 is the Lebesgue space of square integrable $\mathbb{P}$-measurable functions with respect to the sub-σ-algebra $\mathfrak{B}(\mathcal{M})$. If the join domain $\mathcal{M}$ is not considered, the same construction applies to $\mathcal{X}$ and $\mathcal{Y}$ as co-domains individually. In case of ambiguity random variables are distinguished from deterministic quantities by the attached (ω), thereby making the parametric dependence on ω to be explicit.

4.2.1. Fourier Representation of Stationary Processes

A one dimensional stochastic space with a finite interval $\mathcal{T} = [-T, T]$ is considered. If the mean $\bar{\boldsymbol{s}}$ is constant and the covariance of function of distance is $C_{\boldsymbol{s}}(t_1, t_2) = c_{\boldsymbol{s}}(t_1 - t_2)$ then by trigonometric identity the Fourier series [121, 115, 130] representing the tensor product structure of $C_{\boldsymbol{s}}(t_1, t_2)$ is written as

$$C_{\boldsymbol{s}}(t_1, t_2) = c_{\boldsymbol{s}}(t_1 - t_2) = \frac{a_0}{2} + \sum_{k=0}^{\infty} a_k \, [\cos(\pi\nu_k t_1)\cos(\pi\nu_k t_2)] + b_k \, [\sin(\pi\nu_k t_1)\sin(\pi\nu_k t_2)], \tag{4.2}$$

where $\nu_k = k/T$ refers to the temporal frequency [130, 121, 115]. Considering $c_{\boldsymbol{s}}$ and a_k as non-negative, the stochastic process is synthesized in a tensor product form from its spectrum for a function of two variables $\tilde{\boldsymbol{s}}(t, \omega)$:

$$\tilde{\boldsymbol{s}}(t, \omega) = \sqrt{\frac{a_0}{2}} \, \xi_0(\omega) + \sum_{k=1}^{\infty} \sqrt{a_k} \, [\xi_k(\omega)\cos(\pi\nu_k t) + \eta_k(\omega)\sin(\pi\nu_k t)], \tag{4.3}$$

where $\xi_k(\omega)$ and $\eta_k(\omega)$ are random variables computed by the orthogonal projection of the stochastic process as the trigonometric Fourier functions are orthogonal to each other on $\mathcal{T}$ [122]. Hence the ξ_k and η_k are uncorrelated random variables of unit variance and vanishing mean mathematically expressed as:

$$\forall k, j: \quad \mathbb{E}(\xi_k) = \mathbb{E}(\eta_k) = \mathbb{E}(\xi_k \eta_j) = 0 \quad \mathbb{E}(\xi_k \xi_j) = \mathbb{E}(\eta_k \eta_j) = \delta_{kj}. \tag{4.4}$$

If $\boldsymbol{s}(t, \omega)$ is Gaussian, then the random variables ξ_k and η_k are independent and uncorrelated as a linear combination of Gaussian variables [130, 123, 115]. The formulations in Subsection 4.2.2 will be seen as the general extended case of formulations in this subsection.

4.2.2. Karhunen-Loève Expansion

Karhunen-Loève expansion (KLE) [123, 130, 115, 124, 125, 142, 126] known as proper orthogonal decomposition is an expansion that decomposes into products of deterministic functions on the considered region where the functions are only dependent on simple random variables similar to spectral synthesis as in Equation 4.3 [119] which is an example of Karhunen-Loève expansion.

Considering the special condition, the covariance a function of distance $C_{\boldsymbol{s}}(t_1, t_2)$ being given as described in Subsection 4.2.1, Fredholm eigenproblem [143, 115] results in Equation 4.5

$$\int_{-T}^{T} C_{\boldsymbol{s}}(t_1, t_2)\, \phi_k(t_2)\, \mathrm{d}t_2 = \int_{-T}^{T} c_{\boldsymbol{s}}(t_1 - t_2)\, \phi_k(t_2)\, \mathrm{d}t_2 = \lambda_k\, \phi_k(t_1), \tag{4.5}$$

where $\{\lambda_k\}_{k=1,..,N}$ are non-negative decreasing order eigenvalues for $N \in \mathbb{N}$ and ϕ_k representing a complete and orthonormal set of eigenfunctions [128]. The Equation 4.5 is a convolution equation which can be solved by applying Fourier transform as described in Subsection 4.2.1. On solving for $\phi_k(t)$, two solutions are found such as

$\phi_k(t) = 2\cos(\pi\nu_k t)$ and $\phi_k(t) = 2\sin(\pi\nu_k t)$.

Similar to the special form as in Equation 4.5, generalized form for a random field $\boldsymbol{r}(x,\omega)$ for $x \in \mathcal{G}$ by synthesizing the random field through its Karhunen-Loève expansion can be given in Equation 4.6 [115, 130, 110].

$$\tilde{\boldsymbol{r}}(x,\omega) = \sum_{k=1}^{N} \sqrt{\lambda_k}\ \rho_k(\omega)\,\phi_k(x) \tag{4.6}$$

In Equation 4.6, uncorrelated centered random variables with unit variance are defined by $\rho_k(\omega)$ i.e. $\mathbb{E}(\rho_k\rho_m) = \delta_{km}$. These random variables can themselves be expressed in terms of projection as in Equation 4.7.

$$\sqrt{\lambda_k}\ \rho_k(\omega) = \int_{\mathcal{G}} \tilde{\boldsymbol{r}}(x,\omega)\,\phi_k(x)\,\mathrm{d}x \tag{4.7}$$

Equation 4.8 is obtained by defining $\lambda_0 = 1$, $\rho_0(\omega) = 1$ and $\phi_0(x) = \bar{\boldsymbol{r}}(x)$.

$$\boldsymbol{r}(x,\omega) = \bar{\boldsymbol{r}}(x) + \sum_{k=1}^{N} \sqrt{\lambda_k}\ \rho_k(\omega)\,\phi_k(x) = \sum_{k=0}^{N} \sqrt{\lambda_k}\ \rho_k(\omega)\,\phi_k(x) \tag{4.8}$$

Since a linear combination of Gaussian variables is again Gaussian, the random variables $\rho_k(\omega)$ in Equation 4.8 are Gaussian when the given random field $\boldsymbol{r}(x,\omega)$ is Gaussian. In this case, the random variables are not only uncorrelated but also independent [129].

To consider for the actual numerical computation, Equation 4.8 is truncated at a finite number $M < N$ as given in Equation 4.9.

$$\boldsymbol{r}(x,\omega) \approx \boldsymbol{r}_M(x,\omega) = \sum_{k=0}^{M} \sqrt{\lambda_k}\ \rho_k(\omega)\,\phi_k(x) \tag{4.9}$$

The resulting approximation is the best approximation achieved in the $L_2(\mathcal{G}\times\Omega) \cong L_2(\mathcal{G}) \otimes L_2(\Omega)$-norm by that number M of random variables [115, 130].

4.2.3. Polynomial Chaos Expansion

When the random variables are used as the case, then the other coordinate system should be defined other than the Cartesian coordinate system. The introduced coordinate system should be in the space of random variables preferably in the set of Ω as it provides the capability of computing with random variables $\rho_k(\omega)$ by considering the series of Karhunen-Loève expansion as given by Equation 4.9 [130, 115]. The coordinate system should also facilitate in computing the expectation value for $\Psi(u)$ as a considered state function of our system i.e. $\mathbb{E}(\Psi(u)) = \int_\Omega \Psi(\omega, u(\omega))\mathbb{P}(\mathrm{d}\omega)$. The proposed space is a

space of random variables such as $L_2(\Omega)$ in which the basis of random variables $\{X_\iota\}_{\iota\in J}$ are considered [130, 131, 115].

The space $L_2(\Omega)$ is considered and any random variable can be expressed as a series of polynomials of Gaussian random variables $\boldsymbol{\theta} = (\theta_1, ..., \theta_\jmath, ...)$ which are independent and uncorrelated. This series of polynomials is a well-known polynomial chaos expansion (PCE) and it was proposed by Wiener [131, 142, 130, 115] as given in Equation 4.10.

$$\boldsymbol{r}(\omega) = \sum_{\alpha\in\mathcal{J}} r^{(\alpha)} H_\alpha(\boldsymbol{\theta}(\omega)), \qquad \text{with} \qquad ||\boldsymbol{r}||^2_{L_2(\Omega)} = \sum_{\alpha\in\mathcal{J}} (r^{(\alpha)})^2\, \alpha!\,, \tag{4.10}$$

where $H_\alpha(\boldsymbol{\theta}(\omega)) = \prod_{\jmath=1}^{\infty} h_{\alpha_\jmath}(\theta_\jmath(\omega))$, in which $h_\ell(\vartheta)$ are the very famous well-known Hermite polynomials. $\mathcal{J} := \{\alpha \in \mathbb{N}_0^{(\mathbb{N})} | \alpha = (\alpha_1, ..., \alpha_\jmath, ...), \alpha_\jmath \in \mathbb{N}_0, |\alpha| := \sum_{\jmath=1}^{\infty} \alpha_\jmath < \infty\}$ are multi-indices and only finite $\alpha_\jmath$ are non-zero. Similar to Subsection 4.2.1, it is discussed that $\langle H_\alpha, H_\beta\rangle_{L_2(\Omega)} = \mathbb{E}(H_\alpha H_\beta) = \alpha!\,\delta_{\alpha\beta}$, where $\alpha! := \prod_{\jmath=1}^{\infty}(\alpha_\jmath!)$ [115, 131, 132, 142].

The polynomial chaos expansion is used and random variables $\rho_k(\omega) = \sum_{\alpha\in\mathcal{J}} r_k^{(\alpha)} H_\alpha(\boldsymbol{\theta}(\omega))$ are substituted in Equation 4.9 to determine random variable $\boldsymbol{r}(x,\omega)$ as shown in Equation 4.11. It is a convenient expression of random variable in independent identical distributed (iid) standard Gaussian variables and it is derived from the combination of polynomial chaos expansion and Karhunen-Loève expansion [115, 142, 130].

$$\boldsymbol{r}(x,\omega) = \sum_{k=0}^{N} \sum_{\alpha\in\mathcal{J}} \sqrt{\lambda_k}\; r_k^\alpha\, H_\alpha(\boldsymbol{\theta}(\omega))\, \phi_k(x) \tag{4.11}$$

It is inferred from the Equation 4.11 that instead of computing on Ω to determine random variables $\rho_k(\omega)$, it can be carried out on the range Θ of the $\boldsymbol{\theta}(\omega)$ with a Gaussian product measure Γ as the transformed measure. Hence the random variables are defined on (Θ, Γ) [115, 130].

By employing polynomial chaos expansion the random variables are not only considered in $L_2(\Omega)$ spaces but in general form the random variable $\boldsymbol{r}$ has p-th order moments as in Equation 4.11. Karhunen-Loève expansion and polynomial chaos expansion provides a mathematical setting for the random variables as given in Equation 4.11 [115, 142, 130, 132].

It should be pointed out that the combination of Karhunen-Loève expansion and polynomial chaos expansion is only one of the approaches in the context of stochastic finite element method to discretize random fields. The main goal of this combination is to approximate the random variables by the simpler function.

4.3. Methods for Solving the Stochastic Forward Problem

Once the uncertainty defined by random variables is propagated in the model, the stochastic model or so-called the forward model is prepared. The forward model is solved by quantifying the uncertainty into the response of the model and this is done usually by computing some functional $\mathbb{E}(\Psi(\mathsf{u}))$ but however different methods can also be differentiated based on estimate of these methods. The direct integration method via sampling and stochastic collocation method are introduced and discussed in subsection 4.3.1 and 4.3.2.

4.3.1. Direct Integration

In this approach the functional $\mathbb{E}(\Psi(\mathsf{u}))$ is an integral over the probability space as given in Equation 4.12 and it is approximated by the direct approach, i.e. direct numerical integration [115, 130, 110]. The main aim is to compute the response statistics as it refers to the expected response values of functions. The integration points or a selected set of Z realization $\{\omega_z\}_{z=1}^{z}$ is a major concern in this approach. The system of equations are solved z times to compute $\mathbb{E}(\Psi(\mathsf{u}))$ for all z results in large computational cost [115, 130, 148, 149, 113].

$$\Psi(u) = \int_{\mathcal{G}} \Psi_u(x)\,\mathrm{d}x, \quad \text{with} \quad \Psi_u(x) = \mathbb{E}(\Psi(x,\omega,u(x,\omega))) = \int_{\Omega} \Psi(x,\omega,u(x,\omega))\mathbb{P}(\mathrm{d}\omega) \tag{4.12}$$

To solve Equation 4.12, the Monte Carlo (MC) methods [152, 134, 135, 153] or the modifications of this method are used to approximate the integral numerically by a weighted sum of samples of the integrand [133, 140]. Considering M random variables, i.e. Θ_M is finite dimensional, the Equation 4.12 is estimated as Equation 4.13.

$$\Psi_u(x) \approx \boldsymbol{\Psi}_Z = \sum_{z=1}^{Z} \omega_z(\Psi(x,\boldsymbol{\theta}_z,\boldsymbol{u}(\boldsymbol{\theta}_z)) = \sum_{z=1}^{Z} \omega_z \Psi_Z(\boldsymbol{\theta}_z) \tag{4.13}$$

The approximate solution for the realization $\boldsymbol{\theta}_z$ is represented by $\boldsymbol{u}(\boldsymbol{\theta}_z)$. $\boldsymbol{\theta}_z$ are the points chosen randomly by Monte Carlo method according to the underlying measure. The weights $\omega_z = 1/Z$ and evaluation points $\boldsymbol{\theta}_z \in \Theta_M$ are the Monte Carlo parameters. The Monte Carlo approach is a very time consuming approach as $\boldsymbol{u}(\boldsymbol{\theta}_z)$ is estimated for each realization $\boldsymbol{\theta}_z$ [152, 153, 133, 140].

The procedure is described below in steps [115, 130].

1. Select points $\boldsymbol{\theta}_z | z = 1, ..., Z \subset \Theta_M$ based on the integration rule.
2. The deterministic problem with fixed realization for each $\boldsymbol{\theta}_z$ is solved and it results in $\boldsymbol{u}(\boldsymbol{\theta}_z)$.

3. For each $\boldsymbol{\theta}_z$ compute the integrand $\Psi_u(x, \boldsymbol{\theta}_z, \boldsymbol{u}(\boldsymbol{\theta}_z))$ with aid of Equation 4.13.

4. Perform the summation as given in Equation 4.13.

If the integration points are chosen randomly, based on probability measure the basic Monte Carlo method is applied. If other modification of Monte Carlo methods like quasi Monte Carlo method is used then the points from quadrature rule can be chosen. The convergence rate of Monte Carlo methods are independent of the dimension and hence it is so robust. On the other hand the computational time of the Monte Carlo methods to compute the integral over a high dimensional space requires more time which is the main disadvantage of Monte Carlo methods [115, 130, 141, 148, 149].

The examples are given below to understand the concepts of direct integration better.

Example 4.1. For a sphere π is to be estimated and the volume of a sphere with radius r is $\frac{4}{3}\pi r^3$. The volume of a sphere by integration is given by Equation 4.14.

$$I = \int_{-r}^{r}\int_{-r}^{r}\int_{-r}^{r} I(x^2 + y^2 + z^2 \leq r^2)\,\mathrm{d}x\mathrm{d}y\mathrm{d}z. \tag{4.14}$$

From Equation 4.14, it is inferred that $\pi = I/((4/3)r^3)$. The Monte Carlo integration is applied to approximate π using random variables $x, y, z \sim \mathcal{U}(-r, r)$ inside the sphere i.e. the accepted samples by using the Equation 4.13 [127]. After the computation of the integral in Equation 4.14 using the Monte Carlo method, the calculated estimated π is equal to 3.1458 by using 10000 samples. The accepted points in blue color and rejected points in cyan color are shown in Figure 4.2.

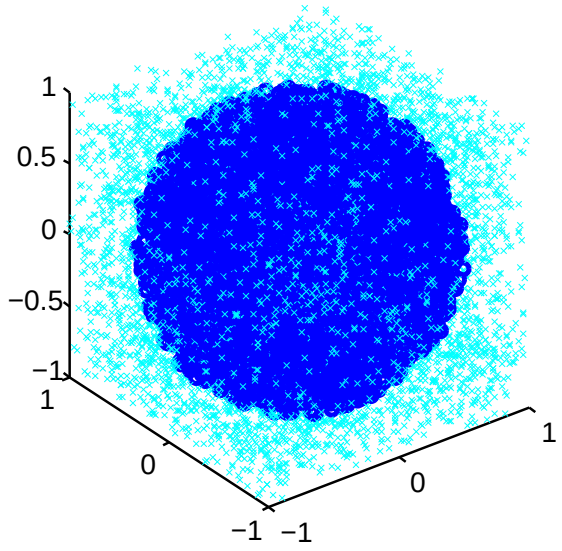

Figure 4.2.: Accepted and rejected samples

A method to draw samples is to be crucially considered. Rejection sampling approaches are better for low-dimensional problems and the Markov Chain Monte Carlo method is recommended as discussed in Chapter 5 for the high-dimensional problem.

Example 4.2. ***Uncertainty Quantification of a Viscoplastic Model with Isotropic Hardening using Monte Carlo Method***

The isotropic hardening behavior is considered for the model in Section 3 and the yield function is given in Equation 4.15 where the scalar hardening parameter is given by α, modulus of hardening is given by the constant H and the deviatoric part of $\boldsymbol{\sigma}$ is represented by σ_D [148, 88].

$$f(\boldsymbol{\sigma}, \alpha) = |\sigma_D| - \sigma_y(1 + H\alpha) \tag{4.15}$$

The schematic of the studied phenomenological model is illustrated in Figure 4.3.

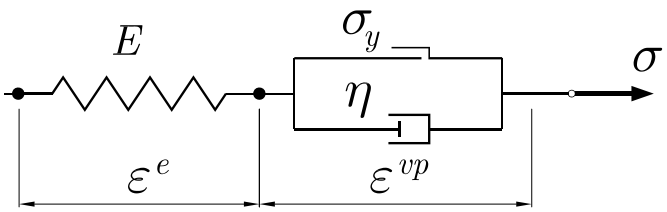

Figure 4.3.: The phenomenological model schematic

The uncertainty represented by random variables ω is introduced into the model and the uncertainty is quantified from the response of the system. Direct integration as in section 4.3.1 is applied for a well-known model called as Cook's membrane problem [150, 148] as seen in Figure 4.4 where the left side is clamped and a force in y direction with magnitude of 100 N is applied as Neumann boundary condition on the other side.

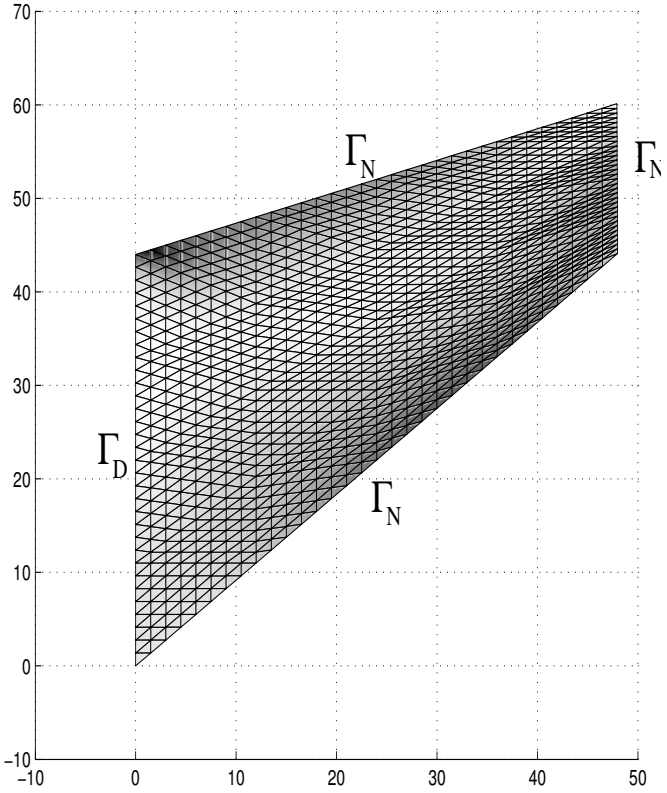

Figure 4.4.: 2D Cook's membrane problem

The model parameters bulk modulus (κ) and shear modulus (G) are considered as uncertain parameters. The mean and variance of the displacements calculated from the stochastic approach are shown in Figure 4.5 after computing the uncertainty in the response of the model using direct integration.

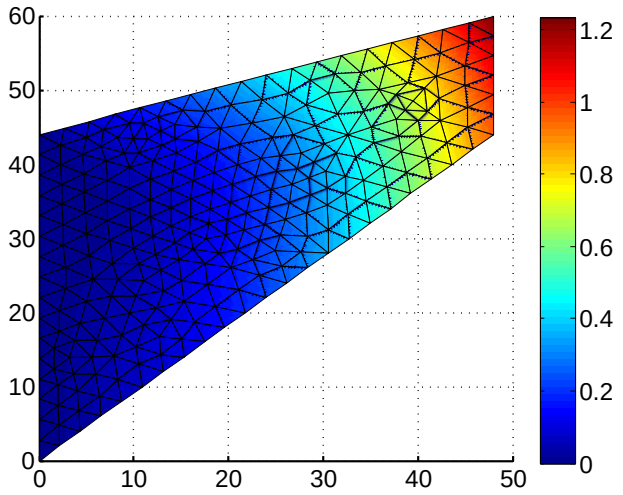

(a) Mean of displacements

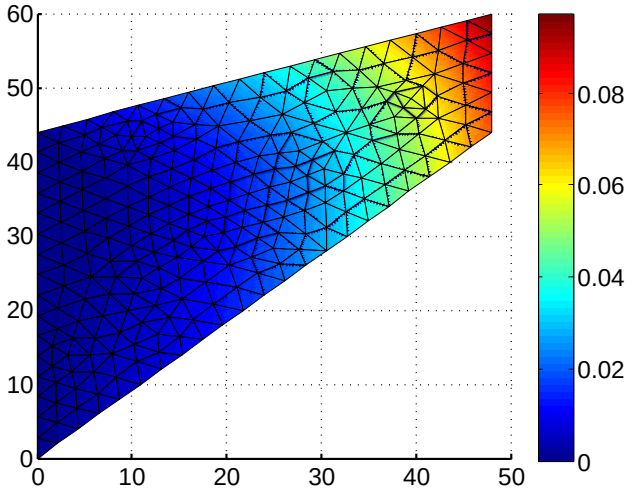

(b) Standard deviation of displacements

Figure 4.5.: Mean and standard deviation of the displacements

The maximum displacement of nodes are observed in the nodes on right upper corner as its displacement distribution illustrated in Figure 4.6.

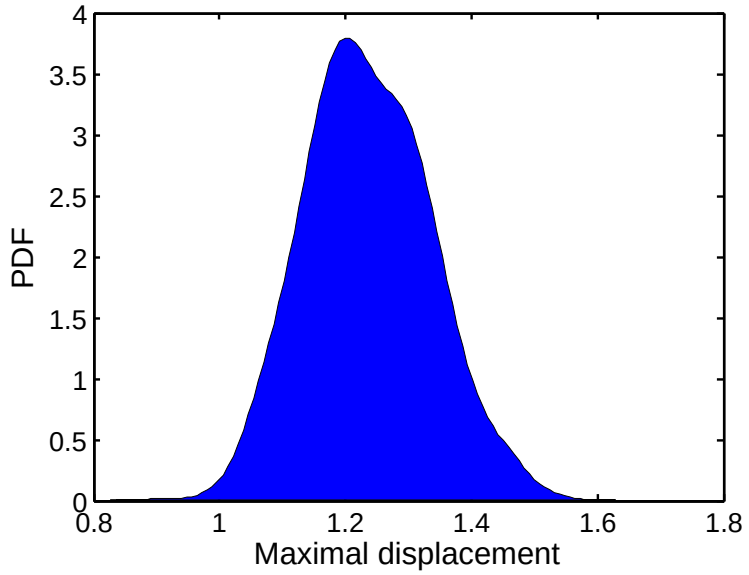

Figure 4.6.: Probability distribution function of the right upper corner node displacement

The considered problem is in two dimension and a coarse mesh is generated. For a few samples used for direct integration a considerable time is needed to compute the displacements of the nodes. Hence in this approach much time is required to evaluate problem. Therefore the direct integration approach using samples are generally inappropriate for the problems represented by the partial differential equation (PDE).

4.3.2. Stochastic Collocation-Projection Method

A function of ω is employed to approximate the random variables $\boldsymbol{u}(\omega)$ and this function is computed as approximation by collocation method called as stochastic collocation method [136, 137, 138, 139, 110]. This method is in contrast to direct integration where the random variables are represented by samples. Initially the approximation of $\boldsymbol{u}(\omega)$ is evaluated and then $\mathbb{E}(\Psi(\mathsf{u}))$ is computed similar to direct integration approach to quantify the uncertainty and to solve the forward model. The number of integration points required to approximate the random variables are less than the required integration points in direct integration method and hence the stochastic collocation method is computationally cheaper [115, 142, 130]. A considerable computational time is required if the system is defined by partial differential equation in which the solution is approximated at each integration point. According to stochastic collocation method the desired

response is evaluated at certain points in stochastic parameter space and then an analytical expression such as a low order Hermite polynomial is made to fit at the response points. Stochastic collocation method is much appreciated in the sense of computation time [115, 130, 142, 145, 146, 148].

In this method if the model is represented by partial differential equation then the spatial discretization of the stochastic partial differential equation is estimated by Galerkin method i.e by Finite Element Method [115, 130, 142]. It is assumed that the Galerkin method gives a measure of unity in the spatial domain as the stochastic space is taken into consideration in the Galerkin method. Considering a finite dimensional subspace $\mathcal{U}_N \subset \mathcal{U}$ with basis $\{s_1(x), ..., s_N(x)\}$ in $\mathcal{U}_N$ the approximated solution is given by Equation 4.16 where the $\{u_k(\omega)\}$ are random variables in $\mathcal{S}$ and vectors like $\boldsymbol{s}(x) = [s_1(x), ..., s_N(x)]$ and $\boldsymbol{u}(\omega) = [u_1(\omega), ..., u_N(\omega)]^T$ are introduced [147, 148].

$$u(x, \omega) = \sum_{k=1}^{N} s_k(x)\, u_k(\omega) = \boldsymbol{s}(x)\, \boldsymbol{u}(\omega) \tag{4.16}$$

Equation 4.17 is obtained by considering the spatial Galerkin condition and substituting the ansatz where the $\boldsymbol{K}(\omega)$ is defined similarly to finite element stiffness matrix. The right hand side of the equation is given by $\boldsymbol{f}(\omega) = [f_1(\omega), ..., f_N(\omega)]^T$ with components $f_J(\omega) = \int_{\mathcal{G}} s_J(x) f(x, \omega) dx$. By semi-discretization Equation 4.17 is determined and it includes the computationally intractable variable $\omega \in \Omega$ where infinitely many coordinates required to parametrize Ω.

$$\boldsymbol{K}(\omega)\, \boldsymbol{u}(\omega) = \boldsymbol{f}(\omega) \tag{4.17}$$

Considering the Gaussian random variables Equation 4.18 in a weak sense is obtained from Equation 4.17 [147, 148].

$$\boldsymbol{K}(\boldsymbol{\theta})\, \boldsymbol{u}(\boldsymbol{\theta}) = \boldsymbol{f}(\boldsymbol{\theta}) \tag{4.18}$$

The spatial discretization is carried out by applying direct integration method in Equation 4.18 and the samples from the integration points $\boldsymbol{\theta}_z$ are generated [115, 130, 142]. A further procedure is carried out as described in the Subsection 4.3.1.

When the realizations are generated either through the polynomial chaos expansion as given in Equation 4.10 or through the combination of Karhunen-Loève expansion and polynomial chaos expansion as in Equation 4.11, a truncation to a finite number of terms should be carried out [115, 130, 142]. As the truncated terms are expressed in polynomial ($\boldsymbol{\theta}(\omega)$) and this expansion violates for some $\boldsymbol{\theta}_z$ after truncation as the polynomials are not bounded and they only converge in $L_2(\Theta)$. Hence, according to Hadamarad [144] the computational procedure is not well-posed. To overcome this

problem $\mathcal{S}$ is discretized and the approximation of the component $\mathcal{U}$ is furnished by the discretization methods. For instance the finite element method and its subspace span $\{s_1, ..., s_N\} = \mathcal{U}_N \subset \mathcal{U}$ but the tensor product is in $\mathcal{U} \otimes \mathcal{S}$. This discretization which is called stochastic discretization is carried out after spatial discretization. The collocation approach of finite dimensional subspaces $\mathcal{S}_M$ of $\mathcal{S}$ is considered with a basis $\{X_\iota\}_{\iota \in J}$ of $\mathcal{S}$. Hence it is possible to truncate a finite subset $J_{M,p} \subset J$ resulting in the finite dimensional subspace $\mathcal{S}_{M,p} = \text{span}\{X_\iota | \iota \in J_{M,p}\} \subset \mathcal{S}$ and the introduced ansatz function is given in Equation 4.19 where the coefficients $u_k^{(\iota)}$ is to be computed [115, 142, 130, 148].

$$u_{N,M,p}(x, \omega) = \sum_{k \leq N} \sum_{\iota \in J_{M,p}} u_k^{(\iota)} s_k(x) X_\iota(\omega) \tag{4.19}$$

From the idea of polynomial chaos expansion the collocation method is extended to polynomial and hence the random variables $\boldsymbol{u}(\omega)^T = [u_1(\omega), ..., u_N(\omega)]$ are expanded in a polynomial chaos expansion series as given in Equation 4.20 where the $\mathsf{H}(\boldsymbol{\theta}^T) = [..., H_\alpha(\boldsymbol{\theta}), ...]$, $\mathsf{u}_k = [..., u_k^{(\alpha)}, ...]$ and the considered basis is $\{H_\alpha | \alpha \in \mathcal{J}\}$ [115, 130, 148].

$$\forall k: \quad u_k(\boldsymbol{\theta}(\omega)) = \sum_\alpha u_k^{(\alpha)} H_\alpha(\boldsymbol{\theta}(\omega)) = \mathsf{u}_k \mathsf{H}(\boldsymbol{\theta}(\omega)) \tag{4.20}$$

Using the orthogonality of the Hermite basis, the coefficients of the polynomial chaos expansion of the solution can be computed directly, as they are given by

$$u^{(\alpha)} = \frac{\mathbb{E}(u(\omega) H_\alpha(\boldsymbol{\theta}(\omega))}{\alpha!}. \tag{4.21}$$

Similar to direct integration approach by using the Monte Carlo method, the coefficients of the polynomial chaos expansion in Equation 4.21 can be solved by the least squares regression approach and it is approximated by Equation 4.22 that may be seen as the approximation obtained from the collocation-projection method [136, 137, 138, 130, 139, 110] where the integration weights in the case of Monte Carlo are $\omega_z = 1/Z$.

$$u^{(\alpha)} \approx \frac{1}{\alpha!} \sum_{z=1}^{Z} \omega_z H_\alpha(\boldsymbol{\theta}_z) u(\boldsymbol{\theta}_z) = \frac{1}{\alpha!} \sum_{z=1}^{Z} \omega_z H_\alpha(\boldsymbol{\theta}_z) \boldsymbol{K}^{-1}(\boldsymbol{\theta}_z) \boldsymbol{f}(\boldsymbol{\theta}_z) \tag{4.22}$$

On actual computation, a finite dimensional approximation $\mathcal{S}_{M,p} = \text{span}\{H_\alpha | \alpha \in \mathcal{J}_{M,p}\} \subset \mathcal{S}$ is defined after truncating the expansion to finitely many terms $\alpha \in \mathcal{J}_{M,p}$ as given in Equation 4.20. The set $\mathcal{J}_{M,p} \subset \mathcal{J}$ is defined by benefiting the effective length function $\ell(\alpha) := \min\{m \,|\, \forall k > m : \alpha_k = 0\}$ of a multi-index α for $M, p \in \mathbb{N}$ as given in Equation 4.23. It is to be noted that the dimensions of the subspaces $\mathcal{S}_{M,p}$ increases quickly with M and p and hence it requires finer control.

$$\mathcal{J}_{M,p} = \{\alpha \in \mathcal{J} \,|\, \ell(\alpha) \leq M, \ |\alpha| \leq p\} \tag{4.23}$$

For instance the considered partial differential equation is a desired equation of a finite number of random variables which are transformed to a set of independent identically distributed Gaussian and the solution depends analytically on random parameters.

Example 4.3. ***Uncertainty Quantification of a Viscoplastic Model with Isotropic Hardening using Functional Approximation***

The example described in Subsection 4.3.1 is studied for the same problem. Hermite function in form of polynomial chaos expansion is employed instead of samples. The bulk modulus (κ), shear modulus (G) and output displacement are introduced as an ansatz.

$$\kappa(\omega) = \sum_{\alpha} \kappa^{(\alpha)} H_\alpha(\boldsymbol{\theta}(\omega)) \tag{4.24a}$$

$$G(\omega) = \sum_{\alpha} G^{(\alpha)} H_\alpha(\boldsymbol{\theta}(\omega)) \tag{4.24b}$$

$$u(x,\omega) = \sum_{\alpha} u^{(\alpha)}(x) H_\alpha(\boldsymbol{\theta}(\omega)) \tag{4.24c}$$

The Gaussian standard random variables are represented by $\boldsymbol{\theta}(\omega)$ and the Hermite function is represented by H_α as in Equations 4.24a and 4.24b, where the bulk modulus and shear modulus are not dependent on the position, and in Equation 4.24c the output displacement is a function of position. The coefficients of bulk modulus, shear modulus and displacement are computed as in Equations 4.25a, 4.25b and 4.25c.

$$\kappa^{(\alpha)} = \frac{\mathbb{E}(\kappa(\omega) H_\alpha(\boldsymbol{\theta}(\omega)))}{\alpha!} \tag{4.25a}$$

$$G^{(\alpha)} = \frac{\mathbb{E}(G(\omega) H_\alpha(\boldsymbol{\theta}(\omega)))}{\alpha!} \tag{4.25b}$$

$$u^{(\alpha)}(x) = \frac{\mathbb{E}(u(x,\omega) H_\alpha(\boldsymbol{\theta}(\omega)))}{\alpha!} \tag{4.25c}$$

Considering the third order Hermite function, the mean and standard deviation of the displacement of the nodes are shown in Figure 4.7 where the stochastic collocation method is employed.

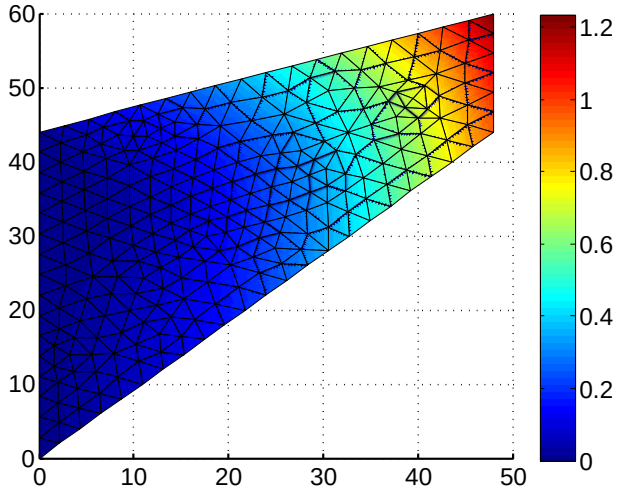

(a) Mean of displacements

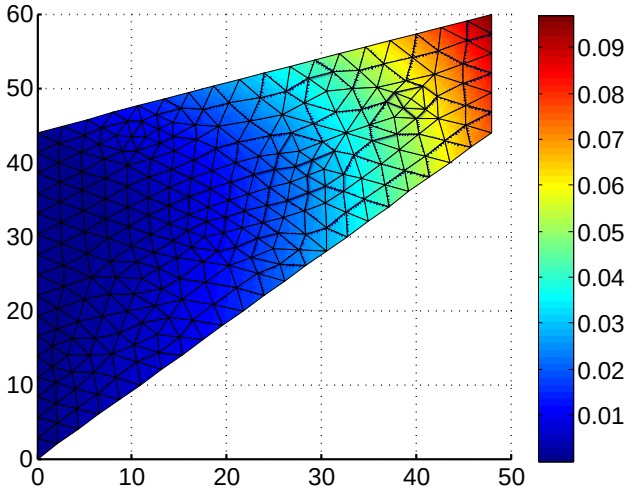

(b) Standard deviation of displacements

Figure 4.7.: Mean and standard deviation of the displacements

The distribution of displacement of node on the right upper corner representing the maximal displacement of the nodes is illustrated in Figure 4.8.

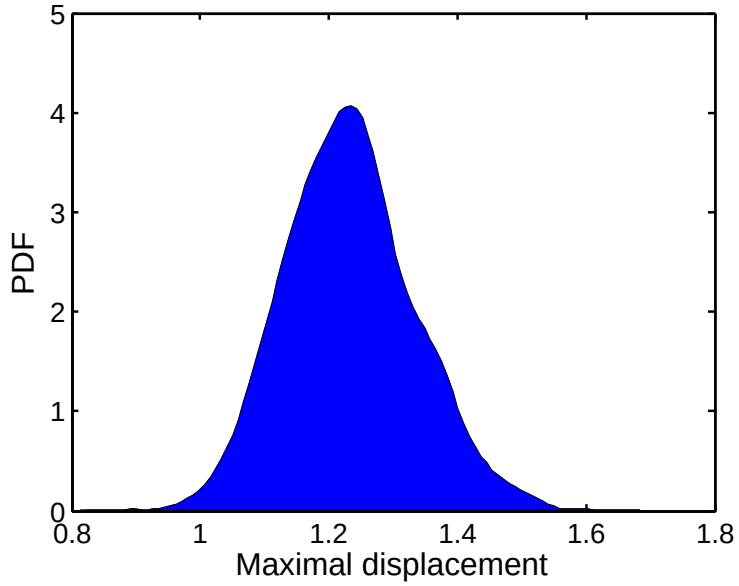

Figure 4.8.: Probability distribution function of the right upper corner node displacement

The direct integration and stochastic collocation method are applied on the cook's membrane problem and its results are compared. It is inferred that the less computational time is needed when functional approximation is used in order to quantify the uncertainty into the response of system. Hence in this thesis the Hermite function through the polynomial chaos expansion is used in Chapter 7 and 8 to solve the forward model by functional approximation.

4.4. Conclusion

In this chapter the uncertainty is introduced, addressed and how it can be mathematically propagated in the model is described. Further the forward model, the calculation of uncertainty in response of the system and the discretization method are also described in this chapter. The procedure of solving the forward problem using direct integration method by sampling and stochastic collocation method by spectral decomposition are investigated. Two types of expansions i.e. the Karhunen-Loève expansion and polynomial chaos expansion and their combinations are also discussed in this chapter.

From the results of the provided examples it can be concluded that the direct integration using sampling technique and stochastic collocation method using Hermite function provide almost similar results. However the computation time of the latter approach is much less than the former method. Hence for the PDE systems the stochastic colloca-

tion approach using functional approximation such as the polynomial chaos expansion is preferred than the direct integration using sampling. Chapter 5 and 6 are dedicated to the approaches which aid to solve the inverse problems and validation of these approaches for the desired deterministic forward model as described in Chapter 3 is given in Chapter 7. Finally the parameters of the viscoplastic-damage model on a well-known mechanical engineering test are identified using stochastic methods as given in Chapter 8.

5. Bayesian Updating via Markov Chain Monte Carlo

The introduction about the viscoplastic-damage model was discussed in Chapter 3 and the propagation of uncertainty in the model was described in Chapter 4. One of the main random walk approaches which provides the ability to solve the very high conditional ill-posed problem stochastically is discussed in this chapter and also in this chapter it is explained how to identify the parameters of the desired models by using the samples obtained form the measurements of the model. It is shown in this chapter that the Bayesian updating provides a rigorous approach to the considered inverse problem when the developed stochastic simulation algorithm such as Transitional Markov Chain Monte Carlo method [168] is applied on it. The parameter identification based on updating of finite element models using the measured response of the model is challenging and the other problem to be considered is due to the large number of uncertain parameters associated with these models.

The aim of the stochastic simulation method is to generate samples that are distributed based on the probability density function (PDF). The posterior PDF aids in the plausibility of each candidate models in the model class which is specified by the corresponding vector of model parameters based on the data. In this chapter Markov Chain Monte Carlo methods [151, 152, 153, 157, 158] are considered. The main advantage of this method is the samples determination from the non-normalized PDF such that the samples are generated from the posterior PDF without evaluating the evidence $\mathbb{P}(\mathcal{M}_y)$ in Equation 2.12 or $Z_s(y)$ in Equation 2.16 in Bayes' theorem, discussed in Subsection 2.2.1, as it is very expensive to calculate a high dimensional integral over the parameter space. As the posterior PDF has a smaller volume in the parameter space as compared to the prior PDF [153], it is challenging to determine samples from posterior PDF using stochastic simulation, considering the data which is very sparse. As the other advantage of this method is that, these approaches are popular for solving inverse problems while the combination of them by other spectral representations can be also applied for solving the forward problem [152, 153].

5.1. Markov Chain Monte Carlo

There are numerous stochastic simulation algorithms to generate samples from a distribution of probability density function (PDF) such as acceptance-rejection algorithm, Gibbs sampler, ziggurat algorithm, etc. [154, 155, 156]. But majority of these methods

are unable to address the problem of Bayesian model updating because of the following reason.

- The evidence is mostly a high-dimensional integral over the parameter space and its evaluation is difficult or intractable
- The algorithms are unable to generate samples taking into account of all the higher probability regions when dealing with high-dimensional parameter space

These problems are overcome by the MCMC method which is essentially a Monte Carlo integration using Markov chains. The Monte Carlo integration considers the samples for the required distribution followed by approximating the expectation from the determined average values. But the Markov Chain Monte Carlo method ascertain these samples by using a Markov Chain method for a long time which has the target distribution as its stationary distribution [157]. With the increasing use of super computers all over the world, this method which requires such computers to solve the complex problem can be easily employed.

The Markov Chain Monte Carlo method is developed to generate samples from an arbitrary distribution. The samples are statistically consistent from the target function without considering the other distribution for the rejection of certain samples. Therefore, this approach is useful for evaluating the integrals and visualizing the uncertainties in a model and its variation. MCMC approaches depend on the forward model as well as on the associated likelihood calculations. These methods are suitable to apply on linear problems as well as nonlinear problems. The main disadvantage of Markov Chain Monte Carlo method is its low convergence speed and it is major issue when a high dimensional problem is analyzed. Hence the MCMC method is not recommended for high dimensional problem [158].

5.2. Metropolis Algorithm

The Metropolis algorithm is a type of MCMC method which is used to generate samples from a posterior probability distribution function. The Metropolis method was developed by Nicholas Metropolis [187, 188, 155] and it is the most used approach of all MCMC method.

In the Metropolis algorithm at any defined time t the next state θ_{t+1} is chosen to determine the sample at a candidate point $\theta^\star$ from a symmetric proposal distribution $g(.|\theta_t)$. The candidate point $\theta^\star$ is acknowledged only when a random number from the uniform PDF ($\mathcal{U}(0,1)$) satisfies the condition as in Equation 5.1.

$$\alpha(\theta_t, \theta^\star) = \min(1, \frac{f(\theta^\star)}{f(\theta_t)}) \tag{5.1}$$

If the random number u from the PDF ($\mathcal{U}(0,1)$) is greater than α then the chosen point is declined. But if the candidate point is accepted then the density increases and the algorithm is moved to next state which is defined as $\theta_{t+1} = \theta^{\star}$. If the point is rejected then the chain does not proceed and the next state becomes $\theta_{t+1} = \theta_t$. Through this procedure the entire collection of points are generated and it is indicated by $\boldsymbol{\theta}$, where $\boldsymbol{\theta} = [\theta_1, \theta_2, ..., \theta_n]$ represents set of samples.

By the Metropolis algorithms the samples are generated as seen in Algorithm 1 where the number of samples involved in the problem is given by n.

Algorithm 1 Metropolis algorithm

1: Initializing θ_1
2: **for** each integer from i to n **do**
3: Sampling $u \sim \mathcal{U}(0,1)$
4: **if** $u \leq \alpha(\theta_t, \theta^{\star})$ **then**
5: accepting the sample $\theta_{i+1} = \theta^{\star}$
6: **else**
7: rejecting the sample $\theta_{i+1} = \theta_i$
8: Returning θ

The main advantage of the Metropolis algorithm is that the samples of distributions can be determined without considering any other extra factors and hence this algorithm is much faster than the other algorithms where the determination of samples from complex density functions requires calculation of normalization factors in each step resulting in complicated and time consuming algorithm.

The main disadvantage of the Metropolis algorithm is that it is not suitable for high dimensional problems due to the slow convergence of chain i.e. the increase in dimension of the problem results in generation of large number of repeated samples.

Example 5.1. A simple target function $f(x) = x \exp(-2x + 5)$ which is wished to simulate draws from its distribution is considered as an example. The start value of the algorithm is 5.0 and the number of samples of 10000 are considered and the frequency of the samples are obtained by deploying the Metropolis algorithm as shown in Figure 5.1 [160]. It should be noted that the uniform distribution $\mathcal{U}(0,\, 5)$ is taken as proposal distribution.

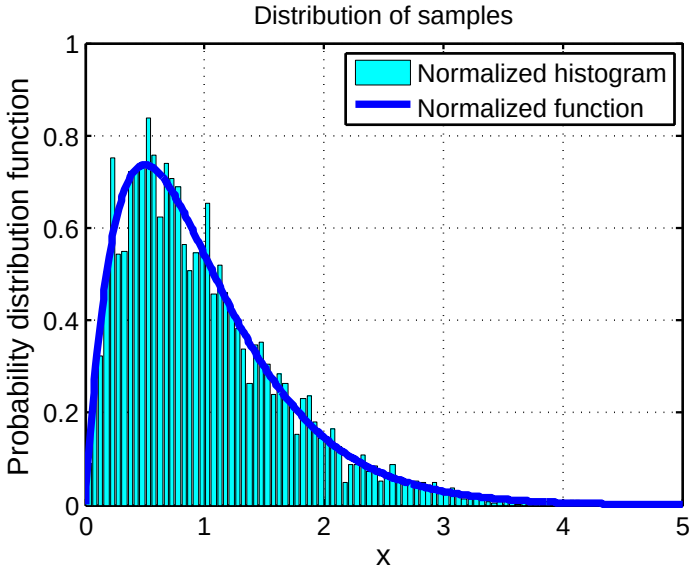

Figure 5.1.: Frequency of samples generated by Metropolis algorithm

In Figure 5.1, the defined probability density function is represented in blue color and the samples provided by Metropolis algorithm is shown in the green color columns. It is observed that the target distributed function does not properly represent the samples even though lots of samples are generated from PDF.

5.3. Metropolis-Hastings Algorithm

In 1970 Keith Hastings developed the modified Metropolis algorithm called as Metropolis-Hastings algorithm [155, 189, 190] and it is discussed in this section.

At any defined time t, the next state θ is chosen by first sampling a candidate point $\theta^{\star}$ from an arbitrary transition probability function or proposal distribution $g(\theta_t|\theta_{t+1})$. The candidate point $\theta^{\star}$ is acknowledged only when a random number from the uniform PDF ($\mathcal{U}(0,1)$) satisfies the condition as in Equation 5.2.

$$\alpha(\theta_t, \theta^{\star}) = \min(1, \frac{f(\theta^{\star})g(\theta_t|\theta^{\star})}{f(\theta_t)g(\theta^{\star}|\theta_t)}) \tag{5.2}$$

If the random number u from the PDF ($\mathcal{U}(0,1)$) is greater than α then the chosen point is declined. The main significant advantage of Metropolis-Hastings algorithm over the Metropolis algorithm is that the Metropolis-Hastings algorithm can use a proposal distribution function which is not necessarily symmetrical.

By the Metropolis-Hastings algorithms the samples are generated as seen in Algorithm 2 where the number of samples involved in the problem is given by n.

Algorithm 2 Metropolis-Hastings algorithm

Initializing θ_1
for each integer from i to n **do**
    Sampling $u \sim \mathcal{U}(0,1)$
    Sampling $\theta^\star \sim g(.|\theta_i)$
    if $u \leq \alpha(\theta_t, \theta^\star)$ **then**
        accepting the sample $\theta_{i+1} = \theta^\star$
    else
        rejecting the sample $\theta_{i+1} = \theta_i$
Returning θ

5.4. Tricks to Improve Metropolis-Hastings Algorithm Performance

Suitable sample sets are not generated from the Metropolis-Hastings algorithm for complex functions and hence this algorithm is improved by techniques as discussed in this section.

Start value
The start values depends on the initial distribution of the sampling function i.e. if the distribution causes a good mix in the chain then the influence of start value reduces and proportionally any start value results in a same value [157]. On the other hand if the distribution causes a well mix in the sampling function then the start value plays a crucial role and it has to be chosen carefully otherwise it will result in inaccurate result. Hence it is recommended to define the start values as close as possible to the center of the distribution.

Lag time
The multiple iterations of the algorithm is executed between the accepted samples to store the lag-th position and this technique will result in decrease of autocorrelation [160]. This technique is most useful when the algorithm got stuck in a location for a long time and this happens for the distribution function which has a lot of rejected rate. Hence the time of this algorithm is reduced resulting in less cost.

Burn-in period
The number of iterations till the chain becomes stationary is called Burn-in time length [160] and this time length is affected by parameters such as,

- Rate of convergence to stationary distribution
- Start value
- Required similarity between the generated chain and stationary distribution
- Applied distribution

These factors can result in large range of difference of Burn-in period length.

Example 5.2. To determine the effect of Burn-in period and lag time of this algorithm a target function $f(x) = x \exp(-2x + 5)$ along with the PDF discussed in Section 5.2 is considered. The input parameters such as start value of 5.0 and number of samples of 10000 are considered. The Burn-in and lag periods are considered as 1000 and 100 respectively. The frequency of the samples obtained by employing the Metropolis-Hastings algorithm with the considered input parameters is shown in Figure 5.2.

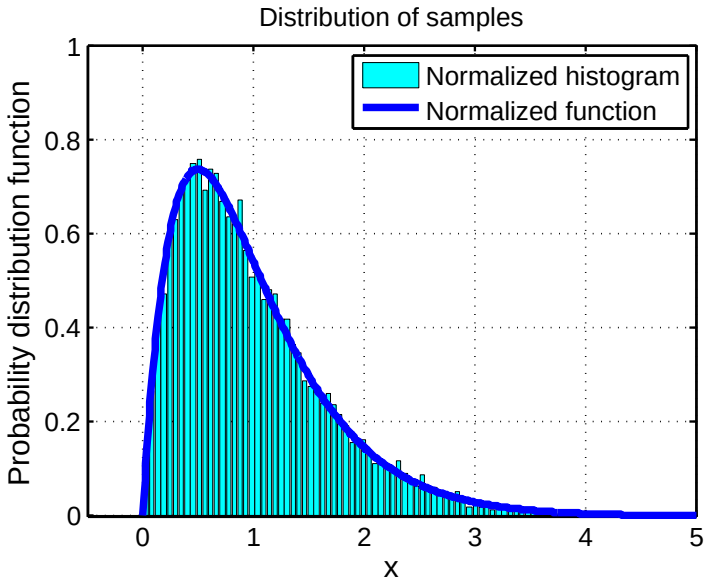

Figure 5.2.: Frequency of samples generated by Metropolis-Hastings algorithm

As can be seen in Figure 5.2, the defined probability density function is represented in blue color and the green color represents the samples from Metropolis-Hastings algorithm. It is observed that the samples are placed appropriately to the target distribution function and the accuracy of this algorithm for the probability density function can be determined.

Comparison of the samples from the Metropolis algorithm and the enriched Metropolis-Hastings algorithm for the same function is shown in Figure 5.3. It is observed from the Figure 5.3 that the enriched Metropolis-Hastings algorithm provides the more accurate result which suitably correspond to the target function and for complicated function there is a significant difference.

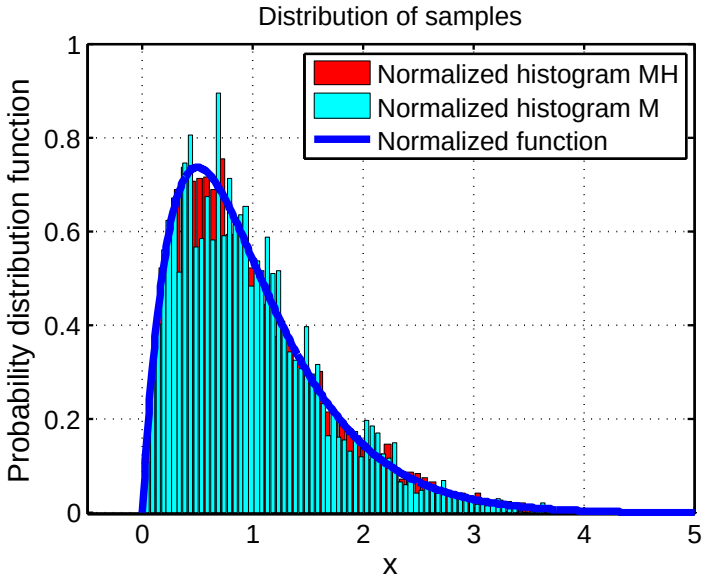

Figure 5.3.: Comparison of samples generated by Metropolis and Metropolis-Hastings algorithms

5.5. Implementation of Transitional Markov Chain Monte Carlo

It is found from section 5.3 that the Metropolis-Hastings algorithm is best suitable algorithm to determine samples from the probability density function and difficulties in employing this algorithm along with the Markov Chain Monte Carlo method to determine samples from the determined distributed function is discussed in this section. In this section, the disadvantages of direct deployment of Metropolis-Hastings algorithm and the features of Markov chain Monte Carlo method are discussed. Further the Transitional Markov Chain Monte Carlo (TMCMC) method is also clearly discussed. Though TMCMC has been already used in different fields like molecular dynamics [163], adaptronics and robotics [164], discrete element simulations [165] etc., it has not been applied on the mechanical material model in order to identify the model parameters to the best of the author's knowledge.

5.5.1. Metropolis-Hastings Algorithm Drawbacks

Though the Metropolis Hastings algorithm is one of the best algorithms in this field but direct application of the Metropolis-Hastings algorithm is not feasible due to the following constraints.

- If there is not enough information regarding the region of concentration of the posterior PDF for the model parameters then in the Metropolis-Hastings it is difficult to choose an appropriate proposal distribution [166].
- The algorithm does not give good result when the parameters of the model are highly correlated, i.e. it is very difficult to determine the samples which covers all the regions of high-probability content [166].

In order to overcome these issues the gradual updating of the model from a sequence of target PDFs is suggested by Beck and Au [166, 167]. In this proposed approach, M-H algorithm is employed and each target PDF is the posterior PDF based on the fraction of the available data which causes the broad prior PDF converge to the final narrow posterior PDF.

5.5.2. Ching's Transitional MCMC Method

Ching and Chen [168] modified the approach by Beck and Au to develop Transitional Markov Chain Monte Carlo method. This approach is based on Markov Chain Monte Carlo method and its adaptive capability is inspired from adaptive Metropolis–Hastings method developed by Beck and Au in 2002 [166]. This approach employs a sequence of PDFs where the entire data set of the available data is used for each stage of the sampler which is proportional to the local posterior with some power times likelihood with change of power between 0 and 1. As the same idea was used in the simulated annealing approach [169], this power is called as tempering parameter. TMCMC and Beck and Au approach also differs in method of employing the M-H algorithm. In each stage a local proposed PDF is constructed instead of a global proposed PDF and it is also to be noted that to improve the rate of convergence in TMCMC re-sampling is used.

Based on the formulation of Bayes's theorem as described in Equation 2.12, it is difficult to generate samples from the posterior PDF due to lack of information about the geometry of the probability density function. In order to overcome this problem, TMCMC algorithm employs a sequence of intermediate PDFs which converge to the target posterior PDF as defined in the Equation 5.3 where the index j denotes the stage number [168, 170]. Considering the reformulation of the Bayes's theorem for the model class $\mathcal{M}$ which is defined by the parameter vector $\boldsymbol{\theta}$, the prior PDF of this model class over the parameter vector $f(\boldsymbol{\theta}|\mathcal{M})$ is updated with the measurement data $\mathcal{D}$ where the likelihood function is $f(\mathcal{D}|\mathcal{M}, \boldsymbol{\theta})$.

$$f_j(\boldsymbol{\theta}) \propto f(\boldsymbol{\theta}|\mathcal{M}) f(\mathcal{D}|\mathcal{M}, \boldsymbol{\theta})^{r_j} \tag{5.3a}$$

$$j = 0, 1, 2, ..., M \qquad 0 = r_0 \leq r_1 \leq r_2 \leq ... \leq r_M = 1 \tag{5.3b}$$

The stage number fulfills the desirable properties such as developing of series of intermediate PDFs ($f_j(\boldsymbol{\theta})$) from the prior PDF, i.e. it starts with $r_j = 0$ stating that the initial prior is proportional to the prior PDF ($f_0(\boldsymbol{\theta}) \propto f(\boldsymbol{\theta}|\mathcal{M})$) and it ends with $r_j = 1$ stating that the final PDF is proportional to the posterior PDF ($f_M(\boldsymbol{\theta}) \propto f(\boldsymbol{\theta}|\mathcal{M}) f(\mathcal{D}|\mathcal{M}, \boldsymbol{\theta})$). The right hand side of the latter relation represents the posterior PDF $f(\boldsymbol{\theta}|\mathcal{M}, \mathcal{D})$ and its proportionality is shown in Equation 5.4.

$$r_j = 0 \qquad f_0(\boldsymbol{\theta}) \propto f(\theta|\mathcal{M}) \tag{5.4a}$$

$$r_j = 1 \qquad f_M(\boldsymbol{\theta}) \propto f(\boldsymbol{\theta}|\mathcal{M}, \mathcal{D}) \tag{5.4b}$$

Although the geometry change from $f(\boldsymbol{\theta}|\mathcal{M})$ to $f(\boldsymbol{\theta}|\mathcal{M}, \mathcal{D})$ is large, the change between two adjacent intermediate PDFs can be small. Due to this possible transition it is possible to determine samples efficiently from $f_{j+1}(\boldsymbol{\theta})$ based on samples from $f_j(\boldsymbol{\theta})$.

The significant advantage of this adaptive approach is that initially in first stages, a wide free exploring sample space is available but as the number of stages increases the samples are determined from the narrower neighborhood of the sample space. Moreover the proposed PDF may change within the same distribution stage in such a way that it results in proper local behavior. The TMCMC is compared with other similar methods and the following unique features are inferred from it [168, 170].

- It is based on MCMC method but unlike most MCMC methods, it is applicable to multi-modal $f(\boldsymbol{\theta}|\mathcal{M}, \mathcal{D})$
- It is applicable to both very peaked and flat $f(\boldsymbol{\theta}|\mathcal{M}, \mathcal{D})$
- It can estimate the evidence $f(\mathcal{D}|\mathcal{M})$ as a by-product

In the next subsection the algorithm of TMCMC is explained in detail.

5.5.3. Transitional MCMC Algorithm

In this section, the entire algorithm of TMCMC is described in following steps in detail [168, 170, 171].

1. As a first step, $j = 0$ is set and from $f_0(\boldsymbol{\theta}) = f(\boldsymbol{\theta}|\mathcal{M})$ a set of N samples are generated.

2. It is to be noted that r_{j+1} is selected in such a way that the coefficient of variation of $f(\mathcal{D}|\mathcal{M}, \boldsymbol{\theta}_k^{(j)})^{r_{j+1}-r_j}$ where $k = 1, 2, ..., N$ is a prescribed value and $\boldsymbol{\theta}_k^{(j)}$ stands for the k-th sample that belongs to level j. Accordingly, the coefficient of variation serves as an indicator to measure the closeness of $f_j(\boldsymbol{\theta})$ to $f_{j+1}(\boldsymbol{\theta})$.

3. The plausibility weight $w(\boldsymbol{\theta}_k^{(j)}) = f(\mathcal{D}|\mathcal{M}, \boldsymbol{\theta}_k^{(j)})^{r_{j+1}-r_j}$ is obtained for $k = 1, 2, ..., N$ and by which the parameter $S^j = \sum_{k=1}^{N} w(\boldsymbol{\theta}_k^{(j)})/N^j$ is computed.

4. Samples $\boldsymbol{\theta}_k^{j+1}$ where $k = 1, 2, ..., N$ determined from $f(\boldsymbol{\theta})^{j+1}$ by Metropolis-Hastings technique are given, i.e. the k-th sample is chosen randomly from a Markov chain which has samples starting from one of the samples $\boldsymbol{\theta}_i^j$ where $i = 1, 2, ..., N$. The i-th initial sample $\boldsymbol{\theta}_i^{(j)}$ is chosen with probability $w(\boldsymbol{\theta}_i^{(j)})/\sum_{l=1}^{N} w(\boldsymbol{\theta}_l^{(j)})$. As in proposed distribution a Gaussian which is centered at the current sample in the k-th chain is applied in the Metropolis-Hastings algorithm and the determined covariance matrix is shown in Equation 5.5 and 5.6 where β is a prescribed scaling factor that scales the proposal distribution and $\beta = 0.2$ is suggested by Ching and Chen [168].

$$\boldsymbol{\Sigma}_j = \beta^2 \frac{\sum_{i=1}^{N} w(\boldsymbol{\theta}_i^{(j)}) \left[\boldsymbol{\theta}_i^{(j)} - \boldsymbol{\mu}_j\right] \left[\boldsymbol{\theta}_i^{(j)} - \boldsymbol{\mu}_j\right]^T}{\sum_{k=1}^{N} w(\boldsymbol{\theta}_k^{(j)})} \tag{5.5}$$

where

$$\boldsymbol{\mu}_j = \frac{\sum_{l=1}^{N} w(\boldsymbol{\theta}_l^{(j)}) \boldsymbol{\theta}_l^{(j)}}{\sum_{l=1}^{N} w(\boldsymbol{\theta}_l^{(j)})}. \tag{5.6}$$

5. Steps two to four are repeated until $r_M = 1$. At final step, samples $\boldsymbol{\theta}_k^{(M)}$ for $k = 1, 2, ..., N$ are distributed according to $f(\boldsymbol{\theta}|\mathcal{M}, \mathcal{D})$ and it is found that $S = \Pi_{j=0}^{M} S_j$ is asymptotically unbiased for $f(\mathcal{D}|\mathcal{M})$.

The significant advantage of the modified Metropolis-Hastings algorithm applied in TMCMC is that initially it allows a large and a free sample space to explore but in the final stages the samples are generated from the narrow neighborhood of sample space. Furthermore the proposal distribution will change within a simulation level and this will result in better local behavior. This is accomplished by modifying the proposal distribution for each level in such a way that its standard deviation is small for higher simulation levels. But the average value drives the generation of samples towards the most important neighborhood of the sample space [168, 170, 171].

5.5.4. Parameter Identification of Ordinary Differential Equations using TMCMC

This subsection discusses the applicability of the above described methods on a set of ordinary differential equations (ODEs) and it is also discussed the working of this method on ODEs in general. Based on the obtained results this method can be extended to apply on the viscoplasticity-damage model as discussed in Chapter 3 which is basically a partial differential equation (PDE) and a set of ODEs.

Example 5.3. ***Parameter Identification of Bouc-Wen-Wang-Wen Model***

Bouc-Wen model [173, 174, 172] is a first order nonlinear differential equation that transposes the displacement to the restoring force via hysteretic shape. The phenomenological Bouc-Wen model schematic is illustrated in figure 5.4. The model is represented by Equation 5.7 where k and c represents the lateral stiffness of the system and viscous damping coefficient respectively. The velocity in x direction is represented by $\dot{x}(t)$ and acceleration in x direction is represented by $\ddot{x}(t)$. Similarly the linear restoring force is represented by $\alpha kx(t)$ and the hysteretic storing force is represented by $(1-\alpha)kz(t)$ where $z(t)$ is the hysteretic displacement. The hysteretic displacement $z(t)$ comprises the hysteretic component of the system.

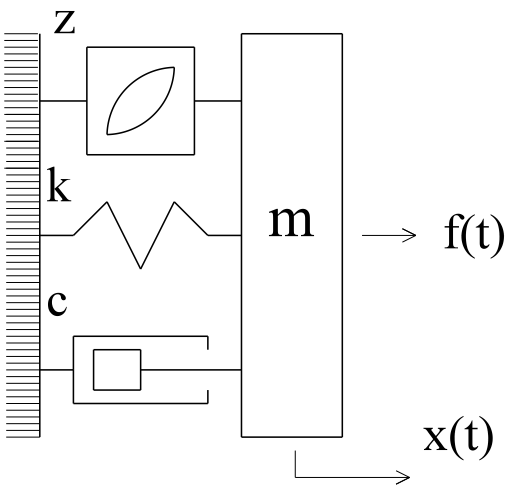

Figure 5.4.: The phenomenological Bouc-Wen model schematic

$$m\ddot{x}(t) + c\dot{x}(t) + \alpha kx(t) + (1-\alpha)kz(t) = f(t) \tag{5.7}$$

The Equation 5.7 is divided by the mass of the system m to determine the damping ratio

$\zeta = \frac{c}{c_{cr}} = \frac{c}{2m\omega}$ and the circular frequency $\omega = \sqrt{\frac{k}{m}}$ [175] as shown in Equation 5.8 where $f(t)$ is the new external excitation with the initial conditions $\dot{x} = v_0$ and $\ddot{x} = a_0$ in which v_0 and a_0 represents the initial velocity and acceleration of the system respectively. The stiffness ratio in the range of $(0, 1)$ is represented by α and it is obtained by $\alpha := k_f/k_i$. The post-yield elastic stiffness is represented by k_f and the pre-yield elastic stiffness is represented by k_i. The pre-yield elastic stiffness is determined from the ratio of initial yield force f_y to the initial yield displacement x_y i.e. $k_i := f_y/x_y$.

$$\ddot{x}(t) + 2\zeta\omega\dot{x}(t) + \alpha\omega^2 x(t) + (1-\alpha)\omega^2 z(t) = f(t) \tag{5.8}$$

The term $z(t)$ introduced by Wang and Wen [176] is directly proportional to the time history of displacement and it is defined by the first order nonlinear differential equation as shown in Equation 5.9 with the initial condition $z(0) = 0$.

$$\dot{z}(t) = \dot{x}(t)\left\{A - \left[\gamma + \beta\,\mathrm{sign}(z(t)\dot{x}(t)) + \phi(\mathrm{sign}(\dot{x}(t)) + \mathrm{sign}(z(t)))\right]|z(t)|^n\right\} \tag{5.9}$$

In Equation 5.9, the amplitude of hysteresis loops is represented by A and the constants that control the hysteresis shape of the model are β, γ, ϕ and n. These constants are called as hysteretic shape parameters.

The hysterical energy giving the energy dissipated by the hysteretic component is represented by $\epsilon(t)$. It is defined by evaluation of area of graph of mass normalized hysteretic restoring force $F^h(z(t)) := (1-\alpha)k_i z(t)$ vs the total displacement. Hence, the absorbed hysteretic energy per unit mass is quantified as in Equation 5.10 [177, 178, 176].

$$\epsilon(t) = \int_{x(0)}^{x(t)} \frac{F^h(x)}{m} dx = (1-\alpha)\omega_0^2 \int_0^t z(\tau)\dot{x}(\tau)d\tau \tag{5.10}$$

On considering the vector $Y = (Y_1(t), Y_2(t), Y_3(t), Y_4(t))^T = (x(t), \dot{x}(t), z(t), \epsilon(t))^T$, the equations above can be rewritten as set of equations below where the derivatives are in first power and the variables vary at different rates with respect to time.

$$\begin{aligned}
\dot{Y_1} &= Y_2 \\
\dot{Y_2} &= -2\zeta\omega_n Y_2 - \alpha\omega_n^2 Y_1 - (1-\alpha)\omega_n^2 Y_3 + f(t) \\
\dot{Y_3} &= AY_2 - Y_2|Y_3|^n(\gamma + \beta|Y_2Y_3| + \phi(|Y_2| + |Y_3|)) \\
\dot{Y_4} &= (1-\alpha)\omega_0^2 Y_2 Y_3
\end{aligned}$$

Hence, the hysteretic model consists of a stiff set of ODEs which can be solved numerically by using the Fourth-order Runge-Kutta method. Therefore, the state-space

model in the discrete form is given in Equation 5.11 where $Y(l)$ is the state vector and $\boldsymbol{\theta} = [\zeta, \alpha, \beta, \gamma, n, \phi]$ is a set of model parameters. This model parameters are unknown for the real systems and it has to be determined as accurately as possible. The input is represented by $u(k) = f(l \cdot \Delta t)/m$ where the Runge-Kutta time step is represented by l [179, 180].

$$Y(l+1) = f(l, Y(l), u(l), \boldsymbol{\theta}) \tag{5.11}$$

The parameters such as $m = 1000\ kg$, $k_i = 10\ kN/mm$ are given as input. The External excitation force $f(t) = t\cos(\pi t)$ is applied for 15 s and a Runge-Kutta time step k of 0.02 s is given as a input. Response of the system in terms of displacement with respect to time is shown in Figure 5.5 and it is obtained by considering the parameters of the model $A = 1$, $\zeta = 0.15$, $\alpha = 0.50$, $\beta = 4.00$, $\gamma = 0.50$, $n = 4.0$ and $\phi = -0.50$. The response of system in terms of absorbed hysteresis energy with respect to time is shown in Figure 5.6. The variation of hysteresis force with respect to displacement is shown in Figure 5.7.

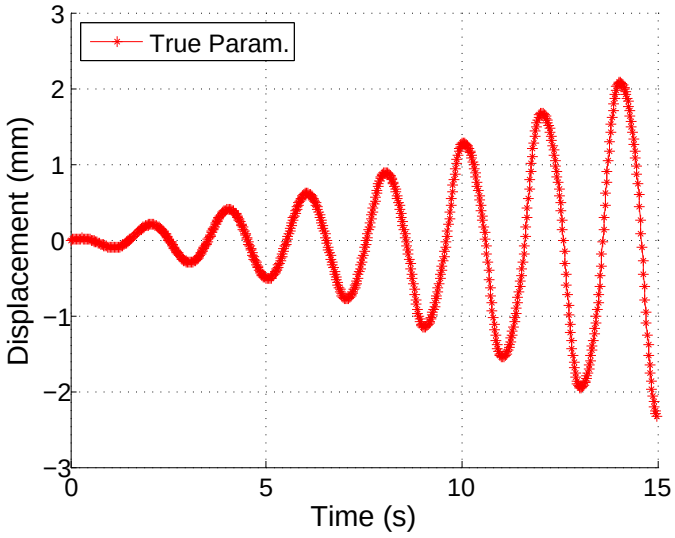

Figure 5.5.: Displacement of the model according to time variation

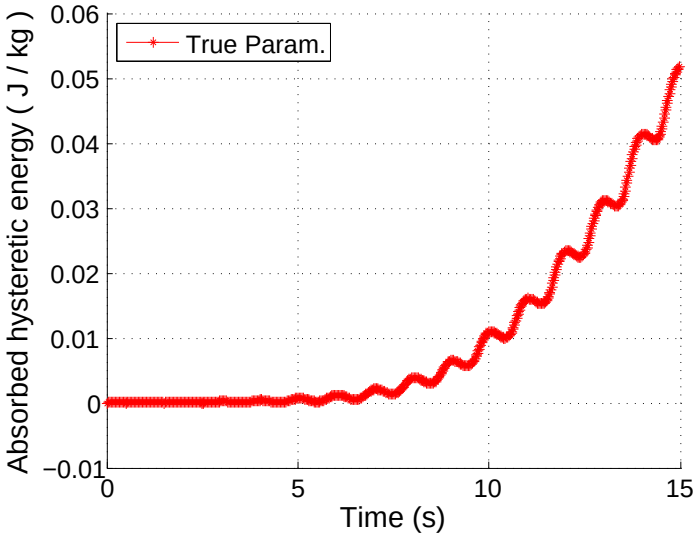

Figure 5.6.: Absorbed hysteretic energy of the model according to time variation

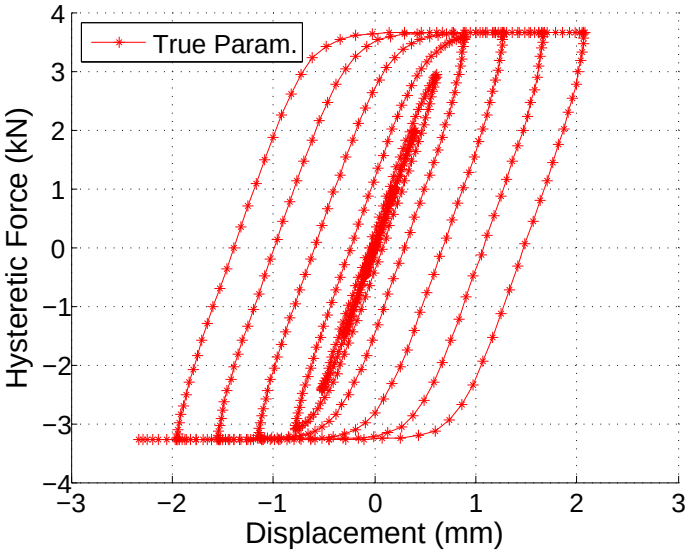

Figure 5.7.: Hysteresis force of the model according to the displacement

The samples for TMCMC are generated from the displacement and hysteresis energy

of the structure. 751 samples are generated for the next step from the force which is applied for 15 seconds and from the Runge-Kutta time step l of 0.02 second. As the exact response of the structure is not an exact approximation in natural phenomena so the simulated displacement (Y_1) of the structure is computed using very different initial values and also it is contaminated by an additive Gaussian white noise with a variance (σ^2) of 0.04 as shown in Equation 5.12 to bring our problem closer to the reality.

$$Y_1^{\text{noisy}} = Y_1 + \mathcal{N}(0, \sigma^2) \tag{5.12}$$

In Equation 5.12, Y_1^{noisy} represents the noisy simulated displacement of the system considered as the measurement data and RV_n is normally distributed random numbers. The number of sample generations Nj is taken into account as 1000. The burn-in period is considered as 200 in all iterations but in last iteration it is considered as 500 to ensure that the accuracy is higher in the last iteration than in the other iterations. Further the scaling parameter (β) is considered in TMCMC as 0.2.

The evolution of the estimated model parameters and their convergence in the generation steps i.e. only first and last step is shown in Figure 5.8.

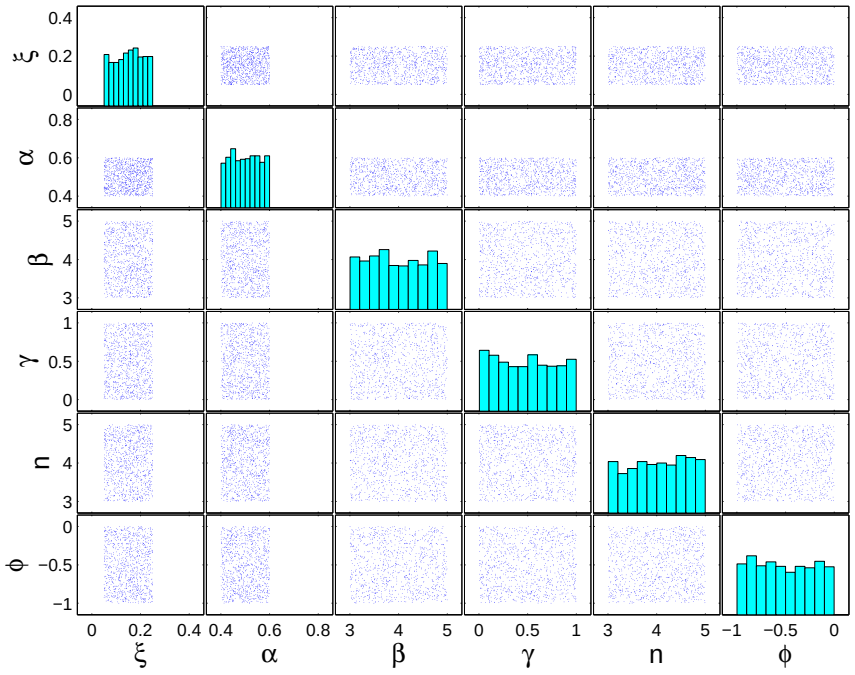

(a) Prior

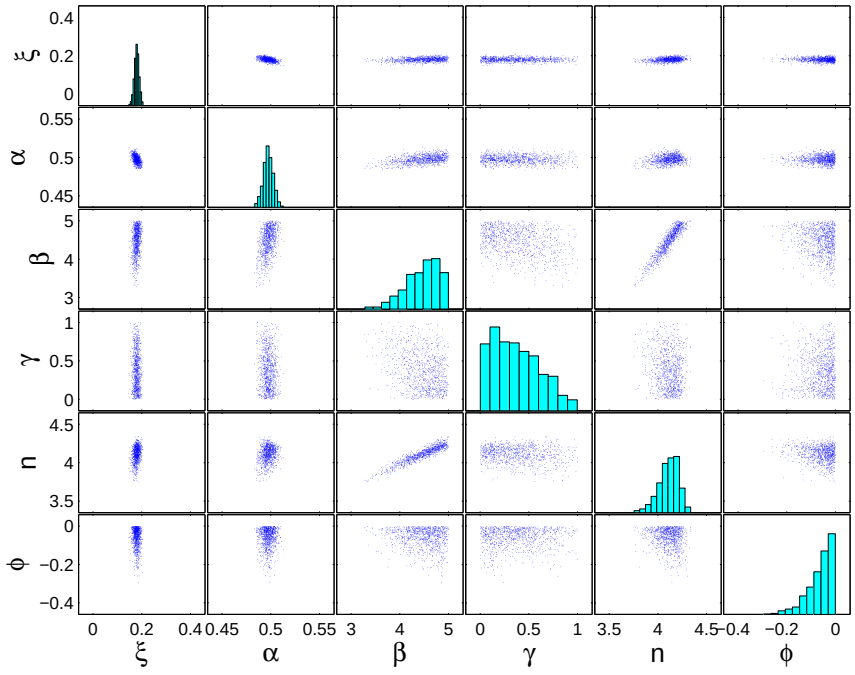

(b) Posterior

Figure 5.8.: Comparing the prior and posterior of model parameters

It is observed from Figure 5.8 that the final posterior distribution functions of the parameters from the samples generated by using TMCMC are centered at certain values which are basically the estimation of the true values. In addition, the off-diagonal cells representing the correlation between each two parameters are very clustered while in the initial prior they are completely scattered.

The estimated prior probability distributed functions for all true parameters ($\boldsymbol{\theta}$) and the restricted regions are represented as $\boldsymbol{\theta}_{\text{min}}$ and $\boldsymbol{\theta}_{\text{max}}$ respectively. The mean and standard deviation of the final posterior estimated parameters are represented as $\boldsymbol{\theta}_{\text{est}}$(mean) and $\boldsymbol{\theta}_{\text{est}}$(std) respectively. This parameters are summarized in Table 5.1.

Table 5.1.: Parameter identifications of simulated data

Param.	$\boldsymbol{\theta}_{\text{min}}$	$\boldsymbol{\theta}$	$\boldsymbol{\theta}_{\text{max}}$	$\boldsymbol{\theta}_{\text{est}}$(mean)	$\boldsymbol{\theta}_{\text{est}}$(std)
ζ	0.05	0.15	0.25	0.1791	0.0096
α	0.40	0.50	0.60	0.4974	0.0050
β	3.00	4.00	5.00	4.4643	0.3438
γ	0.00	0.50	1.00	0.3738	0.2425
n	3.00	4.00	5.00	4.1099	0.1017
ϕ	-1.00	-0.50	0.00	-0.0617	0.0504

Despite considering a very big noise, the all estimated mean values by TMCMC are close enough to the true values except for ϕ. In order to determine the efficiency of the method to estimate the parameters, the displacement and the hysteresis energy of the system with the estimated and true parameters are shown in Figure 5.9 and 5.10 respectively which compares the considered first step true parameters with the estimated parameters. The hysteresis force with respect to displacement is compared for true and estimated parameters as shown in Figure 5.11. In Figure 5.9, 5.10 and 5.11, the model simulation with true parameters is represented in red color and the model simulation with the estimated parameters is represented in blue color.

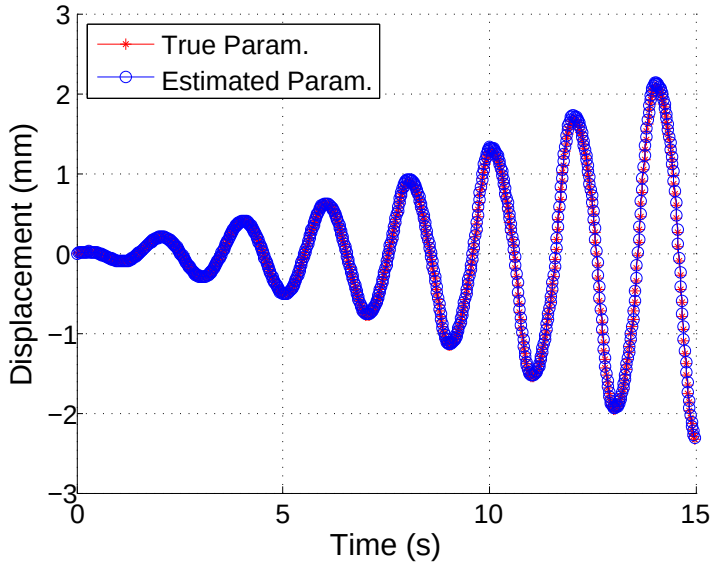

Figure 5.9.: Displacement of the model according to time variation

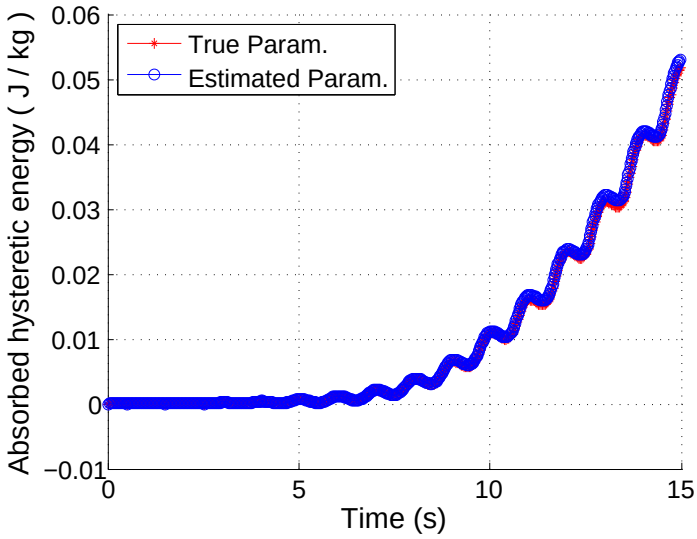

Figure 5.10.: Absorbed hysteretic energy of the model according to time variation

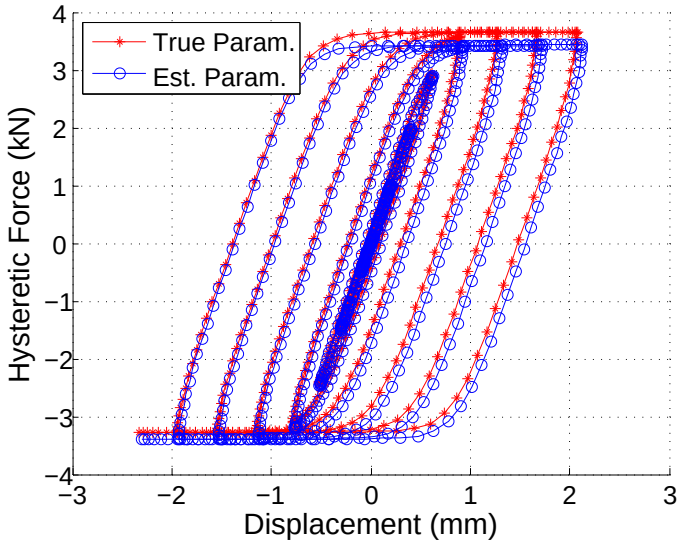

Figure 5.11.: Hysteretic force of the model according to the displacement

The efficiency of the TMCMC method for identifying the parameters of the ODE system is evaluated and as it turned out the results are accurate enough even by considering the noise on displacement of structure and it is represented in Figure 5.9, 5.10 and 5.11. It is also to be noted that the accuracy is determined by choosing the defined effective values in this method.

5.6. Conclusion

In this chapter the random walk Monte Carlo approach is explained in detail. A modification of Markov Chain Monte Carlo method which is so-called Transitional Markov Chain Monte Carlo approach is employed by considering the improved Metropolis-Hastings algorithm which leads to a more efficient method. Indeed, Transitional Markov Chain Monte Carlo method is a multi-level adaptive Markov Chain Monte Carlo method which by introducing some intermediate probability distribution functions leads to generation of samples from the final posterior in a much more appropriate way. Generation of samples from the posterior is difficult especially for some flat manifold, multi-model or peaked PDFs where Transitional Markov Chain Monte Carlo method efficiency and applicability is more appreciated. This method is applied on an ODE system to identify its model parameters and as it is shown in this chapter that the parameters are estimated good enough and the uncertainty of its parameters are reduced, although very different measurement data than the identification model is considered. It should also be noted that the probabilistic identification is still possible by considering the prior in such a way that no information from them is provided and so they are set as uniform prob-

ability distributions. Transitional Markov Chain Monte Carlo method will be applied on the desired mechanical material model as discussed in Chapter 3 and this method's validation on the mentioned model will be evaluated in Chapter 7.

6. Bayesian Updating via Conditional Expectation

In Chapter 3 the viscoplastic-damage model is introduced and Chapter 4 dedicated how uncertainty is propagated into the model. In this chapter, one of the main approaches based on the approximation of Bayes's theorem with the capability to solve the very high conditional ill-posed problem in the Bayesian setting is discussed. Further in this chapter the functional approximation of this estimation is described which can provide us the capability of identifying the model parameters probabilistically.

The original Kalman filter [181, 182, 183, 184, 201] is most famous instance of spectral methods for recursive linear conditional expectations where the Gaussian random variables are used [185]. Hence the model random variables will always be a multivariate Gaussian. The presented filter estimates the exact value for the linear problem mostly without any difficulties as the stochastic spectrum of a multivariate Gaussian random variables are represented by its mean and covariance structure similar to the representation in Kalman filter.

An extension of the linear conditional expectation approach to non-Gaussian random variables represented by spectral decomposition is discussed in this chapter. Indeed this approach is obtained by a direct projection of the linear conditional expectation onto a spectral representation.

6.1. Conditional Expectation

The author follows the conditional expectation described in Section 4.2 by considering the theorem of Bayes and Laplace discussed in Subsection 2.2.1. The conditional expectation is defined on the Hilbert space where the random variables are considered with finite variance as shown in Equation 6.1 where the considered sub-σ-algebra $\mathfrak{B}$ is a subset of the underlying σ-algebra $\mathfrak{A}$, i.e. $\mathfrak{B} \subset \mathfrak{A}$. It should be noted that the σ-algebra is basically representing the collection of subsets of Ω on which statements about their probability can be made. Therefore it has a continuous orthogonal projection $P_{\mathfrak{B}} : \mathcal{S} \to \mathcal{S}_{\mathfrak{B}}$ from the whole σ-algebra to sub-σ-algebra $\mathfrak{B}$ that has the collection of subsets of Ω based on which their probability is determined [186, 191].

$$\mathcal{S}_{\mathfrak{B}} := L_2(\Omega, \mathfrak{B}, \mathbb{P}) := \{r : \Omega \to \mathbb{R} \ : \ \text{r measurable w.r.t. } \mathfrak{B}\,, \mathbb{E}\left(|r|^2\right) < \infty\} \subset \mathcal{S} \quad (6.1)$$

Thus the conditional expectation (CE) of a random variable $r \in \mathcal{S}$ with respect to a sub-σ-algebra $\mathfrak{B}$ can be defined by the orthogonal projection as shown in Equation 6.2.

$$\mathbb{E}(r|\mathfrak{B}) := P_{\mathfrak{B}}(r) \in \mathcal{S}_{\mathfrak{B}} \tag{6.2}$$

The conditional expectation minimizes the squared error as it is an orthogonal expectation as shown in Equation 6.3.

$$\mathbb{E}(|r - \mathbb{E}(r|\mathfrak{B})|^2) = \min\{\mathbb{E}(|r - \tilde{r}|^2) \ : \ \tilde{r} \in \mathcal{S}_{\mathfrak{B}}\} \tag{6.3}$$

Equation 6.3 leads to the orthogonality relation $\forall \tilde{r} \in \mathcal{S}_{\mathfrak{B}} \ : \ \mathbb{E}(\tilde{r}(r - \mathbb{E}(r|\mathfrak{B}))) = 0$. Also a form of Pythagoras theorem [192] can be considered as shown in Equation 6.4.

$$\mathbb{E}(|r|^2) = \mathbb{E}(|r - \mathbb{E}(r|\mathfrak{B})|^2) + \mathbb{E}(|\mathbb{E}(r|\mathfrak{B})|^2) \tag{6.4}$$

Therefore it can be concluded that conditional expectation is a form of a minimum mean square error estimator. The conditional probability, for instance, the posterior in Bayes's theorem can be characterized by the conditional expectation [186, 193]. For instance the conditional probability for $A \subset \Omega$, $A \in \mathfrak{B}$ is obtained by Equation 6.5 where the random variable χ_A becomes unity if $\omega \in A$ and it vanishes otherwise.

$$\mathbb{P}(A|\mathfrak{B}) := \mathbb{E}(\chi_A|\mathfrak{B}) \tag{6.5}$$

Based on Equation 6.5, if the conditional expectation $\mathbb{E}(\chi_A|\mathfrak{B})$ is known then everything about the conditional probability $\mathbb{P}(A|\mathfrak{B})$ is known and thus the posterior density is defined by this. If the distribution of a random variable representing the prior density is characterized by the prior characteristic function then the conditional characteristic function is determined by using the conditional expectation and this characterizes the conditional distribution. If the prior probability was the distribution of some random variable r, then it is completely characterized by the prior characteristic function, i.e. in the sense of probability theory, it can be expressed as $\phi_r(s) := \mathbb{E}(\exp(irs))$ [195]. To determine the conditional characteristic function $\phi_{r|\mathfrak{B}}(s) := \mathbb{E}(\exp(irs)|\mathfrak{B})$, conditional expectation is used instead of the unconditional expectation and this completely characterizes the conditional distribution.

For an instance if a random variable y is the observation and the sub-σ-algebra $\mathfrak{B}$ is generated from the observation y resulting in $\mathfrak{B} = \sigma(y)$, the information about the observation can be obtained only on $\mathfrak{B} = \sigma(y)$ which are some subsets of Ω [186]. According to the Doob-Dynkin lemma [194, 85], the Equation 6.6 represents the subspace $\mathcal{S}_{\sigma(y)}$ as the functions of observation.

$$\mathcal{S}_{\sigma(y)} := \{r \in \mathcal{S} \,:\, r(\omega) = \phi(y(\omega)), \phi \text{ measurable}\} \subset \mathcal{S} \tag{6.6}$$

It can be inferred from the Equation 6.6 that an observation is a function of the observation and where the information from the measurement is lying is represented by the subspace $\mathcal{S}_{\sigma(y)} \subset \mathcal{S}$ [186].

The conditional expectation $\mathbb{E}(r|\sigma(y)) = \mathbb{E}(r|y)$ and the conditional probability $\mathbb{P}(A|\sigma(y)) = \mathbb{P}(A|y)$ are random variables as y is a random variable. If a fixed value $\hat{y} \in \mathcal{Y}$ is observed for the random variable y, i.e. an observation is established then the posterior expectation is just a number $\mathbb{E}(r|\hat{y}) \in \mathbb{R}$ and the posterior probability is $\mathbb{P}(A|\hat{y}) = \mathbb{E}(\chi_A|\hat{y})$. Accordingly, Equation 6.7 can be determined for some function ϕ_r from the Equation 6.6 which means for each random variable r it is a possibly different function.

$$\mathbb{E}(r|y) = \phi_r(y) \quad \text{and} \quad \mathbb{E}(r|\hat{y}) = \phi_r(\hat{y}) \tag{6.7}$$

Considering Bayes's theorem as discussed in Subsection 2.2.1, it can be concluded that if it is possible to compute the conditional expectation with respect to an observation y then the conditional probability with respect to observation $\hat{y}$ can also be computed and this leads to determine the posterior probability as in Bayes's theorem described. Thus the Bayesian estimation can be done by using the concept of conditional expectation [186, 195, 196].

The conditional expectation can be extended for the considered vector random variables. The considered vector-valued random variables as an element of the tensor Hilbert space $\mathscr{Y} = \mathcal{Y} \otimes \mathcal{S}$ i.e. $\mathscr{Y} = \mathcal{Y} \otimes \mathcal{S} \cong L_2(\Omega, \mathfrak{B}, \mathbb{P}; \mathcal{Y})$ has a finite total variance as in Equation 6.8 [196].

$$|||\tilde{y}|||^2_{\mathscr{Y}} = \int_{\Omega} ||\tilde{y}(\omega)||^2_{\mathcal{Y}} \, \mathbb{P}(\mathrm{d}\omega) < \infty \tag{6.8}$$

Equation 6.9 is obtained by simplifying the Equation 6.8 by considering the total L_2-norm of an elementary tensor $y \otimes r \in \mathcal{Y} \otimes \mathcal{S}$ with $y \in \mathcal{Y}$ and $r \in \mathcal{S}$ where $\langle r, r\rangle_{\mathcal{S}} = ||r||^2_{\mathcal{S}} := \mathbb{E}(|r|^2)$ is the usual inner product of scalar random variables.

$$|||y \otimes r|||^2_{\mathscr{Y}} = \langle\langle y \otimes r, y \otimes r\rangle\rangle_{\mathscr{Y}} = ||y||^2_{\mathcal{Y}} \, ||r||^2_{\mathcal{S}} = \langle y, y\rangle_{\mathcal{Y}} \, \langle r, r\rangle_{\mathcal{S}} \tag{6.9}$$

Eventually the Equation 6.10 is obtained showing the conditional expectation on $\mathscr{Y}$ where the $I_{\mathcal{Y}}$ is the identity operator on $\mathcal{Y}$ [196].

$$\mathbb{E}_{\mathscr{Y}}(.|\mathcal{B}) = I_{\mathcal{Y}} \otimes \mathbb{E}(.|\mathcal{B}) : \mathscr{Y} = \mathcal{Y} \otimes \mathcal{S} \to \mathcal{Y} \tag{6.10}$$

The conditional expectation in simplified form is shown in Equation 6.11.

$$\mathbb{E}_{\mathscr{Y}}(y \otimes r|\mathcal{B}) = y \otimes \mathbb{E}(r|\mathcal{B}) \tag{6.11}$$

Conditional expectation of vector random variables denoted by $\mathbb{E}_{\mathscr{Y}}(.|\mathcal{B}) = P_{\mathcal{B}}$ is an orthogonal projection similar to the scalar random variables but in $\mathcal{Y}$ [186, 196].

6.2. Constructing a Posterior Random Variable

Equation 6.12 which is the probabilistic model of the observation is obtained by considering the random variables and the observation equation of the model as discussed in Equation 2.11 in Chapter 2 where the mapping Y is observed. This mapping is on the Hilbert space of the random variables with finite variance.

$$\hat{y} = y + \epsilon = Y(\boldsymbol{q}) + \epsilon \tag{6.12}$$

6.2.1. Updating Random Variables

Let's assume a random variable $\boldsymbol{q}_n \in \mathscr{Q}$, the next state $\hat{\boldsymbol{q}}_{n+1} \in \mathscr{Q}$ and the measurement $y_{n+1} \in \mathscr{Y}$ at time t_n goes to t_{n+1} can be predicted. The conditional expectation of the measurement prediction y_{n+1} calculated based on Equation 6.12 is shown in Equation 6.13 and the posterior expectation operator is computed by considering the actual observation $\hat{y}_{n+1}$ as shown in Equation 6.14.

$$\mathbb{E}(\Psi(\boldsymbol{q}_{n+1})|\sigma(y_{n+1})) = \phi_{\Psi}(y_{n+1}) \tag{6.13}$$

$$\mathbb{E}(\Psi(\boldsymbol{q}_{n+1})|\hat{y}_{n+1}) = \phi_{\Psi}(\hat{y}_{n+1}) \tag{6.14}$$

As the conditional expectation of the posterior is known and thereby all the information of the posterior probability is available [186, 195, 196].

It is to be noted that the Equation 6.12 requires every time new random variables $\boldsymbol{q}_{n+2}$ to be computed from t_{n+1} to t_{n+2} and this new random variables has the posterior distribution given by the mappings $\phi_{\Psi}(\hat{y}_{n+1})$ as shown in Equation 6.14. Although there are many random variables which have this posterior density but only one particular distribution should be chosen via the method as discussed in Section 6.3.

To simplify the notations, the forecast random variable is considered as $\boldsymbol{q}_f = \hat{\boldsymbol{q}}_{n+1}$ and the forecast measurement is considered as $y_f = y_{n+1}$. The measurement is represented

as $\hat{y} = \hat{y}_{n+1}$. Therefore the update of the forecast random variable $\boldsymbol{q}_f$ also called as the assimilated random variable $\boldsymbol{q}_a = \boldsymbol{q}_{n+1}$ results in Equation 6.15 where B represent a Bayesian update and Ξ represents an innovation map which plays the role of a transformation so-called filter i.e. update by filtering the measurement $\hat{y}$ [195, 196].

$$\boldsymbol{q}_a = B(\boldsymbol{q}_f, y_f, \hat{y}) = \boldsymbol{q}_f + \Xi(\boldsymbol{q}_f, y_f, \hat{y}) \tag{6.15}$$

6.2.2. Correcting the Mean

To correct the mean value of the new random variable $\bar{\boldsymbol{q}}_a = \mathbb{E}(\boldsymbol{q}_a|\hat{y})$, it should be considered that $\mathbb{E}(\boldsymbol{q}_a|\sigma(y_f)) = \phi_{\boldsymbol{q}_f}(y_f) := \phi_{\boldsymbol{q}}(y_f)$ is an orthogonal projection $P_{\sigma(y_f)}(\boldsymbol{q}_f)$ from $\mathscr{Q} = \mathcal{Q} \otimes \mathcal{S}$ onto $\mathscr{Q}_\infty := \mathcal{Q} \otimes \mathcal{S}_\infty$, where $\mathcal{S}_\infty := \mathcal{S}_{\sigma(y)} = L_2(\Omega, \sigma(y_f), \mathbb{P})$ by considering the Equation 6.2 and 6.14 [186]. Therefore the orthogonal decomposition can be shown as in Equation 6.16.

$$\mathscr{Q} = \mathcal{Q} \otimes \mathcal{S} = \mathscr{Q}_\infty \oplus \mathscr{Q}_\infty^\perp = (\mathcal{Q} \otimes \mathcal{S}_\infty) \oplus (\mathcal{Q} \otimes \mathcal{S}_\infty^\perp) \tag{6.16}$$

$$\boldsymbol{q}_f = P_{\sigma(y_f)}(\boldsymbol{q}_f) + (I_{\mathscr{Q}} - P_{\sigma(y_f)})(\boldsymbol{q}_f) = \phi_{\boldsymbol{q}}(y_f) + (\boldsymbol{q}_f - \phi_{\boldsymbol{q}}(y_f)) \tag{6.17}$$

Equation 6.18 can be determined as the conditional expectation of the second term in Equation 6.17 is zero as this term is representing the projection part of the decomposition, i.e. $\mathbb{E}(\boldsymbol{q}_f - \phi_{\boldsymbol{q}}(y_f)|\sigma(y_f)) = P_{\sigma(y_f)}(I_{\mathscr{Q}} - P_{\sigma(y_f)})(\boldsymbol{q}_f) = 0$ [186, 195, 196]. It can be also explained in this way that when the measurement is obtained, the Equation 6.17 is changed by fixing the component $\phi_{\boldsymbol{q}}(y_f) \in \mathscr{Q}_\infty$ and leaving the orthogonal rest unchanged.

$$\boldsymbol{q}_{a,1} = \phi_{\boldsymbol{q}}(\hat{y}) + (\boldsymbol{q}_f - \phi_{\boldsymbol{q}}(y_f)) = \boldsymbol{q}_f + (\phi_{\boldsymbol{q}}(\hat{y}) - \phi_{\boldsymbol{q}}(y_f)) \tag{6.18}$$

The posterior mean as seen in Equation 6.19 can be obtained from Equation 6.18.

$$\bar{\boldsymbol{q}}_{a,1} = \mathbb{E}(\boldsymbol{q}_{a,1}|\hat{y}) = \phi_{\boldsymbol{q}}(\hat{y}) = \mathbb{E}(\boldsymbol{q}_a|\hat{y}) \tag{6.19}$$

By defining the projection part of the decomposition by $\boldsymbol{q}_\perp := (\boldsymbol{q}_f - \phi_{\boldsymbol{q}}(y_f))$ where it is a zero mean random variable in Equation 6.18, the covariance and total variance of $\boldsymbol{q}_{a,1}$ are computed as shown in Equation 6.20 and 6.21, respectively [195, 196].

$$\mathrm{cov}(\boldsymbol{q}_{a,1}) = \mathbb{E}(\boldsymbol{q}_\perp \otimes \boldsymbol{q}_\perp) = \mathbb{E}(\boldsymbol{q}_\perp^{\otimes 2}) =: \boldsymbol{C}_1 \tag{6.20}$$

$$\mathrm{var}(\boldsymbol{q}_{a,1}) = \mathbb{E}(||\boldsymbol{q}_\perp(\omega)||_{\mathcal{Q}}^2) = \mathrm{tr}(\mathrm{cov}(\boldsymbol{q}_{a,1})) \tag{6.21}$$

6.3. The Gauss-Markov-Kalman Filter (GMKF)

Practically the computations where the Monte Carlo method or any other variation of it e.g. Marko Chain Monte Carlo or Transitional Markov Chain Monte Carlo method which is discussed in Chapter 5 is used, are very time consuming [168, 170, 171, 165, 164].

Some methods used for estimation of Bayes's theorem unlike Monte Carlo methods do not use all information but only part of information as approximations are considered. Hence the balance between time consumption, considered amount of information and the accuracy of approximations can be achieved. Incidentally, this leads to Kalman filter (KF) [199, 200, 198] method as it was related to Gauss-Markov theorem which is developed without any reference to Bayes's theorem. Moreover the polynomial chaos expansion is also used along with the ensemble Kalman filter (EnKF) [201, 186] in order to be completely independent from any time consuming computational implementations such as Monte Carlo method. This leads to the Gauss-Markov-Kalman filter [186, 195, 196, 203] which is discussed in this section.

6.3.1. Building the Filter

The algorithm to update the random variable with a map $g : \mathcal{Y} \to \mathcal{Q}$ to approximate $\phi_{\boldsymbol{q}}$ is obtained by inserting the Equation 6.12 into Equation 6.18 to obtain the Equation 6.22.

$$\begin{aligned} \boldsymbol{q}_{n+1} =& \boldsymbol{q}_n + (g(\hat{y}_{n+1}) - g(Y(\boldsymbol{q}) + \epsilon)) \\ =& \boldsymbol{q}_n - g(Y(\boldsymbol{q}) + \epsilon) + g(\hat{y}_{n+1}) \end{aligned} \tag{6.22}$$

It is inferred from the Equation 6.22 that the model Equation 6.12 is corrected by an innovation term and the Equation 6.22 can be named as the filter equation for identifying the extended uncertain parameters of Equation 6.12 which is an unbiased filter with the minimum mean square error estimate is represented by $\phi(\hat{y})$.

The map ϕ_Ψ is defined by Equation 6.23. It is obtained by introducing ϖ ranging over all measurable maps $\varpi : \mathcal{Y} \to \mathcal{Q}$ and by using the Equation 6.3 representing the combination of minimization property and the Equation 6.4 representing the Doob-Dynkin lemma [194, 85].

$$||\Psi(\boldsymbol{q}) - \phi_\Psi(y)||^2_{\mathcal{Q}} = \min_{\varpi} ||\Psi(\boldsymbol{q}) - \varpi(y)||^2_{\mathcal{Q}} = \min_{z \in \mathcal{Q}_\infty} ||\Psi(\boldsymbol{q}) - z||^2_{\mathcal{Q}} \tag{6.23}$$

As $\mathcal{Q}_{\sigma(y)} = \mathcal{Q}_\infty$ is $\mathcal{L}$-closed, it can be concluded that $\forall z \in \mathcal{Q}_\infty : \mathbb{E}(z \otimes (\Psi(\boldsymbol{q}) - \phi_\Psi(y)))$ [202]. Hence the random variable $(\Psi(\boldsymbol{q}) - \varpi(y))$ is orthogonal in the $\mathcal{L}$-invariant sense to all random variables $z \in \mathcal{Q}_\infty$. In other words, the correlation operator of $(\Psi(\boldsymbol{q}) - \varpi(y))$ is zero [186, 195, 196]. It should also be noted that the measurement operator evaluating y need not necessarily be linear in $\boldsymbol{q}$ and hence the optimal map $\phi_{\boldsymbol{q}}(y)$ is also need not

necessarily be linear in y. However the conditional expectation $\mathbb{E}(\boldsymbol{q}|y) = P_{\sigma(y)}(\boldsymbol{q})$ is basically an orthogonal projection.

6.3.2. The Linear Filter

The minimization problem as in the Equation 6.23 is to be solved and it lies in infinite dimensional space. Hence it is to be approximated using Galerkin method in finite dimensional subspaces. The chosen desired subspace to solve the problem is $\mathscr{Q}_1 \subset \mathscr{Q}_\infty \subset \mathscr{Q}$. Hence the desired subspace is shown in Equation 6.24 where the affine maps Φ are certainly measurable [186, 195, 196, 185].

$$\mathscr{Q}_1 = \{z : z = \Phi(y) = L(y(\omega)) + b,\ L \in \mathscr{L}(\mathcal{Y}, \mathcal{Q}),\ b \in \mathcal{Q}\} \subset \mathscr{Q}_\infty \subset \mathscr{Q} \tag{6.24}$$

The Equation 6.25 is obtained from the minimization problem as given by the Equation 6.23 where the optimal affine map is introduced via so-called Kalman gain $K \in \mathscr{L}(\mathcal{Y}, \mathcal{Q})$. The Kalman gain is represented as $\boldsymbol{K} := \text{cov}(\boldsymbol{q}, y)\text{cov}(y)^{-1}$ where $\text{cov}(\boldsymbol{q}, y)$ is the covariance of $\boldsymbol{q}$ and y, $\text{cov}(y)$ is the auto-covariance of y and $a \in \mathcal{Q}$ read as $a := \bar{\boldsymbol{q}} - \boldsymbol{K}(\bar{y})$.

$$||\boldsymbol{q} - (\boldsymbol{K}(y) + a)||^2_{\mathscr{Q}} = \min_{L,b} ||\boldsymbol{q} - (L(y) + b)||^2_{\mathscr{Q}} \tag{6.25}$$

It should be noted that as $\mathscr{Q}_1 \subset \mathscr{Q}_\infty$ is a true subspace then obviously some information is disregarded when using this approximation $g(y) = \boldsymbol{K}(y) + a$. Although the computation becomes easier, some information that we may learn from the measurement is neglected. Equation 6.26 is determined from the Equation 6.18 and from the described algorithm.

$$\boldsymbol{q}_{a,1L} = \boldsymbol{q}_f + (\boldsymbol{K}(\hat{y}) - \boldsymbol{K}(y)) = \boldsymbol{q}_f + \boldsymbol{K}(\hat{y} - y) \tag{6.26}$$

This linear filter is called Gauss-Markov-Kalman filter (GMKF) with the linear minimum mean square error $\boldsymbol{K}(\hat{y})$ defined as in [186, 195, 196, 203]. It should be noted that Gauss-Markov-Kalman filter is a general form of the original Kalman filter which is considered only for the mean values of the random variables of the parameters included in Equation 6.26. Accordingly the Equation 6.22 representing the algorithm turns to the Equation 6.27.

$$\begin{aligned} \boldsymbol{q}_{n+1} =& \boldsymbol{q}_n + \boldsymbol{K}((\hat{y}_{n+1}) - (Y(\boldsymbol{q}_n) + \epsilon)) \\ =& \boldsymbol{q}_n - \boldsymbol{K}(Y(\boldsymbol{q}_n) + \epsilon)) + \boldsymbol{K}(\hat{y}_{n+1}) \end{aligned} \tag{6.27}$$

Equation 6.28 is determined from the Equation 6.26 by introducing the Kalman gain and by considering the random variables as the argument. By considering the error the

Kalman gain is defined as $\boldsymbol{K} := \mathrm{cov}(\boldsymbol{q}_f, y)(\mathrm{cov}(y) + \mathrm{cov}(\epsilon))^{\dagger}$.

$$\boldsymbol{q}_a(\omega) = \boldsymbol{q}_f(\omega) + \boldsymbol{K}(\hat{y} - y(\omega)) \tag{6.28}$$

The Gauss-Markov-Kalman filter as described in Equation 6.28 needs to be discretized in order to implement numerically as it is related with the random variables.

6.3.3. Sequential Gauss-Markov-Kalman Filter

The process of updating can be done several times on the whole time interval. Once a high non-linear chaotic system is divided to very small time steps, the problem turns to plenty of continuous linear systems so that the GMKF approach can update the model parameters in a much better way if it is applied several times to update the model parameters on each time step. Eventually this approach helps to update the uncertain parameters of a non-linear system. Therefore the Gauss-Markov-Kalman filter as in Equation 6.28 can be written as like in Equation 6.29 on the k-th time step for the n total time steps, where the Kalman gain reads $\boldsymbol{K}^{(k)} := \mathrm{cov}(\boldsymbol{q}_f^{(k)}, y^{(k)})(\mathrm{cov}(y^{(k)}) + \mathrm{cov}(\epsilon))^{\dagger}$.

$$\boldsymbol{q}_a^{(k)}(\omega) = \boldsymbol{q}_a^{(k-1)}(\omega) + \boldsymbol{K}^{(k)}(\hat{y}^{(k)} - y^{(k)}(\omega)) \tag{6.29}$$

The Equation 6.29 is called sequential Gauss-Markov-Kalman filter. Schematically the process of sequential Gauss-Markov-Kalman filter is shown in Figure 6.1 where the posterior of one update is the prior of the next update.

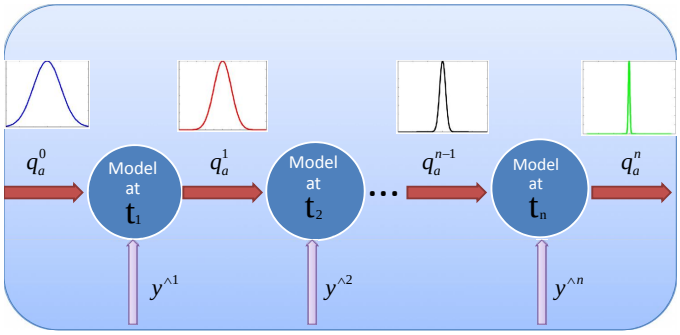

Figure 6.1.: Sequential GMKF method

6.4. Numerical Realization

The approaches such as sampling and spectral approximation or functional approximations to compute the linear filter approximations are discussed in this section to compute

the linear filter approximations.

6.4.1. Sampling

Considering N random variables then an ensemble of sampling points $\boldsymbol{\omega} = [\omega_1, ..., \omega_N]$ are taken into account [201]. The Gauss-Markov-Kalman filter as shown in Equation 6.28 for the considered ensemble of sampling points results in Equation 6.30.

$$\forall \ell = 1, ..., N: \quad \boldsymbol{q}_a(\omega_\ell) = \boldsymbol{q}_f(\omega_\ell) + \boldsymbol{C}_{\boldsymbol{q}_f y}(\boldsymbol{C}_y + \boldsymbol{C}_\epsilon)^\dagger(\tilde{y} - y(\omega_\ell)) \tag{6.30}$$

The Equation 6.30 is the basis of ensemble Gauss-Markov-Kalman filter where $\boldsymbol{C}_{\boldsymbol{q}_f y} = \text{cov}(\boldsymbol{q}_f, y)$, $\boldsymbol{C}_y = \text{cov}(y)$ and $\boldsymbol{C}_\epsilon = \text{cov}(\epsilon)$. $\boldsymbol{q}_f(\omega_l)$ and $\boldsymbol{q}_a(\omega_l)$ are shown as particles in the extended version.

6.4.2. Parameter Identification of Ordinary Differential Equations using Ensemble Gauss-Markov-Kalman Filter

The method described in this section is applied on a model represented by the set of Ordinary Differential Equation (ODE) and from the obtained results the efficiency of filter method for ODE are discussed. Further these method can be extended to apply on the viscoplastic-damage model as discussed in Chapter 3 which is represented by the Partial Differential Equation (PDE) and a set of ODEs.

Example 6.1. ***Parameter Identification of Lorenz-1996 Model by Ensemble Gauss-Markov-Kalman Filter***

The Lorenz-1996 is a variable size, low-order, strongly non-linear and chaotic dynamical model used by Lorenz (1996). The model has N state variables, X_1, X_2,...,X_N, and is governed by the Equation 6.31 with a periodic boundary condition as shown in Equation 6.32 where $i = 1, ..., N$ are cyclic indices [205, 206].

$$\frac{dX_i}{dt} = (X_{i+1} - X_{i-2})X_{i-1} - X_i + F \tag{6.31}$$

$$X_0 = X_i, \quad X_1 = X_{i+1}, \quad X_{-1} = X_{i-1} \tag{6.32}$$

The considered initial conditions are : $N = 40$, $F = 8.0$. A fourth order Runge-Kutta time step of $dt = 0.05$ is applied to solve the problem.

The parameters represented by independent Gaussian random variables are to be modeled and hence the deterministic model results in a system of stochastic differential

equation as shown in the Equation 6.33.

$$\frac{dX_i(\boldsymbol{\omega})}{dt} = (X_{i+1}(\boldsymbol{\omega}) - X_{i-2}(\boldsymbol{\omega}))X_{i-1}(\boldsymbol{\omega}) - X_i(\boldsymbol{\omega}) + F \tag{6.33}$$

The state variables are to be updated by applying ensemble Gauss-Markov-Kalman filter where the perturbed observation is considered that refers to the virtual experiment which is basically a simulation of the model with different initial value. Initially the model is updated every 10 time steps for the total time steps of 240. The estimated number of variables is 40 but only the first five variables are shown in Figure 6.2 and the rest of the variables can be found in Appendix A.

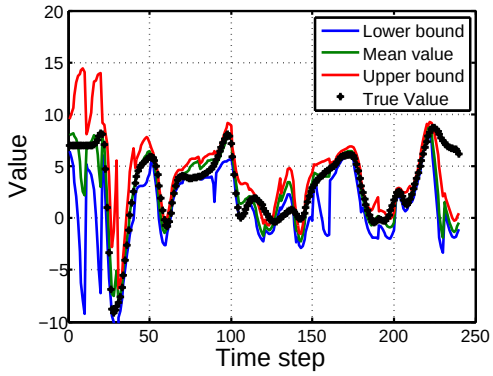

(a) First variable X_1 update

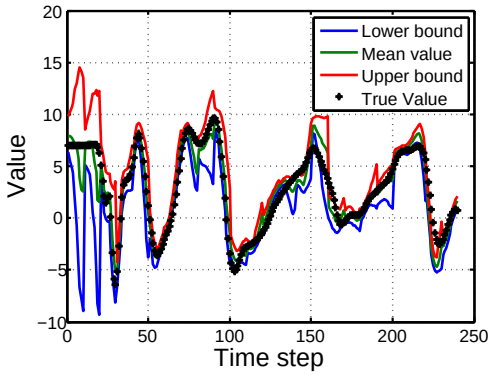

(b) Second variable X_2 update

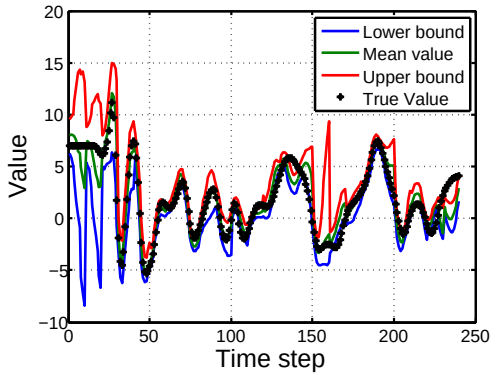

(c) Third variable X_3 update

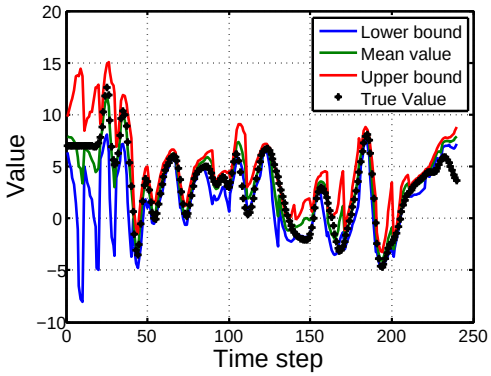

(d) Fourth variable X_4 update

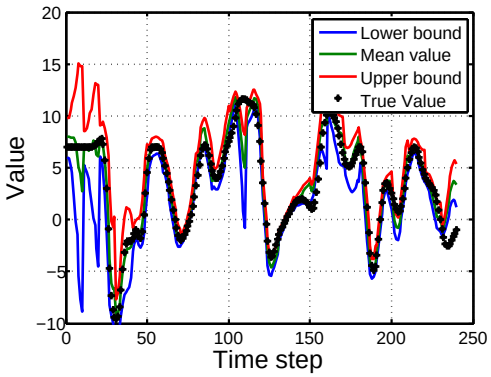

(e) Fifth variable X_5 update

Figure 6.2.: Updating the first 5 state variables of the model using ensemble Gauss-Markov-Kalman filter according to the time

In Figure 6.2, the true value is represented by the black color. The estimated Mean value using the ensemble Gauss-Markov-Kalman filter is plotted via green color. The

red and blue colors representing 95% and 5% of distribution called as upper bound and lower bound of the distribution respectively estimated by the ensemble Gauss-Markov-Kalman filter approach. The width of the distribution shrinks every time a measurement is performed, i.e. every 10 time step and it increases again due to the chaotic and noisy dynamics. It can be inferred that as time increases the estimated distribution becomes narrower and the mean value is very close to the true value. This indicates the capability of the Kalman filter method. However it is also to be noted that it takes a while to predict the true value by the estimated distributions. In Subsection 6.4.4 the Gauss-Markov-Kalman filter using functional approximation on the same problem is applied and the results of both approaches are compared.

The first state variable is updated for every 10, 20, 30 and 40 time steps as illustrated in Figure 6.3 to determine the effectiveness of time update.

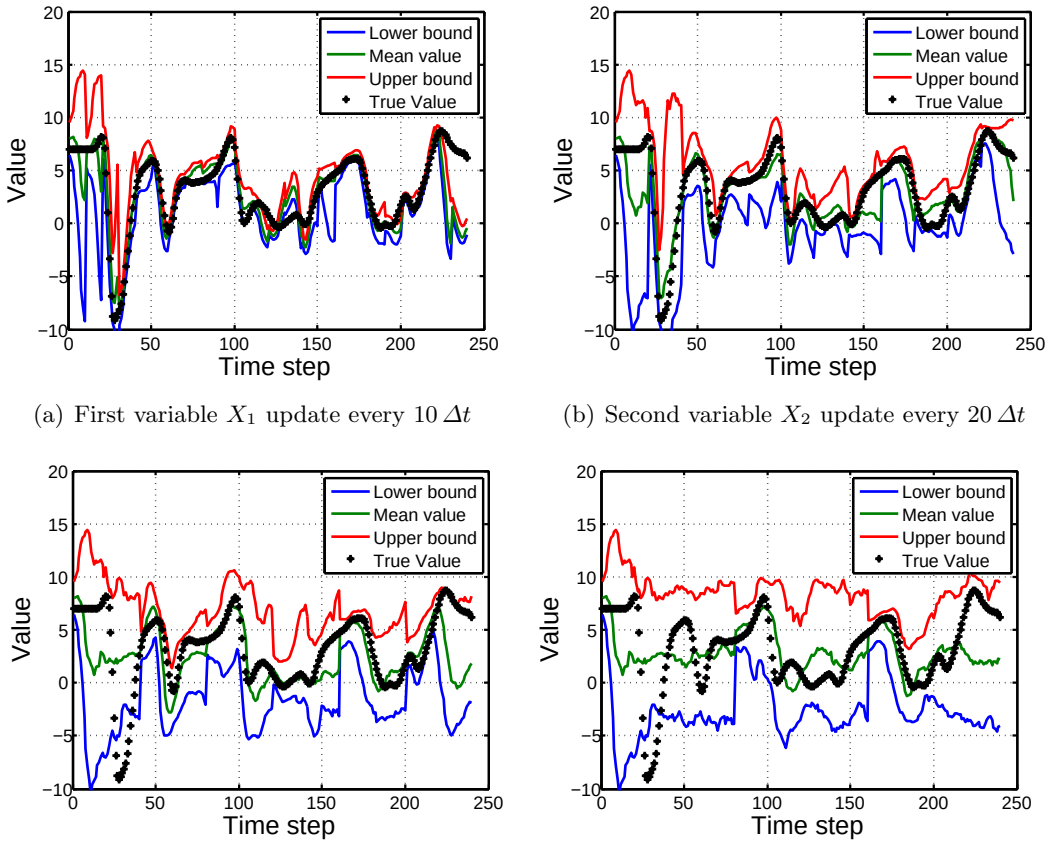

(a) First variable X_1 update every $10\,\Delta t$

(b) Second variable X_2 update every $20\,\Delta t$

(c) Third variable X_3 update every $40\,\Delta t$

(d) Fourth variable X_4 update every $80\,\Delta t$

Figure 6.3.: Comparing the different update time for the first state variable of the model using ensemble Gauss-Markov-Kalman filter according to the time

Better result is obtained by updating more often as it provides the better estimation of the model parameters, i.e. updating every 10 time step as shown in Figure 6.3(a) provides a better parameter prediction of the model in comparison with 20, 40 and 80 time steps as shown in Figure 6.3(b), 6.3(c) and 6.3(d) respectively.

6.4.3. Functional Approximation

The discretization of the random variables are performed by spectral or functional approximations instead of sampling [115, 195, 204]. Hence the desired random variables are described as functions of known random variables $\{\theta_1(\omega), ..., \theta_l(\omega), ...\}$. As only finite random variables can be dealt, a finite vector random variables in functional representation $\boldsymbol{\theta}(\omega) = [\theta_1(\omega), ..., \theta_n(\omega)]$ can be considered where n random variables $\boldsymbol{\theta}$ are taken into account.

The polynomial chaos expansion described in Chapter 4 is chosen as system of functions but also other possibilities exist. It should be noted that the finite set of linear independent Hermite functions $\{H_\alpha\}_{\alpha \in \mathcal{J}_M}$ of variables $\boldsymbol{\theta}(\omega)$ should include all the linear functions of $\boldsymbol{\theta}$ with polynomials such as polynomial chaos expansion [186, 195, 196, 207, 208]. The multi-index is represented by α and the set $\mathcal{J}_M$ is a finite set with cardinality M. The functional approximation of a random variable $\boldsymbol{q}(\omega)$ is shown in Equation 6.34.

$$\boldsymbol{q}(\omega) = \sum_{\alpha \in \mathcal{J}_M} \boldsymbol{q}_\alpha H_\alpha(\boldsymbol{\theta}(\omega)) = \sum_{\alpha \in \mathcal{J}_M} \boldsymbol{q}_\alpha H_\alpha(\boldsymbol{\theta}) = \boldsymbol{q}(\boldsymbol{\theta}) \tag{6.34}$$

The argument ω is neglected in the Equation 6.34 because the probability measure $\mathbb{P}$ on Ω is transported to $\boldsymbol{\Theta} = \Theta_1 \times ... \times \Theta_n$. The range of $\boldsymbol{\theta}$ showing $\mathbb{P}_\theta = \mathbb{P}_1 \times ... \times \mathbb{P}_n$ as a product measure, where $\mathbb{P}_\ell = (\theta_\ell)_* \mathbb{P}$ is the distribution measure of the random variable θ_ℓ and it is noted that the random variables θ_ℓ are independent. Therefore all computations are performed on $\boldsymbol{\Theta}$ which is typically a subset of $\mathbb{R}^n$. Hence the Gauss-Markov-Kalman filter as shown in Equation 6.28 for the considered expansion results in Equation 6.35 which is known as spectral Gauss-Markov-Kalman filter.

$$\boldsymbol{q}_a(\boldsymbol{\theta}) = \boldsymbol{q}_f(\boldsymbol{\theta}) + \boldsymbol{C}_{\boldsymbol{q}_f y}(\boldsymbol{C}_y + \boldsymbol{C}_\epsilon)^\dagger(\check{y} - y(\boldsymbol{\theta})) = \boldsymbol{q}_f(\boldsymbol{\theta}) + \boldsymbol{K}(\check{y} - y(\boldsymbol{\theta})) \tag{6.35}$$

It should also be noted that in spectral approximation the Gauss-Markov-Kalman filter as shown in the Equation 6.28 has the same form as of the sampling approach but the only difference is the functional approximation of random variables, i.e. the Hermite functions are used to calculate the covariance matrices. For instance $\boldsymbol{C}_{\boldsymbol{q}_f y}$ can be easily computed as given in Equation 6.36.

$$\boldsymbol{C}_{\boldsymbol{q}_f y} = \sum_{\alpha > 0} \alpha! \, (\boldsymbol{q}_f^{(\alpha)}(\boldsymbol{\theta}))(y^{(\alpha)}(\boldsymbol{\theta}))^T \tag{6.36}$$

While the Equation 6.28 is applied on samples or particles in sampling approach, in

spectral approximations it is applied on the coefficients as shown in Equation 6.34 which are the functional approximation of the random variables.

6.4.4. Parameter Identification of Ordinary Differential Equations using Gauss-Markov-Kalman Filter by Functional Approximation

The Gauss-Markov-Kalman filter approach using functional approximation is applied on the same problem as seen in Subsection 6.4.2 to estimate the state variables and the obtained results are compared with the results determined from the Subsection 6.4.2.

Example 6.2. ***Parameter Identification of Lorenz-1996 Model by Gauss-Markov-Kalman Filter using Functional Approximation***

The Gauss-Markov-Kalman filter is applied on the problem to estimate the state variables and functional approximation is employed to represent the random variables. The Hermite function introduced in Subsection 4.2.3 is considered for each of the 40 variables and only at the eighth time step an update is done. The updated distribution of the first 5 parameters and their comparison with estimated distribution obtained by ensemble Gauss-Markov-Kalman filter using polynomial chaos expansion are shown in Figure 6.4.

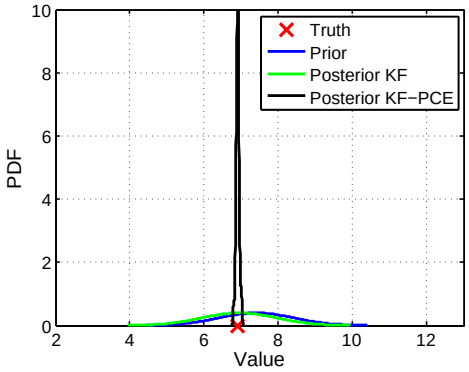

(a) 25th variable X_{25} update

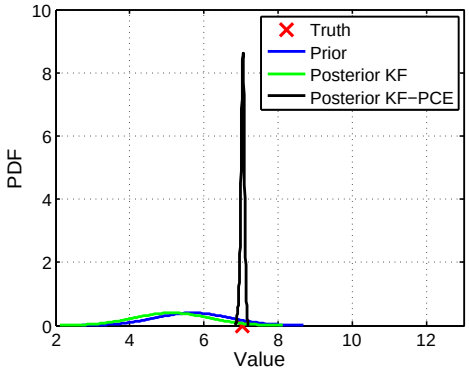

(b) 26th variable X_{26} update

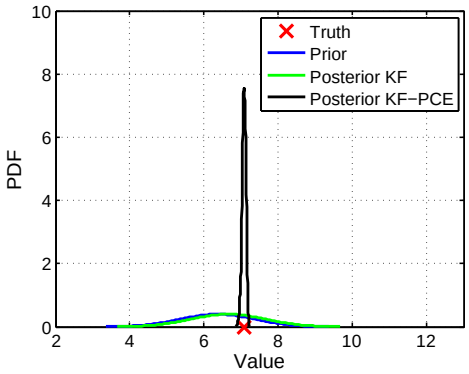

(c) 27th variable X_{27} update

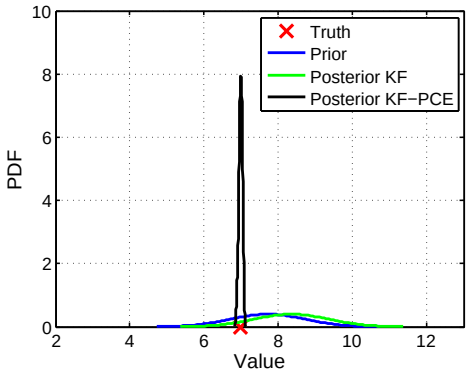

(d) 28th variable X_{28} update

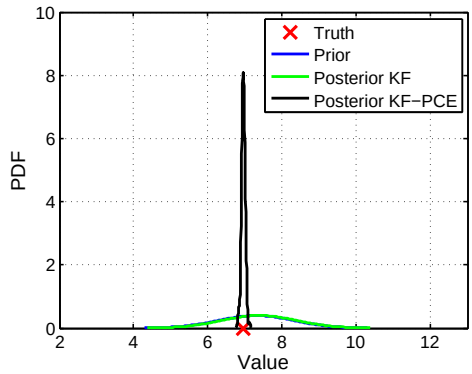

(e) 29th variable X_{29} update

Figure 6.4.: Updating the X_{25} to X_{29} variables of the model using GMKF by PCE at eighth Δt

It can be inferred from the Figure 6.4 that even in a short time the state variables of very high non-linear model can be estimated by using the Gauss-Markov-Kalman filter

by updating based on polynomial chaos approximation. The probability distributions of the state variables as shown in Figure 6.4 shrinks significantly after only one update, i.e. the updated distributions have a very little standard deviations and also the estimations of the true values are so close to them which indicates that the Gauss-Markov-Kalman filter using polynomial chaos expansion computes accurate results on a chaotic ODE system. It is also to be noted that the updated random variables obtained from the ensemble Gauss-Markov-Kalman filter using sampling after an update is compared with the Gauss-Markov-Kalman filter update based on polynomial chaos expansion. The distributions predicted by ensemble Gauss-Markov-Kalman filter using sampling have the mean values close to the true values. However, the width of distributions are not much narrowed. On comparing with the ensemble Gauss-Markov-Kalman filter using samples the Gauss-Markov-Kalman filter based on polynomial chaos expansion provides a better result in less computation time.

6.5. Conclusion

In this chapter a linear approximation of the conditional expectation is described in detail. The conditional expectation of the random variables and its relation to the Bayes's theorem is considered unlike Transitional Markov Chain Monte Carlo method as discussed in Chapter 5 where the samples of the posterior are generated. Indeed this approach is obtained by a direct projection of the linear conditional expectation. Accordingly, the Gauss-Markov-Kalman filter is extracted and it is introduced as an approach to solve the ill-posed problems probabilistically. Gauss-Markov-Kalman filter approach is applied on an ODE system to identify the states of the model using sampling and functional approximation approach where Hermite polynomial chaos expansion is employed and it is found out that the significant computational time difference can be observed between sampling and functional approximation approach. The efficiency of this method on the considered ODE system is approved and this method's validation will be evaluated in Chapter 7 on the desired mechanical material models as discussed in Chapter 3. The numerical results of this method on the mentioned material models for a well-known engineering test are explained in Chapter 8.

7. Bayesian Parameter Identification for Mechanical Material Models

The viscoplastic-damage model, forward and inverse model are fully discussed in previous chapters along with examples to clarify the concepts and its methods and ODE and PDE systems representing the capability of the studied stochastic approaches are verified. In this chapter, applicability of the Bayesian approaches on our desired viscoplastic model which is basically a system of PDE and ODEs are verified. Thereby the forward model of the considered viscoplastic model as in Subsection 3.1.1 is recalled and solved. Two main stochastic approaches are employed for inverse problem and the methods on our case study model are verified. The results of each approaches are fully discussed and the efficiency and accuracy of the methods are also studied. Finally, the suitable method for the most complicated model is selected with a valid reason and the effects of load path are discussed.

A step by step verification procedure is followed as lot of factors can have partial influence on identification of the model parameters in the Bayesian setting. A 3-dimensional element is considered for the verification. The methods for the elasticity and viscoplasticity are verified followed by verification of stochastic methods for viscoplasticity, isotropic and kinematic hardening, and finally the whole viscoplastic-damage model with the isotropic and kinematic hardening is verified. In this case, realizing the possible problem is much easier compared to identifying the model parameters from the most complicated model with a complex shape. Bayesian approaches, TMCMC and GMKF methods as in Chapter 5 and 6 respectively, are employed to solve the inverse problem in each case and they are discussed and compared in detail.

7.1. Validation Procedure for the Purely Elastic Model

In this section, the capability of the two Bayesian approaches discussed in the previous chapters are presented. The first approach is the Transitional Markov Chain Monte Carlo method and the other one is the Gauss-Markov-Kalman filter using the polynomial chaos expansion which will be applied on an elastic model. The forward model representing the considered elastic part of the model is summarized in the Table 7.1.

Table 7.1.: Forward model of Elasticity

Elastic strains $\dot{\tilde{\boldsymbol{\epsilon}}}_{el}(t,\omega) = \boldsymbol{C}^{-1}(\omega) : \dot{\tilde{\boldsymbol{\sigma}}}(t,\omega) \quad$ with $\quad \boldsymbol{C}\left(G(\omega), \kappa(\omega)\right)$
Initial conditions $\tilde{\boldsymbol{\epsilon}}_{el}(0) = \mathbf{0}$
Parameters $\kappa(\omega)$, $G(\omega)$ (elastic strains)

The only uncertain parameters, which are considered while elasticity model is the case, are the bulk modulus (κ) and the shear modulus (G). Hence the vector of unknown parameters is $\boldsymbol{q} = \left[\kappa(\omega), G(\omega)\right]$.

Preliminary study is on a regular cube, modeled with one 8 node element. The minimal number of freedoms that have to be constrained is six and many combinations are possible. As shown in Figure 7.1, all three degrees of freedom at point B are fixed. This prevents all rigid body translations, and leaves three rotations to be taken care of. The x displacement component at point A is constrained to prevent rotation about z, and the z component is fixed at point C to prevent rotation about y. The y component is constrained at point D to prevent rotation about x [209].

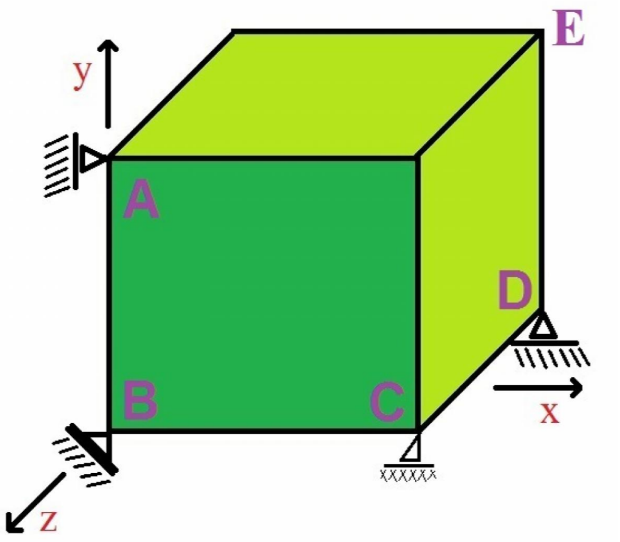

Figure 7.1.: Boundary condition considered

The normal tractions which is a Neumann boundary condition are applied cyclically in x, y and z directions on front and back faces and the magnitude of tractions in all directions are shown in Figure 7.2 where green, red and blue colors represent the stress values in x, y and z directions respectively.

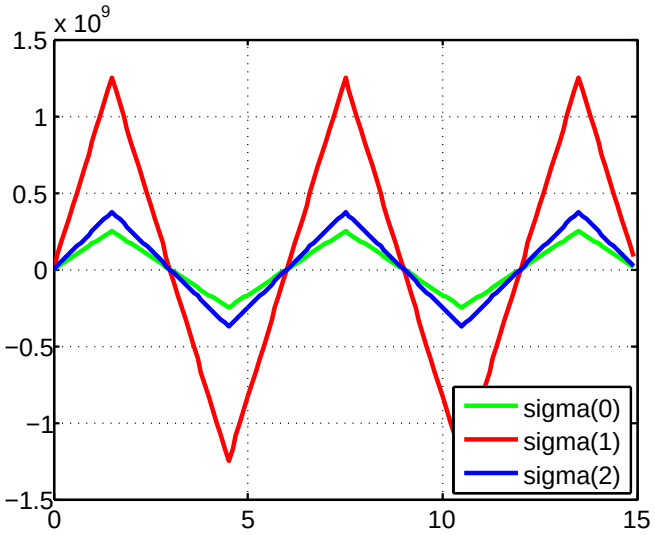

Figure 7.2.: Decomposed applied force at point E according to time

By considering the parameters listed in Table 7.2, for the top right corner node on back face, point E, as shown in Figure 7.1, the related displacement graph is obtained as shown in Figure 7.3 where green, red and blue colors represent the displacement of point E in x, y and z directions respectively.

Table 7.2.: The model parameters

κ	G	σ_y	n	k
1.66e9	7.69e8	1.7e9	1	1.5e8

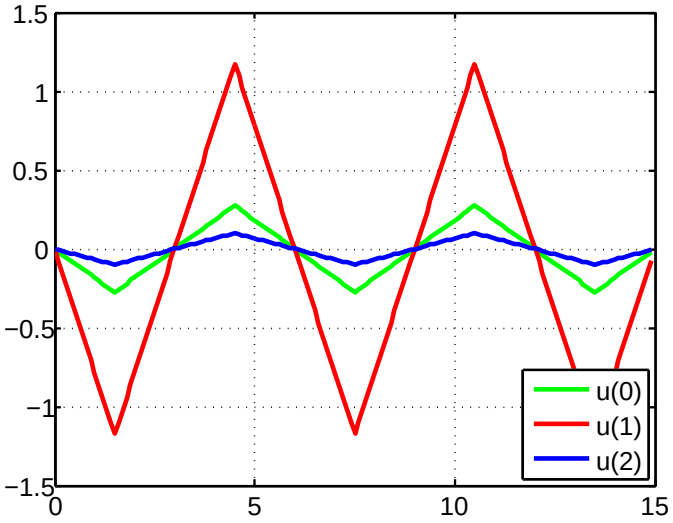

Figure 7.3.: Displacement of point E in x, y and z directions according to time

The displacements of point E in x, y and z directions are noted as the virtual data in this case.

7.1.1. TMCMC Method

The Transitional Markov chain Monte Carlo method is applied using sampling by which 1000 samples are generated and the history of the displacement of point E is noted. The determined prior and posterior probability density functions are compared and illustrated in Figure 7.4. It should be noted that the Burn-in period is considered as 200 in all iterations but in last iteration it is considered as 500. Further, the scaling parameter (β) in TMCMC is considered as 0.2. The initial prior of the material model parameters are defined as uniform distributions which literally means no pre-knowledge of them is considered, without any attention to the forward model. From the prior and posterior distributions of the bulk modulus (κ) and shear modulus (G), it is found that the model parameters are detected by using TMCMC. The obtained results are acceptable however it should be mentioned that the TMCMC method is a very time consuming approach particularly when the case study is a PDE system.

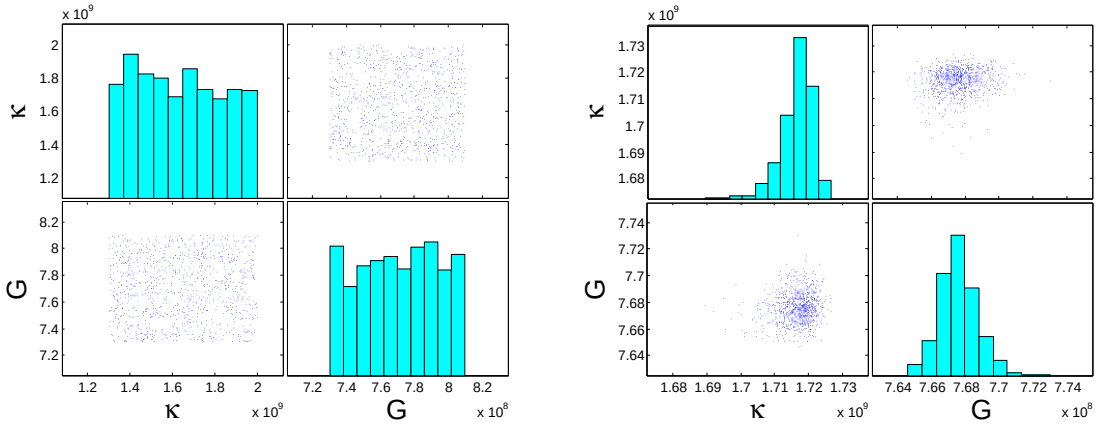

Figure 7.4.: PDF of identified parameters

The determined true values, the mean and standard deviation of the estimated parameters via TMCMC approach are shown in Table 7.3.

Table 7.3.: The identified model parameters

Parameters	$\boldsymbol{q}_{\text{true}}$	$\boldsymbol{q}_{\text{est}}$(mean)	$\boldsymbol{q}_{\text{est}}$(standard deviation)
κ	1.66e9	1.71e9	6.10e6
G	7.69e8	7.67e8	1.01e6

7.1.2. GMKF Approach

The Gauss-Markov-Kalman filter using the polynomial chaos expansion is applied here in two ways. In the first approach, the whole history of displacement is considered once to identify the model parameters and it is called as history matching updating as discussed in Subsection 6.3.2. In the second approach, the uncertain parameters are updated for several time steps and only on the interested time step which depends on the need the displacement is considered. This approach is called sequential updating as presented in Subsection 6.3.3. The results from both these approaches are discussed in the next subsections.

Hermite function in form of polynomial chaos expansion is employed instead of samples. The uncertain parameters and output displacement are introduced as an ansatz.

$$\kappa(\omega) = \sum_{\alpha} \kappa^{(\alpha)} H_\alpha(\boldsymbol{\theta}(\omega)) \tag{7.1a}$$

$$G(\omega) = \sum_{\alpha} G^{(\alpha)} H_\alpha(\boldsymbol{\theta}(\omega)) \tag{7.1b}$$

$$u(x,\omega) = \sum_{\alpha} u^{(\alpha)}(x) H_\alpha(\boldsymbol{\theta}(\omega)) \tag{7.1c}$$

The Gaussian standard random variables are represented by $\boldsymbol{\theta}(\omega)$ and the Hermite function is represented by H_α as given in Equation 7.1a, 7.1b and 7.1c. The coefficients of bulk modulus and shear modulus which are described through random variables are not dependent of the position and coefficients of displacement which are also described through random variables are the function of position. These coefficients are computed as discussed in Subsection 4.3.2.

The forward model of elasticity is solved by using stochastic collocation approach as discussed in Subsection 4.3.2 where the different order of Hermite function (α) and different number of samples are considered. Thereby the relative error (e) is determined according to the Equation 7.2 where u^α represents the displacement calculated from the forward model with different number of samples and order of the Hermite function and u^α_{5000} is the displacement obtained by considering 5000 samples for the related order of Hermite function. It should be noted that the displacement in y direction is considered. The computed relative error of mean and standard deviation are shown in Figure 7.5 by using a base 10 logarithmic scale for the y-axis.

$$e = \frac{||u^\alpha - u^\alpha_{5000}||}{||u^\alpha_{5000}||} \tag{7.2}$$

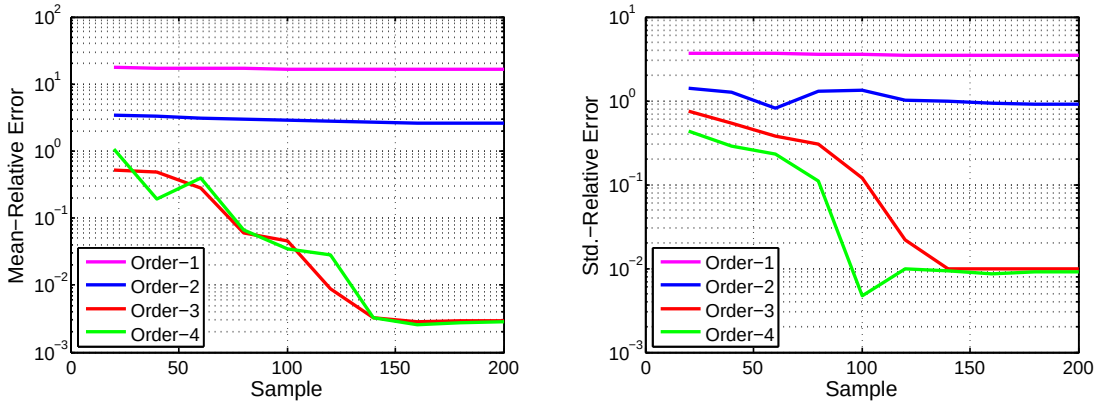

Figure 7.5.: Mean and standard deviation relative error by number of samples

Figure 7.5 indicates that the relative error of the mean and standard deviation decreases as the number of samples and order increases. It is also inferred from the Figure 7.5 that the same value of error is observed for the third and fourth order Hermite function after some certain of samples' number. Therefore, a balance between the computational cost and the accuracy of results is achieved by considering a third order of Hermite function and 180 samples as the basis of Hermite function for the computation of forward problem. Further the relative error stays constant for the considered third order Hermite function.

7.1.2.1. History Matching Updating

The prior and posterior probability density functions of the identified parameters as shown in Figure 7.6 are obtained by applying GMKF approach using functional approximation as discussed in Subsection 6.3.2. The whole time interval is considered and updated only once by comparing the predicted value with the recorded displacement history.

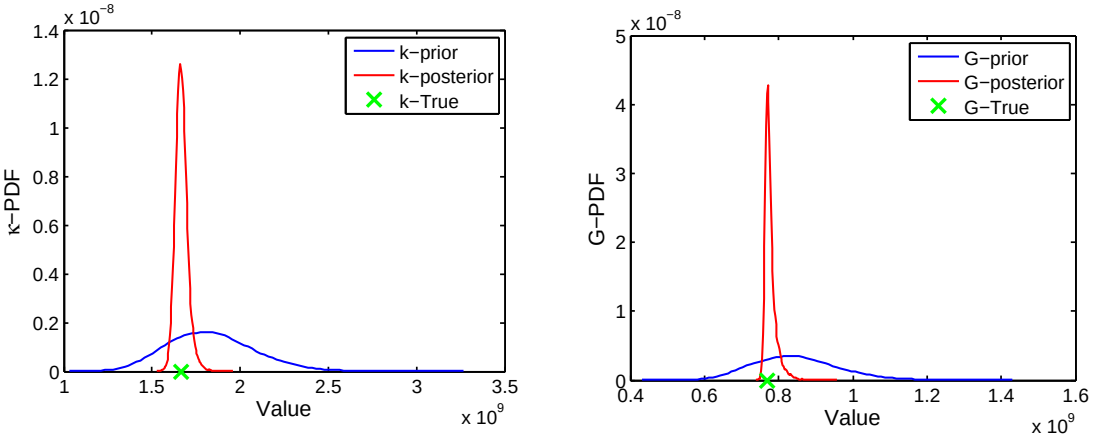

Figure 7.6.: PDF of identified parameters

The enough information from the virtual data is caught in the whole process and it is concluded from the sharpness of the posterior PDF of the bulk modulus (κ) and shear modulus (G). From the posterior distributions of parameters, it is concluded that updating the parameters by using the history matching updating of GMKF approach is possible in this case.

The summarized results are shown in Table 7.4, where the true values, mean and variance of the estimated parameters via history matching updating are compared.

Table 7.4.: The identified model parameters

Parameters	$\boldsymbol{q}_{\text{true}}$	$\boldsymbol{q}_{\text{est}}$(mean)	$\boldsymbol{q}_{\text{est}}$(standard deviation)
κ	1.66e9	1.66e9	3.52e7
G	7.69e8	7.77e8	1.63e7

7.1.2.2. Sequential Updating

The prior and posterior probability density functions of the identified parameters as shown in Figure 7.7 are obtained by GMKF approach using functional approximation as discussed in Subsection 6.3.3. The parameters are updated several times by comparing the measured displacement with the prediction.

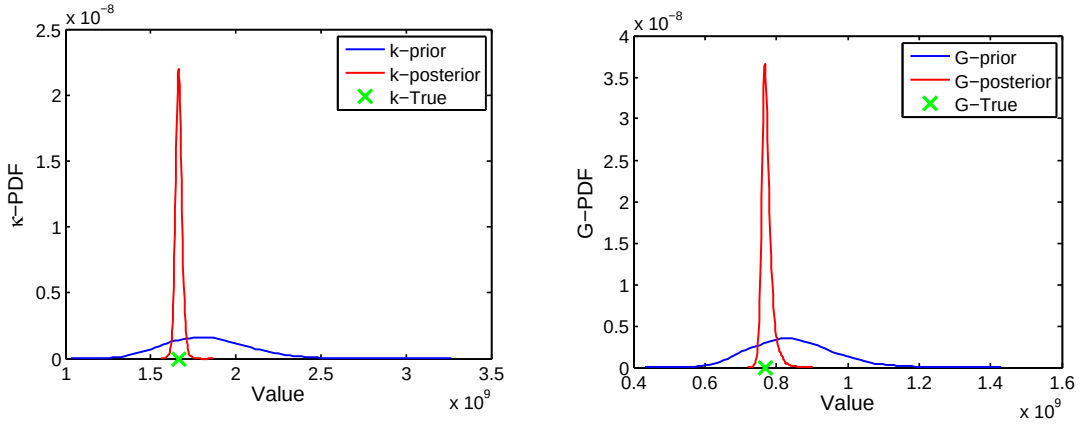

Figure 7.7.: PDF of identified parameters

The enough information from the virtual data is caught in the whole process and it is concluded from the sharpness of the posterior PDF of the bulk modulus (κ) and shear modulus (G). From the posterior distributions of parameters, it is concluded that updating the parameters by employing sequential updating of GMKF approach is not a tough task in this case.

The summarized true values of the parameters, mean and variance of the estimated parameters via sequential updating are shown in Table 7.5.

Table 7.5.: The identified model parameters

Parameters	$\boldsymbol{q}_{\text{true}}$	$\boldsymbol{q}_{\text{est}}$(mean)	$\boldsymbol{q}_{\text{est}}$(standard deviation)
κ	1.66e9	1.66e9	1.99e7
G	7.69e8	7.73e8	1.55e7

7.1.3. Discussion and Comparison

It should be noted that these two main methods could not be compared. The Transitional Markov Chain Monte Carlo method generates the samples of the posterior distribution of the parameters while the Gauss-Markov-Kalman filter approach evaluates the posterior random variables. Further, the initial prior considered in these methods are different. Generally the uniform distributions representing the initial prior distributions considered for Transitional Markov Chain Monte Carlo method are narrower than the distribution of random variables in Gauss-Markov-Kalman filter approach as Transitional Markov Chain Monte Carlo method needed significantly much more time of calculation and therefore by considering the narrower distributions the cost of calculation is reduced. Considering this fact in the following only the estimated values of both approaches are discussed.

By observing the results from the two main approaches, it can be concluded Transitional Markov Chain Monte Carlo and Gauss-Markov-Kalman filter method provide accurate result and identify the uncertain parameters for the elasticity model properly. The difference between results of the Transitional Markov Chain Monte Carlo method and Gauss-Markov-Kalman filter method is that the uncertainty of the parameters are reduced in a more proper way via Transitional Markov Chain Monte Carlo than Gauss-Markov-Kalman filter method as the results of Transitional Markov Chain Monte Carlo show smaller values of standard deviation for uncertain parameters. This might be due to considering the narrower initial prior of parameters for Transitional Markov Chain Monte Carlo method than Gauss-Markov-Kalman filter.

Although the elasticity case is a linear case, little difference in results is observed between the history updating and sequential updating of Gauss-Markov-Kalman filter approach. As in the sequential Gauss-Markov-Kalman filter after each update the computations are done from the initial time step with the updated parameters, i.e. the calculations start from the beginning with a new set of samples. Therefore the information obtained is at least a few times more than the history updating of Gauss-Markov-Kalman filter approach which leads to a little bit better identification via sequential Gauss-Markov-Kalman filter even for the elasticity model as a linear case. It is also to be noted that the computation time of Transitional Markov Chain Monte Carlo is significantly higher than the other approach. For the sequential updating of the Gauss-Markov-Kalman filter approach the computational time is slightly more than the history matching update

approach as the multiple updating is performed.

7.2. Validation Procedure for the Viscoplasticity Model

Similar to the validation of the elastic model, the Transitional Markov Chain Monte Carlo method and Gauss-Markov-Kalman filter using the polynomial chaos expansion are applied on a viscoplasticity model without considering the isotropic and kinematic hardening behavior. The forward model representing the considered viscoplasticity model is summarized in the Table 7.6.

Table 7.6.: Forward model of viscoplasticity

Elastic strains $\dot{\tilde{\boldsymbol{\epsilon}}}_{el}(t,\omega) = \boldsymbol{C}^{-1}(\omega) : \dot{\tilde{\boldsymbol{\sigma}}}(t,\omega) \quad \text{with} \quad \boldsymbol{C}\left(G(\omega), \kappa(\omega)\right)$
Viscoplastic strains $\dot{\tilde{\boldsymbol{\epsilon}}}_{vp}(t,\omega) = \left\langle \frac{\tilde{\sigma}_{eq}(t,\omega) - \sigma_y(\omega)}{k} \right\rangle^n \frac{\partial \tilde{\sigma}_{ex}}{\partial \tilde{\boldsymbol{\sigma}}}$
Parameters $G(\omega)$, $\kappa(\omega)$, (elastic strains) $\sigma_y(\omega)$ (viscoplastic strains)

The uncertain parameters here are bulk modulus (κ), shear modulus (G) and the yield stress (σ_y). Hence the vector of unknown parameters is $\boldsymbol{q} = \left[\kappa(\omega),\, G(\omega),\, \sigma_y(\omega)\right]$.

Similar to the elastic model, preliminary study is on a regular cube, modeled with one 8 node element as shown in Figure 7.1 in Section 7.1. Similarly the same Dirichlet boundary condition is considered. Also the same tractions which is a Neumann boundary condition are applied cyclically in x, y and z directions on front and back faces and the magnitude of tractions in all directions are shown in Figure 7.8 where green, red and blue colors represent the stress values in x, y and z directions respectively.

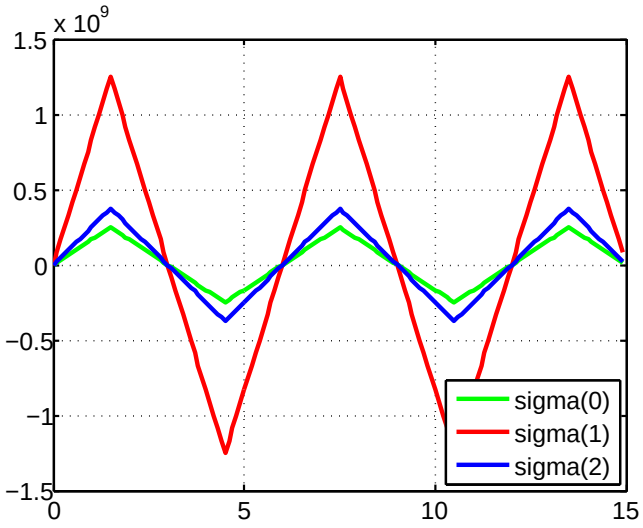

Figure 7.8.: Decomposed applied force at point E according to time

By considering the parameters listed in Table 7.7, for the top right corner node on back face, point E, as shown in Figure 7.1, the related displacement graph is obtained as shown in Figure 7.9 where green, red and blue colors represent the displacement of point E in x, y and z directions respectively.

Table 7.7.: The model parameters

κ	G	σ_y	n	k
1.66e9	7.69e8	1.7e8	1	1.5e8

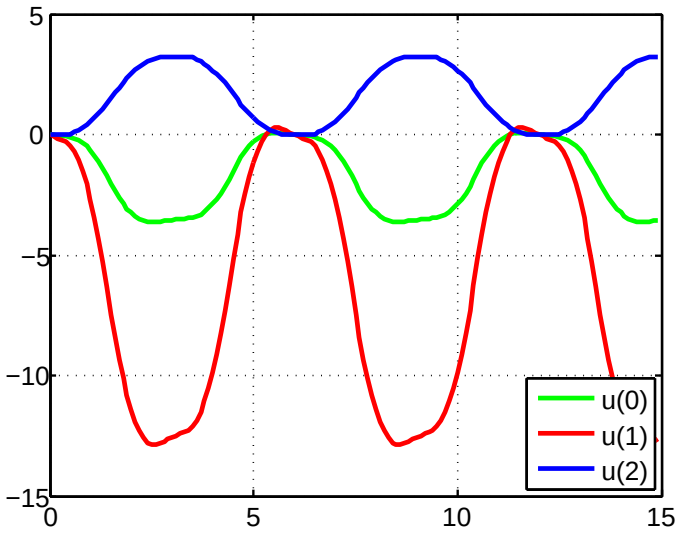

Figure 7.9.: Displacement of point E in x, y and z directions according to time

The displacements of point E in x, y and z directions are noted as the virtual data in this case.

7.2.1. TMCMC Method

Similar to the elastic model, by applying the Transitional Markov Chain Monte Carlo method using sampling, the prior and posterior probability density functions are obtained. The probability density functions are compared and illustrated in Figure 7.10. As discussed in the Subsection 7.1.1, similar number of samples, Burn-in period and scaling parameter (β) are applied. The displacement history is also observed as the data measurement. The uniform distributions are considered to represent the initial prior of model parameters. TMCMC method is used to estimate the model parameters, i.e. the bulk modulus (κ), shear modulus (G) and the yield stress (σ_y) where the amount of these estimations can be inferred by comparing the prior and posterior distributions of the parameters with their true values. The determined results are fair but it is also to be noted that the TMCMC method is a very time consuming approach for such a system.

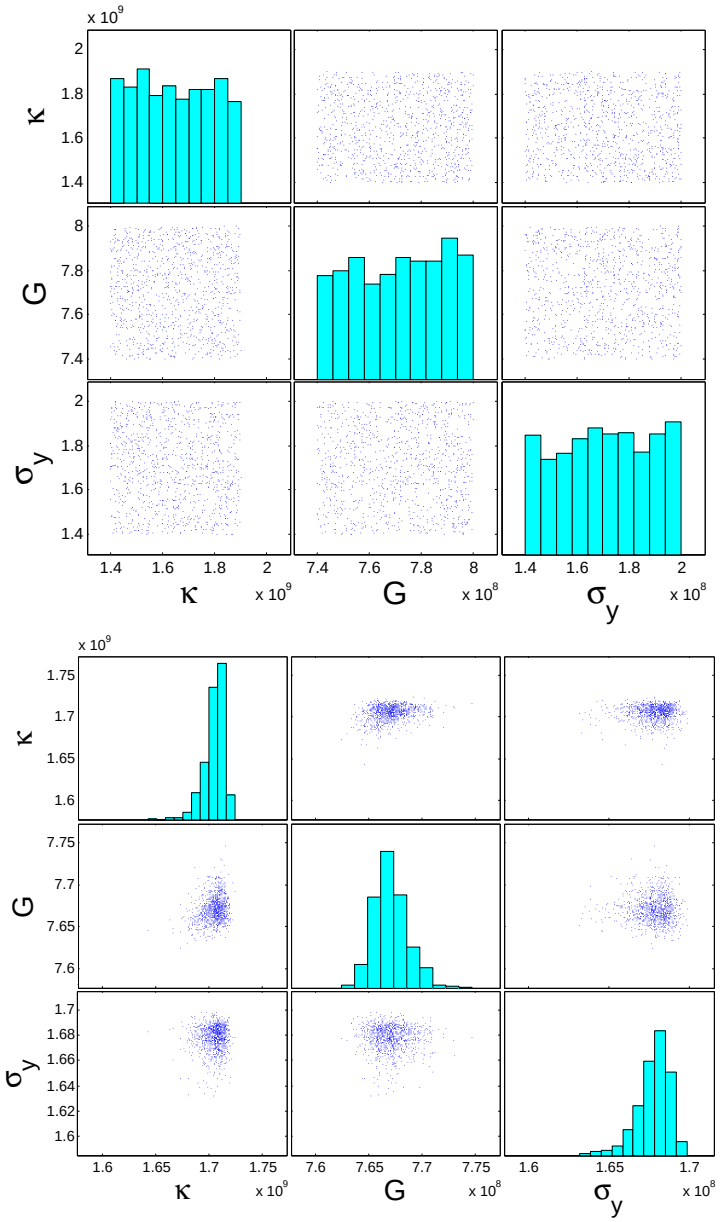

Figure 7.10.: PDF of identified parameters

The determined true values, the mean and standard deviation of the estimated parameters via TMCMC are shown in Table 7.8.

Table 7.8.: The identified model parameters

Parameters	$\boldsymbol{q}_{\text{true}}$	$\boldsymbol{q}_{\text{est}}$(mean)	$\boldsymbol{q}_{\text{est}}$(standard deviation)
κ	1.66e9	1.70e9	9.17e6
G	7.69e8	7.67e8	1.55e6
σ_y	1.7e8	1.68e8	1.02e6

7.2.2. GMKF Approach

The application of Gauss-Markov-Kalman filter using the polynomial chaos expansion and its approaches are discussed in Subsection 7.1.2. The results from both these approaches for the viscoplasticity model are discussed in the Subsection 7.2.2.1 and 7.2.2.2.

Similar to the elastic model, Hermite function in form of polynomial chaos expansion is employed instead of samples. Similarly, the uncertain parameters and output displacement are introduced as an ansatz. The coefficients of the bulk modulus, shear modulus, yield stress and displacement are also computed as discussed in Subsection 4.3.2.

Similar to forward model of elasticity as discussed in Subsection 7.1.2, a third order Hermite function and 180 samples as the Hermite functions basis are considered in order to solve the forward model using stochastic collocation approach as discussed in Subsection 4.3.2.

7.2.2.1. History Matching Updating

Similar to history matching updating method applied in Subsection 7.1.2.1, the prior and posterior probability density functions of the identified parameters are shown in Figure 7.11 and characteristics of probability density functions are similar to elastic model.

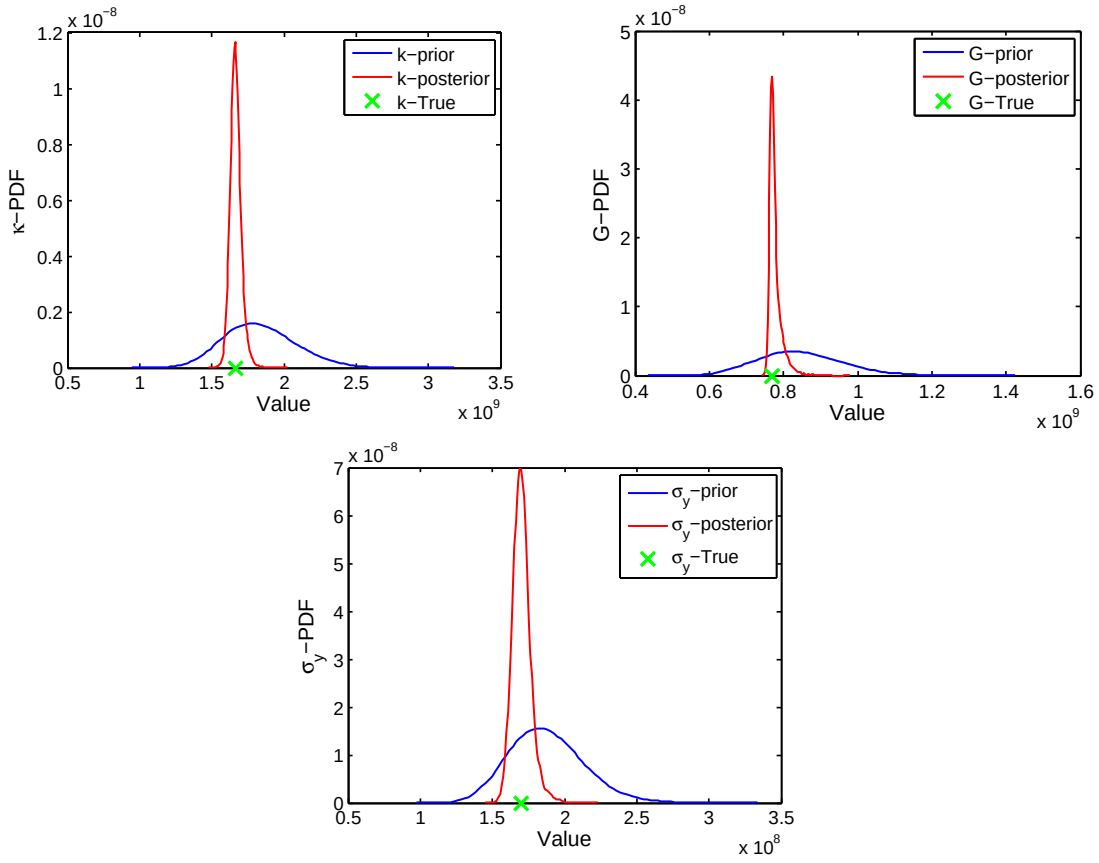

Figure 7.11.: PDF of identified parameters

It is determined from the sharpness of the posterior PDF of the bulk modulus (κ), shear modulus (G) and yield stress (σ_y) that enough information from the virtual data is considered in the whole process. The parameters are updated correctly by applying the history matching update method as it can be seen from the prior and posterior distributions of uncertain parameters and related true values as shown in Figure 7.11.

The comparison of the true values, mean and variance of the estimated uncertain parameters via GMKF approach in history matching updating method are summarized in Table 7.9.

Table 7.9.: The identified model parameters

Parameters	$\boldsymbol{q}_{\text{true}}$	$\boldsymbol{q}_{\text{est}}$(mean)	$\boldsymbol{q}_{\text{est}}$(standard deviation)
κ	1.66e9	1.66e9	3.97e7
G	7.69e8	7.77e8	1.72e7
σ_y	1.7e8	1.7e8	6.39e6

7.2.2.2. Sequential Updating

Similar to sequential updating method in elastic model in Subsection 7.1.2.2, the prior and posterior probability density functions of the identified parameters are shown in Figure 7.12 and characteristics of probability distribution functions are similar to elastic model.

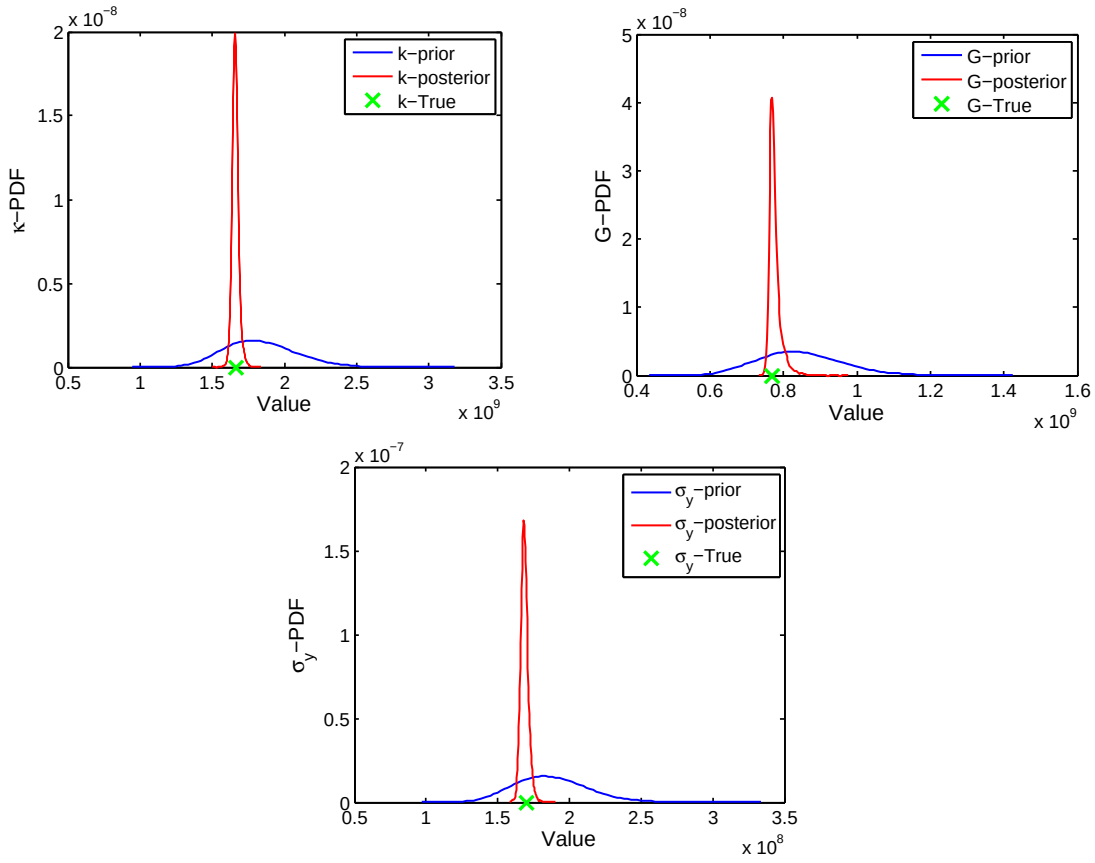

Figure 7.12.: PDF of identified parameters

It is concluded from the sharpness of the posterior PDF of the bulk modulus (κ), shear modulus (G) and yield stress (σ_y) that the enough information from the virtual data is caught in the whole process. From the distributions of parameters and their true values in Figure 7.12, it is concluded that the parameters are updated properly in this case by applying sequential updating approach.

The summarized true values of the parameters, mean and variance of the estimated parameters via GMKF method in sequential updating manner for the viscoplastic model are shown in Table 7.10.

Table 7.10.: The identified model parameters

Parameters	$\boldsymbol{q}_{\text{true}}$	$\boldsymbol{q}_{\text{est}}$(mean)	$\boldsymbol{q}_{\text{est}}$(standard deviation)
κ	1.66e9	1.66e9	2.26e7
G	7.69e8	7.76e8	1.64e7
σ_y	1.7e8	1.69e8	2.66e6

7.2.3. Discussion and Comparison

It can be concluded by comparing the results of the two main approaches that the Transitional Markov Chain Monte Carlo method and Gauss-Markov-Kalman filter method provide accurate result and identify the parameters for the viscoplasticity model. There is no much difference in the results of the standard deviation of the uncertain parameters between these two methods for the viscoplasticity model. Each of the both Gauss-Markov-Kalman filter approaches provides almost the same amount of update for each considered uncertain parameters as the influence of each of these uncertain parameters is almost same on the output measured displacement. The other point to mention is that the uncertainty of the parameters determined using the sequential updating of Gauss-Markov-Kalman filter approach is reduced a little bit more and hence the narrower distributions of the parameters can be seen in comparison with the history matching of Gauss-Markov-Kalman filter approach. This is because after each update the computations are evaluated from the beginning with new set of samples and therefore more information are observed which leads to a better reduction of uncertainty of the parameters in sequential Gauss-Markov-Kalman filter approach. The computational time for the sequential updating of the Gauss-Markov-Kalman filter approach is slightly more than the history matching update approach as multiple updating is performed for the sequential updating of the Gauss-Markov-Kalman filter approach. It should also be noted that the computation time of Transitional Markov Chain Monte Carlo method is significantly higher than the other approach.

7.3. Validation Procedure for Viscoplasticity Model with Isotropic and Kinematic Hardening Behavior

Similar to the validation of the elastic model and viscoplasticity model, the Transitional Markov Chain Monte Carlo method and Gauss-Markov-Kalman filter using the polynomial chaos expansion are applied on a viscoplastic model considering both the isotropic and kinematic hardening behavior. The forward model representing the considered viscoplastic model with hardening is summarized in the Table 7.11.

Table 7.11.: Forward model of viscoplasticity with isotropic and kinematic hardening

Elastic strains

$$\dot{\tilde{\boldsymbol{\epsilon}}}_{el}(t,\omega) = \boldsymbol{C}^{-1}(\omega) : \dot{\tilde{\boldsymbol{\sigma}}}(t,\omega) \qquad \text{with} \qquad \boldsymbol{C}\left(G(\omega), \kappa(\omega)\right)$$

Viscoplastic strains

$$\dot{\tilde{\boldsymbol{\epsilon}}}_{vp}(t,\omega) = \left\langle \frac{\tilde{\sigma}_{eq}(t,\omega) - \sigma_y(\omega) - R(t,\omega)}{k} \right\rangle^n \frac{\partial \tilde{\sigma}_{ex}}{\partial \tilde{\boldsymbol{\sigma}}}$$

Isotropic and kinematic hardening

$$\dot{R}(t,\omega) = b_R(\omega)\left(H_R - R\right)\dot{p}$$

$$\dot{\boldsymbol{\chi}}(t,\omega) = b_{\boldsymbol{\chi}}(\omega)\left(\frac{2}{3}H_{\boldsymbol{\chi}}\frac{\partial \tilde{\sigma}_{eq}}{\partial \tilde{\boldsymbol{\sigma}}} - \boldsymbol{\chi}\right)\dot{p}$$

Initial conditions

$$\tilde{\boldsymbol{\epsilon}}_{el}(0) = \mathbf{0}, \quad \tilde{\boldsymbol{\epsilon}}_{vp}(0) = \mathbf{0}, \quad R(0) = 0 \text{ and } \boldsymbol{\chi}(0) = \mathbf{0}$$

Parameters

$G(\omega)$, $\kappa(\omega)$,	(elastic strains)
$\sigma_y(\omega)$,	(viscoplastic strains)
$b_R(\omega)$, $b_{\boldsymbol{\chi}}(\omega)$	(hardenings)

The parameters which are set as the uncertain parameters are bulk modulus (κ), shear modulus (G), the isotropic hardening coefficient (b_R), the kinematic hardening coefficient (b_χ) and the yield stress (σ_y). Hence the vector of unknown parameters is $\boldsymbol{q} = \left[\kappa(\omega),\, G(\omega),\, b_R(\omega),\, b_\chi(\omega),\, \sigma_y(\omega)\right]$.

Similar to the elastic model and viscoplasticity model, preliminary study is on a regular cube, modeled with one 8 node element as shown in Figure 7.1 in Section 7.1. Similarly the same Dirichlet boundary condition is considered. Also the same tractions which is a Neumann boundary condition are applied cyclically in x, y and z directions on front and back faces and the magnitude of tractions in all directions are shown in Figure 7.13

where green, red and blue colors represent the stress values in x, y and z directions respectively.

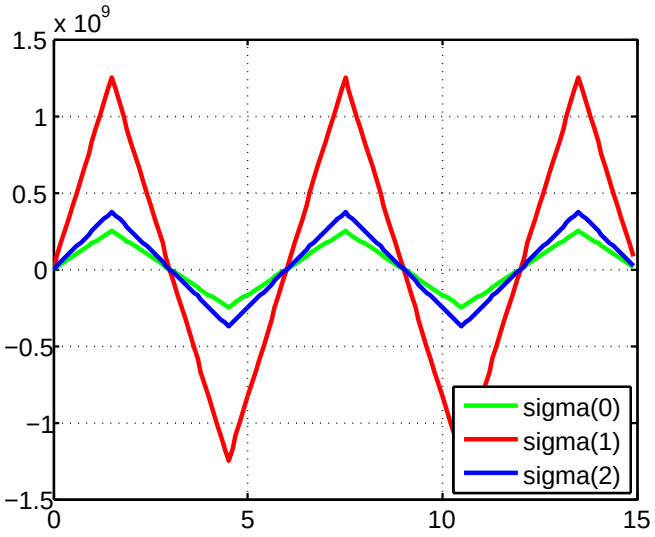

Figure 7.13.: Decomposed applied force at point E according to time

For the top right corner node on back face represented by point E as shown in Figure 7.1, the related displacement graph is obtained as shown in Figure 7.14 where green, red and blue colors represent the displacement of point E in x, y and z directions respectively by considering the parameters listed in Table 7.12.

Table 7.12.: The model parameters

κ	G	σ_y	n	k	b_R	H_R	b_χ	H_χ
1.66e9	7.69e8	1.7e8	1	1.5e8	50	2.75e8	50	2.75e8

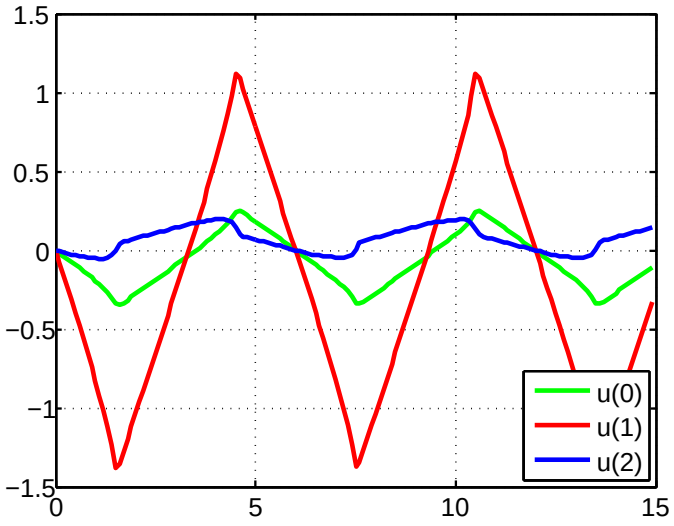

Figure 7.14.: Displacement of point E in x, y and z directions according to time

Again the displacements of point E in x, y and z directions are noted as the virtual data in this case.

7.3.1. TMCMC Method

Similar to the elastic model and viscoplasticity model as discussed in Subsection 7.1.1 and 7.2.1, Figure 7.15 compares and illustrates the determined prior and posterior probability density functions of the parameters such as bulk modulus (κ), shear modulus (G), the isotropic hardening coefficient (b_R), the kinematic hardening coefficient (b_χ) and the yield stress (σ_y) which are obtained by applying the Transitional Markov chain Monte Carlo method using sampling. For viscoplastic model with hardening, the similar number of samples, Burn-in period and scaling parameter (β) are applied similar to the Subsection 7.1.1 and 7.2.1. Also, uniform distributions are again considered to represent the initial prior of model parameters. Further, uniform distributions are considered again to represent the initial prior of model parameters. It is found that the model parameters are updated at first step by using TMCMC approach. The obtained results are acceptable however it should be mentioned that the TMCMC method is a very time consuming approach for such a PDE system.

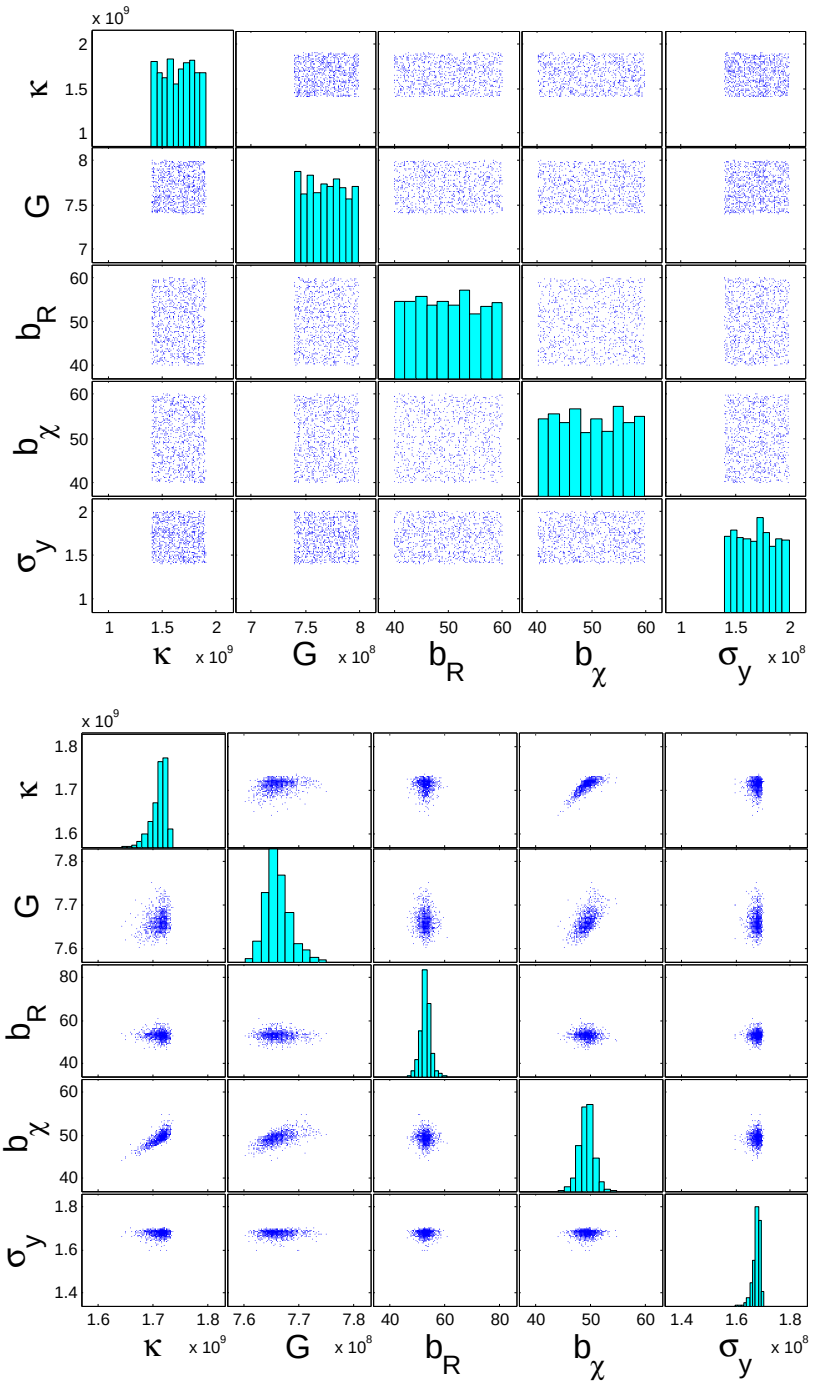

Figure 7.15.: PDF of estimated parameters

The determined true values, the mean and standard deviation of the estimated parameters via TMCMC are shown in Table 7.13.

Table 7.13.: The identified model parameters

Parameters	$\boldsymbol{q}_{\text{true}}$	$\boldsymbol{q}_{\text{est}}$(mean)	$\boldsymbol{q}_{\text{est}}$(standard deviation)
κ	1.66e9	1.71e9	1.33e7
G	7.69e8	7.66e8	2.24e6
b_R	50	53.00	1.83
b_χ	50	49.30	1.32
σ_y	1.7e8	1.67e8	1.37e6

7.3.2. GMKF Approach

The application of Gauss-Markov-Kalman filter using the polynomial chaos expansion is discussed in Subsection 7.1.2 and 7.2.2. The results from both these approaches for the viscoplasticity model with isotropic and kinematic hardening behavior are discussed in the next subsections.

Similar to the elastic model and viscoplasticity model, Hermite function in form of polynomial chaos expansion is employed instead of samples. Similarly the uncertain parameters and output displacement are introduced as an ansatz. The coefficients of the bulk modulus, shear modulus, isotropic and kinematic hardening parameters, yield stress and displacement are also computed as discussed in Subsection 4.3.2.

The relative error of the viscoplasticity forward model with isotropic and kinematic hardening is determined based on the Equation 7.2 with the assumptions described as in Subsection 7.1.2 and 7.2.2. The stochastic collocation approach as discussed in Subsection 4.3.2 is applied to solve the forward problem by considering the different order of Hermite function and different number of samples. The computed relative error of mean and standard deviation are shown in Figure 7.16 by using a base 10 logarithmic scale for the y-axis.

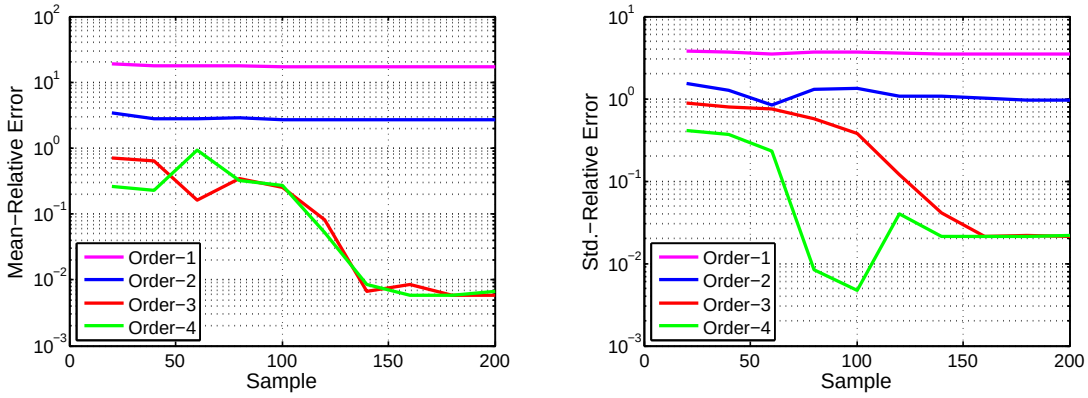

Figure 7.16.: Mean and standard deviation relative error by number of samples

Figure 7.16 indicate that the relative error of the mean and standard deviation decreases as the number of samples increases and the order of Hermite function increases. It can also be inferred from Figure 7.16 that the same value of error is obtained for the third and fourth order Hermite function after a certain number of samples. Therefore, a balance between the cost of calculation and accuracy of the results are achieved by considering the third order Hermite function and 200 samples as the basis of the Hermite function. Further the relative error is constant for the mentioned number of samples of the third order Hermite function.

7.3.2.1. History Matching Updating

Similar to history matching updating method discussed in Subsection 7.1.2.1 and 7.2.2.1 the prior and posterior probability density functions of the identified parameters are shown in Figure 7.17 and characteristics of probability density functions are similar to elastic model and viscoplasticity model.

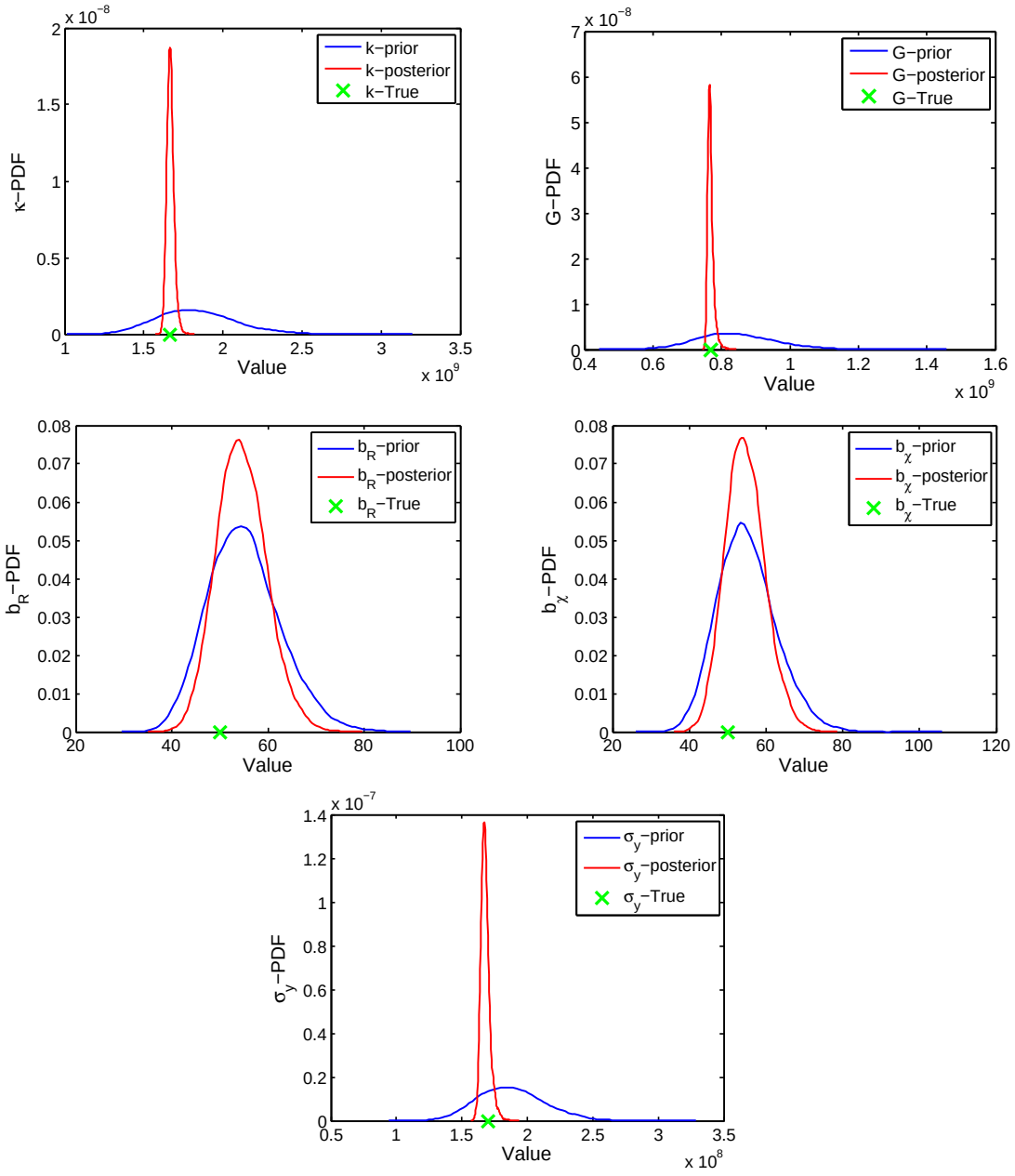

Figure 7.17.: PDF of identified parameters

Considering the sharpness of the posterior probability density functions of bulk modulus (κ), shear modulus (G) and yield stress (σ_y), these uncertain parameters are updated much easier than the hardening parameters, the isotropic hardening coefficient (b_R) and the kinematic hardening coefficient (b_χ). This is because that the process was not always in the states that the hardening equations are involved. Reminding this fact that

hardening equations are only involved when the process is in the plastic states. Hence the less information is available from the whole simulation to estimate the hardening parameters and with this information the hardening parameters are updated but not as much as rest of the parameters.

The summarized identification results for the viscoplasticity with isotropic and kinematic hardening behavior via GMKF approach in history matching updating manner are shown in Table 7.14.

Table 7.14.: The identified model parameters

Parameters	$\boldsymbol{q}_{\text{true}}$	$\boldsymbol{q}_{\text{est}}$(mean)	$\boldsymbol{q}_{\text{est}}$(standard deviation)
κ	1.66e9	1.66e9	2.28e7
G	7.69e8	7.68e8	9.09e6
b_R	50	54.78	5.16
b_χ	50	54.58	5.15
σ_y	1.7e8	1.67e8	3.48e6

7.3.2.2. Sequential Updating

Similar to sequential updating method discussed in Subsection 7.1.2.2 and 7.2.2.2, Figure 7.18 represents the prior and posterior probability density functions of the identified parameters. The determined characteristics of the probability density functions are similar to elastic and viscoplasticity model.

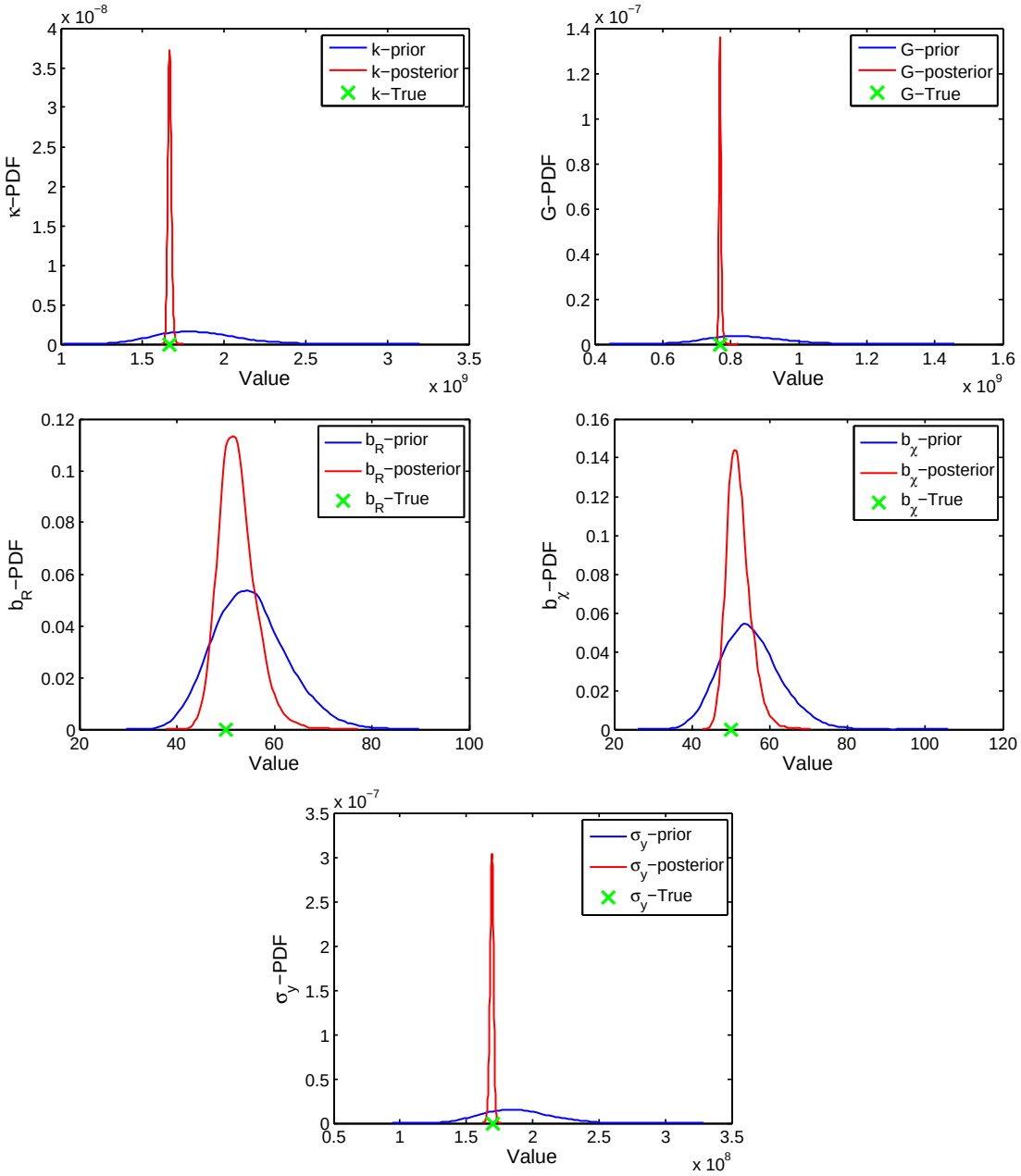

Figure 7.18.: PDF of identified parameters

Owing to reason provided in the history matching updating of GMKF method discussed in Subsection 7.3.2.1, the hardening parameters are updated but not as much as the rest of the parameters using sequential updating.

The summarized true values of the parameters, mean and variance of the estimated pa-

rameters via GMKF method in sequential updating manner for the viscoplastic model enriched with isotropic and kinematic hardening behavior are shown in Table 7.15.

Table 7.15.: The identified model parameters

Parameters	$\boldsymbol{q}_{\text{true}}$	$\boldsymbol{q}_{\text{est}}$(mean)	$\boldsymbol{q}_{\text{est}}$(standard deviation)
κ	1.66e9	1.66e9	1.12e7
G	7.69e8	7.68e8	3.46e6
b_R	50	52.38	3.74
b_χ	50	52.05	3.04
σ_y	1.7e8	1.69e8	1.36e6

7.3.3. Discussion and Comparison

By comparing the results from the two main approaches that it can be concluded Transitional Markov Chain Monte Carlo and Gauss-Markov-Kalman filter method provide accurate result and identify the known parameters for the viscoplasticity model with isotropic and kinematic hardening behavior except in the history matching update approach as the Gauss-Markov-Kalman filter method for the hardening parameters are not as narrow as the rest of parameter's distributions as shown in Figure 7.17. This is because the hardening parameters have no direct and strong influence on the measured displacement and so the uncertainty are not reduced good enough than rest of the parameters as there is no enough information. As the other reason it can be mentioned that updating is done only one time when history matching Gauss-Markov-Kalman filter is applied and hence the posterior distributions of hardening parameters are not as narrow as when sequential Gauss-Markov-Kalman filter is employed. In addition, as the computations are evaluated from the initial time step after each update in the sequential Gauss-Markov-Kalman filter, more information is recorded in total. Therefore, better identification and reduction of uncertainty can be obtained in comparison with history matching Gauss-Markov-Kalman filter.

There is not much difference between the standard deviation of the uncertain parameters between Transitional Markov Chain Monte Carlo approach and Gauss-Markov-Kalman filter approach for sequential updating of viscoplasticity with isotropic and kinematic hardening behavior. It should also be noted that the Transitional Markov Chain Monte Carlo method computational time is significantly higher than the other approach. The computational time is more in the Gauss-Markov-Kalman filter approach as multiple updating is involved in the sequential updating of Gauss-Markov-Kalman filter approach.

As Transitional Markov Chain Monte Carlo approach which is applied on viscoplasticity model with isotropic and kinematic hardening is computationally too much expen-

sive, Gauss-Markov-Kalman filter method is only considered for the viscoplastic-damage model in Section 7.4 and further.

7.4. Validation Procedure on Viscoplastic-Damage Model with Isotropic and Kinematic Hardening

In this section the capability of only one of the Bayesian approaches discussed in the previous sections is studied. Gauss-Markov-Kalman filter using the polynomial chaos expansion is applied on a viscoplastic-damage model with both the isotropic and kinematic hardening behavior. The forward model representing the considered viscoplastic-damage model with both hardening is summarized in the Table 7.16.

Table 7.16.: Forward model of viscoplasticity-damage with isotropic and kinematic hardening

Elastic strains

$$\dot{\tilde{\boldsymbol{\epsilon}}}_{el}(t,\omega) = \boldsymbol{C}^{-1}(\omega) : \dot{\tilde{\boldsymbol{\sigma}}}(t,\omega) \qquad \text{with} \qquad \boldsymbol{C}\left(G(\omega), \kappa(\omega)\right)$$

Viscoplastic strains

$$\dot{\tilde{\boldsymbol{\epsilon}}}_{vp}(t,\omega) = \left\langle \frac{\tilde{\sigma}_{eq}(t,\omega) - \sigma_y(\omega) - R(t,\omega)}{k} \right\rangle^n \frac{\partial \tilde{\sigma}_{ex}}{\partial \tilde{\boldsymbol{\sigma}}}$$

Isotropic and kinematic hardening

$$\dot{R}(t,\omega) = b_R(\omega)\left(H_R - R\right)\dot{p}$$

$$\dot{\boldsymbol{\chi}}(t,\omega) = b_{\boldsymbol{\chi}}(\omega)\left(\frac{2}{3}H_{\boldsymbol{\chi}}\frac{\partial \tilde{\sigma}_{eq}}{\partial \tilde{\boldsymbol{\sigma}}} - \boldsymbol{\chi}\right)\dot{p}$$

Local damage

$$\dot{D}(t,\omega) = \left(c_1(\omega) + c_2(\omega)e^{-c_3(\omega)p^+}\right)\dot{p}^+ + c_4\left(c_5 - \bar{D}\right)\left\langle \mathrm{tr}\left(\frac{\partial \tilde{\sigma}_{eq}}{\partial \tilde{\boldsymbol{\sigma}}}\,\dot{p}^+\right)\right\rangle$$

Initial conditions

$$\tilde{\boldsymbol{\epsilon}}_{el}(0) = \mathbf{0},\ \ \tilde{\boldsymbol{\epsilon}}_{vp}(0) = \mathbf{0},\ \ R(0) = 0,\ \ \boldsymbol{\chi}(0) = \mathbf{0} \text{ and } D(0) = 0$$

Parameters

$G(\omega)$, $\kappa(\omega)$,	(elastic strains)
$\sigma_y(\omega)$,	(viscoplastic strains)
$b_R(\omega)$, $b_{\boldsymbol{\chi}}(\omega)$,	(hardenings)
$c_1(\omega)$, $c_2(\omega)$, $c_3(\omega)$	(local damage)

The parameters which are set as the uncertain parameters are bulk modulus (κ), shear modulus (G), the isotropic hardening coefficient (b_R), the kinematic hardening coefficient (b_χ) and the yield stress (σ_y) as well as damage parameters ((c_1), (c_2) and (c_3)). Hence the vector of unknown parameters is $\boldsymbol{q} = \big[\kappa(\omega),\, G(\omega),\, \sigma_y(\omega),\, b_R(\omega),\, b_\chi(\omega),\, c_1(\omega),\, c_2(\omega),\, c_3(\omega)\big]$.

Similar to the elastic model, viscoplasticity model and viscoplastic model with isotropic and kinematic hardening, preliminary study is on a regular cube, modeled with one 8 node element as shown in Figure 7.1 in Section 7.1. Similarly the same Dirichlet boundary condition is considered. Also the same tractions which is a Neumann boundary condition are applied cyclically in x, y and z directions on front and back faces and the magnitude of tractions in all directions are shown in Figure 7.19 where green, red and blue colors represent the stress values in x, y and z directions respectively.

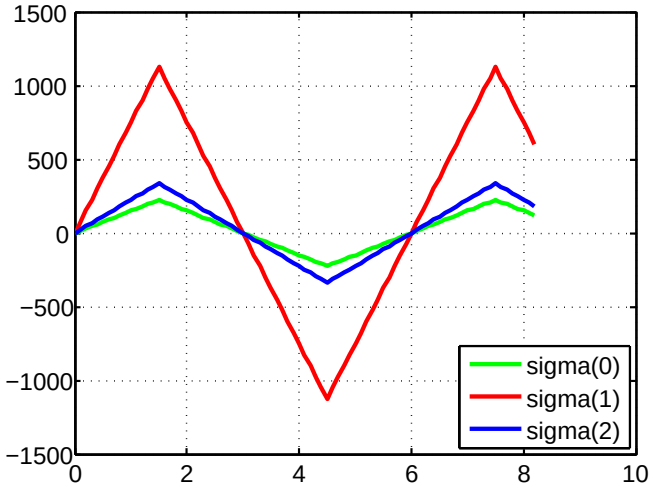

Figure 7.19.: Decomposed applied force at point E according to time

By considering the parameters listed in Table 7.17, for the top right corner node on back face, point E, as shown in Figure 7.1, the related displacement graph is obtained as shown in Figure 7.20 where green, red and blue colors represent the displacement of point E in x, y and z directions respectively.

Table 7.17.: The model parameters

κ	G	σ_y	n	k	b_R	H_R	b_χ	H_χ	c_1	c_2	c_3
1.66e5	7.69e4	266	1	23500	298.6	117.2	100	150	7	8	−80

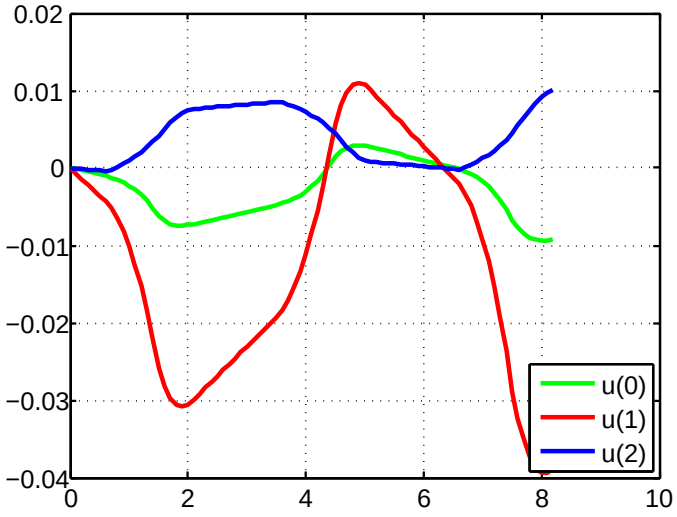

Figure 7.20.: Displacement of point E in x, y and z directions according to time

Again the displacements of point E in x, y and z directions are noted as the virtual data in this case.

7.4.1. GMKF Approach

The application of Gauss-Markov-Kalman filter using the polynomial chaos expansion and its approaches are discussed in Subsection 7.1.2. The results from both these approaches for the viscoplastic-damage model with isotropic and kinematic hardening are discussed in the next subsections.

Similar to the elastic model, viscoplasticity model and viscoplastic model with isotropic and kinematic hardening, Hermite function in form of polynomial chaos expansion is employed instead of samples. Similarly as discussed in Subsection 4.3.2, the uncertain parameters and output displacement are introduced as an ansatz. Further, the coefficients of the bulk modulus, shear modulus, yield stress, isotropic and kinematic hardening parameters, damage parameters and displacement are also computed.

Similar to forward model of viscoplasticity with isotropic and kinematic hardening as discussed in Subsection 7.3.2, a third order Hermite function and 200 samples as the Hermite functions basis are considered in order to solve the forward model using stochastic collocation approach as discussed in Subsection 4.3.2.

7.4.1.1. History Matching Updating

Similar to history matching method discussed in Subsection 7.1.2.1, 7.2.2.1 and 7.3.2.1 the prior and posterior probability density functions of the identified parameters are shown in Figure 7.21 and the characteristics of the probability density functions are similar to elastic model, viscoplastic model, viscoplastic model with isotropic and kinematic hardening behavior.

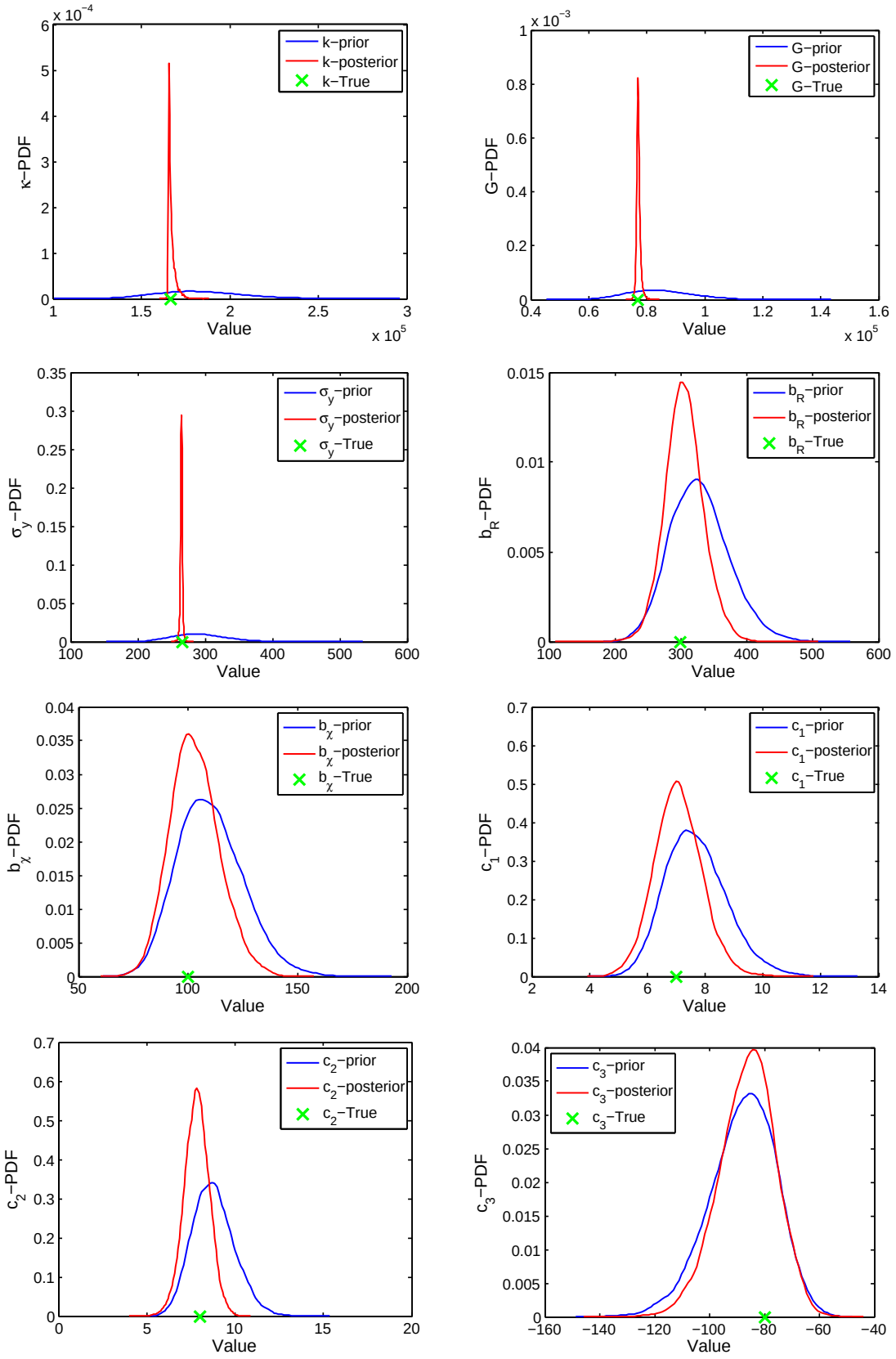

Figure 7.21.: PDF of identified parameters

Similar to the Subsection 7.3.2.1, the bulk modulus (κ), shear modulus (G) and the yield stress (σ_y) are updated much easier than the hardening and damage parameters. From the evaluation of hardening and local damage as seen in Figure 7.22, it was found that the hardening and damage equations are involved and activated only in the time intervals [0.8 2.0], [3.5 5.0] and [6.6 8.2] and only at these time intervals the hardening and damage parameters, isotropic hardening coefficient (b_R), the kinematic hardening coefficient (b_χ) and damage parameters ((c_1), (c_2) and (c_3)), are updated unlike the rest of the parameters which are updated at all time.

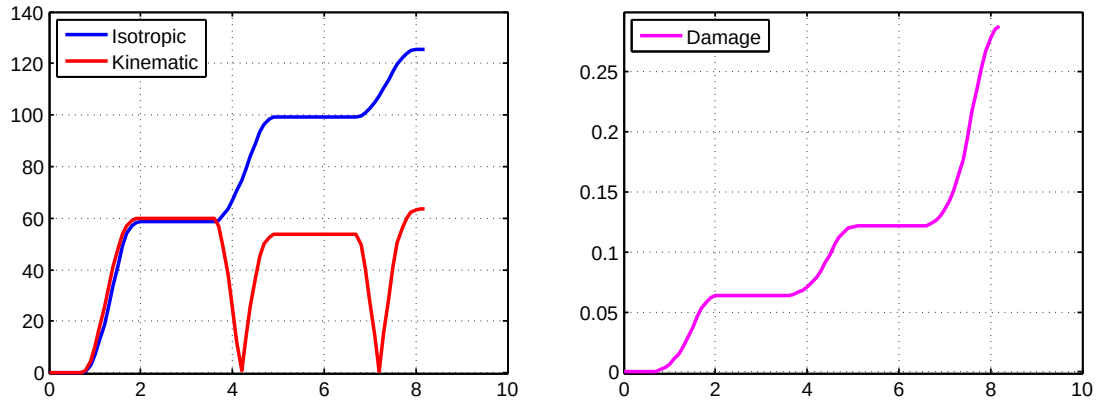

Figure 7.22.: Isotropic and kinematic hardening and non-local damage evaluation

The summarized results for the viscoplasticity-damage model with isotropic and kinematic hardening behavior via history matching updating are shown in Table 7.18.

Table 7.18.: The identified model parameters

Parameters	$\boldsymbol{q}_{\text{true}}$	$\boldsymbol{q}_{\text{est}}$(mean)	$\boldsymbol{q}_{\text{est}}$(standard deviation)
κ	1.66e5	1.66e5	2.03e3
G	7.71e4	7.70e4	710.34
σ_y	266	264.75	1.81
b_R	298.6	304.75	29.02
b_χ	100	103.12	11.18
c_1	7	7.07	0.82
c_2	8	7.82	0.70
c_3	-80	-86.29	10.29

7.4.1.2. Sequential Updating

Similar to Subsection 7.1.2.2, 7.2.2.2 and 7.3.2.2, the prior and posterior probability density functions of the identified parameters are shown in Figure 7.23 and the characteristics of probability density functions are similar to elastic, viscoplastic and viscoplastic model with hardening.

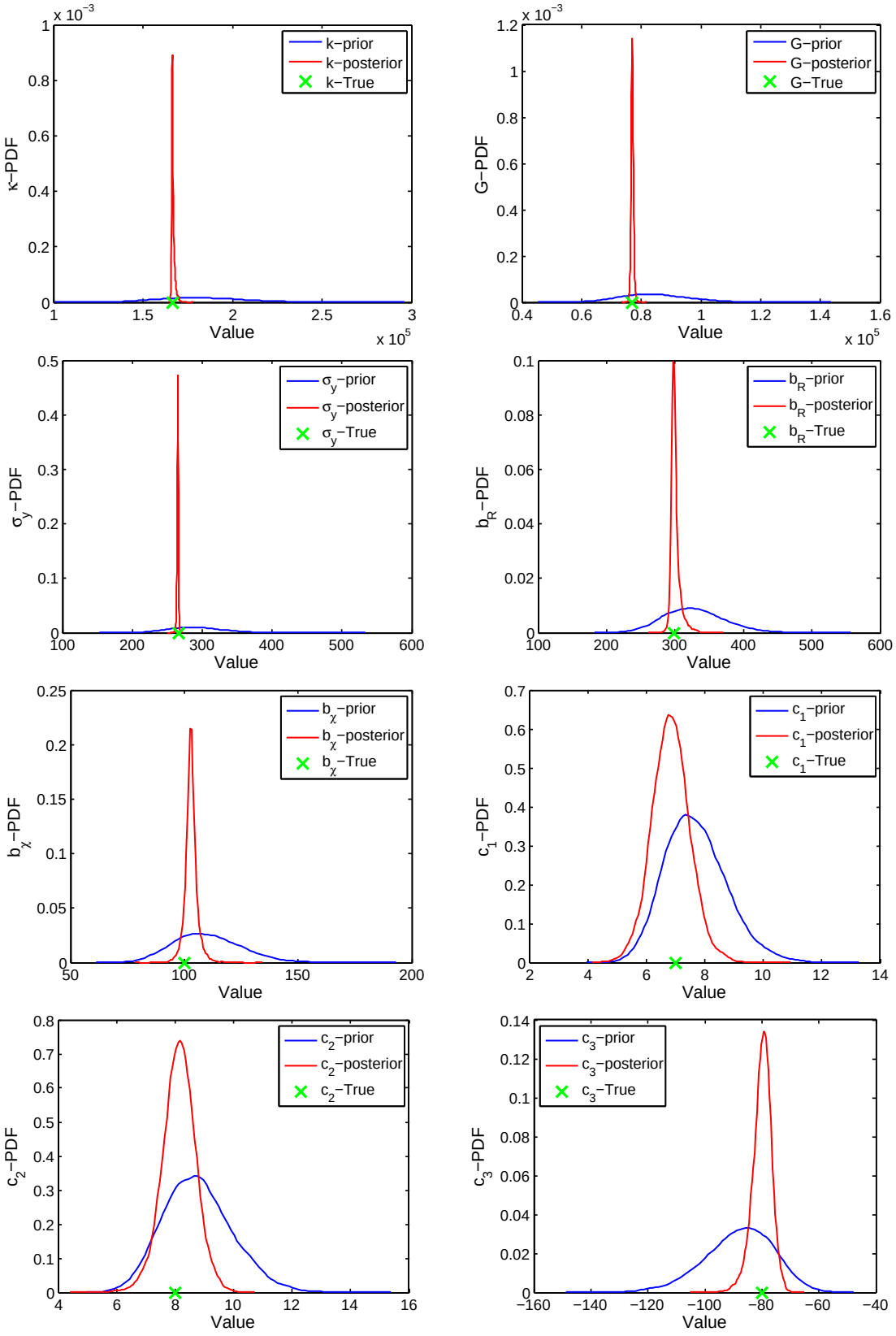

Figure 7.23.: PDF of identified parameters

Similar to the Subsection 7.3.2.2, the bulk modulus (κ), shear modulus (G) and the yield stress (σ_y) are updated much easier than the hardening and damage parameters. From the evaluation of hardening and local damage as seen in Figure 7.22, it was found that the hardening and damage equations are involved only in the time intervals [0.8 2.0], [3.5 5.0] and [6.6 8.2] and only at these time intervals the hardening and damage parameters, isotropic hardening coefficient (b_R), the kinematic hardening coefficient (b_χ) and damage parameters ((c_1), (c_2) and (c_3)), are updated unlike the rest of the parameters which are updated at all time. Therefore, updating the parameters are done only on some time steps which are within the mentioned time intervals and it leads the procedure in such a way that all of the uncertain parameters are updated, and not only few of them, although effect of each parameter on the measured displacement is different than others and it causes different update of each parameter.

The summarized true values of the parameters, mean and variance of the estimated parameters via sequential updating approach for the viscoplastic-damage model enriched with isotropic and kinematic hardening behavior are shown in Table 7.19.

Table 7.19.: The identified model parameters

Parameters	$\boldsymbol{q}_{\text{true}}$	$\boldsymbol{q}_{\text{est}}$(mean)	$\boldsymbol{q}_{\text{est}}$(standard deviation)
κ	1.66e5	1.66e5	937.87
G	7.69e4	7.70e4	430.05
σ_y	266	265.1	1.07
b_R	298.6	300.35	7.06
b_χ	100	102.98	2.77
c_1	7	6.84	0.65
c_2	8	8.13	0.57
c_3	-80	-79.98	3.34

7.4.2. Discussion and Comparison

The updating is possible by Gauss-Markov-Kalman filter approach for the viscoplastic-damage model with isotropic and kinematic hardening as the updating is performed according to the history matching or sequentially updating method. However it should be pointed out that for the parameters such as hardening and damage parameters, which do not have much strong influence on the measured displacement than the rest of parameters, the identification can not be done well as compared to the rest of parameters. Hence a better identification is achieved when the more information is available from the measurement.

Moreover the uncertainty of the parameters is reduced in the such a way that the pos-

terior distribution functions of the hardening and damage parameters are not as narrow as the rest parameters for the history matching and sequential updating methods.

The sequential updating has more computational time as the updating process is performed for several times than the history updating approach. By considering the fact that the computations are done from the initial time step after each update which leads to observe more information as well. On the other hand, the identification and reduction of the parameter uncertainty as inferred from the update of the parameters is more accurate and acceptable for the sequential updating method than the history matching update as it is seen from the posterior densities of hardening and damage parameters by both approaches shown in Figure 7.21 and Figure 7.23 respectively. In Section 7.5 it is better understood whether different load path can lead to a better parameter identification where sequential Gauss-Markov-Kalman filter method is used.

7.5. Effect of Load Path on Parameter Identification by Sequential GMKF Approach

The model considered is a viscoplastic model with isotropic and kinematic hardening discussed in Section 7.3. Similarly the forward model is also prepared seen in Table 7.11. Again the parameters which are set as the uncertain parameters are bulk modulus (κ), shear modulus (G), the isotropic hardening coefficient (b_R), the kinematic hardening coefficient (b_χ) and the yield stress (σ_y) and hence the vector of unknown parameters is $\boldsymbol{q} = \big[\kappa(\omega),\, G(\omega),\, b_R(\omega),\, b_\chi(\omega),\, \sigma_y(\omega)\big]$.

Preliminary study is on a regular cube, modeled with one 8 node element. The Dirichlet boundary condition is applied in such a way that the cube is completely restrained on the back face and with normal traction on opposite (front) face. Two cases are considered in order to compare the effect of applied force on identified parameters. For the both cases the magnitude of the normal traction and a stress in the plane of the front face are plotted in Figure 7.24 and Figure 7.25 respectively. Blue and red colors represent the stress value in normal and in plane directions respectively. As it is seen, the magnitude of the applied force for the case 1 is constant all time but for the case 2 the magnitude of the applied force grows gradually by time.

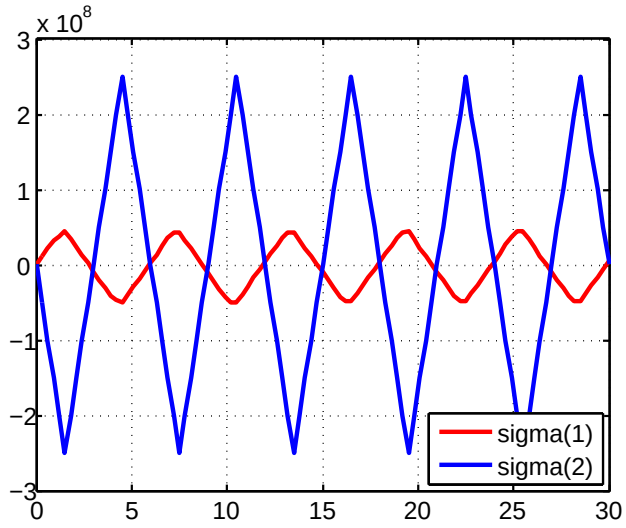

Figure 7.24.: Decomposed applied force on desired node according to time- Case 1

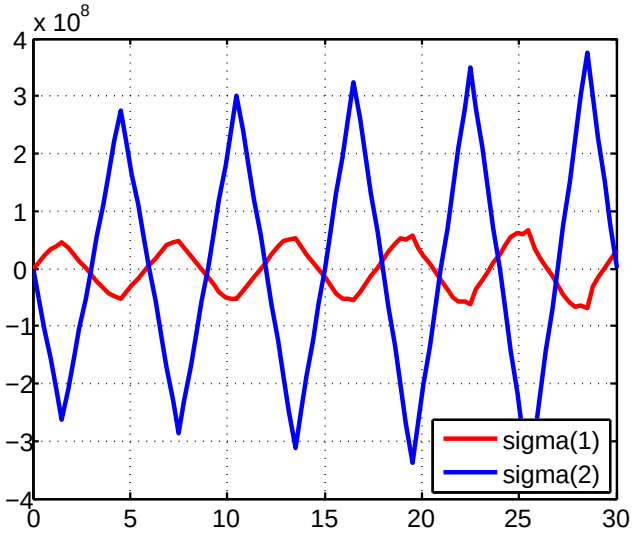

Figure 7.25.: Decomposed applied force on desired node according to time- Case 2

By considering the parameters listed in Table 7.20, for the top right corner node on front face, the related σ-ϵ hysteresis graph is obtained as shown in Figure 7.26 for case 1 and Figure 7.27 for case 2.

Table 7.20.: The model parameters

κ	G	σ_y	n	k	b_R	H_R	b_χ	H_χ
1.66e9	7.69e8	1.7e8	1	1.5e8	50	0.5e8	50	0.5e8

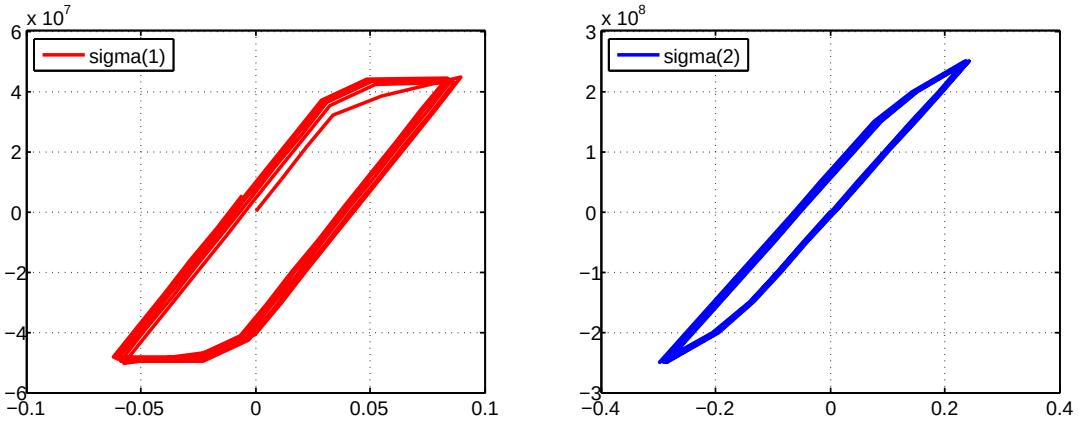

Figure 7.26.: σ-ϵ for the node on front surface in plane and normal directions- Case 1

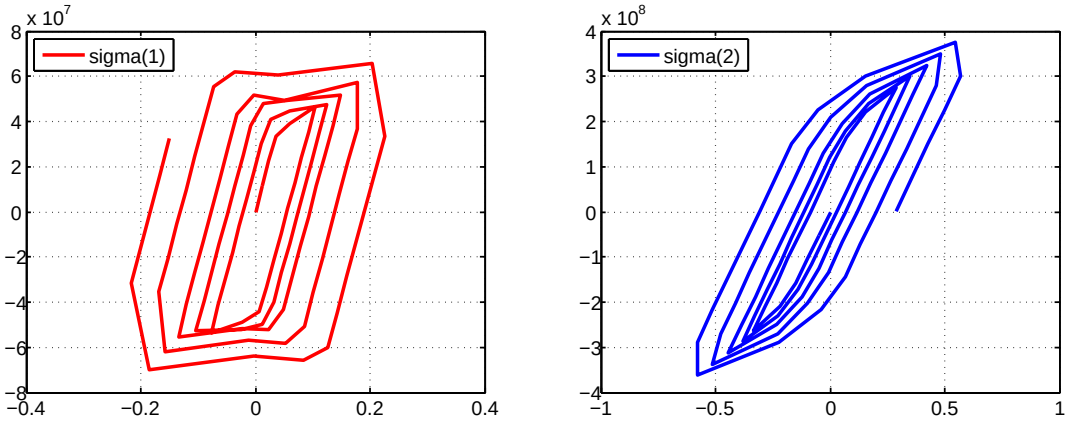

Figure 7.27.: σ-ϵ for the node on front surface in plane and normal directions- Case 2

Again the displacements of top right corner node on front face in normal and plan directions are noted as the virtual data in this case.

7.5.1. GMKF Approach by Sequential Updating

The application of Gauss-Markov-Kalman filter using the polynomial chaos expansion and its approaches are discussed in Subsection 7.3.2.

Similar to the viscoplastic model with isotropic and kinematic hardening, Hermite function in form of polynomial chaos expansion is employed instead of samples. The uncertain parameters and output displacement are introduced as an ansatz as discussed in Subsection 7.3.2. Similarly, Gaussian standard random variables are represented by $\boldsymbol{\theta}(\omega)$ and the third order Hermite function and 200 samples as the basis of the Hermite function are considered. The forward model is again solved using stochastic collocation approach as discussed in Subsection 4.3.2.

7.5.1.1. Sequential Updating

Similar to Subsection 7.3.2.2 the GMKF approach when updating is done sequentially is employed. Figure 7.28 shows the probability density function of prior and posterior of the identified parameters for the constant magnitude force and Figure 7.29 shows the probability density function of prior and posterior of the identified parameters for the gradually varying force.

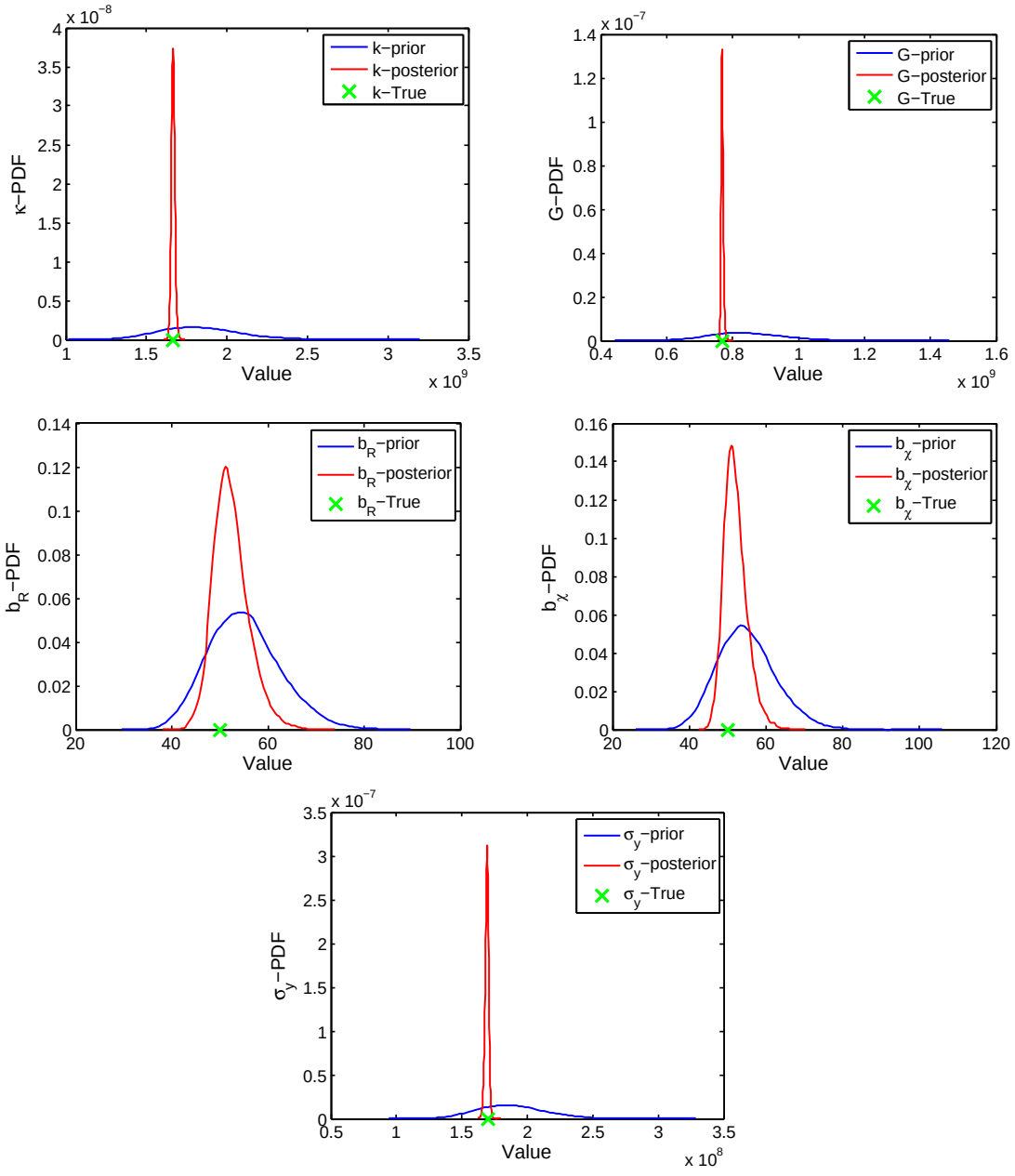

Figure 7.28.: PDF of identified parameters- Case 1

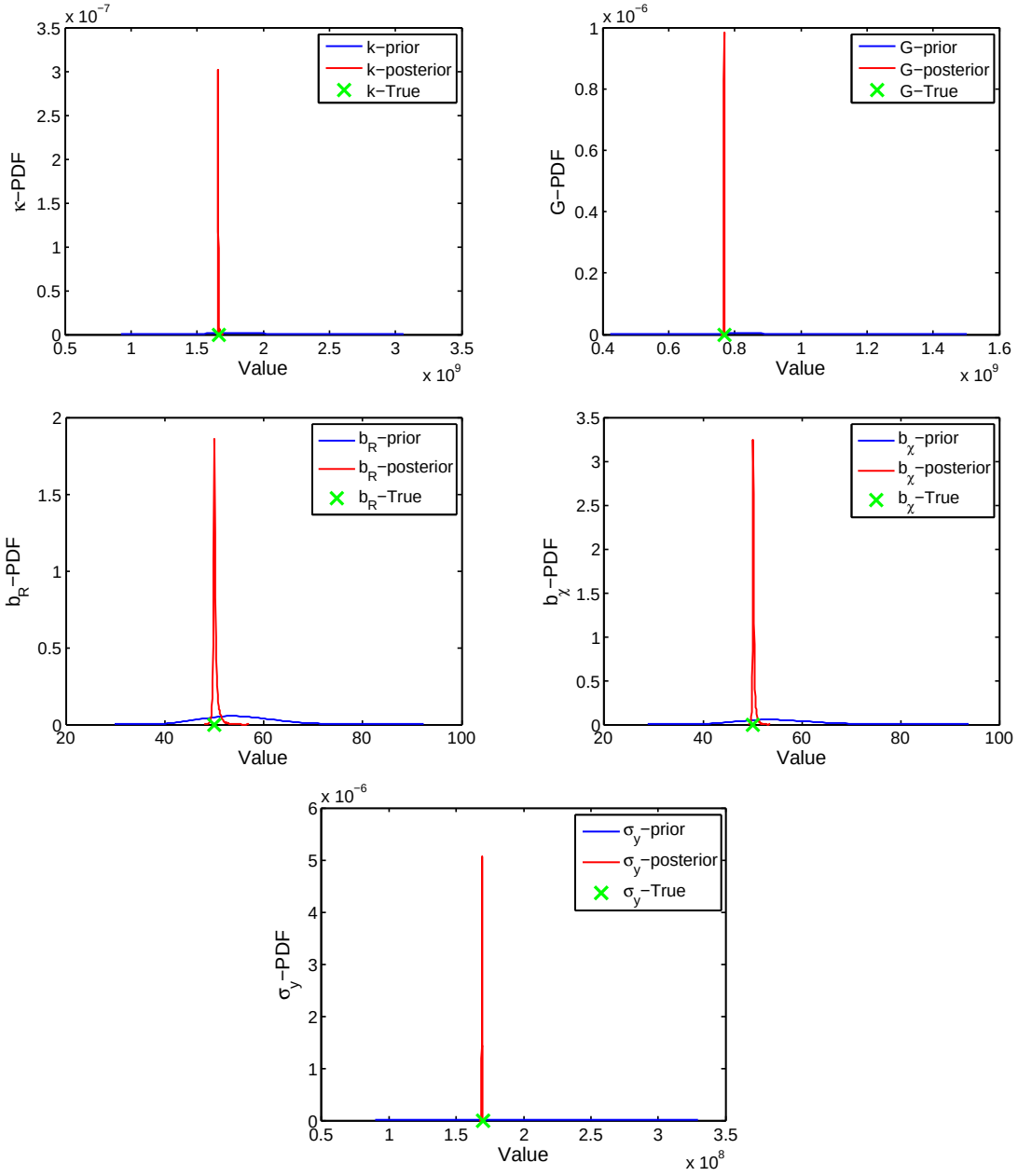

Figure 7.29.: PDF of identified parameters- Case 2

The summarized results for the constant magnitude applied force and gradually varying the applied force are shown in Table 7.21, where the true values q_{true} and the mean and standard deviation of the estimated parameters, $\boldsymbol{q}_{\text{est}}^{m}$ and $\boldsymbol{q}_{\text{est}}^{\text{std}}$ respectively, for both cases are compared [210, 211].

Table 7.21.: The identified model parameters

Parameters	$\boldsymbol{q}_{\text{true}}$	$\boldsymbol{q}^{m}_{\text{est-1}}$	$\boldsymbol{q}^{\text{std}}_{\text{est-1}}$	$\boldsymbol{q}^{m}_{\text{est-2}}$	$\boldsymbol{q}^{\text{std}}_{\text{est-2}}$
κ	1.66e9	1.66e9	1.13e7	1.66e9	2.59e6
G	7.69e8	7.68e8	3.47e6	7.68e8	6.39e5
b_R	50	52.36	3.71	50.19	0.53
b_χ	50	52.04	3.01	50.27	0.29
σ_y	1.7e8	1.69e8	1.35e6	1.69e8	1.52e5

7.5.2. Discussion and Comparison

The parameters are updated for both the cases by using the information from the virtual data. The enough information is used for updating and it is determined from the sharpness of the posterior PDF of bulk modulus (κ), shear modulus (G) and yield stress (σ_y).

It is inferred from the posterior PDF of isotropic and kinematic hardening parameters, (b_R) and (b_χ), these parameters are updated better for the gradually varying applied force than the constant magnitude force. The exact hardening parameters, (b_R) and (b_χ), are predicted more accurately for the gradually varying applied force with the less uncertainty of the estimated hardening parameters.

One reason that can be mentioned is that the process is not always in the states where the hardening equations are involved such as in elastic states and due to this fact that the less information from the whole simulation are used to estimate the hardening parameters. The other reason that why the better estimation for hardening parameters for the case 2 is obtained is that for the gradually varying increasing applied force more states involving the hardening equations are available to estimate the hardening parameters than for the constant magnitude force and it is shown in Figure 7.30 and Figure 7.31 for the both cases respectively. In other words, the hardening equations are more activated for gradually varying increasing applied force as described in case 2 in contrast with the constant magnitude force as described in case 1. The von Mises yield criterion is illustrated by green cylinder in Figure 7.30 and Figure 7.31 where the inside and outside of the cylinder refers to elastic and plastic states respectively and principal stresses are represented by blue color.

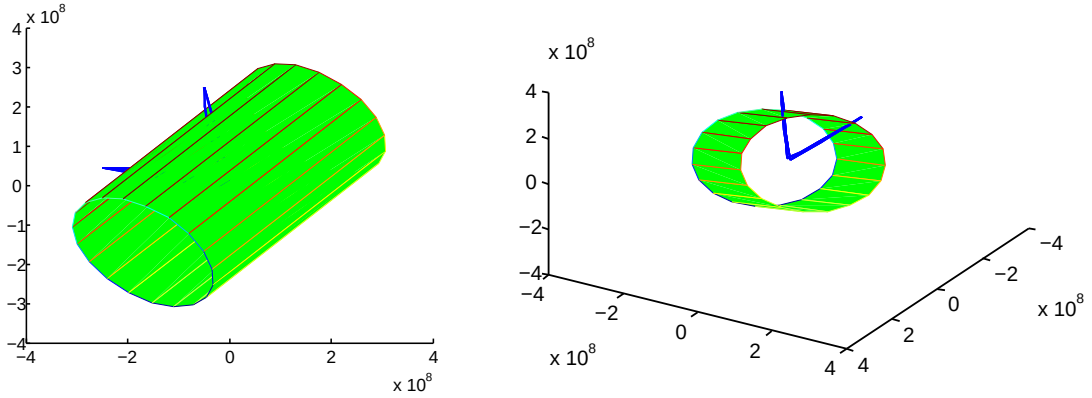

Figure 7.30.: Principal stresses of applied force- Case 1

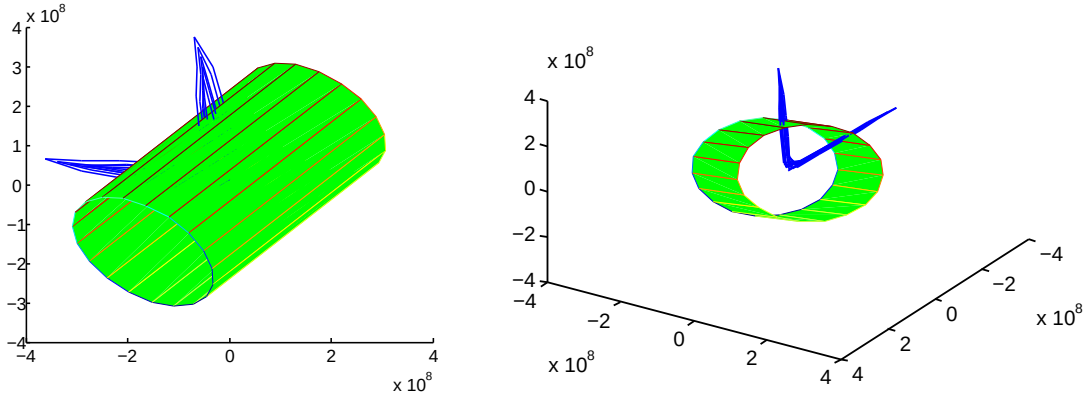

Figure 7.31.: Principal stresses of applied force- Case 2

As it is seen, for the case 2, gradually varying increasing applied force, there are more states outside of the von Mises yield criterion in comparison to case 1, constant magnitude applied force, and therefore the better identification of hardening parameters, (b_R) and (b_χ), can be done for case 2 comparing to case 1. From this comparison it can be noted that the parameters are identified more accurately when more information is available while using sequential Gauss-Markov-Kalman filter method.

7.6. Conclusion

In this chapter, Transitional Markov Chain Monte Carlo method and Gauss-Markov-Kalman filter approach in two approaches are applied on large verity of mechanical material models. The investigated results confirm the validation of these two methods

on the considered mechanical material models. The conclusions inferred from the discussions and comparisons as in Subsection 7.1.3, 7.2.3, 7.3.3, 7.4.2 and 7.5.2 are described below by considering the posterior distribution functions of the parameters obtained by using the Transitional Markov Chain Monte Carlo method and Gauss-Markov-Kalman filter approach on different models as described in Section 7.1, 7.2, 7.3, 7.4 and 7.5.

- There is not much difference in the probability distribution functions of the estimated parameters for all the considered models such as the elasticity model which is the simplest model to the most enriched model i.e. the viscoplastic-damage model with isotropic and kinematic hardening behavior by employing the Transitional Markov Chain Monte Carlo method.

- A considerable difference in results is observed between the updated random variables of the uncertain parameters for the considered models such as the viscoplasticity model with hardening to the most enriched model which is the viscoplastic-damage model with isotropic and kinematic hardening behavior which are determined by employing the Gauss-Markov-Kalman filter approach. This is because of the fact that the hardening and damage parameters do not have a strong and direct influence as like the bulk modulus, shear modulus and the yield stress which have a dominant influence on the considered measured displacement output data.

- The Gauss-Markov-Kalman filter approach in a history matching update approach is not an optimized method to identify the parameters of the viscoplasticity which includes hardening model and viscoplastic-damage model. This is because, the hardening and damage parameters are not identified well and their uncertainties are not properly reduced as updating is done only once. Further, it is also to be noted that the number of observed states where the bulk modulus, shear modulus and yield stress are involved and identifiable, i.e. the number of states where the elasticity and plasticity part are involved and identifiable are more than the number of states where the hardening and damage parameters are involved and identifiable i.e. only plasticity part.

- The most suitable method among the employed methods is the sequential Gauss-Markov-Kalman filter approach for the viscoplastic model with isotropic and kinematic hardening and also for the viscoplastic-damage model enriched with hardening behavior. The parameters such as hardening parameters, damage parameters, bulk modulus, shear modulus and yield stress are well updated and posterior distributions representing their uncertainties are much narrow for these parameters.

- The computational time of the Transitional Markov Chain Monte Carlo method for all models from the elasticity model to the viscoplastic model with isotropic and kinematic hardening is very high and this results in no sense of applying this method in the economical point of view on the complicated material models.

- Gauss-Markov-Kalman filter approach by history matching updating is the fastest approach as the updating procedure is done only one time by comparing the history

of the measured data i.e. the measured displacement in this study.

- The sequential Gauss-Markov-Kalman filter approach for all variety of the considered models is not as fast as the history matching approach as updating is done multiple times but still the computation time needed is reasonable and acceptable as a stochastic approach to identify the parameters of a PDE system.

- Based on the reliability, accuracy and computational time, the sequential Gauss-Markov-Kalman filter approach is chosen for the further application and its application is discussed in the forthcoming chapter.

- Using a sequential Gauss-Markov-Kalman filter approach it should be significantly noted that the load path should be applied in such a way that enough information from the measured data i.e. the measured displacement is obtained. In other words, in order to identify the hardening and damage parameters as well as the rest of the parameters, enough observation of the involved hardening and damage equations should be known, i.e. the states outside the yield stress criterion such as the von Mises yield criterion representing the plasticity should be observed extensively and recorded as the measured data since only on these states the hardening and damage parameters can be updated. In contrast to hardening and damage parameters, the bulk and shear modulus can be updated not only on elasticity states but also on plasticity states as well.

- Using sequential Gauss-Markov-Kalman filter approach the parameters should be updated at proper time intervals to save time and to reduce cost. Lesser number of update, results in the less computation time. Hence a particular times should be selected to identify the parameters as discussed in Subsection 7.4.1.2 where the hardening and damage parameters are changing continuously. Considering this fact results in a better parameter identification and better reduction of parameter uncertainties in a very less time.

- It should be noted that the damage evolution is restricted in such a way that non-local damage should not exceed certain value, i.e. only minor damage is considered for the Gauss-Markov-Kalman filter approach on a viscoplastic-damage model to identify its parameters. Obviously the damage parameters are identified better by using the Gauss-Markov-Kalman filter approach when an immense damage is considered, i.e. the measured displacement data is influenced more by a bigger damage and results in better identification of damage parameters from the provided data.

Considering the above mentioned comparisons, observations, discussions and facts, the sequential Gauss-Markov-Kalman filter approach is chosen for further application in the next chapter.

8. Parameter Identification of a CT-Test using SGMKF

The Bayesian approaches are discussed in Chapter 5 and 6 and their capabilities are verified on different mechanical material models in Chapter 7 and finally sequential Gauss-Markov-Kalman filter method using the polynomial chaos expansion is chosen to update the uncertain parameters sequentially for further applications. In this chapter, the material model parameters for well-known CT-Test are updated by this selected method in order to verify the applicability of this method for real experiment.

8.1. Bayesian Parameter Identification on CT-Test Considering Different Measurements

A very well-known Compact Tension Test (CT-Test) [212] is carried out on a notched sample. The Dirichlet boundary condition is applied by assigning two reference points at the center of two holes of the specimen as seen in Figure 8.1.

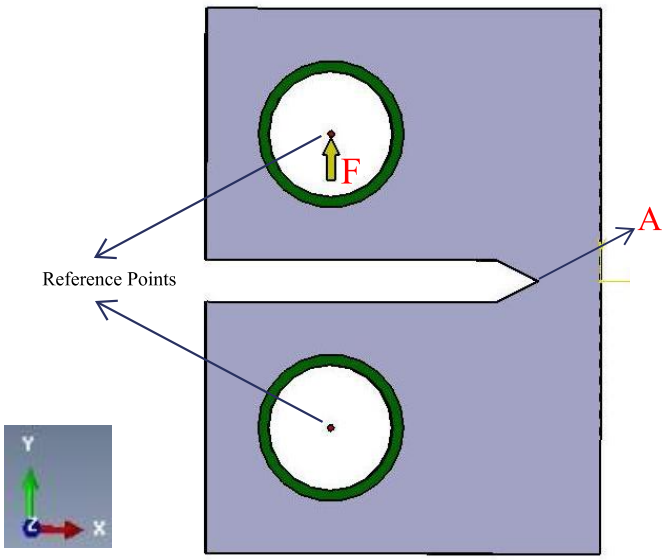

Figure 8.1.: Boundary conditions of CT-Test

The reference points are kinematically coupled with the corresponding holes. The displacement of the reference point at upper hole is constrained in x and z directions and the displacement of reference point at the lower hole is constrained in x, y and z directions. Moreover, to depict a soft transition of the constraints in the specimen the first layer of the elements around the holes are defined with much softer material than the rest of the elements. The first layer of the elements around the holes are shown in green color in Figure 8.1. As a Neumann boundary condition, a cyclic load in y-direction is applied on the reference point of the upper hole as shown with a yellow arrow in Figure 8.1.

The load is applied in such a way that the damage parameter does not exceed relatively small amount of damage parameter, so that it will not probably result in a severe damage or collapsing damage. The minor damage or light cracking is only developed to identify the model parameters in the Bayesian setting so that it can be later may be used for health monitoring purpose where identifying the model parameters and detecting the damage before collapsing the specimen is a crucial issue.

From the above discussion, considered boundary conditions and the parameters as seen in Table 8.1, the related displacement graph as shown in Figure 8.2 was obtained where green, red and blue colors represent the displacement of the node in x, y, and z directions respectively at the notch start point indicated by point A in Figure 8.1.

Table 8.1.: The model parameters

κ	G	σ_y	n	k	b_R	H_R	$b_{\boldsymbol{\chi}}$	$H_{\boldsymbol{\chi}}$	c_1	c_2	c_3
1.66e5	7.69e4	266	1	23500	298.6	117.2	100	150	4.5	5	-11

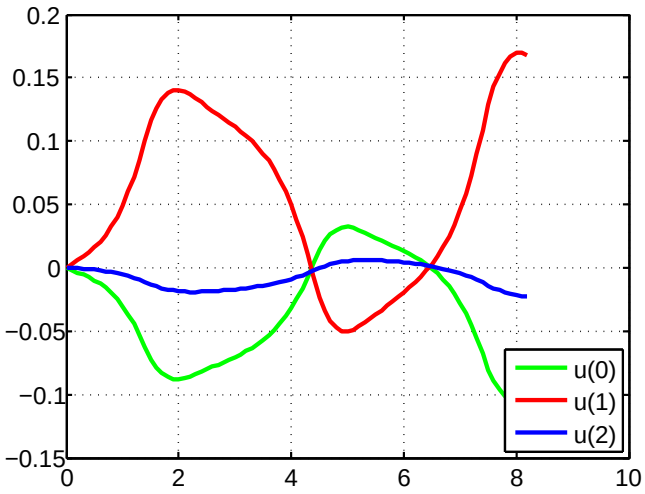

Figure 8.2.: Displacement of point A in x, y and z directions according to time

The mesh generated for the CT-Test model is shown in Figure 8.3, where the meshes are generated in such a way that the very fine meshes are considered near the notch and at far away from the notch coarser meshes are generated. Further, Figure 8.4 shows the damaged specimen.

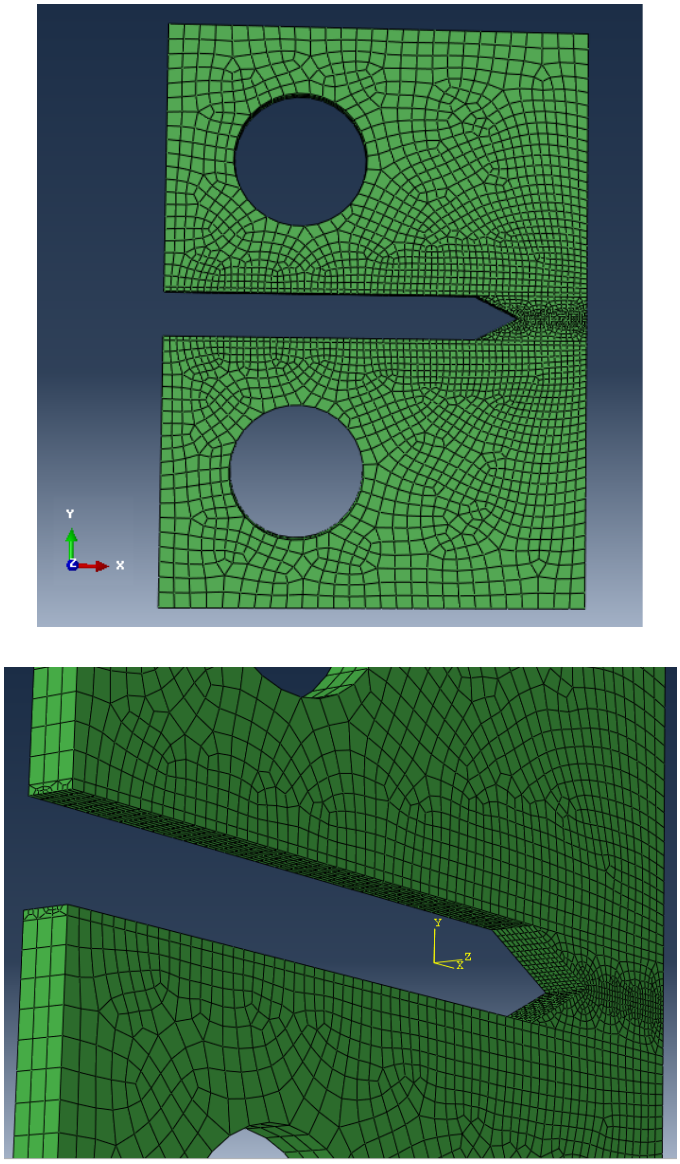

Figure 8.3.: Mesh generation

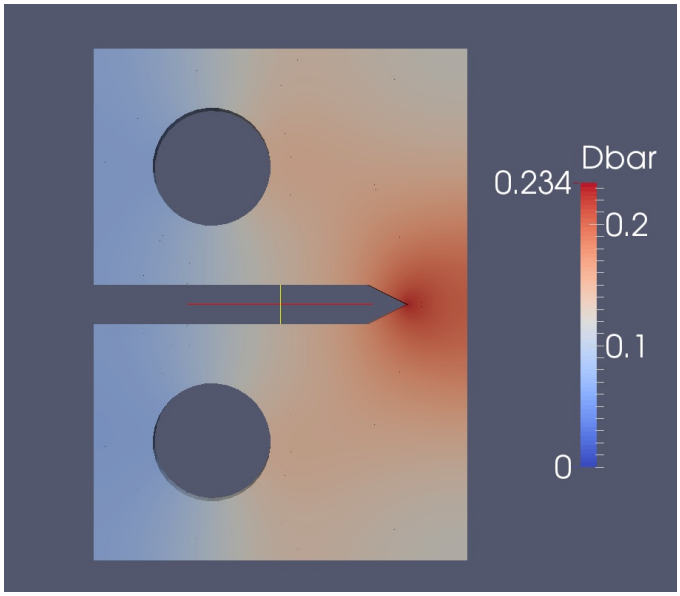

Figure 8.4.: Damaged specimen

Two cases are considered. In the first case we record the displacement of the nodes on the inner surface of notch as it is seen in Figure 8.5 and in the second case the displacement of the nodes on the external surface close to the notch which is seen in Figure 8.6 are caught.

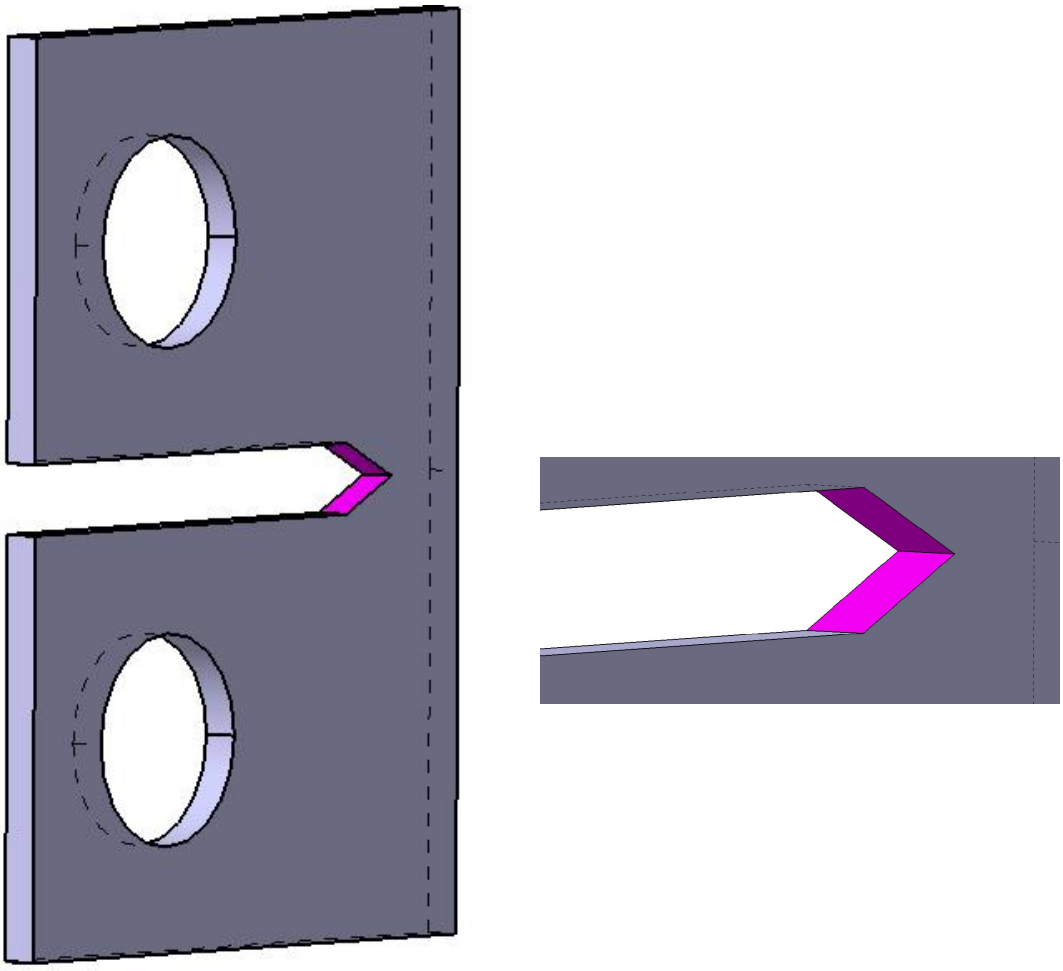

Figure 8.5.: Measurement observed- Case 1

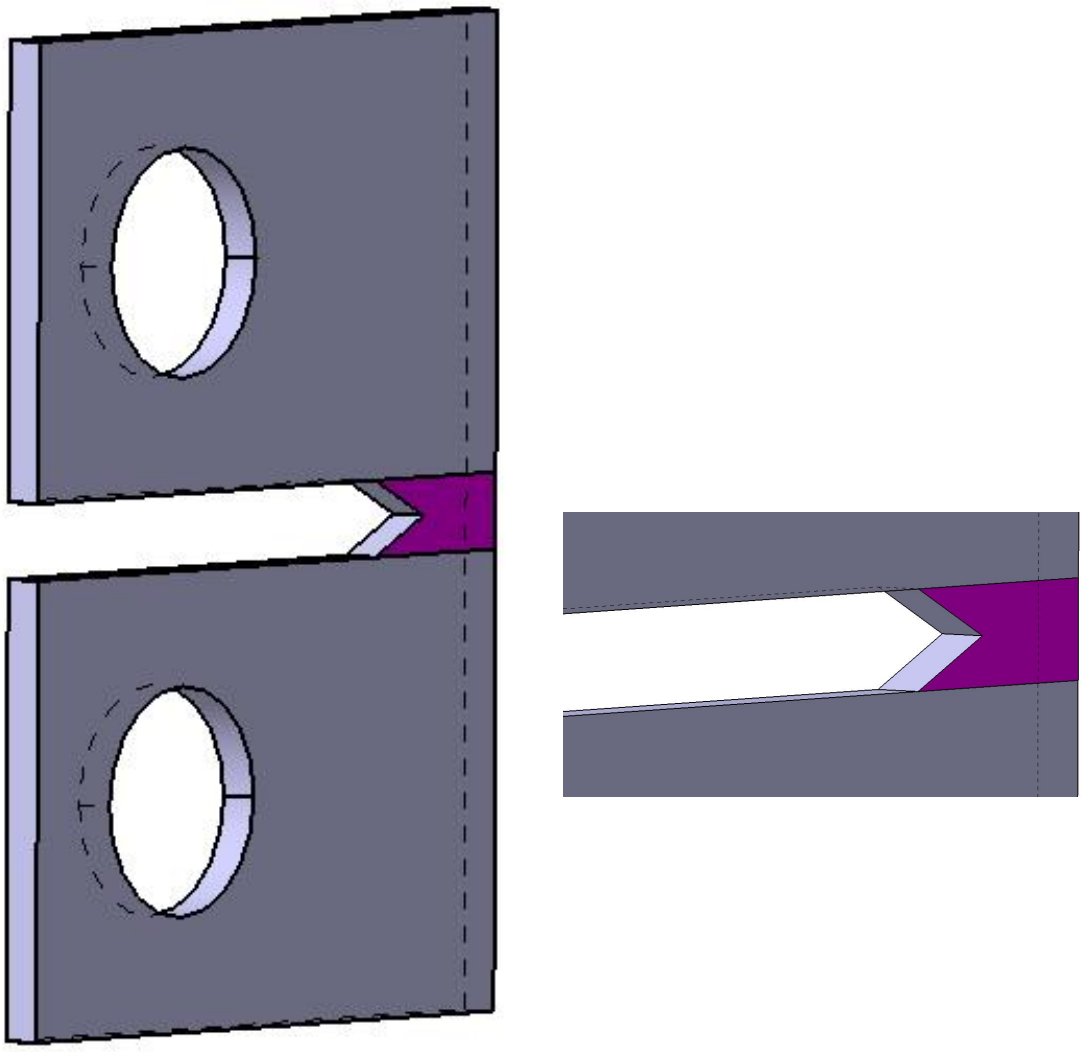

Figure 8.6.: Measurement observed- Case 2

8.1.1. GMKF Approach by Sequential Updating

The same forward model is considered as discussed in Section 7.4. Similarly the same parameters are considered as the uncertain parameters and hence the vector of unknown parameters is $\boldsymbol{q} = \big[\kappa(\omega),\, G(\omega),\, \sigma_y(\omega),\, b_R(\omega),\, b_{\boldsymbol{\chi}}(\omega),\, c_1(\omega),\, c_2(\omega),\, c_3(\omega)\big]$.

Similar to the viscoplastic-damage model with isotropic and kinematic hardening, Hermite function in form of polynomial chaos expansion is employed instead of samples. The uncertain parameters and output displacement are introduced as an ansatz as discussed in Subsection 7.4.1 and similarly Gaussian standard random variables are represented by $\boldsymbol{\theta}(\omega)$. A third order Hermite function and 200 samples as the basis of Hermite func-

tions are considered. The coefficients of the bulk modulus, shear modulus, yield stress, isotropic and kinematic hardening parameters, damage parameters and displacement are also computed as discussed in Subsection 4.3.2. The forward model is solved using stochastic collocation approach as discussed in Subsection 4.3.2.

8.1.1.1. Sequential Updating

Similar to Subsection 7.4.1.2 the GMKF approach when updating is done sequentially is employed. The prior and posterior probability density functions of the identified parameters for the first case are shown in Figure 8.7 and for the second case are shown in Figure 8.8.

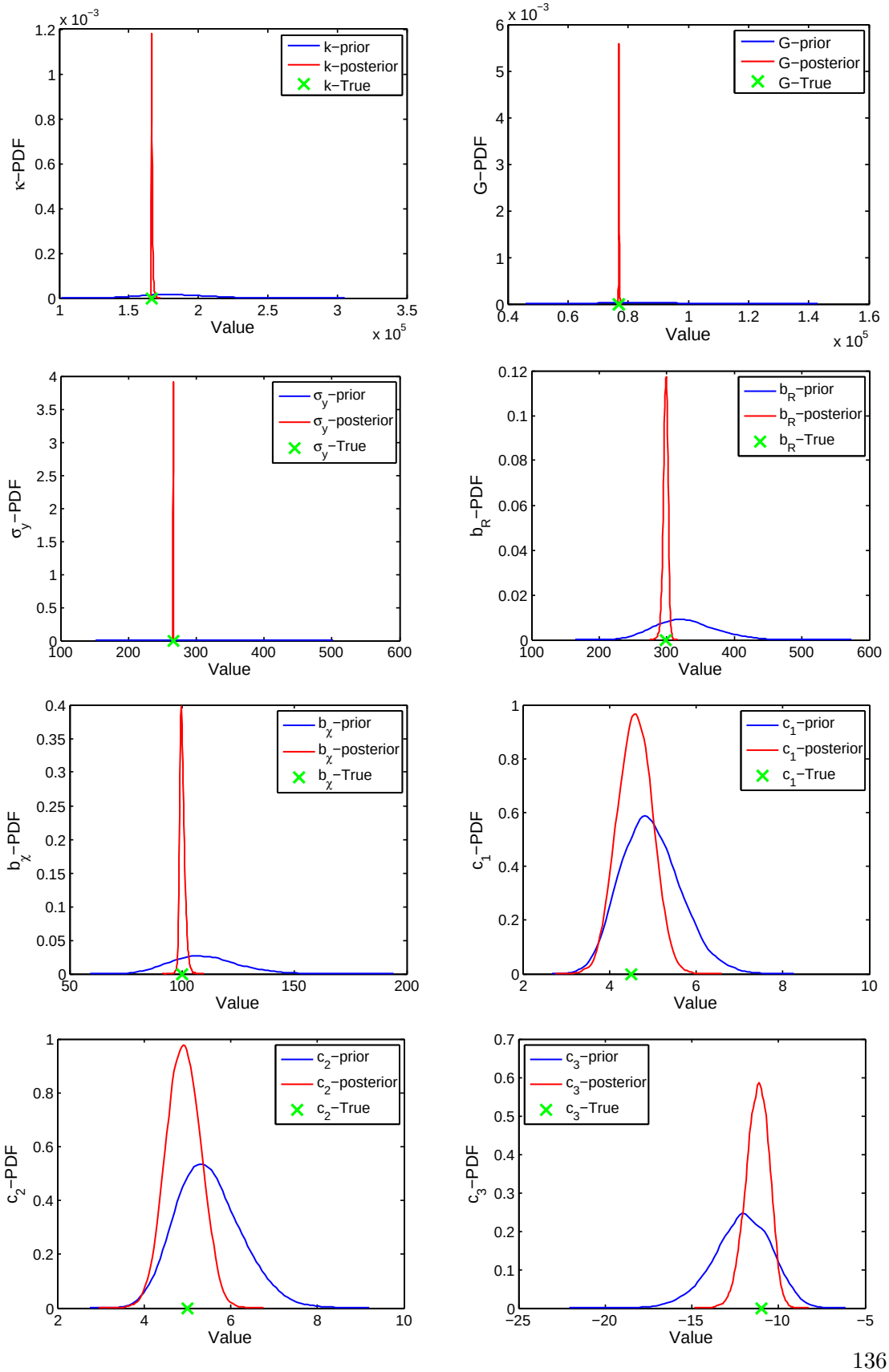

Figure 8.7.: PDF of identified parameters- Case 1

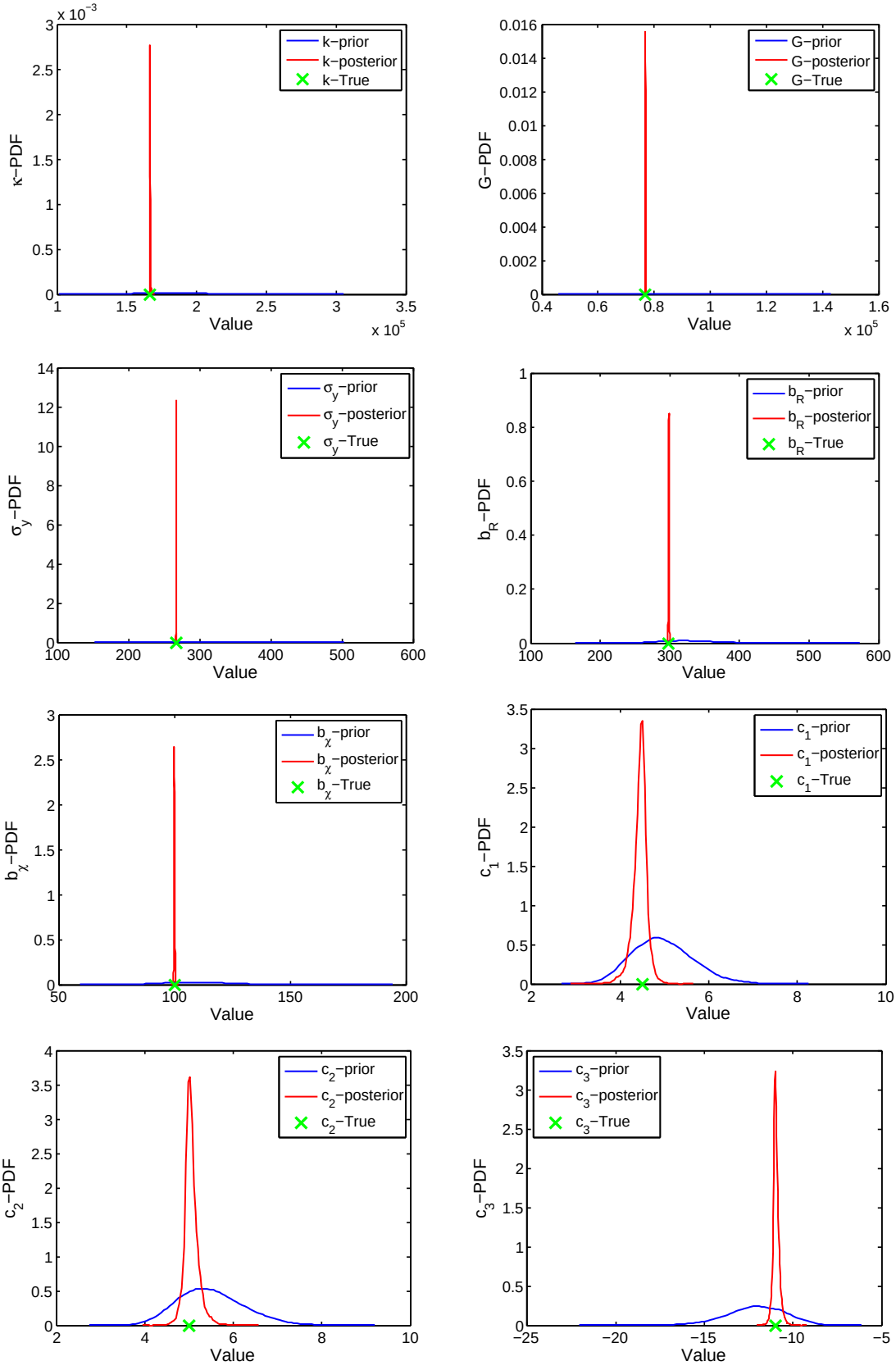

Figure 8.8.: PDF of identified parameters- Case 2

The summarized results for the both cases are shown in Table 8.2.

Table 8.2.: The identified model parameters

Parameters	$\boldsymbol{q}_{\text{true}}$	$\boldsymbol{q}^{m}_{\text{est-1}}$	$\boldsymbol{q}^{\text{std}}_{\text{est-1}}$	$\boldsymbol{q}^{m}_{\text{est-2}}$	$\boldsymbol{q}^{\text{std}}_{\text{est-2}}$
κ	1.66e5	1.66e5	650.91	1.66e5	260.57
G	7.69e4	7.69e4	106.41	7.69e4	33.88
σ_y	266	265.97	0.16	266	0.05
b_R	298.6	298.34	3.51	298.57	0.50
$b_{\boldsymbol{\chi}}$	100	100.13	1.17	100.0	0.18
c_1	4.5	4.58	0.40	4.41	0.17
c_2	5	4.91	0.39	5.05	0.16
c_3	-11	-11.21	0.67	-10.94	0.17

8.1.2. Discussion and Comparison

The parameters such as bulk modulus (κ), shear modulus (G) and yield stress (σ_y) are even identified after updating once as the effect of these parameters on the equation of the displacement are much higher than the rest of the parameters and it is very expensive to update the uncertainty distribution on each time step. Hence the parameters are updated not in elastic states but only in the plastic states where the bulk modulus (κ), shear modulus (G), yield stress (σ_y), hardening parameters ((b_R) and ($b_{\boldsymbol{\chi}}$)) and damage parameters ((c_1), (c_2) and (c_3)) can be updated as updating in the elastic states increases the cost. The evaluation of hardening and local damage on the top node at the notch start point representing the plasticity are shown in Figure 8.9. In order to reduce the time of computation, the displacements of nodes are sequentially updated only in the time intervals [0.4 2.2], [3.5 5.0] and [6.6 8.2]. Although all the nodes do not have the same evaluation of hardening and local damage but with a good approximation the nodes considered on the mentioned surfaces for the both cases have the quite close hardening and damage behaviors on the determined time interval and therefore only updating is done within these time intervals.

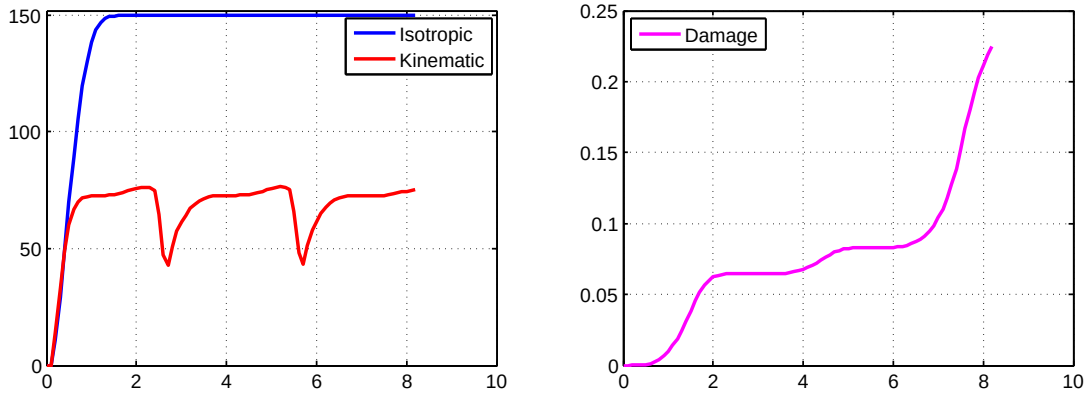

Figure 8.9.: Isotropic and kinematic hardening and non-local damage evaluation

The other fact that should be emphasized is that the observed displacement is directly influenced by the bulk modulus (κ), shear modulus (G), and yield stress (σ_y) as in $u \propto \mathsf{f}(\kappa,\ G\ ,\ \sigma_y)$, i.e. these parameters have a direct strong effect on the measured displacement. The rest of the parameters affect the displacement as in $u \propto \mathsf{f}(\mathsf{g}(\mathsf{k}(\mathrm{b}_R,\ b_{\boldsymbol{\chi}},\ c_1,\ c_2,\ c_3)))$, i.e. the displacement is proportional to these parameters through some more functions. Accordingly, the information received from the constitutive equation from the latter parameters are less and therefore they can be generally estimated not as well as the first group of parameters. However the hardening parameters for both cases are also updated well as a lot of nodes' displacements are observed and considered as the measurement data.

The bulk modulus, shear modulus and yield stress are updated much easier than the hardening and damage parameters for the both cases as enough information from the virtual data are received and this was observed from the sharpness of posterior probability density function of bulk modulus (κ), shear modulus (G), and yield stress (σ_y) of the both cases. However the hardening parameters ((b_R) and ($b_{\boldsymbol{\chi}}$)) are also very well updated for these case studies as large numbers of measurements are considered which provide very good enough information to estimate hardening parameters using sequential Gauss-Markov-Kalman filter approach. Comparing the results of first and second case, as the nodes on the external surface close to the notch are affected strongly by damage and as the more number of nodes are basically observed for the second case than the first case, i.e. more information is observed for the second case, the parameters are identified better for the second case when the probability density functions of the both cases are compared.

The identified parameters of the CT-Test are also compared with the updated parameters of a 8 node element as in 7.4.1.2 and it is found that since for CT-Test more nodes are observed and their displacements are measured but for the 8 node element only one node is observed, the parameters are identified better especially the damage parameters ((c_1), (c_2) and (c_3)) for the CT-Test. Moreover, for the CT-Test, the standard deviation

of parameters representing the uncertainty are updated more than the one element test and their probability density functions are narrowed much more for the CT-Test.

8.2. Bayesian Parameter Identification on CT-Test Considering Different Models

A Compact Tension (CT) test similar to test in Section 8.1 is carried out on a notched sample and the same boundary conditions are applied.

Figure 8.10 shows a displacement graph obtained from the parameters as seen in Table 8.3 and considered boundary conditions. The green, red and blue colors in Figure 8.10 represent the displacement of the node in x, y, and z directions respectively at the notch start point indicated by point A in Figure 8.1.

Table 8.3.: The model parameters

κ	1.66e5
G	7.69e4
σ_y	266
n	1
k	23500
b_R	298.6
H_R	117.2
$b_{\boldsymbol{\chi}}$	100
$H_{\boldsymbol{\chi}}$	150
c_1	4.5
c_2	5
c_3	-11
c_4	15
c_5	3.75

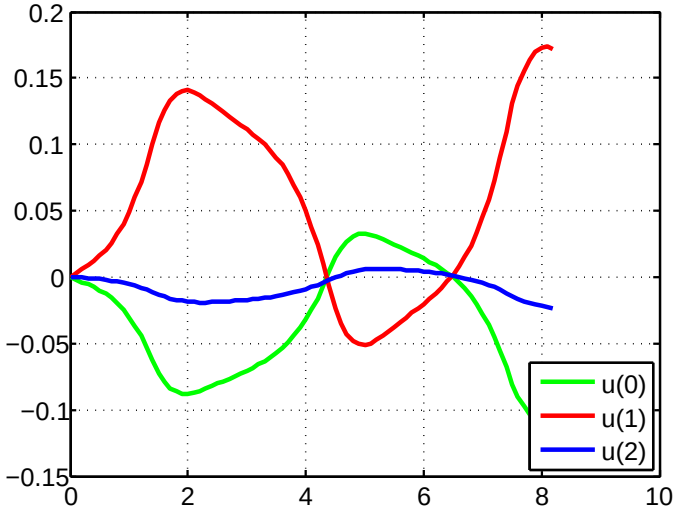

Figure 8.10.: Displacement of point A in x, y and z directions according to time

It should be pointed out that the same mesh generation as seen in Section 8.1 for the CT-Test model is considered. The damaged specimen with the evaluation of damage is shown in Figure 8.11.

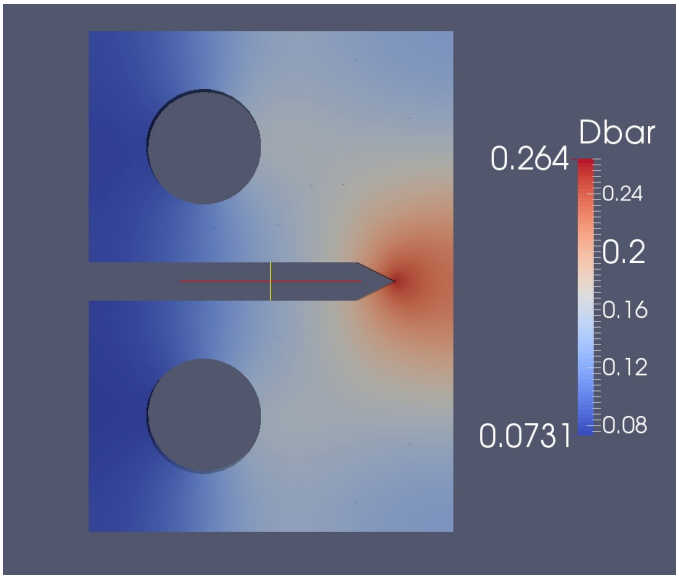

Figure 8.11.: Damaged specimen

Similar to the second case in Section 8.1, the displacement of the nodes on the external surface close to the notch as shown in Figure 8.6 are taken into consideration as the measurement in this section. Some Gaussian white noise like the observed displacement over time is added to the output data to have a perturbed virtual data. In order to consider the model error, data is determined for a full damage model introduced in Section 7.4 but the parameters are identified for a model with different damage equation as shown in Equation 8.1.

$$\dot{D} = (c_1 + c_2 e^{-c_3 p^+})\dot{p}^+ \tag{8.1}$$

These mentioned changes not only results in a very ill-posed problem but proves the applicability of the Gauss-Markov-Kalman filter method on different studied models, i.e. the data model and the identification model, which indeed represents an artificial model error.

8.2.1. GMKF Approach by Sequential Updating

The same forward model is considered as discussed in Subsection 8.1.1. Similarly the same parameters are considered as the uncertain parameters and hence the vector of unknown parameters is $\boldsymbol{q} = \big[\kappa(\omega),\, G(\omega),\, \sigma_y(\omega),\, b_R(\omega),\, b_{\boldsymbol{\chi}}(\omega),\, c_1(\omega),\, c_2(\omega),\, c_3(\omega)\big]$.

The Hermite function in form of polynomial chaos expansion is employed instead of samples like in the viscoplastic-damage model with isotropic and kinematic hardening. As discussed in Subsection 7.4.1, ansatz is defined to represent the uncertain parameters and output displacement where $\boldsymbol{\theta}(\omega)$ represents the Gaussian standard random variables. A third order Hermite function and 200 samples as the Hermite functions basis are considered. As discussed in Subsection 4.3.2, the coefficients of the bulk modulus, shear modulus, yield stress, isotropic and kinematic hardening parameters, damage parameters and displacement are computed. The stochastic collocation approach is used to solve the forward model as discussed in Subsection 4.3.2.

8.2.1.1. Sequential Updating

Similar to Subsection 8.1.1.1 the GMKF approach when updating is done sequentially is employed. The prior and posterior probability density functions of the identified parameters are shown in Figure 8.12.

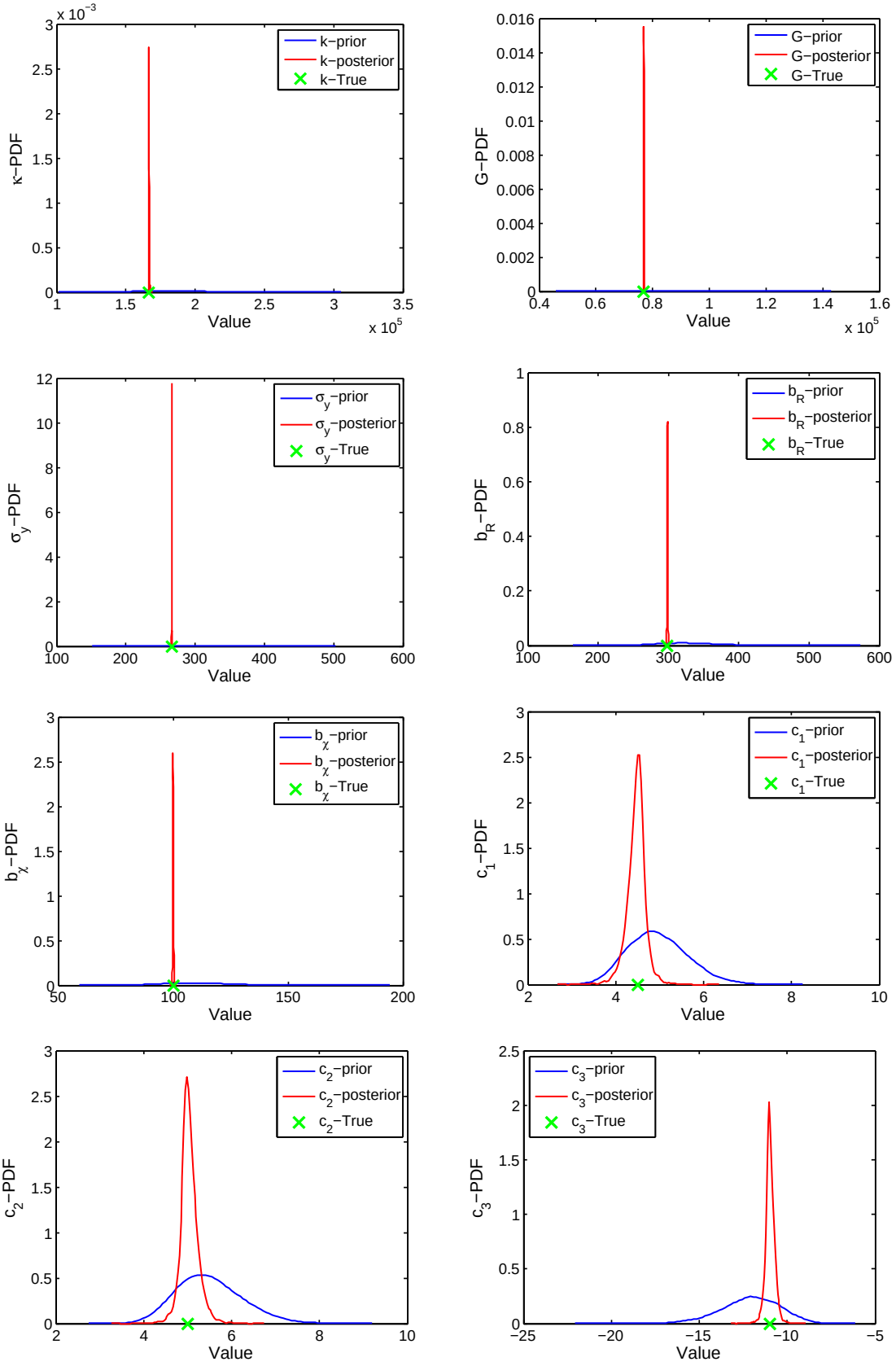

Figure 8.12.: PDF of identified parameters

The summarized results are shown in Table 8.4.

Table 8.4.: The identified model parameters

Parameters	$\boldsymbol{q}_{\text{true}}$	$\boldsymbol{q}_{\text{est}}$(mean)	$\boldsymbol{q}_{\text{est}}$(standard deviation)
κ	1.66e5	1.66e5	255.73
G	7.69e4	7.69e4	34.55
σ_y	266	265.99	0.51
b_R	298.6	298.57	0.51
$b_{\boldsymbol{\chi}}$	100	100.0	1.19
c_1	4.5	4.46	0.21
c_2	5	5.04	0.20
c_3	-11	-10.97	0.25

8.2.2. Discussion and Comparison

The parameters of the model are sequentially updated as discussed in Section 8.1. The evaluation of hardening and local damage on the top node at the notch start point representing the plasticity are shown in Figure 8.13. The update of the parameters such as bulk modulus (κ), shear modulus (G) and yield stress (σ_y) are done very properly. Because of a very large number of measurements considered, the hardening parameters ((b_R) and ($b_{\boldsymbol{\chi}}$)) are also updated significantly and more properly than the left uncertain parameters, i.e. damage parameters ((c_1), (c_2) and (c_3)) as seen in Figure 8.12. The reason behind is similar to the discussion in Section 8.1.

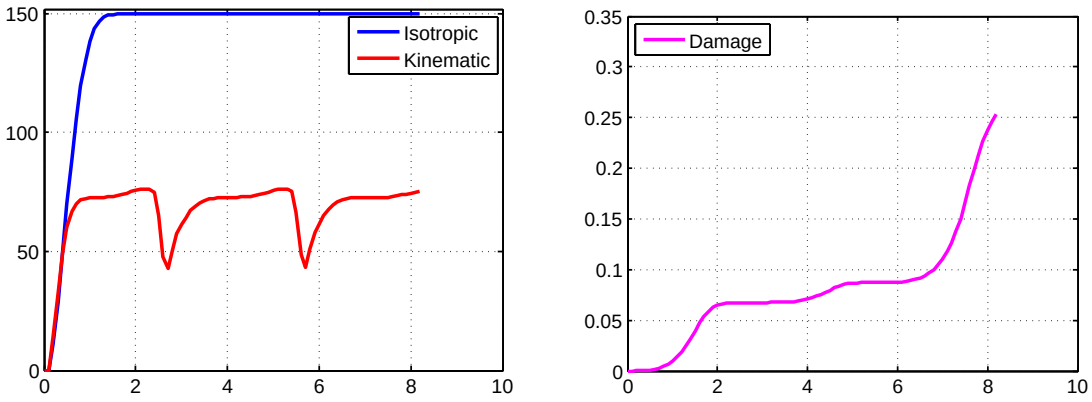

Figure 8.13.: Isotropic and kinematic hardening and non-local damage evaluation

Similar to Section 8.1, the parameters are updated much easier than the hardening and damage parameters. Although by adding noise to the measured data and by considering

a different identification model the estimated parameters using sequential Gauss-Markov-Kalman filter method are almost similar to the results of the second case in Subsection 8.1.1.1. As the results computed are somehow similar to the second case and not the first case, it can be inferred that number of observation data which is here the number of nodes that their output displacements are considered as the measurement data plays a more significant role than the other changes above. In other words, by having more measurement data a good enough identification is possible, as the standard deviations of the residual uncertainties are below 5% of their mean values, even if the data and identification model are different. The results from Figure 8.12 proves that the sequential Gauss-Markov-Kalman filter may be applicable for different models representing the data model or reality and identification model, which represents the model error.

8.3. Conclusion

In this chapter, a sequential Gauss-Markov-Kalman filter approach is applied on a viscoplastic-damage model on a well-known test, so-called CT-Test in order to identify its model parameters. The conclusion from the discussions and comparisons made in Subsection 8.1.2 and 8.2.2 by considering the updated value of the parameters computed using the Gauss-Markov-Kalman filter approach as described in Section 8.1 and 8.2 are classified below.

- The sequential Gauss-Markov-Kalman filter approach can be applied to update the model parameters by considering the surface displacement as the measurement data. The better identification and better reduction in uncertainties of the parameters is achieved by considering the more number of nodes and it is concluded from the comparison as shown in Section 8.1.
- The number of updating can be reduced to reduce the computation time when the more information from the large number of nodal displacement is available. The CT-Test with a very fine mesh takes a lot of time to solve the system of PDE therefore updating is performed only at few certain time steps and these time steps should be chosen smartly in a way as discussed in Subsection 7.4.1.2. The sequential Gauss-Markov-Kalman filter approach updates the model parameters properly where updatings are done on some specified time steps by considering a large observation data available from the surface strain.
- Considering the model error by taking into account different data model and identification model, the sequential Gauss-Markov-Kalman filter approach can still be employed to identify the model parameters by considering the large number of measurement data determined from the surface displacement of a different data model as the parameters are identified properly. The estimated parameters are very close to the truth values as shown in Table 8.4 in Section 8.2.

Considering the above mentioned comparisons, observations, discussions and results, it can be concluded that identification of model parameters is possible using sequential

Gauss-Markov-Kalman filter approach from pure surface measurement of strain which is practically possible in the form of Digital Image Correlation (DIC). Hence this approach can also be used for the health monitoring purposes as the model parameters can be estimated before the occurrence of severe damage and collapse.

9. Conclusions and Outlook

This chapter summarizes the conclusions and in addition in this chapter a brief outlook on future work is presented.

9.1. Conclusions

The main goals which are achieved in this thesis are classified below.

- The Transitional Markov Chain Monte Carlo method was applied on the viscoplasticity model to estimate the model parameters. Although it is computationally expensive, the results of parameter identification on the viscoplastic model with hardening provided by Transitional Markov Chain Monte Carlo are very acceptable.
- The Gauss-Markov-Kalman filter approach is applied on the viscoplastic-damage model to identify the parameters through a history matching update method. The estimated parameters are not all time true for all model parameters and their uncertainties are not reduced greatly. The load path should be carefully designed to identify the parameters as the updating is done only once and also not from all states enough information can be obtained to identify all parameters. Moreover the Gauss-Markov-Kalman filter approach using history matching update does not take much time than the Transitional Markov Chain Monte Carlo method.
- The sequential Gauss-Markov-Kalman filter approach is recommended to apply on a viscoplastic-damage model. The estimated parameters are accurate and the uncertainties of the parameters are reduced significantly. However the updating should be carefully designed in such a way that only at special time steps the parameters should be updated. Although sequential Gauss-Markov-Kalman filter approach is computationally more expensive than the Gauss-Markov-Kalman filter approach using history matching update, the quality of the results are much better.
- The model parameters of the engineering specimen using the sequential Gauss-Markov-Kalman filter approach by considering a lot of measurements can be identified as shown for example in CT-Test model parameter identification.
- The identification of model parameters using sequential Gauss-Markov-Kalman filter approach is still possible by considering a very high number of measurement data gained from a different data model representing the reality than the identification model, which literally means considering a model error.

- The identification of the model parameters are possible using sequential Gauss-Markov-Kalman filter approach from a pure surface measurement of strain as shown in CT-Test, which is practically possible for example in the form of Digital Image Correlation (DIC).
- Sequential Gauss-Markov-Kalman filter approach can be recommended as the selected probabilistic method for Bayesian model parameter identification of real mechanical engineering tests and health monitoring purposes as the model parameters can be estimated before the occurrence of a severe damage and collapse.

9.2. Outlook

Further investigations can be suggested for further studies which are discussed below.

- An automatic approach can be developed for the updating in a sequential Gauss-Markov-Kalman filter approach instead of choosing the time steps on some time intervals. The parameters in different equations which influence the measurements and the amount of their effects are distinguished by this method and then it is updated exactly at these time steps.
- The use of random fields instead of random variables for the inhomogeneous material can also be discussed further.
- The possibility of magnification of the influence of uncertain parameters on the final observed data can also be investigated if the effect of some uncertain parameters on the measurement is not huge. As described in the example, the effect of damage parameters on the final output displacement is not huge as compared to the effect of bulk modulus and shear modulus. Therefore, it can be investigated if it is possible to magnify the impact on the measurement and then the updating of parameters to be performed. Once all uncertain parameters have the same influence on the observed data, then the parameters can be identified with a same amount.
- Similar to the Bayesian identification of model parameters, the Bayesian model selection is also to be discussed where the behavior of an observed measurement can be compared to different range of mechanical material models e.g. plasticity, viscoplastic, plasticity with hardening, viscoplastic-damage model. Then a best fit model to the measurement can be detected.

Bibliography

[1] A. Miller. An inelastic constitutive model for monotonic, cyclic, and creep deformation: part I–equations development and analytical procedures. Journal of Engineering Material Technology 98(2), 97-105, 1976.

[2] E. Krempl, J. J. McMahon and D. Yao. Viscoplasticity based on overstress with a differential growth law for the equilibrium stress. Journal of Mechanics of Materials 5, 35-48, 1986.

[3] R. K. Korhonen, M. S. Laasanen, J. Toyras, R. Lappalainen, H. J. Helminen and J. S. Jurvelin. Fibril reinforced poroelastic model predicts specifically mechanical behavior of normal, proteoglycan depleted and collagen degraded articular cartilage. Journal of Biomechanics 36, 1373-1379, 2003.

[4] M. Aubertin, D. E. Gill and B. Ladanyi. A unified viscoplastic model for the inelastic flow of alkali halides. Journal of Mechanics of Materials 11, 63-82, 1991.

[5] K. S. Chan, S. R. Bodner, A. F. Fossum and D. E. Munson. A constitutive model for inelastic flow and damage evolution in solids under triaxial compression. Journal of Mechanics of Materials 14, 1-14, 1992.

[6] A. F. Fossum. Rate Data and Material Model Parameter Estimation. Journal of Engineering Materials and Technology 120(1), 7-12, 1998.

[7] J. J. Kang, A. A. Becker and W. Sun. Determination of elastic and viscoplastic material properties obtained from indentation tests using a combined finite element analysis and optimization approach. Proceedings of the Institution of Mechanical Engineers, Part L: Journal of Materials Design and Applications 229(3), 175-188, 2013.

[8] F. Yoshida, M. Urabe, V. V. Toropov. Identification of material parameters in constitutive model for sheet metals from cyclic bending tests. International Journal of Mechanical Sciences 40(2-3), 237-249, 1998.

[9] S. Avril, M. Bonnet, A. S. Bretelle, M. Grédiac, F. Hild, P. Ienny, F. Latourte, D. Lemosse, S. Pagano, E. Pagnacco and F. Pierron. Overview of identification methods of mechanical parameters based on full-field measurements. Journal of Experimental Mechanics (48), 381-402, 2008.

[10] M. Becker and M. Teschner. Robust and Efficient Estimation of Elasticity Parameters using the Linear Finite Element Method. SimVis 15-28. SCS Publishing House e.V., 2007.

[11] A. S. Gendy and A. F. Saleeb. Nonlinear material parameter estimation for characterizing hyper elastic large strain models. Journal of Computational Mechanics 25, 66-77, 2000.

[12] J. S. Novak, D. Benasciutti, F. de Bona, A. Stanojevic, A. de Luca and Y. Raffaglio. Estimation of material parameters in nonlinear hardening plasticity models and strain life curves for CuAg alloy. IOP Conference Series: Materials Science and Engineering 119, 012020, 2016.

[13] Y. Lin and M. A. Stadtherr. Deterministic global optimization for parameter estimation of dynamic systems. Journal of Industrial and Engineering Chemistry Research 45(25), 8438-8448, 2006.

[14] S. Rouchier, M. Rabouille and P. Oberle. Calibration of simplified building energy models for parameter estimation and forecasting: stochastic versus deterministic modelling. Journal of Building and Environment 134, 181-190, 2018.

[15] A. Rieger, G. Scheday and C. Miehe. Parameter identification of a finite viscoplastic material model using different deterministic optimization methods. Proceedings in Applied Mathematics and Mechanics 2(1), 525-526, 2003.

[16] A. L. Araujo, C. M. Mota Soares, J. Herskovits and P. Pedersen. Visco-piezo-elastic parameter estimation in laminated plate structures. Inverse Problems in Science and Engineering 17(2), 145-157, 2009.

[17] P. Renard, A. Alcolea and D. Ginsbourger. Stochastic versus Deterministic Approaches. Environmental Modelling: Finding Simplicity in Complexity, Second Edition. Edited by John Wainwright and Mark Mulligan, 2013.

[18] A. L. Araújo, C. M. Mota Soares, M. J. Moreira de Freitas, P. Pedersen, J. Herskovits. Combined numerical-experimental model for the identification of mechanical properties of laminated structures. Journal of Composite Structures 50(4), 363-372, 2000.

[19] P. Kłosowski and A. Mleczek. Parameters' identification of Perzyna and Chaboche viscoplastic models for Aluminum alloy at temperature of 120°C. Journal of Transportation Engineering 62(3), 291-305, 2014.

[20] H. T. Banks, S. Hu and Z. R. Kenz. Material parameter estimation and hypothesis testing on a 1D viscoelastic stenosis model: Methodology. Journal of Inverse and Ill-posed Problems 21(1), 25-57, 2013.

[21] Y. Gong, C. Hyde, W. Sun and T. Hyde. Determination of material properties in the Chaboche unified viscoplasticity model. Proceedings of the Institution of Mechanical Engineers, Part L: Journal of Materials: Design and Applications, 224(1), 19-29, 2010.

[22] T. Harth and J. Lehn. Identification of material parameters for inelastic constitutive models Using stochastic methods. GAMM-Mitt. 30, No. 2, 409-429, 2007.

[23] K. S. Chan, S. R. Bodner and U. S. Lindholm. Phenomenological modelling of hardening and thermal recovery in metals. Journal of Engineering Materials and Technology 110, 18, 1988.

[24] P. D. Arendt, D. W. Apley and W. Chen. Quantification of model uncertainty: calibration, model discrepancy, and identifiability. Journal of Mechanical Design 134(10), 100908, 2012.

[25] A. Cividini, G. Maier and A. Nappi. Parameter estimation of a static geotechnical model using a Bayes' approach. International Journal of Rock Mechanics and Mining Sciences and Geomechanics Abstracts 20(5), 215-226, 1983.

[26] C. Pacheco, G. S. Dulikravich, M. Vesenjak, M. Borovinsek, I. M. A. Duarte, R. Jha, S. R. Reddy, H. R. B. Orlande and M. J. Colaco. Inverse parameter identification in solid mechanics using Bayesian statistics, response surfaces and minimization. Technische Mechanik 36(1-2), 120-131, 2016.

[27] A. Gallina, L. Ambrozinski, P. Packo, L. Pieczonka, T. Uhl and W. J. Staszewski. Bayesian parameter identification of orthotropic composite materials using lamb waves dispersion curves measurement. Journal of Vibration and Control 23(16), 2656-2671, 2017.

[28] L. Pieczonka, A. Gallina, L. Ambrozinski, P. Packo, T. Uhl and W. J. Staszewski. Parameters identification of composite materials using Bayesian approach and guided ultrasonic waves. Proceedings of ISMA 2016 - International Conference on Noise and Vibration Engineering and USD2016, 2016.

[29] M. Arnst, R. Ghanem and C. Soize. Identification of Bayesian posteriors for coefficients of chaos expansions. Journal of Computational Physics 229(9), 3134-3154, 2010.

[30] H. Rappel, L. A. A. Beex, J. S. Hale and S. P. A. Bordas. Bayesian inference for the stochastic identification of elastoplastic material parameters: introduction, misconceptions and insights. arXiv:1606.02422, 2017.

[31] H. Rappel, L. A. A. Beex, L. Noels and S. P. A. Bordas. Identifying elastoplastic parameters with Bayes theorem considering double error sources and model uncertainty. Journal of Probabilistic Engineering Mechanics, 2018.

[32] M. Słonski. Bayesian identification of elastic parameters in composite laminates applying lamb waves monitoring. Computational Methods in Structural Dynamics and Earthquake Engineering, M. Papadrakakis, V. Papadopoulos, V. Plevris (Eds.), 2015.

[33] D. An, J. Cho and N. H. Kim. Identification of correlated damage parameters under noise and bias using Bayesian inference. Structural Health Monitoring 11(3), 293-303, 2011.

[34] W. P. Hernandez, F. C. L. Borges, D. A. Castello, N. Roitman and C. Magluta. Bayesian inference applied on model calibration of a fractional derivative viscoelastic model. Proceedings of the XVII International Symposium on Dynamic Problems of Mechanics, V. Steffen, D. A. Rade, W. M. Bessa (Eds.), 2015.

[35] R. Mahnken. Identification of material parameters for constitutive equations. Encyclopedia of Computational Mechanics Second Edition, Part 2. Solids and Structures, 1-21, 2017.

[36] W. Zheng and Y. Yu. Bayesian probabilistic framework for damage identification of steel truss bridges under joint uncertainties. Advances in Civil Engineering 1-13, 2013.

[37] J. M. Nichols, E. Z. Moore and K. D. Murphy. Bayesian identification of a cracked plate using a population-based Markov Chain Monte Carlo method. Journal of Computers and Structures 89(13-14), 1323-1332, 2011.

[38] E. Zhang, J. D. Chazot and J. Antoni. Parametric identification of elastic modulus of polymeric material in laminated glasses. 16th IFAC Symposium on System Identification, The International Federation of Automatic Control, 2012.

[39] S. Madireddy, B. Sista and K. Vemaganti. A Bayesian approach to selecting hyperelastic constitutive models of soft tissue. Journal of Computational and Applied Mathematics 291, 102-122, 2015.

[40] J. Wang and N. Zabaras. A Bayesian inference approach to the inverse heat conduction problem. International Journal of Heat and Mass Transfer 47(17-18), 3927-3941, 2004.

[41] C. K. Oh, J. L. Beck and M. Yamada. Bayesian learning using automatic relevance determination prior with an application to earthquake early warning. Journal of Engineering Mechanics 134(12), 1013-1020, 2008.

[42] K. Alvin. Finite element model update via Bayesian estimation and minimization of dynamic residuals. The American Institute of Aeronautics and Astronautics Journal 135(5), 879-886, 1997.

[43] T. Marwala and S. Sibusiso. Finite element model updating using Bayesian framework and modal properties. Journal of Aircraft 42(1), 275-278, 2005.

[44] F. Daghia, S. de Miranda, F. Ubertini and E. Viola. Estimation of elastic constants of thick laminated plates within a Bayesian framework. Journal of Composite Structures 80(3), 461-473, 2007.

[45] S. Abhinav and C. Manohar. Bayesian parameter identification in dynamic state space models using modified measurement equations. International Journal of Non-Linear Mechanics 71, 89-103, 2015.

[46] C. Gogu, W. Yin, R. Haftka, P. Ifju, J. Molimard, R. le Riche and A. Vautrin. Bayesian identification of elastic constants in multi-directional laminate from Moire interferometry displacement fields. Journal of Experimental Mechanics 53(4), 635-648, 2013.

[47] C. Gogu, R. Haftka, J. Molimard and A. Vautrin. Introduction to the Bayesian approach applied to elastic constants identification. The American Institute of Aeronautics and Astronautics Journal 48(5), 893-903, 2010.

[48] P. S. Koutsourelakis. A novel Bayesian strategy for the identification of spatially varying material properties and model validation: an application to static elastography. International Journal for Numerical Methods in Engineering 91(3), 249-268, 2012.

[49] P. S. Koutsourelakis. A multi-resolution, non-parametric, Bayesian framework for identification of spatially-varying model parameters. Journal of Computational Physics 228(17), 6184-6211, 2009.

[50] D. D. Fitzenz, A. Jalobeanu and S. H. Hickman. Integrating laboratory creep compaction data with numerical fault models: a Bayesian framework. Journal of Geophysical Research: Solid Earth 112, B08410, 2007.

[51] T. Most. Identification of the parameters of complex constitutive models: least squares minimization vs. Bayesian updating. In: Straub, D. (ed.) Reliability and Optimization of Structural Systems, CRC Press, 119-130, 2010.

[52] S. Sarkar, D. S. Kosson, S. Mahadevan, J. C. L. Meeussen, H. van der Sloot, J. R. Arnold, K. G. Brown. Bayesian calibration of thermodynamic parameters for geochemical speciation modeling of cementitious materials. Journal of Cement and Concrete Research 42(7), 889-902, 2012.

[53] E. Zhang, J. D. Chazot, J. Antoni and M. Hamdi. Bayesian characterization of Young's modulus of viscoelastic materials in laminated structures. Journal of Sound and Vibration 332(16), 3654-3666, 2013.

[54] L. Mehrez, E. Kassem, E. Masad and D. Little. Stochastic identification of linear-viscoelastic models of aged and unaged asphalt mixtures. Journal of Materials in Civil Engineering 27(4), 04014149, 2015.

[55] P. Miles, M. Hays, R. Smith and W. Oates. Bayesian uncertainty analysis of finite deformation viscoelasticity. Journal of Mechanics of Materials 91, 35-49, 2015.

[56] X. Zhao and A. A. Pelegri. A Bayesian approach for characterization of soft tissue viscoelasticity in acoustic radiation force imaging. International Journal for Numerical Methods in Biomedical Engineering 32(4), E02741, 2016.

[57] Z. R. Kenz, H. T. Banks and R. C. Smith. Comparison of frequentist and Bayesian confidence analysis methods on a viscoelastic stenosis model. SIAM/ASA Journal on Uncertainty Quantification 1(1), 348-369, 2013.

[58] D. An, J. Choi, N. H. Kim and S. Pattabhiraman. Fatigue life prediction based on Bayesian approach to incorporate field data into probability model. Journal of Structural Engineering and Mechanics 37(4), 427-442, 2011.

[59] T. Hoshi, Y. Kobayashi, K. Kawamura and M. G. Fujie. Developing an intraoperative methodology using the finite element method and the extended Kalman filter to identify the material parameters of an organ model. Proceedings of the 29th Annual International Conference of the IEEE EMBS Cité Internationale, Lyon, France, 2007.

[60] T. Furukawa and J. W. Pan. Stochastic identification of elastic constants for anisotropic materials. International Journal for Numerical Methods in Engineering 81, 429-452, 2010.

[61] J. P. Conte, R. Astroza and H. Ebrahimian. Bayesian methods for nonlinear system identification of civil structures. MATEC Web of Conferences 24, 03002, 2015.

[62] M. A. N. Hendriks. Identification of the mechanical behavior of solid materials. Ph.D. Dissertation, Department of Mechanical Engineering, Technische Universiteit Eindhoven, 1991.

[63] G. Bolzon, R. Fedele and G. Maier. Parameter identification of a cohesive crack model by Kalman filter. Journal of Computer Methods in Applied Mechanics and Engineering 191(25-26), 2847-2871, 2002.

[64] L. T. Nguyen. Inference of ground condition in mechanized tunneling via inverse analysis using sequential Bayesian filtering. Ph.D. Dissertation, Ruhr-Universität Bochum, 2017.

[65] L. T. Nguyen, M. Datcheva and T. Nestorović. Inference of ground condition in mechanized tunneling via inverse analysis using sequential Bayesian filtering. Journal of Mechanics Research Communications 53, 47-52, 2013.

[66] R. Astroza, L. T. Nguyen and T. Nestorović. Finite element model updating using simulated annealing hybridized with unscented Kalman filter. Journal of Computers and Structures 177, 176-191, 2016.

[67] L. T. Nguyen and T. Nestorović. The extended Kalman filter and the unscented Kalman filter for material parameter identification with application in tunneling. Proceedings in Applied Mathematics and Mechanics 13, 393-394, 2013.

[68] L. T. Nguyen, R. Hölter, T. Nestorović and T. Schanz. Identifying the geological scenario ahead of the tunnel face: The use of elastoplastic and elastodynamic responses. Geotechnics for Sustainable Infrastructure Development - Geotec Hanoi, 2016.

[69] O. Wall and J. Holst. Estimation of parameters in viscoplastic and creep material models. SIAM Journal on Applied Mathematics 61(6), 2080-2103, 2001.

[70] T. Nakamura and Y. Gu. Identification of elastic-plastic anisotropic parameters using instrumented indentation and inverse analysis. Journal of Mechanics of Materials 39(4), 340-356, 2007.

[71] M. Agmell, A. Ahadi and J. Stahl. Identification of plasticity constants from orthogonal cutting and inverse analysis. Journal of Mechanics of Materials 77, 43-51, 2014.

[72] M. Bocciarelli, G. Bolzon and G. Maier. A constitutive model of metal-ceramic functionally graded material behavior: formulation and parameter identification. Journal of Computational Materials Science 43(1), 16-26, 2008.

[73] Y. Gu, T. Nakamura, L. Prchlik, S. Sampath, J. Wallace. Micro-indentation and inverse analysis to characterize elastic-plastic graded materials. Journal of Materials Science and Engineering: A 345(1-2), 223-233, 2003.

[74] A. Corigliano and S. Mariani. Parameter identification of a time-dependent elastic-damage interface model for the simulation of debonding in composites. Journal of Composites Science and Technology 61, 191-203, 2001.

[75] A. Corigliano and S. Mariani. Simulation of damage in composites by means of interface models: parameter identification. Journal of Composites Science and Technology 61(15), 2299-2315, 2001.

[76] H. Ebrahimian, R. Astroza, J. P. Conte and R. A. de Callafon. Nonlinear finite element model updating for damage identification of civil structures using batch Bayesian estimation. Journal of Mechanical Systems and Signal Processing 84, 194-222, 2017.

[77] H. Ebrahimian, R. Astroza and J. P. Conte. Parametric identification of hysteretic material constitutive laws in nonlinear finite element models using extended Kalman filter. Department of Structural Engineering, University of California, San Diego, La Jolla, CA, 2014.

[78] H. Ebrahimian, R. Astroza and J. P. Conte. Extended Kalman filter for material parameter estimation in nonlinear structural finite element models using direct differentiation method. Earthquake Engineering and Structural Dynamics 44, 1495-1522, 2015.

[79] R. Astroza, H. Ebrahimian and J. P. Conte. Material parameter identification in distributed plasticity FE models of frame-type structures using nonlinear stochastic filtering. Journal of Engineering Mechanics 141(5), 04014149, 2015.

[80] A. Yan, P. de Boe and J. Golinval. Structural damage diagnosis by Kalman model based on stochastic subspace identification. International Journal of Structural Health Monitoring 3(2), 103-119, 2004.

[81] R. C. Aster, B. Borchers and C. H. Thurber. Parameter Estimation and Inverse Problems. 2nd Edition, Academic Press, 2012.

[82] M. Dashti and A. M. Stuart. The Bayesian Approach to Inverse Problems. Handbook of Uncertainty Quantification, 1-118. , 2015.

[83] H. W. Engl, M. Hanke and A. Neubauer. Regularization of inverse problems. Dordrecht: Kluwer, 2000.

[84] E. T. Jaynes. Probability theory, the logic of science. Cambridge University Press, Cambridge, 2003.

[85] A. Tarantola. Inverse problem theory and methods for model parameter estimation. Philadelphia: SIAM, 2004.

[86] M. Goldstein and D. Wooff. Bayes linear statisticstheory and methods. Wiley series in probability and statistics, Chichester: Wiley, 2007.

[87] Y. M. Marzouk and H. N. Najm and L. A. Rahn. Stochastic spectral methods for efficient Bayesian solution of inverse problems. Journal of Computational Physics 224(2), 560-586, 2007.

[88] B. V. Rosić, A. Kucerová, J. Sýkora, O. Pajonk, A. Litvinenko and H. G. Matthies. Parameter identification in a probabilistic setting. Journal of Structural Engineering 50, 179-196, 2013.

[89] A. M. Stuart. Inverse problems: a Bayesian perspective. Acta Numerica. 19, 451-559, 2010.

[90] K. C. Le, Introduction to continuum mechanics, Lecture Notes, Ruhr-Universität Bochum, 2013.

[91] K. Hackl and M. Goodarzi. An introduction to linear continuum mechanics. Lecture Notes, Ruhr-Universität Bochum, 2013.

[92] J. Bonet and R. D. Wood. Nonlinear continuum mechanics for finite element analysis, Cambridge University Press, 1997.

[93] J. L. Chaboche and G. Rousselier. On the plastic and viscoplastic constitutive equations part I: rules developed with internal variable concept. Journal of Pressure Vessel Technology 105, 153-158, 1983.

[94] J. L. Chaboche and G. Rousselier. On the plastic and viscoplastic constitutive equations part II: application of internal variable concepts to the 316 stainless steel. Journal of Pressure Vessel Technology 105, 159-164, 1983.

[95] U. Kowalsky, J. Meyer, S. Heinrich and D. Dinkler. A nonlocal damage model for mild steel under inelastic cyclic straining. Computational Materials Science 63, 28-34, 2012.

[96] J. L. Chaboche. Le Concept de Contrainte Effective AppliquElasticit Viscoplasticit Prnce dun Endommagement Anisotrope. Proceedings of the Euromech Colloquium 115, 737-760, 1982.

[97] T. Zümendorf. Ein gradientenabhängiges Modell für Schädigung bei viskoplastischem Materialverhalten. Ph.D. Dissertation, Institut für Statik, Technische Universität Braunschweig, 2006.

[98] J. Velde. 3D non-local damage modeling for steel structures under earthquake loading. Ph.D. Dissertation, Institut für Statik, Technische Universität Braunschweig, 2010.
U. Hoppe. Computational Plasticity. Lecture Notes, Ruhr-Universität Bochum, 2010.

[99] D. Kuhl and G. Meschke. Finite element methods in linear structural mechanics. Lecture Notes, Ruhr-Universität Bochum, 2005.
G. Meschke. Finite element methods for nonlinear analyses of materials and structures. Lecture Notes, Ruhr-Universität Bochum, 2012.
G. Meschke. Advanced finite element methods. Lecture Notes, Ruhr-Universität Bochum, 2013.

[100] A. Ibrahimbegovic. Nonlinear Solid Mechanics. Solid Mechanics and its Applications 160, Springer, 2009.

[101] J. C. Simo and T. J. R. Hughes. Computational inelasticity. Springer, 7th edition, 1998.

[102] J. Velde, U. Kowalsky, T. Zümendorf and D. Dinkler. 3D-FE-Analysis of CT-specimens including viscoplastic material behavior and nonlocal damage. Computational Materials Science 46, 352-357, 2009.

[103] U. Kowalsky, T. Zümendorf and D. Dinkler. Random fluctuations of material behaviour in FE-damage-analysis. Computational Materials Science 39, 8-16, 2007.

[104] A. Pirondi and N. Bonora. Modeling ductile damage under fully reversed cycling. Computational Material Science 26, 129-141, 2003.

[105] T. Hughes and G. Hulbert. Space-time finite element methods for elastodynamics: formulations and error estimates. Computer Methods in Applied Mechanics and Engineering 66, 339-363, 1988.

[106] O. C. Zienkiewicz, R. L. Taylor and J. Z. Zhu. The finite element method: its basis and fundamentals. Elsevier Butterworth-Heinemann, 6th edition, 2005

[107] S. Reinstädler. Modellierung und numerische Analyse der Entleerung von dünnewandigen Silos. Ph.D. Dissertation, Institut für Statik, Technische Universität Braunschweig, 2015.

[108] B. Sudret and A. Der Kiureghian. Stochastic finite element methods and reliability. A state-of-the-art report, Report UCB/SEMM2000/08, Department of Civil and Environmental Engineering, University of California, Berkeley, CA, 2000.

[109] M. A. Gutiérrez and S. Krenk. Stochastic finite element methods. Encyclopedia of Computational Mechanics (2), E. Stein, R. de Borst, and T. J. R. Hughes (Eds), 657-681, 2004.

[110] M. Krosche. A generic component-based software architecture for the simulation of probabilistic models. Ph.D. Dissertation, Institut für Wissenschaftliches Rechnen, Technische Universität Braunschweig, 2013.

[111] R. E. Melchers. Structural reliability analysis and prediction, 2nd edition England: John Wiley and Sons, Inc, 1999.

[112] H. G. Matthies, C. E. Brenner, C. G. Bucher, and C. Guedes Soares. Uncertainties in probabilistic numerical analysis of structures and solids – Stochastic Finite Elements. Journal of Structural Safety 19, 283-336, 1997.

[113] H. G. Matthies. Computational aspects of probability in non-linear mechanics. Multi-physics and Multi-scale Computer Models in Non-linear Analysis and Optimal Design of Engineering Structures under Extreme Conditions, edited by A. Ibrahimbegovic and B. Brank, NATO Science Series III: Computer and System Sciences Vol. 194 IOS Press, Amsterdam, 2005.

[114] M. Grigoriu. Stochastic calculus – applications in science and engineering, Birkhäuser Verlag, Basel, 2002.

[115] H. G. Matthies. Uncertainty quantification with stochastic finite elements. in: Encyclopedia of Computational Mechanics, edited by E. Stein, R. de Borst, T. R. J. Hughes, John Wiley & Sons, Chichester, 2007.

[116] S. Ghahramani. Fundamentals of probability, with stochastic processes. 3rd edition, New Jersey, USA: Pearson, Prentice Hall, 2005.

[117] A. Papoulis. Probability, random variables, and Stochastic Processes. McGraw-Hill, New York, NY, 1984.

[118] A. Keese and H. G. Matthies. Adaptivity and sensitivity for stochastic problems. in: Computational Stochastic Mechanics 4, edited by P. D. Spanos and G. Deodatis, Millpress, Rotterdam, 311-316, 2003.

[119] A. Berlinet and C. Thomas-Agnan. Reproducing Kernel Hilbert spaces in probability and statistics. Kluwer, Dordrecht, 2004.

[120] R. Ghanem. Ingredients for a general purpose stochastic finite elements implementation. Journal of Computer Methods in Applied Mechanics and Engineering (Netherlands) 168, 19-34, 1999.

[121] R. N. Bracewell. The Fourier transform and its applications. McGraw-Hill, New York, NY, 1978.

[122] M. Shinozuka and G. Deodatis. Simulation of stochastic processes and fields. Journal of Probabilistic Engineering Mechanics 14, 203-207, 1997.

[123] M. Loève. Probability theory. Volumes I and II, Springer-Verlag, Berlin, 1977.

[124] C. Bucher and M. Macke. Stochastic computational mechanics. In Proceedings of International Conference on Safety, Risk and Reliability-Trends in Engineering, Malta, 2001.

[125] R. G. Ghanem and S. Dham. Stochastic finite element analysis for multiphase flow in heterogeneous porous media. Transport in Porous Media, 32(3), 239-262, 1998.

[126] A. Keese. Numerical solution of systems with stochastic uncertainties. A general purpose framework for stochastic finite elements. Ph.D. Dissertation, Institut für Wissenschaftliches Rechnen, Technische Universität Braunschweig, 2003.

[127] K. P. Murphy. Markov chain Monte Carlo. Lecture Notes, 2006.

[128] K. E. Atkinson. The numerical solution of integral equations of the second kind. Cambridge University Press, Cambridge, 1997.

[129] P. Krèe and C. Soize. Mathematics of random phenomena. D. Reidel, Dordrecht, 1986.

[130] H. G. Matthies. Stochastic finite elements: computational approaches to stochastic partial differential equations. Journal of Applied Mathematics and Mechanics 88(11), 845-926, 2008.

[131] N. Wiener. The homogeneous chaos. The American Journal of Mathematics 60, 897-936, 1938.

[132] S. Janson. Gaussian Hilbert spaces. Cambridge University Press, Cambridge, 1997.

[133] R. E. Caflisch. Monte Carlo and quasi-Monte Carlo methods. Acta Numerica. 7, 1-49, 1998.

[134] J. S. Liu. Monte Carlo strategies in scientific computing. Springer, New York, 2001.

[135] N. Madras. Lectures on Monte Carlo methods. Fields Institute Monographs. American Mathematical Society, Providence, 2002.

[136] J. Foo and G. E. Karniadakis. Multi-element probabilistic collocation method in high dimensions. Journal of Computational Physics 229(5), 1536-1557, 2010.

[137] G. Blatman and B. Sudret. Adaptive sparse polynomial chaos expansion based on least angle regression. Journal of Computational Physics 230(6), 2345-2367, 2011.

[138] B. Ganapathysubramanian and N. Zabaras. Sparse grid collocation schemes for stochastic natural convection problems. Journal of Computational Physics 225(1), 652-685, 2007.

[139] F. Nobile, R. Tempone and C. G. Webster. A sparse grid stochastic collocation method for partial differential equations with random input data. SIAM Journal on Numerical Analysis 46(5), 2309-2345, 2008.

[140] M. Papadrakakis and V. Papadopoulos. Robust and efficient methods for stochastic finite element analysis using Monte Carlo simulation. Journal of Computer Methods in Applied Mechanics and Engineering (Netherlands) 134, 325-340, 1996.

[141] T. Gerstner and M. Griebel. Numerical integration using sparse grids. Numerical Algorithms (Netherlands) 18, 209-232, 1998.

[142] R. Ghanem and P. D. Spanos. Stochastic finite elements – A spectral approach, Springer-Verlag, Berlin, 1991.

[143] F. Riesz and B. Sz.-Nagy. Functional analysis, Dover Publications, New York, NY, 1990.

[144] J. Hadamard. Sur les problémes aux dérivées partielles et leur signification physique. Princeton University Bulletin, 49-52, 1902.

[145] H. G. Matthies and C. G. Bucher. Finite elements for stochastic media problems. Journal of Computer Methods in Applied Mechanics and Engineering (Netherlands) 168, 3-17, 1999.

[146] H. G. Matthies and A. Keese. Galerkin methods for linear and nonlinear elliptic stochastic partial differential equations. Journal of Computer Methods in Applied Mechanics and Engineering (Netherlands) 194, 1295-1331, 2005.

[147] G. Strang and G. J. Fix. An analysis of the finite element method. Wellesley-Cambridge Press, Wellesley, MA, 1988.

[148] B. V. Rosić. Variational formulations and functional approximation algorithms in stochastic plasticity of materials. Ph.D. Dissertation, Technische Universität Braunschweig and University of Kragujevac, 2013.

[149] B. V. Rosić and H. G. Matthies. Variational theory and computations in stochastic plasticity. Archives of Computational Methods in Engineering 22, 457-509, 2015.

[150] P. Wriggers. Mixed finite element methods - theory and discretization. CISM International Centre for Mechanical Sciences 509, 131-177, 2009.

[151] R. Y. Rubinstein. Simulation and the Monte Carlo method. 1st edition Canada: John Wiley & Sons, 1981.

[152] C. P. Robert and G. Casella. Monte Carlo statistical methods. 2nd edition, Springer, New York, 2004.

[153] M. Muto and J. L. Beck. Bayesian updating and model class selection for hysteretic structural models using stochastic simulation. Engineering and Applied Science, California Institute of Technology, Pasadena, CA 91125 USA, 2006.

[154] N. Metropolis, A. Rosenbluth, M. Rosenbluth, A. Teller and E. Teller. Equations of state calculations by fast computing machines. Journal of Chemical Physics 21, 1087-1092, 1953.

[155] W. Hastings. Monte Carlo sampling methods using Markov Chains and their applications. Biometrika 57, 97-109, 1970.

[156] S. Geman and D. Geman. Stochastic relaxation, Gibbs distribution and the Bayesian restoration of images. IEEE Transactions on Pattern Analysis and Machine Intelligence 6, 721-741, 1984.

[157] W. Gilks, S. Richardson and D. Spiegelhalter. Markov chain Monte Carlo in practice. 1st edition London, UK: Chapman and Hall/CRC, 1996.

[158] C. Andrieu, N. D. Freitas, A. Doucet and M. I. JORDAN. An introduction to MCMC for Machine Learning. Machine Learning 50, 5-43, 2003.

[159] S.K. Au and J. L. Beck. Subset simulation and its application to seismic risk based on dynamic analysis. Journal of Engineering Mechanics 129(8), 901-917, 2003.

[160] B. Walsh. Markov chain Monte Carlo and Gibbs sampling. Lecture Notes, 2004.

[161] F. Miao and M. Ghosn. Modified subset simulation method for reliability analysis of structural systems. Structural Safety 33(45), 251-260, 2011.

[162] S. K. Au and J. L. Beck. Estimation of small failure probabilities in high dimensions by subset simulation. Probabilistic Engineering Mechanics 16(4), 263-277, 2001.

[163] P. Angelikopoulos, C. Papadimitriou and P. Koumoutsakos. Data driven, predictive molecular dynamics for nanoscale flow simulations under uncertainty. Journal of Physical Chemistry B, 117, 14808-14816, 2013.

[164] A. Gallina, R. Krenn, M. Scharringhausen, T. Uhl and B. Schafer. Parameter identification of a planetary rover wheel-soil contact model via a Bayesian approach. Journal of Field Robotics 31(1), 161-175, 2014.

[165] P. E. Hadjidoukas, P. Angelikopoulos, D. Rossinelli, D. Alexeev, C. Papadimitriou and P. Koumoutsakos. Bayesian uncertainty quantification and propagation for discrete element simulations of granular materials. Journal of Computer Methods in Applied Mechanical Engineering 282, 218-238, 2014.

[166] J. L. Beck and S. K. Au. Bayesian updating of structural models and reliability using Markov Chain Monte Carlo simulation. Journal of Engineering Mechanics 128(4), 380-391, 2002.

[167] J. L. Beck and S. K. Au. Updating robust reliability using Markov Chain simulation. in Proceedings of the International Conference on Monte Carlo Simulation, Monte Carlo, Monaco, 2000.

[168] J. Ching and Y. C. Chen. Transitional Markov Chain Monte Carlo method for Bayesian model updating, model class selection and model averaging. Journal of Engineering Mechanics 133(7), 816-832, 2007.

[169] G. S. Fishman. Coordinate selection rules for Gibbs sampling. University of North Carolina, UNC/OR TR-92/15, 1996.

[170] J. Ching and J. Wang. Application of the Transitional Markov Chain Monte Carlo algorithm to probabilistic site characterization. Journal of Engineering Geology 203, 151-167, 2016.

[171] J. Wang, L. S. Katafygiotis and M. N. Noori. Transitional Markov Chain Monte Carlo simulation for reliability-based optimization. Safety, Reliability, Risk and Life-Cycle Performance of Structures & Infrastructures Deodatis, Ellingwood & Frangopol (Eds), 1593-1599, 2014.

[172] G. A. Ortiz, D. A. Alvarez and D. Bedoya-Ruíz. Identification of Bouc-Wen type models using the Transitional Markov Chain Monte Carlo method. Journal of Computers and Structures 146, 252-269, 2015.

[173] M. Ismail, F. Ikhouane and J. Rodellar. Forced vibrations of a mechanical system with hysteresis. Proceeding of 4th conference on nonlinear oscillation, 1967.

[174] Y. Wen. Method for random vibration of hysteretic systems. Journal of Engineering mechanics 102(2), 249-263, 1976.

[175] R. M. Ebelling, R. A. Green and S. E. French. Accuracy of response of single-degree-of-freedom systems to ground motion. US Army Corps of Engineers, Earthquake Engineering Research Program, Technical Report ITL-97-7, 1997.

[176] C. H. Wang and Y. K. Wen. Reliability and redundancy of pre-northridge low-rise steel building under seismic action. Rep No. UILU-ENG-99-2002, Univ. Illinois at Urbana-Champaign, Champaign, Ill, 1998.

[177] M. Ismail, F. Ikhouane and J. Rodellar. The Hysteresis Bouc-Wen Model, a Survey. Computational Methods in Engineering 16, 161-188, 2009.

[178] Wikipedia, Bouc-Wen model of hysteresis, http://en.wikipedia.org/wiki/Bouc-Wenmodel_of_hysteresis, visited on 15/06/2018.

[179] Ye. Meiying and X. Wang. Parameter estimation of the Bouc-Wen hysteresis model using particle swarm optimization. Smart Materials and Structures 16, 2341-2349, 2007.

[180] J. Song and A. Der Kiureghian. Generalized Bouc-Wen model for highly asymmetric hysteresis. Journal of Engineering Mechanics 132(6), 610-618, 2006.

[181] R. E. Kalman. A new approach to linear filtering and prediction problems. Journal of Basic Engineering 82(D), 35-45, 1960.

[182] G. Welch and G. Bishop. An introduction to the Kalman filter. Technical report, Department of Computer Science, University of North Carolina at Chapel Hill, 2006.

[183] A. Andrews. A square root formulation of the Kalman covariance equations. AIAA Journal 6(6), 1165-1166, 1968.

[184] J. E. Potter and R. G. Stern. Statistical filtering of space navigation measurements. In Proceedings of the AIAA Guidance and Control Conference, Massachusetts Institute of Technology, 1963.

[185] O. Pajonk. Stochastic spectral methods for linear Bayesian inference. Ph.D. Dissertation, Institut für Wissenschaftliches Rechnen, Technische Universität Braunschweig, 2012.

[186] H. G. Matthies, E. Zander, B. V. Rosić, A. Litvinenko and O. Pajonk. Inverse problems in a Bayesian setting. Journal of Computational Methods for Solids and Fluids 245-286, 2016.

[187] N. Metropolis. The beginning of the Monte Carlo method. Los Alamos Science 15, 1949.

[188] N. Metropolis and S. Ulam. The Monte Carlo method. Journal of the American Statistical Association 44(247), 335-341, 1949.

[189] S. Chib and E. Greenberg. Understanding the Metropolis-Hastings algorithm. American Statistician 49(4), 327-335, 1995.

[190] B. A. Berg. Markov Chain Monte Carlo simulations and their statistical analysis. Singapore, World Scientific, 2004.

[191] A. Bobrowski. Functional analysis for probability and stochastic processes. Cambridge: Cambridge University Press, 2005.

[192] C. Pritchard. The changing shape of geomtetry. Cambridge University Press, 2003.

[193] M. Rao. Conditional measures and applications. Boca Raton: CRC Press, 2005.

[194] M. Rao and R. J. Swift. Probability theory with applications. Mathematics and Its Applications, Band 582, Springer-Verlag, 2006.

[195] H. G. Matthies, E. Zander, B. V. Rosić and A. Litvinenko. Parameter estimation via conditional expectation: a Bayesian inversion. Advanced Modeling and Simulation in Engineering Sciences 3:24, 2016.

[196] H. G. Matthies, A. Litvinenko, B. V. Rosić and E. Zander. Bayesian parameter estimation via filtering and functional approximations. Technical Gazette 23(1), 1-8, 2016.

[197] T. A. El Moselhy and Y. M. Marzouk. Bayesian inference with optimal maps. Journal of Computational Physics 231(23), 7815-7850, 2012.

[198] S. B. McGrayne. The theory that would not die. New Haven: Yale University Press, 2011.

[199] D. G. Luenberger. Optimization by vector space methods. Chichester: Wiley, 1969.

[200] M. S. Grewal and A. P. Andrews. Kalman filtering: theory and practice using MATLAB, Chichester: Wiley, 2008.

[201] G. Evensen. Data assimilation–the ensemble Kalman filter. Berlin: Springer, 2009.

[202] D. Bosq. Linear processes in function spaces, theory and applications. In: Lecture notes in statistics 149, Berlin: Springer, 2000.

[203] O. Pajonk, B. V. Rosić, A. Litvinenko and H. G. Matthies. A deterministic filter for non-Gaussian Bayesian estimation– Applications to dynamical system estimation with noisy measurements. Physica D: Nonlinear Phenomena 241(7), 775-788, 2012.

[204] D. Xiu. Numerical methods for stochastic computations: a spectral method approach. Princeton: Princeton University Press, 2010.

[205] J. L. Anderson. Ensemble adjustment Kalman filter for data assimilation. Geophysical Fluid Dynamics Laboratory, Princeton, New Jersey, 2001.

[206] K. J. H. Law, D. Sanz-Alonso, A. Shukla and A. M. Stuart. Filter accuracy for the Lorenz 96 model: Fixed versus adaptive observation operators. Physica D 325, 1-13, 2016.

[207] B. V. Rosić, A. Litvinenko, O. Pajonk and H. G. Matthies. Sampling-free linear Bayesian update of polynomial chaos representations. Journal of Computational Physics 231(17), 5761-5787, 2012.

[208] B. V. Rosić and H. G. Matthies. Identification of properties of stochastic elastoplastic systems. Computational Methods in Stochastic Dynamics 26, 237-253, 2013.

[209] C. Felippa. Introduction to FEM, FEM Modeling: Mesh, Loads and BCs.Lecture Notes, University of Colorado Boulder, 2016.

[210] E. Adeli, B. V. Rosić, H. G. Matthies and S. Reinstädler. Bayesian parameter identification in plasticity. XIV International Conference on Computational Plasticity. Fundamentals and Applications COMPLAS XIV E. Oñate, D.R.J. Owen, D. Peric and M. Chiumenti (Eds), 2017.

[211] E. Adeli, B. V. Rosić, H. G. Matthies and S. Reinstädler. Effect of Load Path on Parameter Identification for Plasticity Models using Bayesian Methods. Quantification of Uncertainty: Improving Effieciency and Technology, G. Rozza, M. D'Elia and M. Gunzburger (Eds), 2018.

[212] A. F. Bower. Applied mechanics of solids. CRC Press, 2009.

Appendix A. State Variable Estimation of Lorenz-1996 Model

Here the estimation of the model variables X_6 to X_{40} according to the time evaluation are shown.

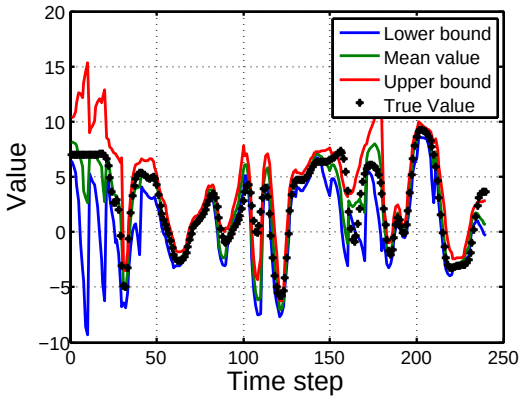

(a) Variable X_6 update

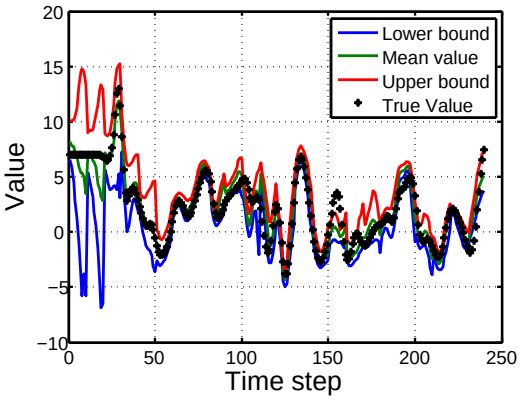

(b) Variable X_7 update

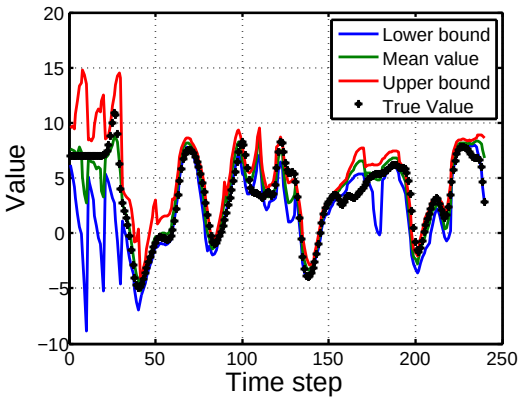

(c) Variable X_8 update

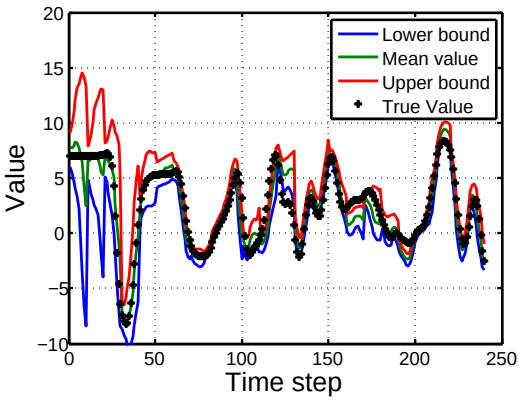

(d) Variable X_9 update

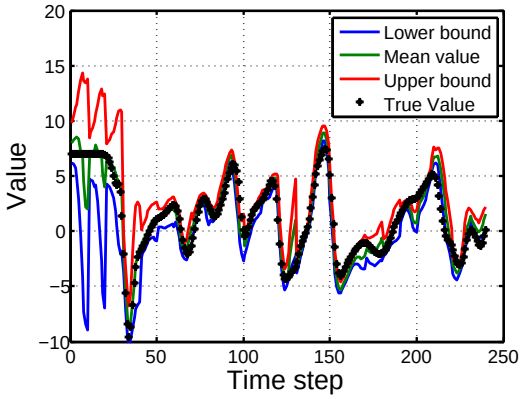

(a) Variable X_{10} update

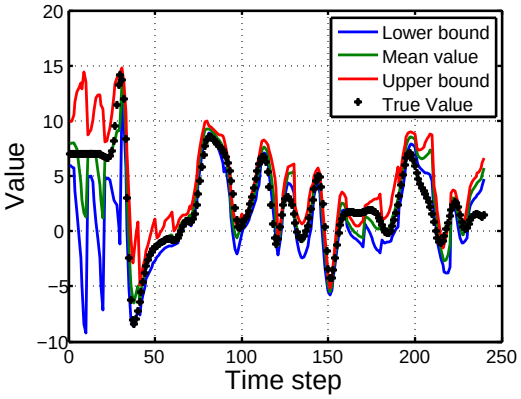

(b) Variable X_{11} update

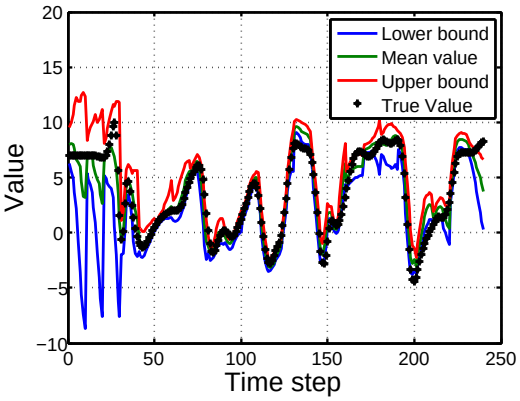

(c) Variable X_{12} update

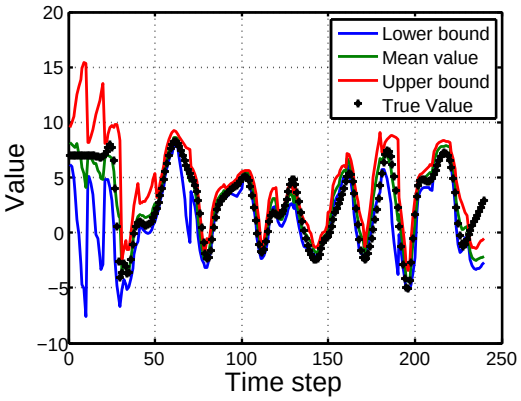

(d) Variable X_{13} update

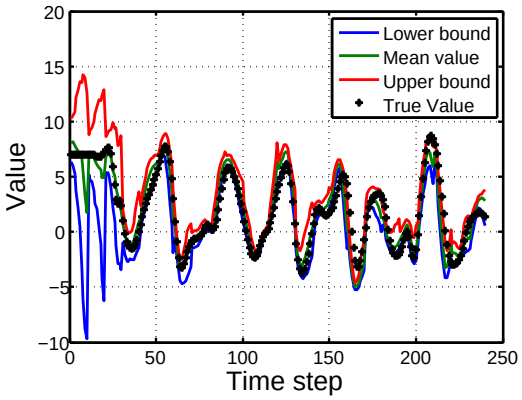

(e) Variable X_{14} update

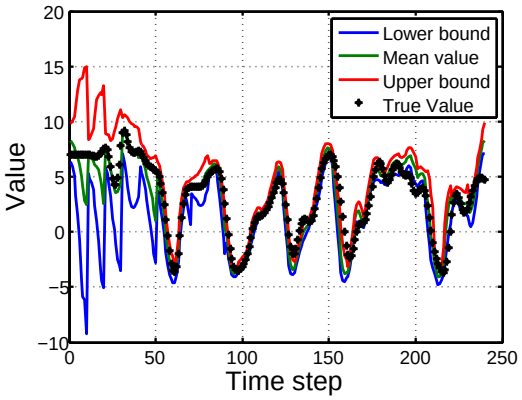

(f) Variable X_{15} update

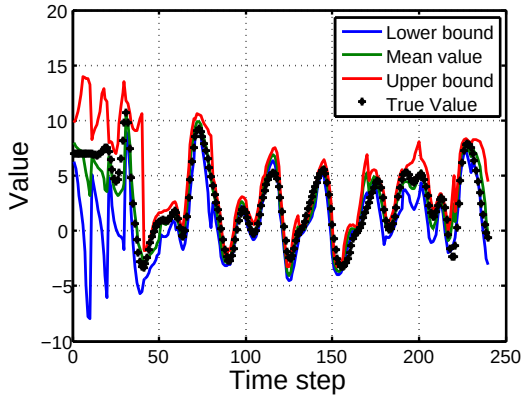

(a) Variable X_{16} update

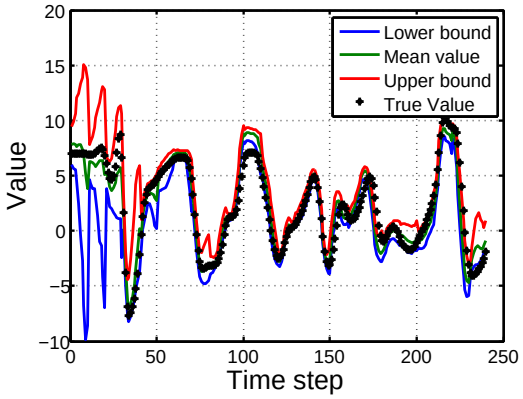

(b) Variable X_{17} update

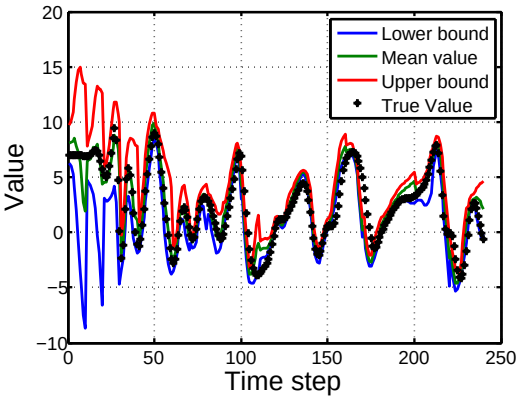

(c) Variable X_{18} update

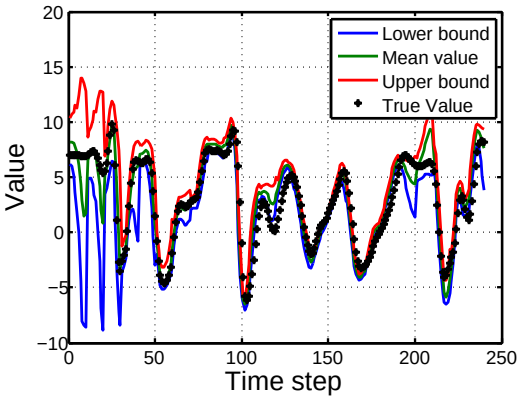

(d) Variable X_{19} update

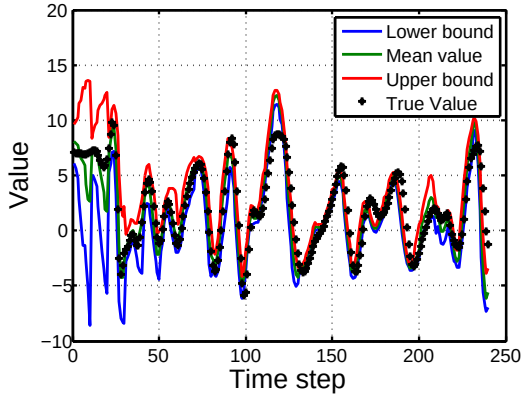

(e) Variable X_{20} update

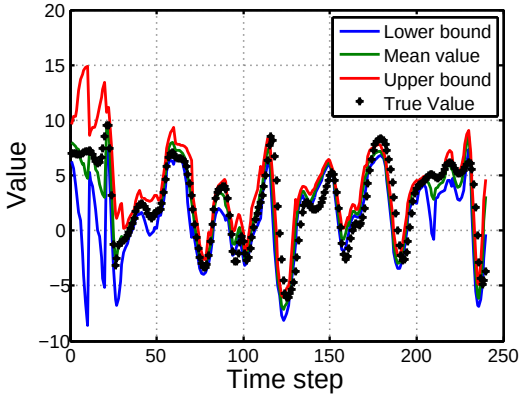

(f) Variable X_{21} update

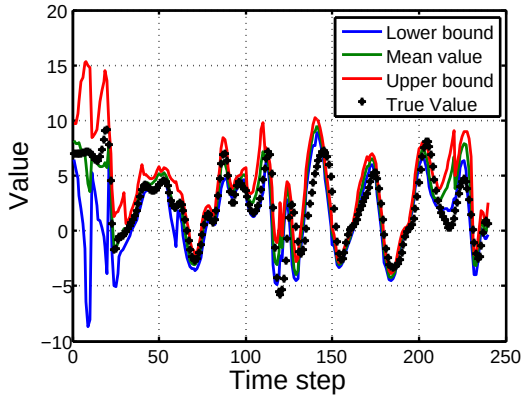

(a) Variable X_{22} update

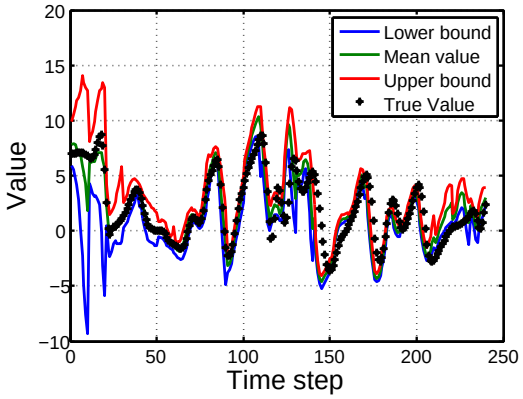

(b) Variable X_{23} update

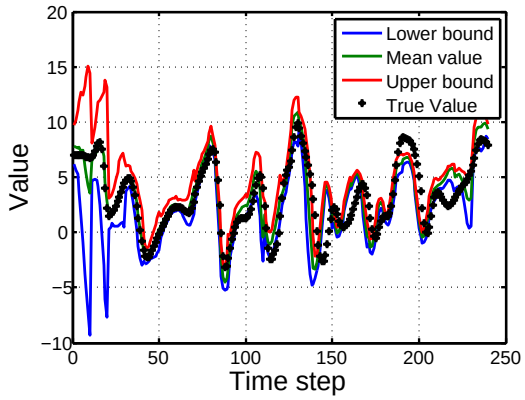

(c) Variable X_{24} update

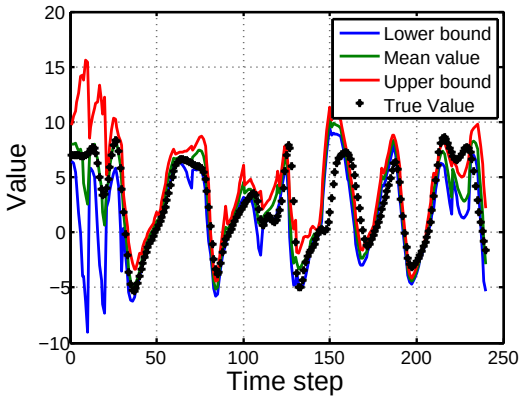

(d) Variable X_{25} update

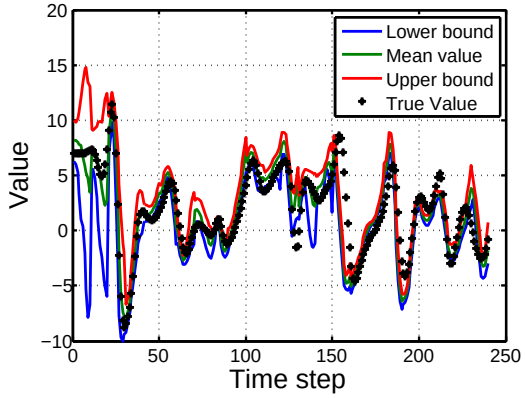

(e) Variable X_{26} update

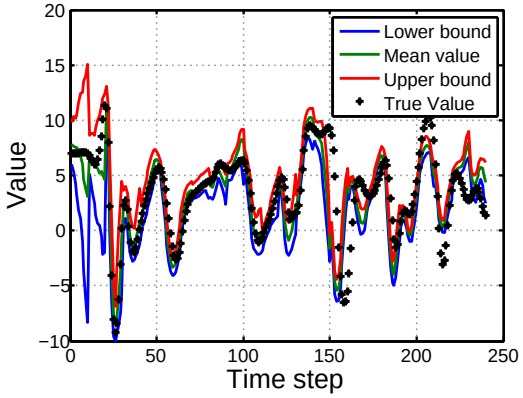

(f) Variable X_{27} update

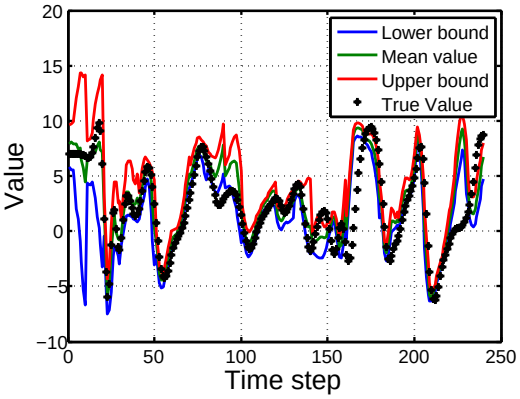

(a) Variable X_{28} update

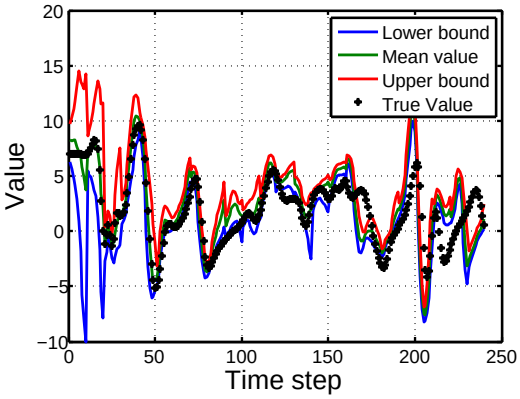

(b) Variable X_{29} update

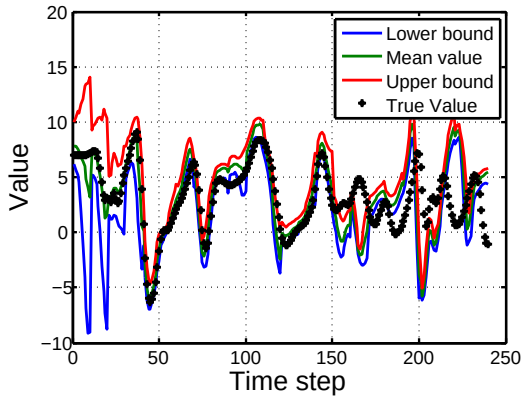

(c) Variable X_{30} update

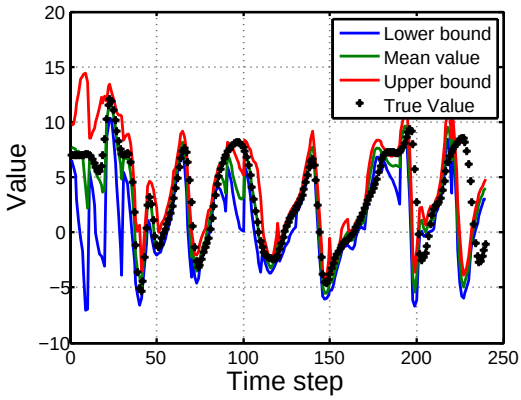

(d) Variable X_{31} update

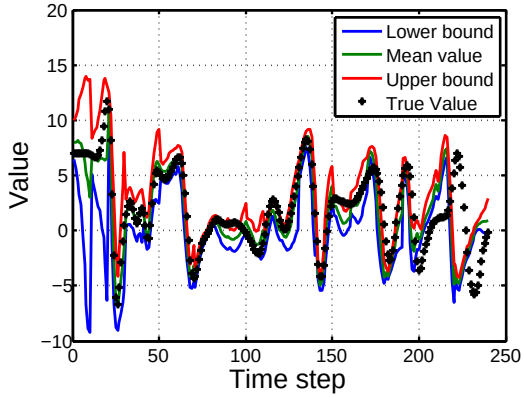

(e) Variable X_{32} update

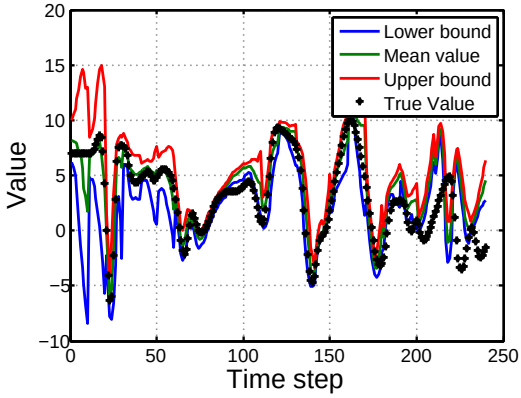

(f) Variable X_{33} update

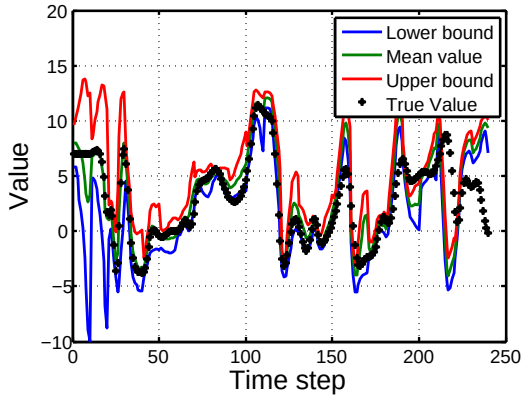

(a) Variable X_{34} update

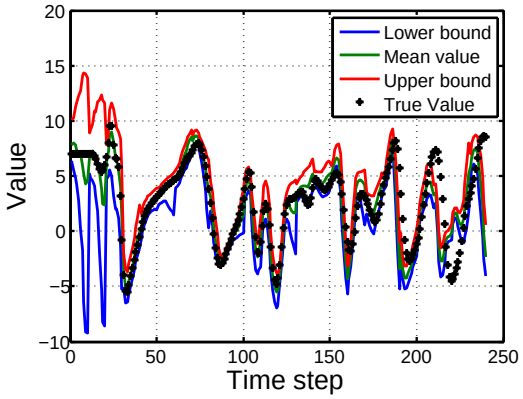

(b) Variable X_{35} update

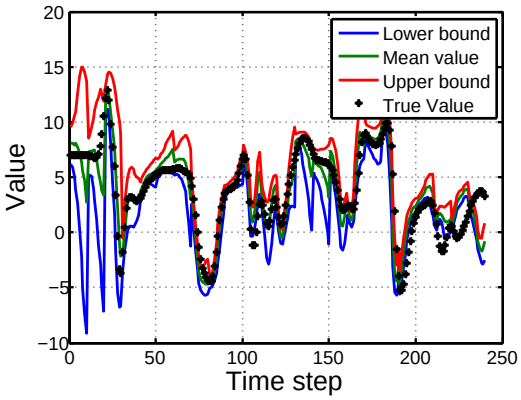

(c) Variable X_{36} update

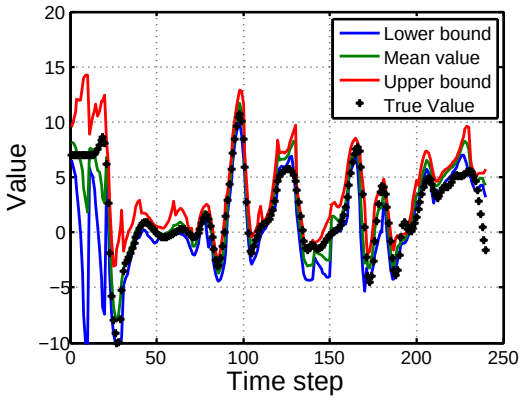

(d) Variable X_{37} update

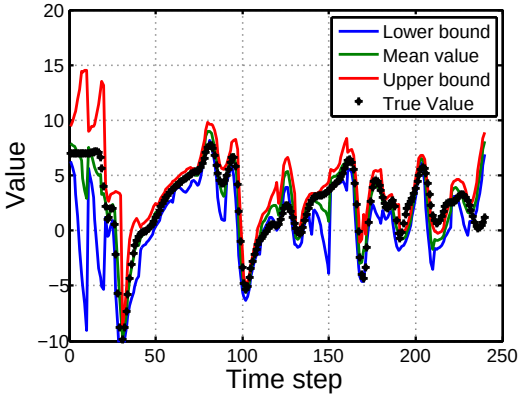

(e) Variable X_{38} update

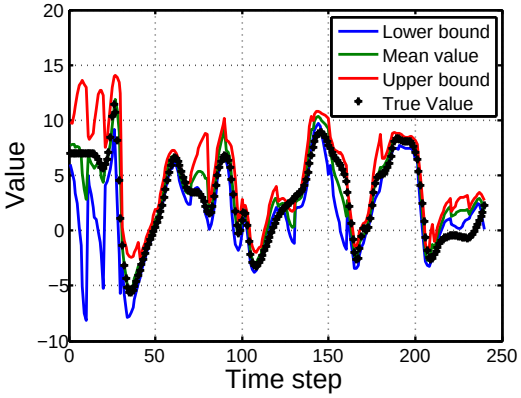

(f) Variable X_{39} update

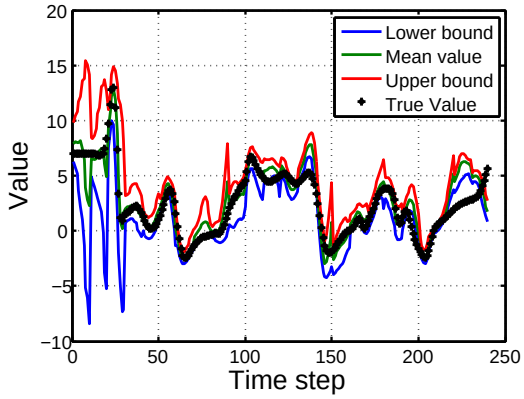

(a) Variable X_{40} update